

# AXIAL FLOW FANS

## DESIGN AND PRACTICE

*by*

R. A. WALLIS

M.E., A.S.T.C., A.I.M.E.Aust., A.F.R.Ae.S.

*Senior Scientific Officer  
Aeronautical Research Laboratories (Melb.)  
Department of Supply  
Australia*



1961

ACADEMIC PRESS  
NEW YORK AND LONDON

© R. A. WALLIS, 1961

U.S. Edition published by  
ACADEMIC PRESS INC.  
111 FIFTH AVENUE  
NEW YORK 3, NEW YORK

*First published 1961*

MADE AND PRINTED IN GREAT BRITAIN BY  
WILLIAM CLOWES AND SONS, LIMITED, LONDON AND BECCLES.

## **FOREWORD**

*by PROFESSOR A. R. COLLAR, University of Bristol*

The design of axial flow fans is a branch of engineering science which has been the subject of a large amount of *ad hoc* study, but in view of the very wide use of the fan, surprisingly little really systematic scientific attention has been devoted to it. This has probably been due in part to the fact that propellers and fans are usually quite remarkably efficient, even when the design is rudimentary, so that refinement of design has been considered not worth the effort involved. The absence of systematic work has, however, resulted in the absence of a satisfactory handbook, and this in turn has had a feedback effect on design philosophy. It is true that a good many scientific papers have derived from the *ad hoc* studies mentioned above, but these have been related to special topics and have not attempted to view the subject as a whole. In the early days of my own interest in this field there were two reference volumes most commonly employed: *Design of Screw Propellers for Aircraft* by H. C. Watts, and *Aerofoil and Airscrew Theory* by H. Glauert. The former contained many experimental data; the latter was almost wholly theoretical. "Glauert", in fact, was the aerodynamicist's *vade-mecum*, and was rightly regarded as indispensable, despite its foundation in inviscid theory and its consequent absence of interest in the effects of Reynolds number. These two volumes could provide basic data and method for a problem, but thereafter one was on one's own, especially in relation to ancillary problems involving ducting. It was a recognition of the paucity of published information that prompted me, two decades ago, to record my own experience relating to the powering of wind tunnels in some half dozen papers in the R. & M. Series, on fan, straightener, and cascade design and the like, papers which, I think, explain (if not justify) the invitation to me to write this Foreword, which I am privileged to do.

In view of the situation outlined above, I am very glad that Mr. Wallis has recognized the need for an authoritative book on fans; moreover, I think his book will quickly become the standard work in this field. Many will note with approval the compendium of boundary layer theory contained in Section 3, which indicates plainly the author's view that this is a subject of major importance for scientific fan design; the insistence on assessment of the characteristics of ducts is also noteworthy. This is to mention only two of the preliminary subjects studied before the book embarks on careful and systematic investigations of fan design, with detailed illustrations.

Of the author, it need only be said that Mr. Wallis had already established a high reputation in Australia before coming to work for a time in England. In this country he quickly won golden opinions for his aerodynamic work, which was both soundly based and original. I am sure that the present volume will add considerably to his reputation.

A. R. COLLAR

*Bristol, 1960.*

## P R E F A C E

The design of a ducted axial flow fan using sheet metal blades was one of my first tasks as an aerodynamicist. I used the simple design method developed at the Aeronautical Research Laboratories by Dr. G. N. Patterson, but experienced difficulty in obtaining reliable information on the aerodynamic characteristics of cambered plate fans. In consequence, a limited research programme on the subject was undertaken. These were the origins of a personal interest in axial flow fans.

Dr. Patterson's pioneer work at A.R.L. on fan design has become widely known, and as a result many inquiries for further information have been received by the Laboratories. At the same time, the need for a modern comprehensive treatment of the aerodynamics of ducted axial flow fans has long been recognized, and the present book seeks to fulfil that need.

In view of the fact that the main potential user of the data contained in this work is probably the ventilating engineer, much thought has been given to the question of suitable presentation. Contacts with members of the ventilating industry and study of professional journals in the field suggest that the industry has perhaps been a little slow to assimilate the great advances which have been made in general aerodynamics. Since ventilation engineers will be compelled to make ever-increasing use of these advances, it has appeared logical to present the material of this book in a modern aerodynamic manner. No apology is offered for the discarding of the traditional hydraulic notation, since I consider this step to be both justified and rendered inevitable by the trend of development. My views in the matter have been reinforced by the ability to deal with a hitherto unfamiliar design concept shown by a group of practising engineers who attended a series of lectures which I delivered on the subject.

No attempt has been made to present the historical and classical development of the momentum theory as applied to fan design. Instead, emphasis has been placed on the derivation of the required equations from well-established basic principles and design assumptions. One of the major aims has been the development of a simply-followed design method, supported by a sufficiency of background data which can be applied in making a rational appraisal of the design. The work should also make it possible to handle any problem of design, testing or analysis by means of either a direct application or a suitable rearrangement of the basic data presented.

Tribute to the author's wife for aid in preparing the manuscript is a familiar feature of prefaces to technical books. The present work is no exception, and I should like to acknowledge my wife's assistance, particularly in the typing of the manuscript. Mr. L. P. Coombes, the Chief Superintendent and Mr. F. W. David, the Aerodynamics Superintendent at A.R.L. have been most helpful during the preparation of the work. I am indebted in particular to Mr. W. Howard, and also to Mrs. B. L. Cumming, for pointing out errors and suggesting improvements. The great assistance given by Mr. N. Ruglen during the proof-reading stage is acknowledged with gratitude.

I am most grateful to Mr. V. J. Smith, who has kindly assisted me in the preparation of the Appendix dealing with free fans.

This book contains material used in a thesis submitted to the University of New South Wales, and I should like to record my appreciation of the readiness with which the University's permission for its publication was given.

The assistance gained from various publications in the preparation of certain of the illustrations is much appreciated; acknowledgments of the sources of the figures concerned will be found in the text.

Finally, the permission given by the Department of Supply for the publication of the book and for the use of photographic material in the possession of the Department is gratefully acknowledged.

R. A. W.

*Melbourne*

## **L I S T   O F   P L A T E S**

*Between pages 182 and 183*

### *Plate*

- 1.(a) Fan unit of wind tunnel at A.R.L. (Melb.)  
(b) Industrial air-moving fan unit
- 2.(a) Wind tunnel fan unit employing cambered sheet metal blades  
(b) Sheet metal blade rotor
3. Construction of 12-bladed fan from wooden laminations
- 4.(a) Straighteners and tail fairing of A.R.L. (Melb.) wind tunnel fan  
(b) Straighteners and drive fairings of industrial fan unit

# INTRODUCTION

## I.I. General

Propeller, or axial flow, type fans have been in use for many decades but it is only during the last two or three that much attention has been paid to their technical refinement. For the first part of this century, centrifugal fans of both the impeller and multi-vaned types enjoyed popularity owing to their greater operating flexibility, efficiency and quietness. The axial flow fan is however now rapidly gaining ground, as is indicated, for example, by the present preference for such fans in large mine ventilating installations. In the compressor field, too, the axial flow machine has virtually superseded the centrifugal compressor in gas turbine engines. This progress is due to the experimental and theoretical studies which have ensured the attainment of very high efficiencies together with satisfactory operation of the fan within the desired range. Marked reductions in noise level have also been achieved.

Important factors affecting the choice of fan unit are (a) manufacturing simplicity, (b) cost of manufacture, (c) fan efficiency, and (d) flow reversal in an emergency. The two former often favour the centrifugal while the two latter favour the axial flow type.

The uses to which fans are put are self-evident and hence will not be outlined here. It is important, however, in choosing or designing a fan to have a precise knowledge of the requirements, as otherwise the fan installed may be completely unsuited for the task. To avoid this predicament, which unfortunately occurs far too often, a basic approach to fan and duct problems is essential. Rule-of-thumb methods cannot take into account all the eventualities likely to be met.

## 1.2. General Types of Axial Flow Fan

Axial flow fans can be placed in three main categories :

(i) *Free fan.* A free fan is one which rotates in a common unrestricted air space (Fig. 1.1). In special cases a shroud ring attached to the blade tips may be employed.

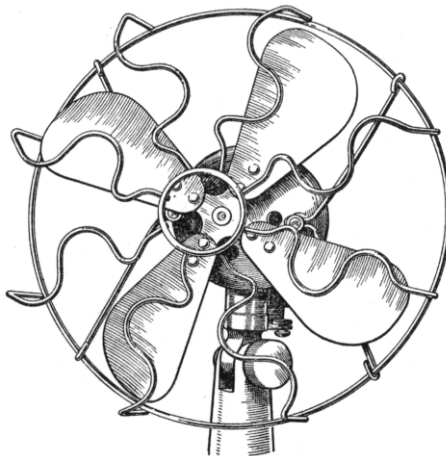


Fig. 1.1. Air circulator, free fan

(ii) *Diaphragm mounted fan.* This type of fan transfers air from one relatively large air space to another (Fig. 1.2). A shroud ring may be attached to the blades or, alternatively, to the partitioning structure.

(iii) *Ducted fan.* A fan is ducted (Plate 1 (a) and (b)) when the enclosing duct constrains the air to enter and leave the blading of the fan unit in an axial direction. The minimum duct length to satisfy this condition will be in excess of the distance between inlet to and outlet from the blading. When additional fan stages are fitted in series, the pressure rise of which the unit is capable increases. In the extreme case, a multi-stage unit becomes a compressor.

The first two types are relatively long-established and are probably the most common fans in use. The task which they perform is, generally speaking, not one for which centrifugal

fans are suitable. Although improvements have been made in the design of these unducted fans, there are still many of a relatively crude type in existence.

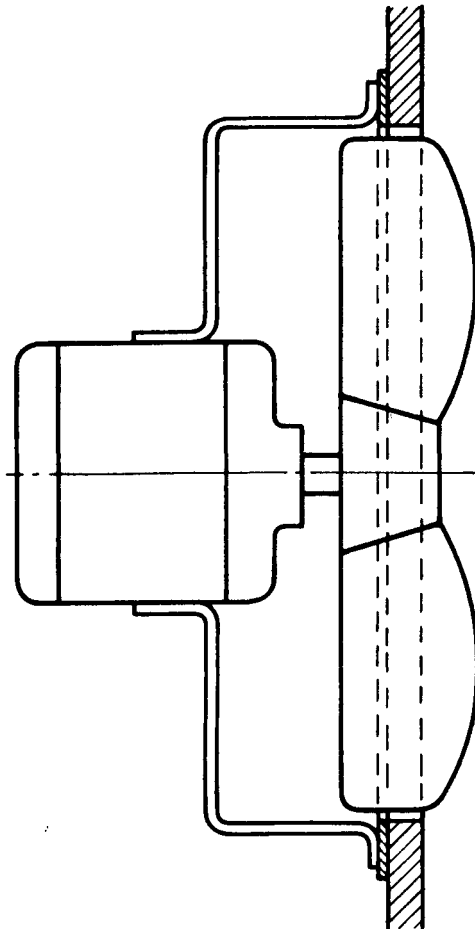


Fig. 1.2. Diaphragm mounted exhaust fan

One of the notable improvements of recent years has been the design of exhaust fans which operate in short compact ducts. These fans are superseding the cheap but crude type of dia-phragm mounted fan illustrated in Fig. 1.2. It might be concluded, therefore, that the second type of fan listed above

represents a passing phase in the development of quiet, high efficiency exhaust fans.

The ducted fan has undergone a rapid evolution and is now the most refined of the axial flow types. This is due in no small measure to the opportunity which the designer usually has to provide favourable aerodynamic working conditions for the fan. The present work will be concerned almost exclusively with this type of fan; some useful data on the other distinct type of fan, namely the free fan, are presented in an appendix.

### I.3. Elements of a Ducted Fan Unit

The various components which go to make up a ducted fan unit are indicated in Fig. 1.3. Rotor blades are a series of aerofoils which, owing to their relative motion with the air, add total head to the air stream. It is desirable that this function should be discharged with minimum losses through friction, flow separation and secondary flows.

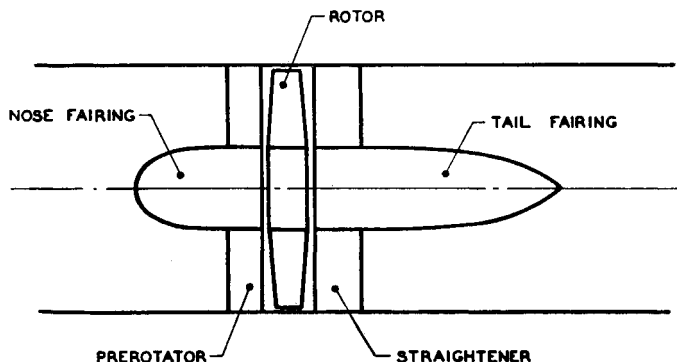


Fig. 1.3. Components of ducted fan unit

Stationary vanes, known as stators, are often located upstream and/or downstream of the rotor for reasons which will be elaborated on in Section 1.6.

In well-designed units the rotor boss diameter will normally be within the range 40–70 per cent of the rotor diameter. Near the axis of the rotor, both the blade velocity and swept areas are very small; as a result, the potential work output here is

very small. The larger boss diameters are usually associated with fans designed for high pressure rises.

Suitably shaped fairings upstream and downstream of the rotor boss are an essential part of good axial flow fan design.

In a multi-stage unit of co-rotating rotors there is a row of stators between each rotor stage.

#### 1.4. General Methods of Manufacture

The method of fan construction often has a marked influence on the aerodynamic design and final blade geometry. A very common type of fan employs sheet metal blades which normally possess some form of local or general cross-sectional camber. The design of such fans is sometimes crude and of an *ad hoc* nature and in consequence they operate with a relatively low efficiency. When design is based on modern aerodynamic principles, however, efficiencies can be high, as demonstrated in later sections. A modern sheet metal bladed wind-tunnel fan is illustrated in Plate 2(a). The blade twist and camber of a similar fan can be observed in Plate 2(b).

High efficiency fans are often made of wood since the material can be readily and accurately worked to the desired shape. The blades and boss are built up in an integral manner out of wooden laminations which are subsequently glued together (see Plate 3); the difficulty of this method increases with the number of blades required. When the laminations are carefully designed, considerable strength can be built into the boss for the purpose of resisting hoop and tensile stresses. Metal reinforcing plates or rings on the upstream and downstream faces of the bosses are, however, usually essential. This method is normally used only for fans in limited production.

The casting method of manufacture is a very common one. Early fans consisted of a few large blades cast integral with the boss, and bore traces of the influence of marine screw design. These fans were relatively crude by present-day standards. The trend is now towards separate blades produced by a modern casting process which provides a smooth surface finish without resort to expensive machining. High efficiency, high pressure rise fans possessing a large number of blades are often produced by this method.

Sufficient has been said to show that the type of construction adopted can exert a definite influence on the aerodynamic design of the fan.

## 1.5. Ducted Fan Duty

The duty of a ducted fan is specified by the amount of air which it forces through the system against resistance comprising skin friction, flow separation, secondary flow and discharge loss.

In many commercial duct systems, the fan exhausts directly to the atmosphere. In such cases the customer is mainly concerned with the pressure losses upstream of the fan and as a consequence manufacturers specify their fans in terms of their ability to overcome a particular upstream loss. The fan static pressure head, as this loss is called, is related to the useful total head rise across the fan by the relation

$$\Delta H_{\text{useful}} = \text{static pressure head} + \text{exit velocity head} \quad (1.1)$$

where the air is discharged direct from the constant-area duct enclosing the fan unit; this equation can be adopted as a formal definition of the term, static pressure head. When a diffuser is used on the exit side of the fan unit, the exhaust velocity is reduced and a static pressure rise occurs in the diffuser (see Section 6.4). The relevant relation is then

$$\begin{aligned} \Delta H_{\text{useful}} = & \text{static pressure head} + \text{exit velocity head} \\ & + \text{diffuser losses} \end{aligned} \quad (1.2)$$

Since the exit velocity head is now lower than it was in the previous case by an amount normally greater than the diffuser losses, the fan has to add less total head to the air for the same upstream pressure losses, that is, static pressure head.

For *exhaust* units of the ducted type, eqs. (1.1) and (1.2) can be written as

$$\Delta H_{\text{useful}} = \text{static pressure head} + \text{downstream loss} \quad (1.3)$$

Axial flow fans are, however, used for many purposes other than that of exhausting air; a few examples of such uses will be discussed briefly. For the case of a fan unit providing a jet of

air for cooling purposes,

$$\Delta H_{\text{useful}} = \text{exit velocity head} + \text{duct losses} \quad (1.4)$$

When no additional ducting is employed, the duct losses are of course zero. With this type of unit the customer is concerned primarily with the capacity of the unit and the outlet velocity from the nozzle.

A fan unit with ducting components connected both upstream and downstream may be part of a system which is either open to the atmosphere or of a closed circuit type. In the former case,

$$\begin{aligned} \Delta H_{\text{useful}} = & \text{upstream duct losses} + \text{downstream duct losses} \\ & + \text{exit velocity head} \end{aligned} \quad (1.5)$$

while in the latter instance the appropriate relation is

$$\Delta H_{\text{useful}} = \text{duct losses} \quad (1.6)$$

Despite the diversity of uses to which a fan unit may be put, it is nevertheless essential to have a unique method of expressing the pressure rise characteristics of the unit. Up to the present eq. (1.1) has been used in determining the fan static pressure head which a fan provides at a given flow condition and this quantity has enjoyed use of a relatively universal nature. From a study of the foregoing relations, however, it will be seen that this pressure, as defined in eq. (1.1), has no physical meaning except in the case of the exhausting unit. It is not difficult, therefore, to appreciate the problems which newcomers to the field of ventilation engineering encounter in dealing with this question of fan pressure. Many serious errors are made and these will be avoided only when a more basic approach to the problem is adopted.

Since fan static pressure head, as determined from eq. (1.1), assumes a more or less nominal character in many cases, the choice of a more appropriate pressure as a means of specifying fan duty is long overdue. The total head rise,  $\Delta H_{\text{useful}}$ , is a convenient pressure since it represents the combined losses in the system external to the fan unit ; this is a quantity basic to

all units, irrespective of the task for which they are used. When relevant, static pressure head can always be readily computed.

The fact that fan static pressure head is *not* the static pressure rise across the fan unit cannot be stressed too strongly; the terminology arises out of duct rather than fan considerations.

Since air compressibility can be neglected in fan design, as opposed to compressor design, the volume of air moved by the fan, known as the capacity, can be specified in terms of volume flow per unit time for ambient pressure and temperature conditions (see Section 2.1).

Duct resistance (Section 6) increases approximately as the square of the velocity for turbulent flow, which is the type normally encountered in industrial installations. The nature of the characteristic curve for the duct system is illustrated in Fig. 1.4. The fan characteristic cuts this curve to give the

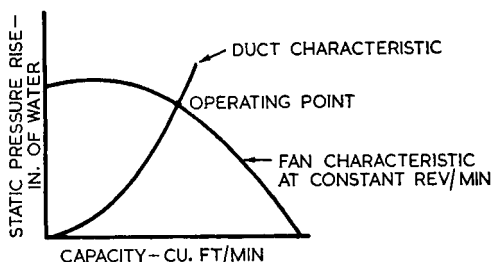


Fig. 1.4. Matching of fan and duct system

operating point of the system for a given fan speed. Provided the fan is not stalled, flow conditions will be steady; this feature is emphasized by the very definite point at which the two characteristics intersect.

For a given duct system the volume flow through the fan is normally varied by changing the rotor speed. Alternative methods which have been devised for the purpose of altering the fan characteristic utilize variable-pitch rotor or stator blades; full data on these methods are presented in Sections 19 to 21.

## I.6. Types of Ducted Fan, Aerodynamic Classification

When a fan rotor adds total head to the air flowing through it, the angular momentum of the stream is altered. For example, a rotor receiving air which is approaching in an axial direction discharges it with a tangential component of velocity, resulting in the appearance of a phenomenon which in the theory of aircraft propellers is known as "slipstream rotation". The change of angular momentum in the airstream is related to the torque on the rotor shaft.

The efficiency of the fan unit is influenced by the amount of swirl left in the air after it has passed the last stage of blading in the unit. The swirl momentum can play no part in overcoming the resistance of the duct system unless the associated tangential component is removed and its velocity head converted into static pressure.

Five main design possibilities arise as a result of the above-mentioned aerodynamic phenomenon of slipstream rotation.

- (i) *Rotor unit.* The swirl passes downstream of the rotor and the associated momentum is lost.
- (ii) *Rotor-straightener unit.* The swirl is removed by stators placed downstream of the rotor and the associated dynamic head is recovered in the form of a static pressure rise.
- (iii) *Prerotator-rotor unit.* Stators are used to impart a preswirl in the opposite sense to the rotor motion and the rotor then removes the swirl.
- (iv) *Prerotator-rotor-straightener unit.* A combination of the preceding two configurations.
- (v) *Contra-rotating rotors.* The second rotor removes the swirl introduced by the first.

The above provides a very convenient method for the classification of ducted fans.

## I.7. On Static Pressure Rise in a Fan Unit

The magnitude of the pressure rise required produces detailed design differences between fans which are nominally of the same type. For example, low pressure rise fans possess a smaller number of blades than the high pressure rise variety;

the relative boss diameter will also be greater in the latter case.

The static pressure rise through the rotor blading is related to the retardation of the air relative to the blade as it passes from inlet to outlet of the rotor stage, as demonstrated in Section 9.3.

The air flowing through prerotating stators is accelerated and, in accordance with Bernoulli's equation (Section 2.2), the static pressure falls. However, the reverse occurs in straighteners, where a static pressure rise accompanies the removal of the tangential velocity component.

Unfortunately, when the static pressure rises along a solid surface in the direction in which the air is flowing, separation of the flow from the surface tends to occur, with undesirable consequences (Section 2.3.9). It is this phenomenon, known as stalling, which restricts the static pressure rise obtainable from a given fan unit.

Static pressure rise considerations have inspired the design of unusual types of fan. In an impulse type of rotor the static pressure rise through the blading is zero. It is designed to have equal inlet and outlet velocities of the air relative to the blades; the direction of the vectors has, however, been changed. In other words, the complete increase in total head exists as swirl velocity head. The straighteners are then charged with the responsibility of converting this dynamic head into static pressure.

An alternative method which has been evolved for the purpose of restricting the static pressure rise through the rotor consists in increasing the axial velocity component from inlet to outlet. This is achieved by a flow contraction due to conical surfaces on either the enclosing duct or rotor boss. A portion of the excess axial velocity head is then recovered as static pressure in a downstream diffuser.

For the above two types of fan, the difficulty of pressure recovery is transferred from the rotor to the straighteners and downstream diffuser respectively. Unfortunately, these components are often less efficient than the rotor in achieving the desired static pressure rise across the unit, and as a result these unusual types of fan are seldom encountered in practice. The designer who endeavours to achieve the maximum static

pressure rise in *each* component of the fan unit, consistent with high or acceptable aerodynamic efficiency, is usually treading on sounder and more conventional ground.

### **I.8. Scope of Treatment**

A comprehensive aerodynamic treatment of ducted axial flow fans is given in the present work. This has necessitated the development of major design and analysis relationships from basic principles. Also, in order to permit a full understanding of the subject, the relevant elements of essential background subjects have been presented as concisely as possible in the sections immediately following this Introduction. The data presented therein are either directly useful in the design of ducting and fan units, or, alternatively, provide the necessary background for informed design decisions.

As usual, a fan is defined as an air-moving unit in which the air can be considered incompressible. Data presented later indicate an approximate air velocity limit below which the assumption of incompressibility can be considered valid.

### **I.9. Final Comments**

The subject matter has been so arranged that each specific topic occupies a separate section. It is considered that this approach will facilitate (a) ready reference, and (b) a clearer understanding of the various distinct features of fan theory and practice. The importance of a particular subject is therefore not necessarily related to the degree of subdivision under which it appears.

The order in which the subjects are presented is designed to provide a gradual development of ideas and working equations. For the reader interested, however, in assessing the magnitude and difficulty of the fan design problem, a direct reading may create many false impressions. In actual fact the mechanics of fan design are far from difficult and the limited computations can be classed as simple. For a first superficial study, Sections 7 and 18 are recommended. This may be followed by a reading of Sections 4 to 5 and 8 to 16 after which the designer should

possess all relevant data. By embracing the remaining sections, the full scope of this aerodynamic subject can be covered.

The section on ducts is included for the purpose of correlating duct and fan design procedures. At the same time reliable duct loss data sufficient for meeting normal requirements are presented.

# 2

---

## INTRODUCTION TO THE FLUID MECHANICS OF DUCTED FANS

### 2.1. The Atmosphere

Air, as the working medium, has a number of physical properties which are of importance in the design of axial flow fans. These are pressure, temperature, density and viscosity ; humidity is neglected as the corrections are small.

**2.1.1. Variation of pressure with altitude.** At mean sea level (M.S.L.), the standard atmosphere is assumed to have a static pressure,  $p_0$ , of 2116.2 lb/ft<sup>2</sup> (760 mm of mercury), at 15°C. The conventional variation of pressure,  $p$ , with altitude has been specified by the International Commission on Air Navigation (I.C.A.N.) as <sup>(1)</sup>

$$\frac{p}{p_0} = \left( \frac{288 - 0.001981h}{288} \right)^{5.256} \quad (2.1)$$

where  $h$  is the altitude in feet from zero to 36,000 ft.

**2.1.2. Variation of temperature with altitude.** The accepted temperature, specified by the above Commission is,

$$t (\text{°C}) = (15 - 0.001981h), \text{ for } h < 36,000 \text{ ft} \quad (2.2)$$

That is, for every 1000 ft of altitude the temperature falls by 1.981°C.

**2.1.3. Density.** The air density,  $\rho$ , can be obtained from the equation of state, namely,

$$\frac{p}{\rho} = RT \quad (2.3)$$

where

$p$  is absolute pressure ( $\text{lb}/\text{ft}^2$ )

$\rho$  is density ( $\text{slug}/\text{ft}^3$ )

$T$  is absolute temperature ( $^{\circ}\text{K}$ )

$R$  is universal constant ( $= 3091 \text{ ft}^2 \text{ sec}^{-2} \text{ deg.}^{-1}$  for a mass of 1 slug).

For standard temperature and pressure at M.S.L.,  $\rho_0 = 0.002378 \text{ slug}/\text{ft}^3$ . (One slug is assumed to be equal to a mass of 32.17 lb in this instance.)

**2.1.4. Viscosity.** The viscosity of air is expressed in terms of a coefficient,  $\mu$ . This coefficient is dependent only on temperature and may be obtained from Sutherland's equation,<sup>(1)</sup>

$$\mu = 3.059 \frac{T^{1.5}}{T+114} \quad (2.4)$$

where  $T$  is absolute temperature ( $^{\circ}\text{K}$ ).

The value for standard conditions at M.S.L. is  $3.719 \times 10^{-7} \text{ slug}/\text{ft sec}$ .

**2.1.5. Compressibility.** In fan design, it is usually assumed that air is incompressible, i.e., the pressure changes in the fluid are too small to change the fluid density to any noticeable extent. This is in contrast to the case of axial flow compressors where large pressure changes are desired and obtained.

In the following theory it will be assumed that the density remains constant at a value calculated for the prevailing atmospheric pressure and temperature conditions. The upper limit at which this assumption can be considered valid is given in Section 7.5.

**2.1.6. Heat addition.** The thermodynamic problems arising from heat addition, e.g. by means of a heat exchanger, will not be considered here.

## 2.2. Bernoulli's Equation

When we consider the flow path of a particle in a fluid in which viscosity can be neglected, changes in the inertia forces must equal the changes in the pressure forces. When the flow at a point is steady with respect to time, the equation of motion for flow along a streamline is

$$\rho U \frac{dU}{dS} = - \frac{dp}{dS} \quad (2.5)$$

where  $U$  is the velocity (ft/sec)

$p$  is the static pressure (lb/ft<sup>2</sup>)

$\rho$  is the density (slug/ft<sup>3</sup>)

$S$  is distance along streamline (ft).

Integrating the above for constant density,

$$\frac{1}{2}\rho U^2 = - p + \text{const.}$$

or

$$\frac{1}{2}\rho U^2 + p = \text{const.} = H \quad (2.6)$$

The constant of integration,  $H$ , is called the total head of the fluid and the quantity  $\frac{1}{2}\rho U^2$  is known as the dynamic or velocity head. The implications of the above equation can be illustrated in Fig. 2.1.

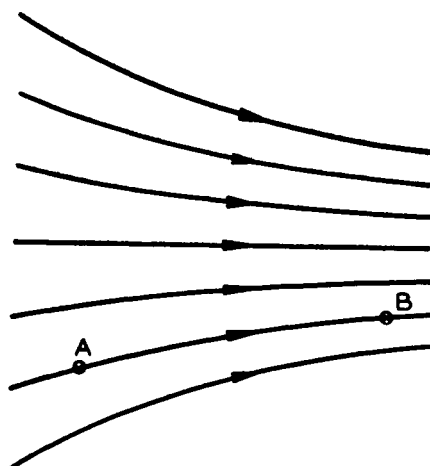


Fig. 2.1. Streamline motion

As a particle moves from A to B, it is accelerated and hence it follows, from the foregoing equation, that the static pressure is progressively reduced.

In the reverse process, the flow is retarded and velocity head is converted into static pressure; this process is called pressure recovery or diffusion. The static pressure rise produced in a fan unit can be attributed to pressure recoveries occurring in various components of the unit (see Section 1.7).

Bernoulli's equation applies strictly to flow paths in which viscosity may be neglected but qualitatively the principle of the interchangeability of static pressure and velocity head remains unaltered even where viscosity has an appreciable influence.

### 2.3. Viscosity and Boundary Layers

**2.3.1. Skin friction.** In developing Bernoulli's equation, viscosity was neglected. This assumption is, however, not valid near a solid surface. Air in direct contact with the surface is at rest and as a result there is a large rate of fluid shear as the velocity,  $u$ , increases rapidly with distance from the surface until it reaches a constant value,  $U$ , in the "free" stream (see Fig. 2.2). This region of flow retardation, called the "boundary layer", represents a loss of fluid momentum which is related to the "skin friction" force acting on the surface.

**2.3.2. Boundary layer thickness.** A boundary layer starts to grow at the point where the airstream first contacts the body. As more and more momentum is taken from the outer flow in order to maintain the forward motion of the air near the surface, the boundary layer thickness, in general, increases with distance  $x$  (see Fig. 2.3).

This thickness,  $\delta$ , is relatively hard to define as the velocity in the boundary layer approaches the free stream velocity asymptotically. The point at which the velocity is 99.5 per cent of its value in the free stream is frequently taken as the edge of the boundary layer. Somewhat more useful quantities are the "displacement" and "momentum" thicknesses.

**2.3.3. Displacement thickness.** Owing to the retarded flow in the boundary layer there is a displacement of the main

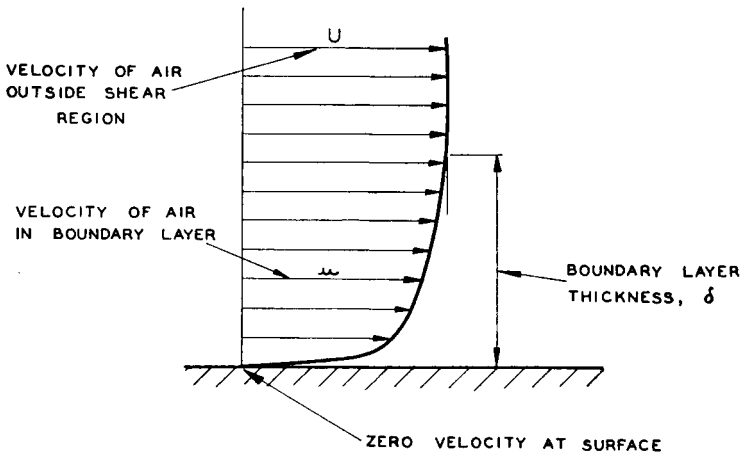


Fig. 2.2. Boundary layer flow

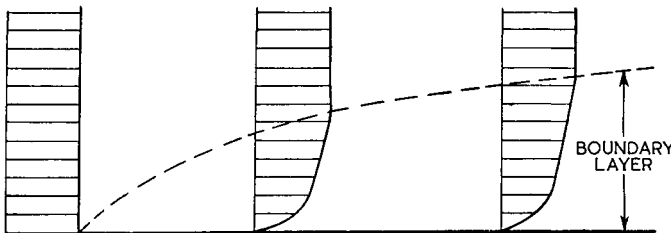


Fig. 2.3. Growth of boundary layer on flat plate

body of fluid away from the surface. When the flow deficiency,  $(U - u)$ , is integrated across the boundary layer in the  $y$  direction and equated to the product of the freestream velocity,  $U$ , and a thickness,  $\delta^*$ , one obtains

$$U\delta^* = \int_0^\delta (U - u) dy,$$

or

$$\delta^* = \int_0^\delta \left(1 - \frac{u}{U}\right) dy \quad (2.7)$$

where  $\delta^*$  is called the displacement thickness. No difficulty is experienced in determining this thickness as the flow deficiency near the outside edge of the boundary layer is negligible and hence the choice of the limit,  $\delta$ , is not critical.

The displacement thickness represents the amount by which the main flow has been displaced from the surface and is equivalent to an increased body thickness.

**2.3.4. Momentum thickness.** Probably the most useful thickness is the one which defines the loss of momentum in the boundary layer. In a similar manner to the foregoing, the loss of momentum is integrated across the layer and equated to the hypothetical case where the whole free stream momentum contained in a width,  $\theta$ , is lost. This gives

$$\rho U^2 \theta = \rho \int_0^\theta u(U-u) dy$$

or

$$\theta = \int_0^\theta \frac{u}{U} \left(1 - \frac{u}{U}\right) dy \quad (2.8)$$

where  $\theta$  is the momentum thickness. This thickness is of fundamental importance when assessing fluid friction losses.

**2.3.5. Transfer of momentum by laminar and turbulent means.** In order to maintain the forward motion of the air particles near the surface, against the retarding action of skin friction, momentum must be transferred inwards from a region possessing higher momentum. The transfer mechanism can be either laminar or turbulent.

The action of a laminar boundary layer can be illustrated from the simple model of an infinite number of thin fluid strata, parallel to each other and the surface; each stratum possesses relative motion with respect to its neighbour and as a consequence exerts a viscous pull on it. In this manner the desired momentum transfer towards the solid surface is effected through the medium of fluid shear.

No simple concept can be advanced for a turbulent boundary layer. It is however known that momentum is transferred in a direct and speedy manner by particles moving in an eddying fashion. The eddy motions passing through a given point are exceedingly numerous and are continually changing their characteristics as they are swept downstream. At any such point, however, the turbulence properties have definite mean statistical values with time; this implies that the mean motion

is a steady one and that the turbulence obeys definite laws. This type of turbulence should not be confused with the violent large scale eddies which exist downstream of bluff bodies, for example cylinders and plates normal to the stream.

The intense mixing which takes place in a turbulent boundary layer implies large fluid shear stresses. As a consequence, turbulent skin friction is greater than that found in a laminar boundary layer of comparable thickness.

**2.3.6. Boundary layer transition.** Laminar boundary layers are normally associated with very low fluid velocities or with the newly formed layers downstream of the point at which the flow meets a solid surface. The leading edge of an aerofoil is such a region. With increasing speed, or increasing distance downstream of the initial contact point, the laminar layer eventually gives way to turbulent flow; the change from laminar to turbulent flow is called transition. The various factors governing transition will be discussed in Section 3.7.

Depending on its cause, transition may occur abruptly or may be prolonged over a finite length of surface. During this period, the skin friction will progressively increase from a laminar to a turbulent value.

**2.3.7. Boundary layer growth.** As indicated in Section 2.3.2, the boundary layer grows as the flow progresses along a solid surface. In a pipe this growth continues until the wall boundary layers meet on the axis. This latter condition is termed "fully developed" pipe flow.

Since skin friction is greater in a turbulent layer than in a laminar one, the turbulent boundary layer grows at a faster rate. This is illustrated in Fig. 2.4 for the case of a flow along a flat plate; the thickness scale has been greatly magnified.

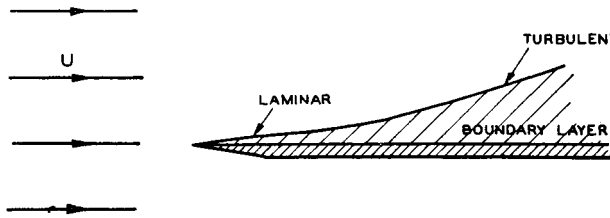


Fig. 2.4. Comparative rates of growth

Other factors influencing skin friction and boundary layer growth are surface roughness and the static pressure gradient in the stream direction.

**2.3.8. Effects of streamwise static pressure gradients.** In an accelerating flow, static pressure head is converted into velocity head and as a result dynamic head is added to the fluid near the surface in addition to that transferred by the shear. Moreover since the flow as a whole is speeded up, appreciable thinning of the layer in the flow direction may occur in highly accelerated flows.

Conversely, when the fluid is decelerating and the pressure rising, the momentum transfer mechanism has to contend with the loss of momentum due to skin friction together with that associated with the conversion of dynamic head into static pressure. Owing to its effective mixing mechanism, a turbulent boundary layer can meet these demands more readily than can a laminar one.

**2.3.9. Boundary layer flow separation.** When, in a decelerating flow, the loss of momentum in the flow immediately adjacent to a surface exceeds the rate at which momentum is being transferred inwards to the surface, the boundary layer approaches the condition where steady flow is impossible. The flow then leaves the surface in the manner shown in Fig. 2.5.

In other words, the particles near the surface no longer have a downstream velocity component and as a consequence the main flow is forced away from the surface. When this occurs, unsteady large-scale eddies are initiated. Large energy losses and drag are associated with such a phenomenon.

The region downstream of the boundary layer separation point is often referred to as a "stagnant" zone, owing to the relatively low air velocities therein. Although this is not a strictly accurate description, it is nevertheless for some purposes convenient to think of it in this manner. The "stagnant" air can be considered to be an extension to the solid surface in so far as the main flow is concerned. Such an extension represents an alleviation of the adverse pressure gradient.

The "stagnant" region is, in effect, a highly inefficient mixing zone, as the losses will imply. It is, however, possible,

when the adverse gradients have been reduced in the above manner, for the eddy mixing to bring about a re-attachment of the main flow to the surface at some downstream location.

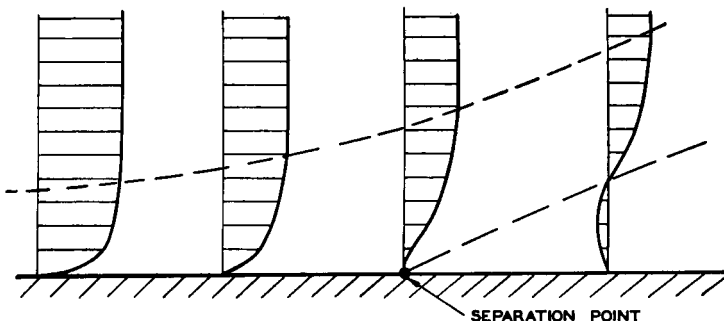


Fig. 2.5. Growth of boundary layer in adverse pressure gradient

This phenomenon of flow separation constitutes one of the major problems in fluid mechanics, as it restricts the lift which can be obtained from aerofoils, increases resistance to flow and produces unsatisfactory conditions where uniformity of flow velocity is essential. Various devices exist for controlling this separation but the additional complication which their installation involves has, in most cases, exerted a deterrent effect. A study of these devices is outside the scope of this book.

## 2.4. Similarity and Non-dimensional Numbers

The subjects of similarity and dimensional analysis are adequately covered by many fluid mechanics textbooks and therefore the discussion in these pages will be limited to the proper use of such data as they affect duct and fan design.

When the results of tests carried out on an item of aerodynamic equipment are expressed in a suitable non-dimensional manner, the data so obtained can be used in predicting the performance of similar items. In aerodynamics, full use must be made of non-dimensional parameters in design methods.

Although the beginner may have initial difficulty in understanding the physical significance of certain parameters, a mastery of their use will facilitate the execution of successful fan designs.

**2.4.1. Similarity.** There are three complementary types of similarity.

(i) *Geometric similarity.* Two units are geometrically similar if the corresponding length dimensions have a constant ratio throughout. In practice, each dimension of a unit is expressed as a ratio of some reference length, e.g. the diameter of a pipe. A unit can then be specified by a number of such ratios and two systems will be similar when the corresponding ratios are identical throughout.

(ii) *Kinematic similarity.* The basic dimension of time has now been added to that of length and this implies that the flow velocity at any point in the system should be in constant ratio to the velocity at a corresponding part of the similar unit. As before, it is more convenient to express the velocities in one unit as a ratio of a reference velocity, for example the mean velocity of flow through a pipe at the station of the reference diameter.

(iii) *Dynamic similarity.* This type of similarity requires the ratio of the forces acting to be similar for both systems. The three basic dimensions of length, time and mass are therefore included.

Three different aspects of dynamic similarity are discussed in the remaining sub-sections.

**2.4.2. Reynolds number.** This is probably the best known of all fluid motion parameters but is unfortunately not always properly understood. When dimensional analysis is applied, it is found that the forces acting on a solid surface and the flow phenomena associated with them are greatly dependent on the ratio of the inertia to the viscous forces, namely,

$$\frac{\rho Ul}{\mu}$$

where  $U$  and  $l$  are characteristic values of velocity and length respectively, and  $\rho$  and  $\mu$  the relevant values of density and viscosity.

It is in the choice of  $U$  and  $l$  that confusion arises and in order to clarify this point a more basic approach than usual will be made. Osborne Reynolds, after whom the ratio is named, demonstrated experimentally in a pipe that the type of boundary

layer flow, i.e. laminar or turbulent, is dependent on a critical value of the relation

$$R_d = \frac{\rho \bar{U} d}{\mu} \quad (2.9)$$

where  $\bar{U}$  is the mean velocity and  $d$  the internal diameter of the pipe.<sup>(2)</sup> For Reynolds' experiments, the flow in the pipe was "fully developed". Hence it follows that an equally suitable number is

$$R_\delta = \frac{\rho U \delta}{\mu} \quad (2.10)$$

where  $U$  is the velocity on the axis, i.e. at the edge of the boundary layer, and  $\delta$  is the boundary layer thickness, which in this case equals  $d/2$ . The characteristic velocity and length are therefore related to the boundary layer. This is very reasonable when it is remembered that the viscous forces are of no practical importance outside the region of the boundary layer. For entry flow to a pipe, this latter Reynolds number is the one with real meaning.

In the general case of flow along a plate, the boundary layer thickness,  $\delta$ , is difficult to define accurately (see Section 2.3.2) and hence it is more convenient to use  $\theta$ , the momentum thickness. This gives

$$R_\theta = \frac{\rho U \theta}{\mu} \quad (2.11)$$

which is the most basic Reynolds number to be discussed here.

It is obvious, however, that for flow over aerofoils and along plates, etc. the above Reynolds number will vary with distance and thus some Reynolds number capable of expressing the integrated effect is required. Such numbers will be discussed in subsequent sub-sections but it must be remembered that they can only be justified if they satisfy the requirements of boundary layer theory.

As suggested above, Reynolds number was first used in the prediction of transition, i.e. the change from laminar to turbulent flow. Reynolds suggested a certain critical value of

$$\frac{\rho \bar{U} d}{\mu} \approx 2000$$

but added the qualification that initial disturbances in the fluid could markedly influence its value. The truth of this has since been strikingly demonstrated by both Ekman and Taylor who, by exercising great care in ensuring a very steady initial flow, obtained critical values of  $5 \times 10^4$  and  $3.2 \times 10^4$  respectively.<sup>(3)</sup> The subject of transition will be treated more fully in Section 3.7.

Since Reynolds number is the ratio of the inertia to the viscous forces, two systems cannot be dynamically similar unless the component Reynolds numbers of one system are identical with those in the geometrically similar unit. It is in this connection that Reynolds number finds its greatest field of application.

**2.4.3. Force coefficients.** For a body immersed in a fluid and having relative motion with respect to that fluid, it can be shown by dimensional analysis that the forces acting on the body can be expressed by the relation

$$F = m\rho l^2 U^2 f\left(\frac{lU\rho}{\mu}\right) \quad (2.12)$$

where  $m$  is a constant and  $f(lU\rho/\mu)$  is a function of Reynolds number. As before,  $l$  and  $U$  are characteristic values of length and velocity.

Dimensional analysis is useful for indicating the correct grouping and presentation of results but actual experience and test data must be employed in choosing the appropriate characteristic dimensions. Although  $l$  appears three times in the above equation, it is not essential to substitute the same dimension in each case.

Some important applications of the above equation will now be considered in detail.

(i) *Skin frictional force in zero pressure gradient.* The element of force,  $dF$ , acting on an elementary area  $dA$ , can be written

$$dF = c_f \frac{1}{2} \rho U^2 dA \quad (2.13)$$

where  $U$  is the local free stream velocity and  $c_f = 2m f(R_\theta)$ .

For two-dimensional flow,  $dA$  can be replaced by  $dx$ , as unit length is assumed in the direction normal to the flow path.

Hence,

$$dF/\text{unit width} = c_f \frac{1}{2} \rho U^2 dx \quad (2.14)$$

In the above it will be seen that the characteristic lengths have been replaced by unity,  $dx$  and  $\theta$  respectively. The non-dimensional coefficient,  $c_f$ , is called the local skin friction coefficient.

Assuming a smooth surface, the process of determining the total force,  $F$ , acting on a surface can be simplified. On integrating the above expression

$$\begin{aligned} F/\text{unit width} &= \frac{1}{2} \rho U^2 \int_0^{x_e} c_f dx \\ &= C_f \frac{1}{2} \rho U^2 x_e \end{aligned} \quad (2.15)$$

where

$$C_f = \frac{1}{x_e} \int_0^{x_e} c_f dx \quad (2.16)$$

and

$x_e$  = effective length of surface.

It follows that  $C_f$  is a mean value of the skin friction coefficient and since the boundary layer will grow with  $x$  in a unique manner, the length,  $\theta$ , in the Reynolds number can be replaced by  $x_e$ . In other words  $C_f$  is a function of  $Ux_e \rho / \mu$  which is unique in the same manner as the  $c_f$  versus  $R_\theta$  relation.

In order to illustrate the above development, the case of a sharp edged, two-dimensional plate in a uniform stream will be considered in Fig. 2.6.

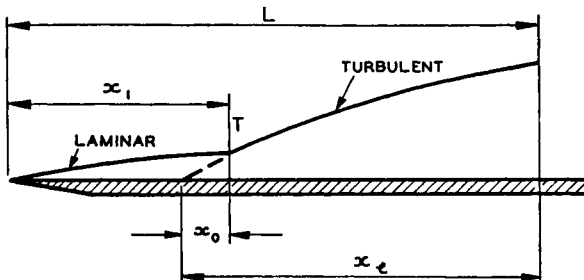


Fig. 2.6. Lengths used in skin friction calculations

For simplicity, transition is assumed to occur abruptly at point T. The effective length in the laminar flow region is obvious but for the turbulent flow the boundary layer thickness must be extrapolated forward to zero in order to obtain the appropriate effective length,  $x_e$ .

The skin frictional force acting on one surface of the above plate, between the limits  $x = 0$  and  $x = L$ , is

$$F/\text{unit width} = (C_{f2}^{\frac{1}{2}}\rho U^2 x_1) + (C_{f2}^{\frac{1}{2}}\rho U^2 x_e) - (C_{f2}^{\frac{1}{2}}\rho U^2 x_0) \quad (2.17)$$

where the values of  $C_f$  are obtained from the appropriate curves of  $C_f$  versus  $Ux\rho/\mu$ .

When the dimension  $L$  is large and the dimension  $x_1$  small, the force  $F$  can be approximated by

$$F/\text{unit width} = C_{f2}^{\frac{1}{2}}\rho U^2 L \quad (2.18)$$

This latter expression is the one usually employed, but the assumptions made in obtaining this simple expression should not be forgotten and each configuration should be examined in order to determine whether the expression may safely be used.

In cases where the velocity is variable with  $x$ , where non-uniform roughness exists, or where other complications are present, good accuracy can be obtained only by boundary layer growth calculations and by subsequent integration of the local elementary skin friction forces. Sufficient data to facilitate such calculations will be given later.

The foregoing paragraphs have illustrated the manner in which non-dimensional coefficients can be used in the calculation of skin friction forces. Flow over various types of solid surfaces will be considered in the relevant sub-sections.

(ii) *Aerofoil forces.* The force experienced by an aerofoil, when situated in an airstream, is usually resolved into two components: the lift force, which acts perpendicular to the direction of the oncoming stream, and the drag force, which acts in the stream direction. By rewriting eq. (2.12), these forces are given by

$$L = C_{L2}\rho U_0^2 A \quad (2.19)$$

and

$$D = C_{D2}\rho U_0^2 A \quad (2.20)$$

where  $U_0$  is the velocity of the oncoming stream,  $A$  is the

planform area of the aerofoil and  $C_L$  and  $C_D$  are the lift and drag coefficients respectively.

The force coefficients are usually obtained experimentally in the following form:

$$C_L = f_1\left(\frac{U_0 c \rho}{\mu}, \alpha\right) \quad (2.21)$$

$$C_D = f_2\left(\frac{U_0 c \rho}{\mu}, \alpha\right) \quad (2.22)$$

where  $c$  and  $\alpha$  represent the aerofoil chord and incidence respectively.

For two-dimensional flow,

$$L/\text{unit span} = C_L \frac{1}{2} \rho U_0^2 c \quad (2.23)$$

$$D/\text{unit span} = C_D \frac{1}{2} \rho U_0^2 c \quad (2.24)$$

In the above development, the chord Reynolds number,  $R_c$ , rather than the boundary layer one,  $R_\theta$ , has been used. It can readily be shown, however, that for a given Reynolds number and incidence, and for complete geometric similarity, the boundary layer thickness at any point on the surface is a fixed proportion of the chord dimension. Hence it follows that the chord is a suitable dimension for expressing the integrated effect of the boundary layers on the lift and drag forces. When the boundary layers are influenced by inadvertent surface roughness or inaccuracy in aerofoil profile, or by appreciable changes in free stream turbulence, inaccuracies may be expected in calculating the forces from chord Reynolds number data. These factors are discussed in greater detail in Section 4.10.

The local velocity at any point on a particular type of aerofoil section is usually determined by the quantities  $U_0$  and  $\alpha$ . Hence kinematic similarity is achieved provided there are no irregular boundary layer effects similar to those just mentioned.

**2.4.4. Pressure coefficients.** When dynamic similarity is achieved, it follows that the pressures which are responsible for the forces must also be capable of non-dimensional treatment. In eq. (2.12),  $\rho U^2$  has the dimensions of pressure; hence the choice of a dynamic head,  $\frac{1}{2} \rho U^2$ , in reducing quantities to a non-dimensional form.

The absolute value of pressure is of limited interest in incompressible aerodynamics and, as a result, pressures are usually measured with respect to some reference value, such as atmospheric pressure.

As an example of the above, the static pressure,  $p$ , at some point on an aerofoil surface, is expressed by the non-dimensional coefficient

$$C_p = \frac{p - p_0}{\frac{1}{2}\rho U_0^2} \quad (2.25)$$

where  $p_0$  and  $U_0$  are the undisturbed values of static pressure and velocity sufficiently far upstream of the aerofoil.

In general, therefore, it can be said that a pressure coefficient consists of three parts, namely, the pressure concerned, a reference pressure level and a reference dynamic head.

# 3

---

## BOUNDARY LAYER AND SKIN FRICTION RELATIONS

One of the usual difficulties encountered when presenting boundary layer theory to engineers lies in the provision of design equations suitable for engineering use. As a result of recent developments, however, it is now possible to present simple and useful methods of calculating certain boundary layer properties.

It is appreciated that more and more boundary layer data useful to the engineer will become available in the next few years and hence the methods chosen are those which are at present undergoing progressive development.

### 3.1. Equations of Motion for Boundary Layer Flow

For two-dimensional steady *laminar* flow, the Prandtl boundary layer equations are

$$u \frac{\partial u}{\partial x} + v \frac{\partial u}{\partial y} = -\frac{1}{\rho} \frac{\partial p}{\partial x} + \nu \frac{\partial^2 u}{\partial y^2} \quad (3.1)$$

$$-\frac{1}{\rho} \frac{\partial p}{\partial y} = 0 \quad (3.2)$$

where  $\nu = \mu/\rho$ , or kinematic viscosity,  $x$  and  $y$  are co-ordinates parallel and normal to the surface respectively and  $u$  and  $v$  are the corresponding velocity components in these directions.

These equations apply to the flow at a point  $(x, y)$  in the boundary layer; when integrated they relate to the boundary layer as a whole. The first relation equates the changes occurring in the inertia, pressure and viscous forces. From the second equation it follows that the static pressure for a given  $x$  co-ordinate remains constant throughout the boundary layer. Experimental aerodynamics makes wide use of this fact.

The above equations contain too many unknowns to be of universal use although isolated solutions have been obtained. One of these is due to Blasius who obtained a solution for the laminar layer in a zero pressure gradient, i.e.  $\partial p/\partial x = 0$ . Another solution exists for fully developed flow in a pipe.

In a *turbulent* boundary layer, the turbulent stresses which provide the turbulent mixing are much greater than the viscous stresses. In an attempt to represent the turbulent stresses, the first equation of motion is empirically modified to include a term,  $\epsilon$ , called the "apparent" kinematic viscosity due to turbulent shear. Hence,

$$u \frac{\partial u}{\partial x} + v \frac{\partial u}{\partial y} = - \frac{1}{\rho} \frac{\partial p}{\partial x} + (\nu + \epsilon) \frac{\partial^2 u}{\partial y^2} \quad (3.3)$$

Despite many attempts, no successful solution of this equation has been obtained. This is not surprising in view of the complexity of the actual boundary layer flow.

The above equations, although of very little direct use, have been included by virtue of their fundamental importance and general interest.

The equation of continuity for two-dimensional flow is usually grouped with the above equations and used in conjunction with them. This states,

$$\frac{\partial u}{\partial x} + \frac{\partial v}{\partial y} = 0 \quad (3.4)$$

In other words, a small loss of fluid in the  $x$  direction is exactly balanced by a gain of fluid in the  $y$  direction since there can be no loss or gain from the fluid as a whole.

Von Karman, by considering the momentum flow into and out of a "control box", developed the well-known momentum equation, namely,

$$\frac{d\theta}{dx} + \left( \frac{\delta^*}{\theta} + 2 \right) \frac{\theta}{U} \cdot \frac{dU}{dx} = \frac{\tau_0}{\rho U^2} \quad (3.5)$$

When  $dU/dx = 0$ ,

$$\frac{d\theta}{dx} = \frac{\tau_0}{\rho U^2} \quad (3.6)$$

or

$$\theta = \int \frac{\tau_0}{\rho U^2} dx \quad (3.7)$$

### 3.2. Laminar Boundary Layers

As illustrated in Fig. 2.3, the velocity in the boundary layer changes continuously from zero at the surface to the free stream value at the outer edge of the layer. Also, for reasons given in Section 2.3.8, the velocity "profile" will be influenced by the pressure gradient in the stream direction. It has been established by Pohlhausen that similarity of profile is achieved when two boundary layers have the same value of the non-dimensional parameter

$$\Lambda = \frac{\delta^2}{\nu} \cdot \frac{dU}{dx} \quad (3.8)$$

Hence it follows that  $\Lambda$  defines a "family" of velocity profiles; these are illustrated in Fig. 3.1.

The approach of boundary layer separation for retarded flow, i.e.  $dU/dx$  negative, is self-evident.

The velocity at any point in the layer is given by<sup>(4)</sup>

$$\frac{u}{U} = 2 \frac{y}{\delta} - 2 \left( \frac{y}{\delta} \right)^3 + \left( \frac{y}{\delta} \right)^4 + \frac{\Lambda}{6} \frac{y}{\delta} \left( 1 - \frac{y}{\delta} \right)^3 \quad (3.9)$$

from which it can be shown that the displacement and momentum thicknesses, as defined in Sections 2.3.3 and 2.3.4, are given by

$$\delta^* = \frac{\delta}{120} (36 - \Lambda) \quad (3.10)$$

and

$$\theta = \frac{\delta}{315} \left( 37 - \frac{1}{3} - \frac{5A^2}{144} \right) \quad (3.11)$$

Of recent times a "shape" parameter defined by

$$\lambda = \frac{\theta^2}{\nu} \cdot \frac{dU}{dx} \quad (3.12)$$

has been gaining favour owing to the greater accuracy with which  $\theta$  can be calculated, as compared with  $\delta$  (see Section 2.3).

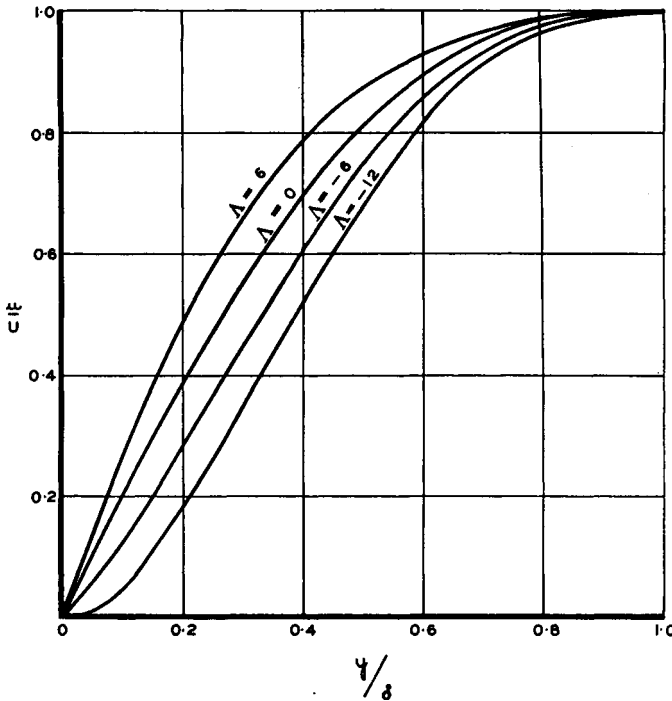


Fig. 3.1. Laminar boundary layer profiles

The growth of the laminar layer can be expressed in the following simple equation due to Thwaites<sup>(5)</sup>:

$$\theta^2 = \frac{0.45\nu}{U^6} \int_0^x U^5 dx \quad (3.13)$$

This integral, which is based on the von Karman relation, eq. (3.5), can be solved graphically.

On account of the inability of a laminar layer to persist far into a region of increasing pressure without separating, it is usually sufficient, for engineering purposes, to assume that separation occurs just downstream of the point where the pressure begins to rise. Hence the use of the above relationships will be limited to positive values of  $\lambda$  and  $A$ ; some useful relations are given graphically in Fig. 3.2.

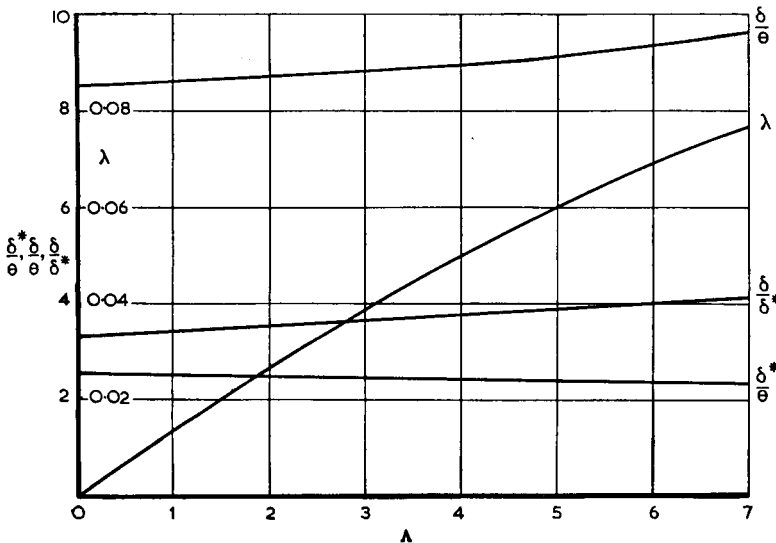


Fig. 3.2. Laminar boundary layer relations

No simple solution is available for an arbitrary three-dimensional flow but for the case of an axisymmetric body, the boundary layer grows<sup>(6)</sup> according to the expression

$$\theta^2 = \frac{0.45\nu}{U^6 r^2} \int_0^x r^2 U^5 dx \quad (3.14)$$

where  $r$  is the local radius and  $x$  is the distance along the surface.

### 3.3. Laminar Skin Friction

There are at least four main simple configurations for which estimates of skin friction are required: two-dimensional flow, fully developed flow in a pipe, initial flow in a pipe prior to

fully developed conditions, and flow over an axisymmetric body. Although small differences are indicated by mathematical studies, these are not sufficient to warrant a separate treatment for each condition.

The shear stress at any point in the boundary layer is given by

$$\tau = \mu \frac{\partial u}{\partial y} \quad (3.15)$$

and hence the surface value, i.e. the skin friction, is

$$\tau_0 = \mu \left( \frac{\partial u}{\partial y} \right)_{y=0} \text{ (lb/ft}^2\text{)} \quad (3.16)$$

From the various two-dimensional boundary layer solutions reviewed by Thwaites,<sup>(5)</sup> it can be shown that for favourable pressure gradients, i.e.  $\lambda$  positive, the parameter,  $T$ , defined as

$$T = \left( \frac{\partial u}{\partial y} \right)_{y=0} \cdot \frac{\theta}{U} \quad (3.17)$$

can be approximated by

$$T = 1.3\lambda + 0.23 \quad (3.18)$$

It follows from a rearrangement of eq. (2.13) that

$$c_f = \frac{\tau_0}{\frac{1}{2}\rho U^2} \quad (3.19)$$

and by using eqs. (3.16) to (3.19),

$$c_f = \frac{2.6\lambda + 0.46}{R_\theta}$$

(3.20)

This is the basic skin friction relationship which is here assumed to hold in a universal manner, provided  $\lambda$  is not negative.

**3.3.1. Zero velocity gradients.** For this condition of flow, certain developments are possible. Since  $\lambda$  is zero,

$$c_f = \frac{0.46}{R_\theta} \quad (3.21)$$

$$\frac{\delta}{\theta} = 8.51 \quad (3.22)$$

and hence

$$c_f = \frac{3.92}{R_\delta} \quad (3.23)$$

where

$$R_\delta = \delta U/\nu$$

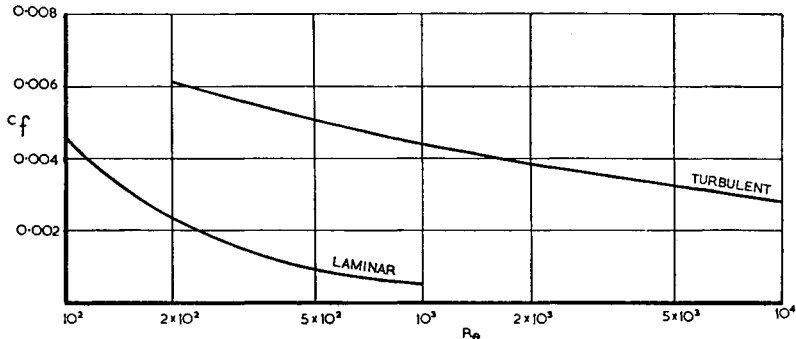


Fig. 3.3. Local skin friction coefficient, zero pressure gradient (eqs. 3.21, 3.42)

(i) *Flow along a two-dimensional flat plate at zero incidence.*  
Integrating eq. (3.13) for  $U = \text{constant}$ ,

$$\theta = 0.671xR_x^{-1/2} \quad (3.24)$$

where

$$R_x = \frac{xU}{\nu}$$

and using eqs. (3.10) and (3.11),

$$\delta^* = 1.71xR_x^{-1/2} \quad (3.25)$$

and

$$\delta = 5.71xR_x^{-1/2} \quad (3.26)$$

Using the relationship between  $\theta$  and  $x$  given in eq. (3.24) and substituting in eq. (3.21),

$c_f = 0.686R_x^{-1/2}$

(3.27)

From eq. (2.16),

$$C_f = \frac{1}{x} \int_0^x 0.686R_x^{-1/2} dx \quad (3.28)$$

therefore,

$$C_f = 1.37 R_x^{-1/2} \quad (3.29)$$

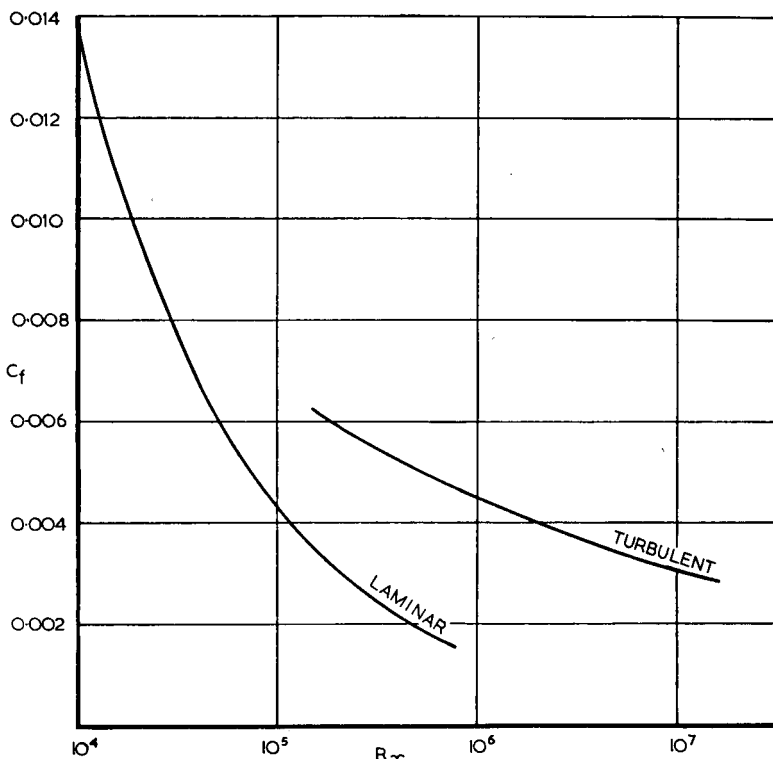


Fig. 3.4. Coefficient of overall skin friction, zero pressure gradient (eqs. 3.29, 3.49)

(ii) *Fully developed flow in a pipe.* In this instance, the velocity at a given radius remains constant along the pipe and the static pressure falls, owing to the viscous losses. At any cross-section, the mean velocity,  $\bar{U}$ , is half the maximum velocity on the axis of the pipe.<sup>(7)</sup> Employing eqs. (3.23) and (3.19) and remembering that  $\delta = d/2$ ,

$$\gamma = \frac{\tau_0}{\frac{1}{2}\rho \bar{U}^2} = 15.7 \left( \frac{\bar{U}d}{\nu} \right)^{-1} \quad (3.30)$$

The constants obtained in eqs. (3.29) and (3.30) for skin friction, namely 1.37 and 15.7, differ from the values 1.33 and 16 obtained by more precise methods. It is believed, however, that these differences are within the order of accuracy required by engineering calculations and hence the use of a single set of universal equations is justified.

**3.3.2. Arbitrary velocity gradients.** For reasons given in Section 3.2, only favourable pressure gradient conditions need be considered. When the distribution of  $U$  with respect to  $x$  is known, the distribution of  $\theta$  can be obtained from eq. (3.13). The variation of  $\lambda$  with  $x$  follows from eq. (3.12) which then permits the computation of the local skin friction coefficients,  $c_f$ , from eq. (3.20).

The total skin friction force is obtained by integrating eq. (2.14), namely,

$$F/\text{unit width} = \frac{1}{2}\rho \int_0^x U^2 c_f \, dx \quad (3.31)$$

This integration can be carried out by simple graphical methods.

### 3.4. Turbulent Boundary Layers

Because of the mathematical difficulties associated with calculating turbulent layer characteristics from the basic equations of motion, most of the formulae available are empirical. There is, however, a marked similarity between the forms of the laminar and turbulent equations and as full a use as possible will be made of this feature.

As in the case of laminar flow, no distinction will be made between flow along a flat plate in a uniform stream and the fully developed flow in a pipe. Research now in progress promises both to disclose the magnitude of the errors inherent in such an assumption and to produce a more refined set of equations suitable for engineering application.

In the case of laminar flow the properties of the layer can, in the presence of a velocity gradient, be expressed in terms of local flow parameters, such as  $A$  and  $\lambda$ . With turbulent flow, however, conditions at a point are definitely influenced by events upstream, e.g., the velocity profile will to some degree be

dependent on the turbulence history of the flow approaching the point in question. Empirical relations, representing averaged conditions, have been formulated on the basis of experimental data.

A widely used parameter in turbulent boundary layer theory is the shape parameter,  $H$ , expressed by

$$H = \frac{\delta^*}{\theta} \quad (3.32)$$

It has been shown experimentally that, for a given value of  $H$ , the boundary layer profile is approximately unique and can be represented<sup>(8)</sup> by an expression of the form

$$\frac{u}{U} = \left( \frac{y}{\delta} \right)^n \quad (3.33)$$

where  $n$  is a function of  $H$  as follows:

$$H = 2n + 1 \quad (3.34)$$

For zero velocity gradient and moderate Reynolds numbers,  $n \approx 1/7$ ; at high Reynolds numbers  $n \approx 1/9$ . With severe adverse pressure gradients,  $n$  increases to a value approaching  $4/5$  at the point of flow separation. The representation given by such a relationship is not particularly accurate in the immediate vicinity of the surface (especially in the case of flows approaching separation), but for the purposes of this book the above expressions are acceptable. A family of boundary layer profiles derived from experimental data<sup>(9)</sup> is illustrated in Fig. 3.5.

When the power law is adopted, the relationships between the boundary layer thicknesses are given by

$$\delta^* = \delta \left( \frac{H-1}{H+1} \right) \quad (3.35)$$

$$\theta = \delta \left[ \frac{H-1}{H(H+1)} \right] \quad (3.36)$$

The growth of the turbulent layer has recently been expressed by Spence<sup>(8)</sup> in the simple relation

$$\theta = \frac{0.0106 R_\theta^{-1/5}}{U^4} \int_{x_i}^x U^4 dx + \text{constant} \quad (3.37)$$

where the constant is  $\theta_i$ , the value of  $\theta$  at  $x_i$ .

For moderate adverse pressure gradients, it is possible to represent the boundary layer growth with the equation<sup>(10)</sup>

$$\frac{\theta}{\theta_i} = \left( \frac{U_i}{U} \right)^{2+G} \quad (3.38)$$

where  $G$  is a function of  $R_\theta$  but has an average value of 2.8.

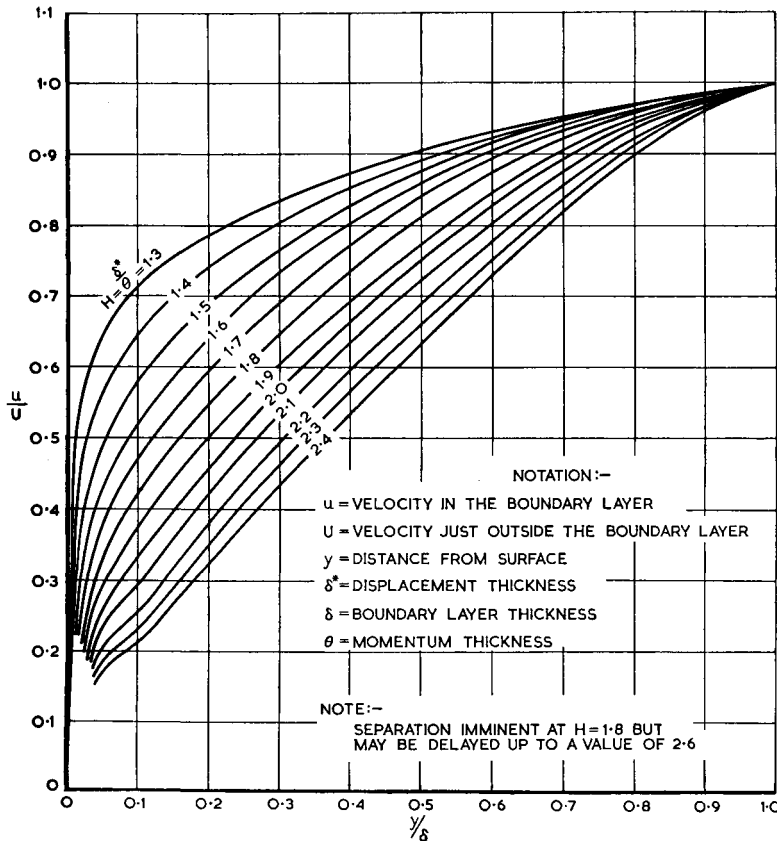


Fig. 3.5. Turbulent boundary layer profiles

In the special case of zero velocity gradient (see eq. (3.7)),

$$\theta = \frac{1}{2} \int_{x_i}^x c_f dx + \theta_i \quad (3.39)$$

When  $c_f$  is known as a function of  $x$ , this expression can be evaluated.

Following a procedure similar to that adopted in Reference 6, it can be shown that eq. (3.37) can, for the axisymmetric case, be written as

$$\theta = \frac{0.0106 R_\theta^{-1/5}}{U^4 r} \int_{x_i}^x U^4 r \, dx + \text{constant} \quad (3.40)$$

### 3.5. Turbulent Skin Friction

Ludwieg and Tillmann<sup>(11)</sup> have shown that turbulent skin friction is a function of the shape parameter,  $H$ , and the Reynolds number,  $R_\theta$ , and they have suggested the relation

$$c_f = 0.246 \times 10^{-0.678H} R_\theta^{-0.268} \quad (3.41)$$

Spence, in developing eq. (3.37), used the expression

$$c_f = 0.01766 R_\theta^{-1/5} \quad (3.42)$$

and found that, in calculating the growth of  $\theta$  with  $x$ , the skin friction can be taken as being independent of  $H$ . Reasons for this seeming contradiction are fully discussed in Reference 8.

It is generally agreed that the variation of skin friction with Reynolds number for the turbulent layer can be very accurately represented on a logarithmic basis. Over moderately wide Reynolds number ranges, however, equally good fits can be obtained with simple power laws; eq. (3.42) is one of a number of such available relations.

In the subsequent developments, eq. (3.42) will be used in a universal manner. The results so obtained, for the various cases of zero pressure gradient, approximate closely to those of Blasius who used a fourth power law.

**3.5.1. Zero velocity gradients.** For this condition it is usually assumed that the power,  $n$ , in eq. (3.33) is given by  $n = 1/7$  and hence,

$$\left. \begin{aligned} H &= \frac{9}{7} \\ \frac{\delta}{\theta} &= \frac{72}{7} \\ \frac{\delta}{\delta^*} &= 8 \end{aligned} \right\} \quad (3.43)$$

and

For fully developed flow in a pipe, the mean velocity,  $\bar{U}$ , is given by

$$\bar{U} = 0.82U \quad (3.44)$$

where  $U$  is the velocity at the centre of the pipe.

(i) *Flow along a two-dimensional flat plate at zero incidence.* Integrating eq. (3.37) for  $U = \text{constant}$ ,

$$\theta = 0.0227xR_x^{-1/6} \quad (3.45)$$

and using the relations in eqs. (3.43),

$$\delta = 0.233xR_x^{-1/6} \quad (3.46)$$

$$\delta^* = 0.0292xR_x^{-1/6} \quad (3.47)$$

Eq. (3.42) can now be rewritten as

$$c_f = 0.0377R_x^{-1/6} \quad (3.48)$$

and, by substituting in eq. (2.16),

$$C_f = 0.0452R_x^{-1/6} \quad (3.49)$$

In developing eqs. (3.45) to (3.49) it is assumed that  $x$  is equal to  $x_e$  (see Section 2.4.3) and hence  $\theta_i$  is zero. When  $R_x$  is large, the difference between  $x_e$  and  $x$  (see Fig. 2.6) will usually be small. Before applying the foregoing equations, it should be established whether the relations are suitable for the task in hand.

(ii) *Fully developed flow in a pipe.* The mean velocity in the pipe and the pipe diameter are usually employed in defining skin friction. From eqs. (3.42) to (3.44), eq. (3.19), and  $\delta = d/2$ ,

$$\gamma = \frac{\tau_0}{\frac{1}{2}\rho \bar{U}^2} = 0.0463 \left( \frac{\bar{U}d}{\nu} \right)^{-1/5} \quad (3.50)$$

### 3.6. Turbulent Boundary Layers in Pressure Gradients

The growth of a turbulent layer in a pressure gradient can be approximately calculated from eq. (3.37) provided there is no

flow separation. The science of predicting flow separation in adverse pressure gradients is, at the present, not an exact one, but a method such as that outlined by Spence<sup>(8)</sup> can be very useful in assessing the deterioration of the layer as it enters a region of rising pressure. Spence's method, like the efforts of other workers, attempts to calculate the distribution of  $H$ , i.e.  $\delta^*/\theta$ , along the surface. The parameter  $H$  increases as flow separation is approached and hence an upper limit is usually set above which flow separation is considered to be imminent. This problem of separation normally takes precedence over that of skin friction and hence accurate estimates of the latter are seldom required.

The reader desiring detailed information is referred to such excellent treatments of this difficult subject as the papers by Spence<sup>(8)</sup> and Coles,<sup>(12)</sup> which also possess extensive bibliographies.

A favourable pressure gradient, such as occurs in a contraction, can lead to a thinning in the turbulent layer. There is in the first place the general contraction of the stream which reduces the boundary layer dimensions. Secondly, there is a large conversion of static pressure into dynamic head. Since there is no variation in static pressure across the duct at entry to the contraction, the conversion will result in a fairly uniform stream at outlet to the contraction. Wind tunnel designers apply this principle in achieving a satisfactory air stream in the working or test section of the tunnel.

### 3.7. Boundary Layer Transition

**3.7.1. General.** Transition is the process which causes a changeover from laminar flow régime to one in which turbulent stresses are predominant. This transformation can be initiated by a variety of circumstances; in no case, however, is the mechanism of transition fully understood.

At very low Reynolds numbers, the viscous forces dominate the boundary layer with the result that turbulent flow cannot exist. If, for instance, turbulence were artificially introduced into such a laminar layer, it would quickly die out under the influence of viscosity.

With increasing Reynolds number, conditions more favourable to the establishment and maintenance of turbulent flow are approached. Beyond a specific Reynolds number, which is a function of flow characteristics, disturbances within the boundary layer grow rapidly as Reynolds number is further increased. The laminar layer is then replaced by a normal turbulent layer and, once this has taken place, additional increases in Reynolds number produce only minor changes in the properties of the turbulent flow within this layer.

The seed of the transition process is an initial disturbance. Since this perturbation need be of only infinitesimal magnitude in the first instance, it can be seen that transition is inevitable in a real fluid at high enough Reynolds numbers.

The most satisfactory Reynolds number which can be used in establishing transition criteria is one based on a boundary layer thickness. For the cases of uniform flow along a flat plate, i.e.  $dU/dx = 0$ , and fully developed laminar flow in a pipe, the following relations exist when eqs. (3.22) and (3.24) are utilized :

$$\left. \begin{aligned} R_\theta &= 0.118 \frac{\bar{U}d}{\nu} \\ R_\theta &= 0.671 R_x^{1/2} \end{aligned} \right\} \quad (3.51)$$

Transition is brought about by one or more of the following circumstances :

- (i) Adverse pressure gradients.
- (ii) Instability with respect to internal flow disturbances.
- (iii) Surface irregularities.

**3.7.2. Adverse pressure gradients.** When the static pressure rises in the direction of flow, the laminar layer rapidly approaches a condition of separation. This occurs when the stream velocity has been reduced to approximately 90 per cent of its value at the start of the diffusion process. The laminar layer leaves the surface and becomes a "free" layer. Except for small Reynolds numbers, transition occurs in the "free" layer ; this may be followed by a re-attachment of the flow to the surface provided the downstream static pressure gradient is not excessively adverse.

The position of laminar separation is independent of Reynolds number but increasing Reynolds number speeds up transition, thus facilitating flow re-attachment. The losses involved in this transition phenomenon are a function of the size of the separated region and may be considerable. For this reason, "trip" wires are often used upstream of a possible danger region in order to ensure that the flow is turbulent at the commencement of diffusion.

**3.7.3. Boundary layer instabilities.** This subject is a very complex one and hence only the salient features will be outlined here. *Large disturbances* in the flow constitute one of the main causes of transition. It is believed that the instantaneous velocity at a point near the surface approaches zero when the component due to the disturbance has a large enough negative value. In other words transition is believed to be related to intermittent separation. Industrial installations contain many disturbance sources and hence information on this aspect is very appropriate. Table 3.1 illustrates the dependence of transition on the free stream turbulence, denoted by  $u'$ , which is the root mean square of the longitudinal fluctuations just outside the boundary layer.

Table 3.1

Ref.	Turbulence level	Values at transition		
		$R_\theta$	$R_x$	$\frac{\bar{U}d}{\nu}$
13	$\frac{u'}{\bar{U}} = 0.03$	210	$1.0 \times 10^5$	1,800
13	$\frac{u'}{\bar{U}} = 0.005$	700	$1.1 \times 10^6$	5,900
3	Very low	5900	$7.7 \times 10^7$	50,000

Some of these values have been derived with the aid of the relations given in eq. (3.51).

From these figures it will be seen that Reynolds' result of

$$\frac{\bar{U}d}{\nu} = 2000$$

corresponds to a moderately high level of turbulence. Provided the flow along a smooth surface is reasonably uniform and steady, laminar flow will almost certainly exist for  $R_\theta < 200$ .

Transition can also stem from a tendency of the viscous forces to amplify infinitesimally *small disturbances* within the flow. The Reynolds number below which disturbances are damped is a function of pressure gradient; the more favourable the pressure gradient, the larger the value. For zero pressure gradient conditions the value is approximately

$$R_\theta \approx 210$$

Transition depends on the initial magnitude of the disturbance and the rate at which it is amplified. The transition Reynolds number will therefore be greater than the value 210.

The last type of instability is a dynamic one and is found where pronounced curvature of the streamlines is experienced. Broadly speaking, the centrifugal force then acting on the boundary layer particles is a function of the velocity distribution and the radii of curvature.

When the surface is concave, an out-of-balance between centrifugal, pressure and viscous forces can promote the growth of a flow disturbance. Instability sets in at a Reynolds number which is a function of surface curvature. Liepmann<sup>(14)</sup> has shown experimentally that the function

$$\left[ R_\theta \sqrt{\frac{\theta}{r}} \right]_{\text{transition}}$$

where  $r$  = radius of curvature, is for most practical purposes dependent only on free stream turbulence; the values of this parameter vary between 9.5 and 6 over the range  $u'/U = 0.0006$  to 0.003. Convex surfaces tend to be stabilizing and are usually treated as flat surfaces in predicting transition.

When the above data are being used for the purpose of assessing the onset of instability, care should be taken to ensure that local laminar separations are avoided. For example, a badly aligned sharp edged flat plate will have a leading edge separation which will invalidate the use of information involving  $R_x$ .

A warning should be noted concerning the improper use of  $\bar{U}d/\nu$  data. For example, transition in a pipe entry possessing

laminar flow initially can be estimated only from  $R_\theta$  or  $R_x$  data; the Reynolds number  $\bar{U}d/\nu$  has no real meaning except where the flow is fully developed.

**3.7.4. Surface irregularities.** When a foreign body is attached to a surface, transition can be accelerated. These bodies usually cause a laminar separation in their vicinity which has the dual effect of increasing the thickness of the downstream layer and introducing large flow disturbances into this layer. Transition, when precipitated, usually occurs close to the excrescence; downstream of "pimples" and the like, transition spreads in a cross flow direction resulting in a turbulent wedge of approximately  $14^\circ$  included angle.

In the following sub-section, quantitative data on critical roughness heights is outlined; it will be seen that surface irregularities play a very important part in transition problems.

### 3.8. Surface Roughness in Laminar Boundary Layers

The main interest in roughness in relation to laminar flow conditions is centred around its effect on transition. If the roughness height for a given Reynolds number is less than the critical value, the disturbance dies out and no noticeable effects on skin friction or boundary layer thickness occur. When the critical height is reached, transition is initiated and hence the skin friction is increased owing to the presence of a turbulent layer. Heights greater than the critical progressively increase the losses by reason of the increased thickness of the initial turbulent boundary layer.

In the last few years, improved methods for predicting the effect of surface roughness have been evolved. Simple relations are presented in Fig. 3.6 for two common types of irregularity.<sup>(15)</sup> The first is similar to sand particles and the second is in popular use as a "tripping" device.

It was found experimentally that these curves, which were obtained from tests on isolated roughnesses, could also be applied to arrangements of sparsely distributed roughnesses; transition sets in at a Reynolds number determined by the most critical irregularity.<sup>(15)</sup>

The curves suggest that the boundary layer is insensitive to

roughnesses which are less than 0.1 of the boundary layer thickness, provided  $R_\theta$  does not exceed 600. At the high Reynolds numbers, however, transition will probably occur owing to other causes.

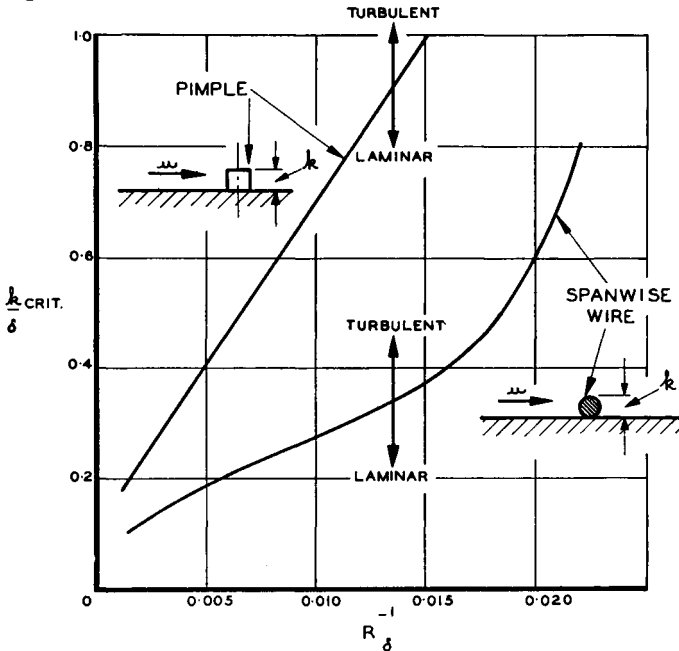


Fig. 3.6. Critical roughness height for laminar flow

In Section 3.7.3, it appeared that viscous damping would prohibit transition for  $R_\theta < 200$ . When roughness is present, however, this value is considerably reduced, owing in no small measure to the thickening effect of the local separation produced by the irregularity. For a grain height of one boundary layer thickness transition will occur at

$$R_\delta \approx 670, \text{ i.e. } R_\theta \approx 80$$

For still greater heights the Reynolds number will drop to

$$R_\theta \approx 50$$

This aspect of the transition problem is thus paramount when appreciable roughness is present.

The thickness of the boundary layer at the position of the

disturbance can be calculated from eqs. (3.13) and (3.11) or from eq. (3.26) for  $dU/dx = 0$ .

### 3.9. Surface Roughness in Turbulent Boundary Layers

**3.9.1. General.** A surface is "aerodynamically smooth" when the roughness height does not exceed the thickness of the "laminar sub-layer". Viscous forces are predominant in this sub-layer, which is that part of the turbulent boundary layer in the immediate vicinity of the surface. The laminar sub-layer has a thickness which is given approximately by<sup>(16)</sup>

$$\delta_s = \frac{4\nu}{\sqrt{(\tau_0/\rho)}} \quad (3.52)$$

The type of roughness encountered in practice rarely shows uniformity of height or shape and hence it is difficult, from uniform sand roughness test data, to assess the overall increase in skin friction. Roughness density, too, can play an important part; an increase in "population" may not always lead to an increase in skin friction.<sup>(17)</sup> It is fairly obvious, therefore, that test data relating to the actual surface are most desirable. The finished products of certain manufacturing processes often possess a similarity in their surface condition. Hence test results from representative specimens of these products can provide useful data in estimating skin friction. Nevertheless, care must always be exercised when applying this information since, for example, cast steel produced by one foundry may have a surface significantly different from that produced by another.

With increasing roughness height, a stage is reached where the eddies produced by the roughness elements virtually control the fluid losses occurring in the boundary layer. Viscous stresses become unimportant and the skin friction in consequence is independent of Reynolds number; the surface is then considered to be "fully rough."

An "equivalent roughness height" can now be defined for surfaces possessing non-uniform roughness. It is the height of a uniform sand roughness which will give the surface a similar skin friction to that experienced by the non-uniform specimen, both being for fully rough conditions.

**3.9.2. Smooth and fully rough limits.** These will naturally be a function of the non-uniformity in roughness height on a given surface. This information is not available in most cases and parameters which are a function of the equivalent roughness height,  $k$ , must be adopted. Averaging out the results of numerous tests gives these approximate relationships<sup>(18)</sup>:

(a) Aerodynamically smooth,

$$\frac{k\sqrt{(\tau_0/\rho)}}{\nu} < 3 \quad \left. \right\}$$

(b) Fully rough,

$$\frac{k\sqrt{(\tau_0/\rho)}}{\nu} > 60 \quad \left. \right\}$$

(3.53)

For values between 3 and 60, the skin friction is a function of both Reynolds number and roughness distribution. In this transitional region between smooth and fully rough conditions, the equivalent roughness rule tends to be inaccurate when the individual heights of the roughness present vary by an appreciable amount. Hence experimental data for a similar class of surface roughness must be available before skin friction on the actual specimen can be assessed accurately in this range.

**3.9.3. Roughness in pipes with fully developed flow.** The skin friction for flow along a smooth surface is obtained from eq. (3.50); when substitution is made in eq. (3.53), the Reynolds number above which a certain roughness size has an influence can be calculated from

$$\frac{k}{d} \approx 20 \left( \frac{\bar{U}d}{\nu} \right)^{-0.9} \quad (3.54)$$

When the surface is fully rough, the skin friction can be expressed empirically by<sup>(16)</sup>

$$\gamma^{-1/2} = \sqrt{\frac{\frac{1}{2}\rho \bar{U}^2}{\tau_0}} = 3.46 + 4.00 \log_{10} \frac{d}{2k} \quad (3.55)$$

Substituting in eq. (3.53), the relation between roughness height and the Reynolds number above which the surface is fully rough is given by

$$\frac{k}{d} \approx 85 \left( \frac{\bar{U}d}{\nu} \right)^{-1} \left( 3.46 + 4.00 \log_{10} \frac{d}{2k} \right) \quad (3.56)$$

Eqs. (3.54) and (3.56) are graphically presented in Fig. 3.7; the various régimes are indicated.

Using the foregoing data, the skin friction coefficient,  $\gamma$ , has been presented as a function of Reynolds number and equivalent roughness height in Fig. 3.8. The transitional curves are completely arbitrary, especially at the lower Reynolds numbers where they may join either the laminar or turbulent skin friction curves for smooth surfaces. In Section 3.8 it was suggested that roughness heights less than  $0.1\delta$  were unlikely

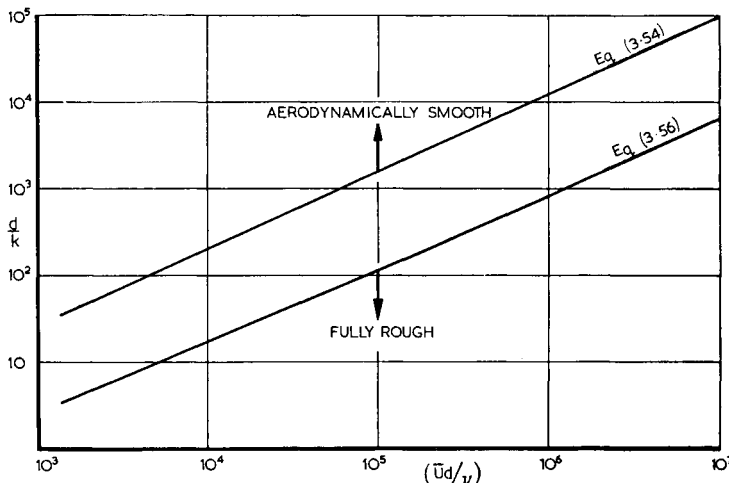


Fig. 3.7. Smooth and rough limits as function of Reynolds number

to cause transition in the laminar layer. For fully developed pipe flow this is equivalent to  $d/k = 20$ . Since all the roughnesses displayed on Fig. 3.8 are of smaller magnitude, it will be seen that the flow over a "smooth" surface can, for

$$\frac{\bar{U}d}{\nu} > 2000$$

be either laminar or turbulent. The dotted curve illustrates the type of transitional curve which might be expected when laminar boundary layer transition is a relevant factor. The data of Fig. 3.8 have been cross-plotted in Fig. 3.9 for the case of fully rough conditions, which of course eliminates Reynolds number as a variable.

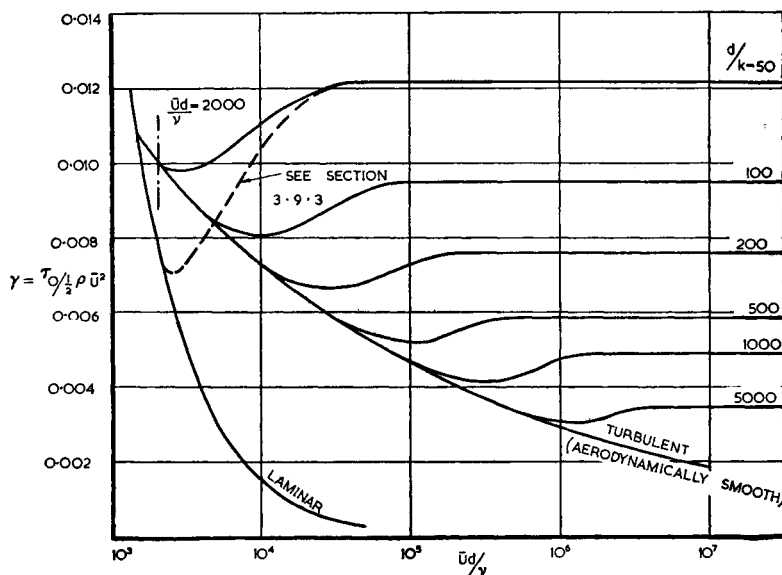


Fig. 3.8. Skin friction in a pipe

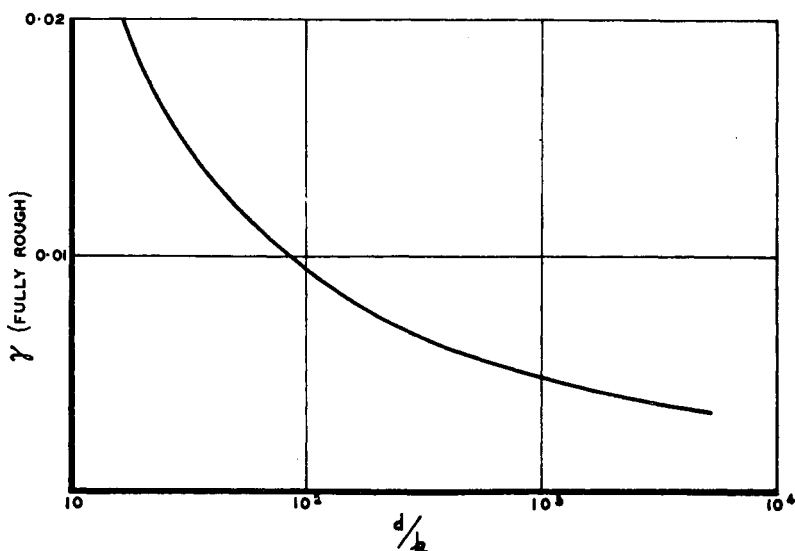


Fig. 3.9. Pipe skin friction for fully rough conditions

**3.9.4. Roughness on flat plates and aerofoils.** A flat plate in a zero pressure gradient has, for fully rough conditions, a skin friction given by<sup>(17)</sup>

$$c_f = \left( 2.87 + 1.58 \log_{10} \frac{x}{k} \right)^{-2.5} \quad (3.57)$$

With a similar procedure to that followed in the previous sub-section, the expression for smooth and fully rough limits is as follows:

$$\frac{k}{x} \approx 22 R_x^{-11/12} \quad (3.58)$$

$$\frac{k}{x} \approx 85 R_x^{-1} \left( 2.87 + 1.58 \log_{10} \frac{x}{k} \right)^{1.25} \quad (3.59)$$

with the usual reminder that  $x$  has been assumed to be approximately equal to  $x_e$ .

The roughness level on aerofoils can usually be kept very small and fully rough conditions are seldom experienced. Owing to the presence of adverse pressure gradients and other variables the effect of roughness on drag can best be determined by experiment on the actual aerofoil or a model of it. By combining eqs. (3.42) and (3.53), however, the following is obtained

$$\frac{k}{\theta} \approx 32 R_\theta^{-0.9} \quad (3.60)$$

as the roughness limit for aerodynamic smoothness.

On fan blades, an increase in drag causes a decrease in efficiency and a possible early onset of the stall; the latter restricts the maximum lift which the blade can supply. If the blades were very rough, as the result of rough casting or the presence of mud, the fan characteristic might be affected owing to a reduced deflection of the stream. An explanation of this feature can be found in the large increase of the boundary layer thickness.

**3.9.5. Effect of roughness in adverse pressure gradients.** There are no quantitative data available on the effect of roughness on skin friction and flow separation in an adverse gradient and here generalities must suffice.

In adverse gradients, roughness usually increases the tendency towards separation. This is due to the greater skin friction losses and hence increased boundary layer thickness.

It has been shown,<sup>(19)</sup> however, that coarse roughness can be used as a means of increasing the mixing rate of the turbulent layer in wide-angle diffusers with the result that separation is prevented. The total head losses associated with the roughness are usually high.

# 4

---

## AEROFOIL DATA FOR BLADE DESIGN

Some reference has already been made to aerofoils, but in this Section the emphasis will be on the main features of aerofoils as they affect fan design and testing.

### 4.1. Definitions

(i) *Aerofoil.* An aerofoil is a lifting surface which, when placed in an airstream, produces a lift force at least 10 times greater than the profile drag force. A flat plate barely qualifies under the above definition.

(ii) *Chord.* The length of the straight line which joins the extreme leading and trailing edges of the aerofoil in a stream-wise direction is known as the aerofoil chord.

(iii) *Span.* The span is the length of the aerofoil in a direction perpendicular to the chord line.

(iv) *Aspect ratio.* The ratio, span/mean chord, is known as the aspect ratio of a wing.

(v) *Incidence.* Incidence is the angle which the oncoming air stream makes with some aerofoil reference line; this line may be the chord line, the flat undersurface of a certain class of aerofoil or any other suitable reference plane provided it is clearly specified.

(vi) *Two-dimensional aerofoils.* For an aerofoil of constant

chord and infinite span, there is no spanwise variation in flow conditions and hence the air flow characteristics can be expressed in terms of two dimensions only.

(vii) *Three-dimensional aerofoils.* The simplest example of a three-dimensional aerofoil is an aircraft wing. As the tip is approached there is a progressive change in lift with which is associated a trailing vortex system. Flow characteristics are now a function of all three dimensions.

(viii) *Free or isolated aerofoils.* The name given to vanes or blades which occur singly or are separated from each other by a distance sufficient to prevent mutual interference.

(ix) *Aerofoils in cascade.* As the perpendicular distance between adjacent blades is decreased, there is an increasing mutual interference between the flow field around one aerofoil and that around the other. The aerofoils are then said to be in cascade.

## 4.2. Types of Aerofoil Section

An orthodox aerofoil may conveniently be considered as a mean line on which is superimposed some thickness form such as a streamlined shape. In the case of a flat plate or cambered plate, the thickness remains constant along the chord except near the leading and trailing edges, where suitable local shaping is often carried out.

When the mean line is straight, the aerofoil is a symmetrical one; with the exception of a certain type of stator blade, such aerofoils are rarely encountered in fan design. By introducing camber into the mean line, greater working loads can be obtained from the blades.

The camber line employed may be of a completely arbitrary shape but circular or parabolic arcs are often used. In the latter case, the curvature decreases as the trailing edge is approached.

The streamlined form with which the camber line is "clothed" is a function of

- (a)  $t/c$
- (b)  $x_{t/c}/c$
- (c) leading edge radius

where  $t$  is the maximum thickness of the section normal to the camber line,  $c$  the aerofoil chord and  $x_{t/c}$  the distance from the leading edge to the point of maximum thickness. The contour over the forward part of the aerofoil is usually of an elliptical nature while aft of the point of maximum thickness the curvatures are small with this portion of the aerofoil resembling a wedge. Small leading edge radii produce large local flow accelerations when the aerofoil is at workable incidences and the subsequent retardations downstream of the leading edge can lead to boundary layer separation from the aerofoil nose. Most aerofoil sections suitable for fan blades possess a moderately large leading edge radius but constant thickness aerofoils such as cambered plates are, of course, an exception. The efficient working range of fans employing cambered plate blades is limited by local flow separations of the type just discussed.

There are in existence numerous families of aerofoils which have been developed with some specific aim in mind. Since, however, the blading requirements of low pressure rise fans are not particularly strict it is possible, in design, to standardize on a very limited number of types; manufacturing expediency plays an important role in the actual choice.

In axial compressor design, however, design methods are being evolved which may lead to a special aerofoil type for each machine, with the aim of increasing the working efficiency to the limit and providing a deterrent to compressor surging.

The method of design here recommended for high pressure rise fans consists in using a standard streamline shape with which circular arcs of designed camber are "clothed."

### 4.3. Lift

An aerofoil at zero incidence constitutes an obstruction in a stream of air and hence local speeding up of the air takes place. With increasing incidence the velocity at any point on the top surface is progressively increased, while, in general, the reverse is true on the lower surface. These velocity changes give, according to Bernoulli's equation, decreasing and increasing static pressures on the top and lower surfaces respectively. The difference in pressure between the two surfaces governs the lifting force acting on the aerofoil.

When the pressure forces are integrated over the entire aerofoil, one force normal to the chord line and one parallel to it are obtained. Resolution of these forces in directions normal and parallel to the oncoming stream gives the lift and drag forces respectively.

The non-dimensional lift coefficient,  $C_L$ , has been previously defined in Section 2.4.3 as

$$C_L = \frac{L}{\frac{1}{2}\rho U_0^2 A}$$

where  $C_L$  is a function of aerofoil incidence and Reynolds number.

There is a limit to the amount of lift which can be obtained by increasing aerofoil incidence. The angle at which maximum lift is obtained is known as the stalling incidence; this phenomenon is further discussed in Section 4.5.1.

#### 4.4. Pitching Moment

The locality in which the resultant lift force acts is generally between the 25 per cent and 50 per cent chord positions, depending largely on the amount of camber in the aerofoil employed. This force produces a turning moment which is usually presented as a moment about the 25 per cent chord line, namely,

$$C_{M_{c/4}} = \frac{\text{P.M.}}{\frac{1}{2}\rho U_0^2 Ac}$$

In fan design, the twisting loads so applied are normally small in comparison with the blade bending loads and the tensile loads due to centrifugal force. Hence, with the exception of flexible blades, pitching moment data can be ignored.

#### 4.5. Drag

The drag associated with a two-dimensional aerofoil is known as profile drag while a three-dimensional wing possesses, in addition, induced or secondary drag.

**4.5.1. Profile drag.** This drag arises from skin friction and pressure forces. The air flowing over the top surface of an

aerofoil is initially accelerated but then suffers retardation as the trailing edge is approached. Owing to the presence of a rapidly growing boundary layer, the rate of diffusion is reduced through the displacement effect of the layer (see Section 2.3.3). As a result, the pressure forces acting on the aerofoil surfaces downstream of the point of maximum thickness are less than they would be if the boundary layer were absent. When resolved along the chord line, the integrated pressure forces upstream of maximum thickness are greater than those downstream and hence there is a resultant downchord component of force. This force gives rise to the pressure drag, towards which the top surface makes the largest contribution.

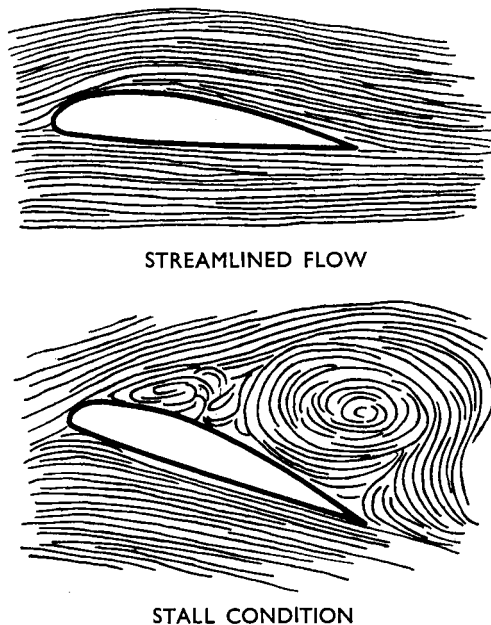


Fig. 4.1. Flow past an aerofoil

With increasing incidence, the adverse pressure gradient on the top surface becomes more severe and the boundary layer thickens; this increases the pressure drag. When boundary layer separation eventually takes place, the static pressure over the rear of the aerofoil is sharply reduced and the pressure drag

rises steeply. This phenomenon of flow separation is directly responsible for the stall, i.e. lift limitation of an aerofoil (see Fig. 4.1).

The skin friction and pressure drags can also be considered as forces arising from the tangential and normal stresses respectively.

**4.5.2. Secondary drag.** On an aerofoil of finite span, e.g. an aircraft wing, the air will tend to flow from the high pressure region on the lower surface around the extreme tip to the low pressure region on the top surface. This phenomenon introduces flows with spanwise components and these combine to form the well-known tip vortex which is present when lift is being obtained from a finite wing. The momentum of this vortex flow passes downstream and is finally dissipated as heat. Vortices are also being shed from the trailing edge along the entire span since conditions at the tip influence the whole flow field. The momentum loss due to this cause is known as the induced drag.

The above vortex flow produces an effective change in the direction of the incident airstream and hence the lift force is inclined backwards at a small angle, thus giving a component in the direction of the drag force. In this way, the momentum losses associated with the secondary flow are experienced by the wing as a pressure force.

Ducted fan installations possess a variety of secondary flows; these are discussed in detail in Sections 5.4.3 and 7.7. In each instance the secondary flows are associated with three-dimensional conditions at the blade extremities and constitute momentum losses which reduce fan efficiency.

## 4.6. Flow Deflection in Cascade of Aerofoils

It is useful to consider the flow-deflecting properties of a cascade of aerofoils as this is an important aspect of rotor or stator blading design. By simple momentum considerations the deflection angles can be related to the lift coefficient acting on the blades. A portion of a cascade possessing an infinite number of aerofoils is presented in Fig. 4.2.

For incompressible, two-dimensional flow, the velocity

component,  $U$ , normal to the cascade must, for continuity reasons, remain constant as shown in Fig. 4.2.

From Fig. 4.2 it will be seen that the velocity component parallel to the cascade has been reduced by the deflecting aerofoils; this reduction involves a rate of change of momentum which is equal to the force acting on the blades in the parallel plane. The force, T.F., per blade is given by

$$\text{T.F.} = \rho s U (U \tan \alpha_1 - U \tan \alpha_2) \quad (4.1)$$

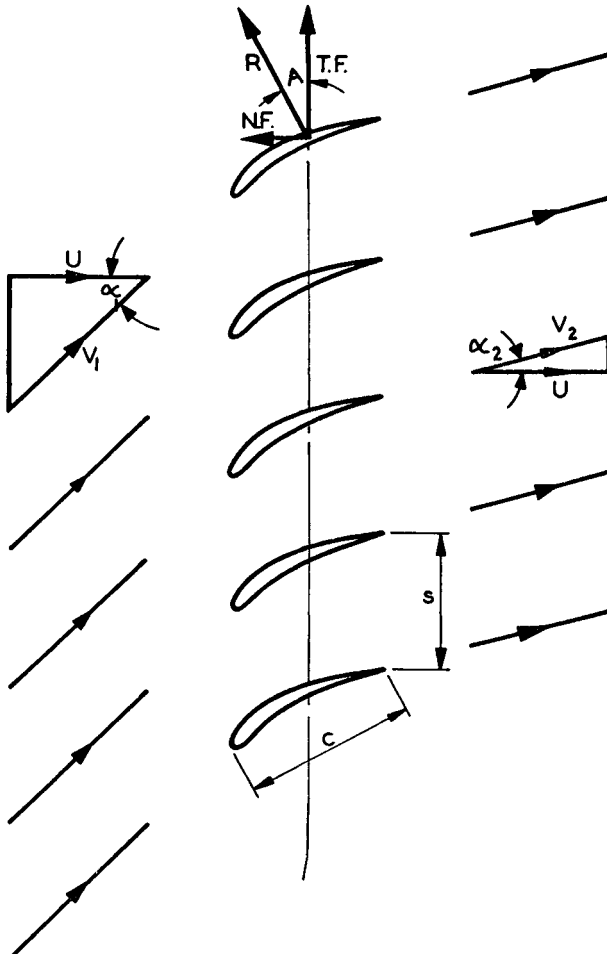


Fig. 4.2. Flow through two-dimensional cascade of aerofoils

Owing to a retardation of the flow from a velocity  $V_1$  to a velocity  $V_2$ , there is, in accordance with Bernoulli's equation, an increase in static pressure which will produce a force normal to the cascade, as shown in Fig. 4.2. Assuming there is no loss in total head through the blade row, the force, N.F., per blade is

$$\begin{aligned} \text{N.F.} &= s(p_2 - p_1) \\ &= s(\frac{1}{2}\rho V_1^2 - \frac{1}{2}\rho V_2^2) \end{aligned} \quad (4.2)$$

It can be shown that the angle by which the resultant force,  $R$ , is inclined back from the line of the cascade is equal to  $\alpha_m$  which is the angle the vector mean of  $V_1$  and  $V_2$  makes with

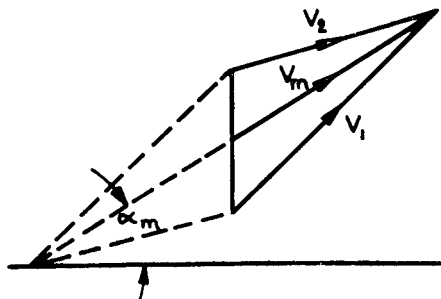


Fig. 4.3. Velocity vectors

the normal to the cascade (see Fig. 4.3). Taking the case of the resultant force, the angle  $A$  is given by

$$\begin{aligned} \tan A &= \frac{\text{N.F.}}{\text{T.F.}} \\ &= \frac{1}{2} \left( \frac{\sec^2 \alpha_1 - \sec^2 \alpha_2}{\tan \alpha_1 - \tan \alpha_2} \right) \\ &= \frac{1}{2} (\tan \alpha_1 + \tan \alpha_2) \end{aligned} \quad (4.3)$$

when  $U \sec \alpha_1$  and  $U \sec \alpha_2$  are substituted for  $V_1$  and  $V_2$  respectively ; this relation is identical to that which follows for  $\tan \alpha_m$  from the geometry of Fig. (4.3).

The foregoing assumption that total head remains constant implies an ideal, non-viscous fluid and hence there is zero drag acting on the aerofoils. The lift force must then be equal to the resultant force and therefore act at right angles to the vector

mean. The lift can then be written

$$L = \frac{1}{2} \rho c C_L V_m^2 \quad (4.4)$$

Taking the component of lift parallel to the cascade and equating to T.F. (eq. (4.1)),

$$C_L = 2 \left( \frac{s}{c} \right) \cos \alpha_m (\tan \alpha_1 - \tan \alpha_2) \quad (4.5)$$

An equivalent equation is developed in Section 8 by a different method.

In developing the above relationship between flow deflection and aerofoil lift, no requirement was set regarding the distance upstream or downstream of the cascade at which uniform conditions, for the purpose of determining  $V_1$  and  $V_2$ , could be assumed. It is generally accepted that, for all practical purposes, the stream approaching the cascade can be considered uniform up to the cascade itself; the same applies to the region downstream of the cascade.

#### 4.7. Flow Deflection in Fan Blading

A stage of rotor or stator blading is fundamentally a circular cascade of aerofoils. Although the amount of flow deflection will usually vary along the span of the blade, conditions at a given radial station can be established from two-dimensional test data for the aerofoil section involved. This independence of a blade section with respect to a neighbouring one on the same blade has long been recognized theoretically<sup>(20)</sup> and experimentally.

Aerofoil characteristics are available in two general classes: isolated or free aerofoil data, and cascade aerofoil data. The first data are, as the name implies, obtained from wind tunnel tests on a single aerofoil whilst the second result from tests on multiple aerofoils installed in a cascade testing tunnel. This leads to two methods of design which are designated here as the "isolated aerofoil method", and the "cascade aerofoil method". The former utilizes lift data in design, while the latter is based mainly on flow deflection information. In view, however, of the relation just established between lift and deflection, this distinction is fundamentally unimportant.

### ISOLATED AEROFOIL DATA

#### 4.8. Isolated Aerofoil Data

The appropriate lift and drag characteristics of single aerofoils of "infinite" span can be determined in a variety of ways. One very popular method<sup>(21)</sup> consists in testing a wing with a span six times the uniform chord dimension. The lift and drag data are finally corrected to infinite aspect ratio by means of well-established equations.

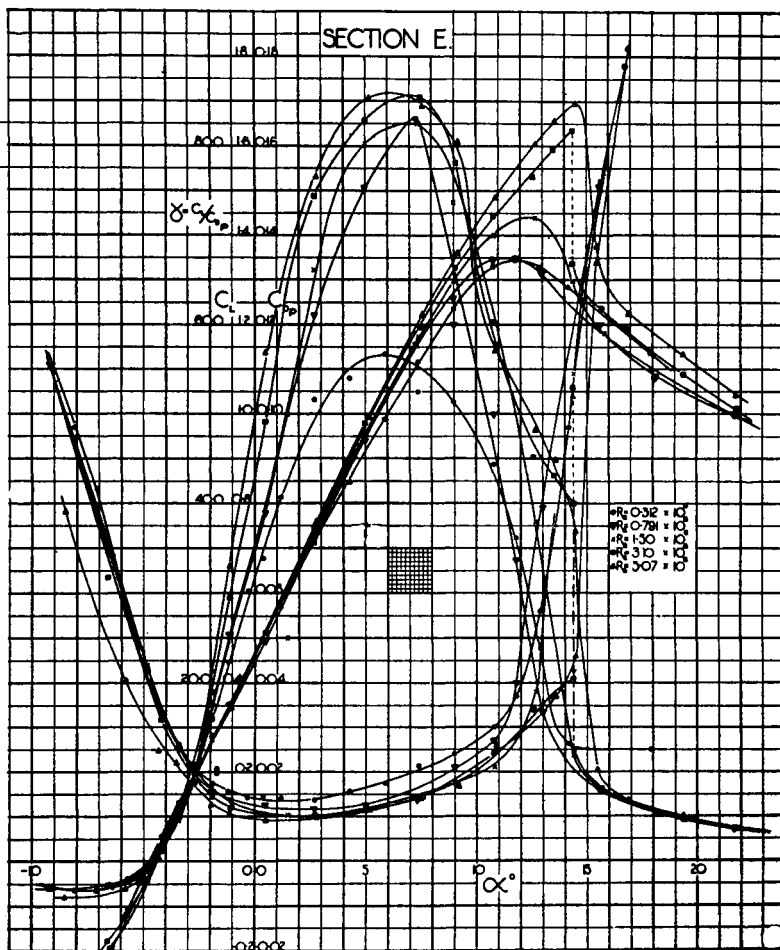


Fig. 4.4. Aerofoil characteristics of RAF 6E section (Reference 22)

## AEROFOIL DATA FOR BLADE DESIGN

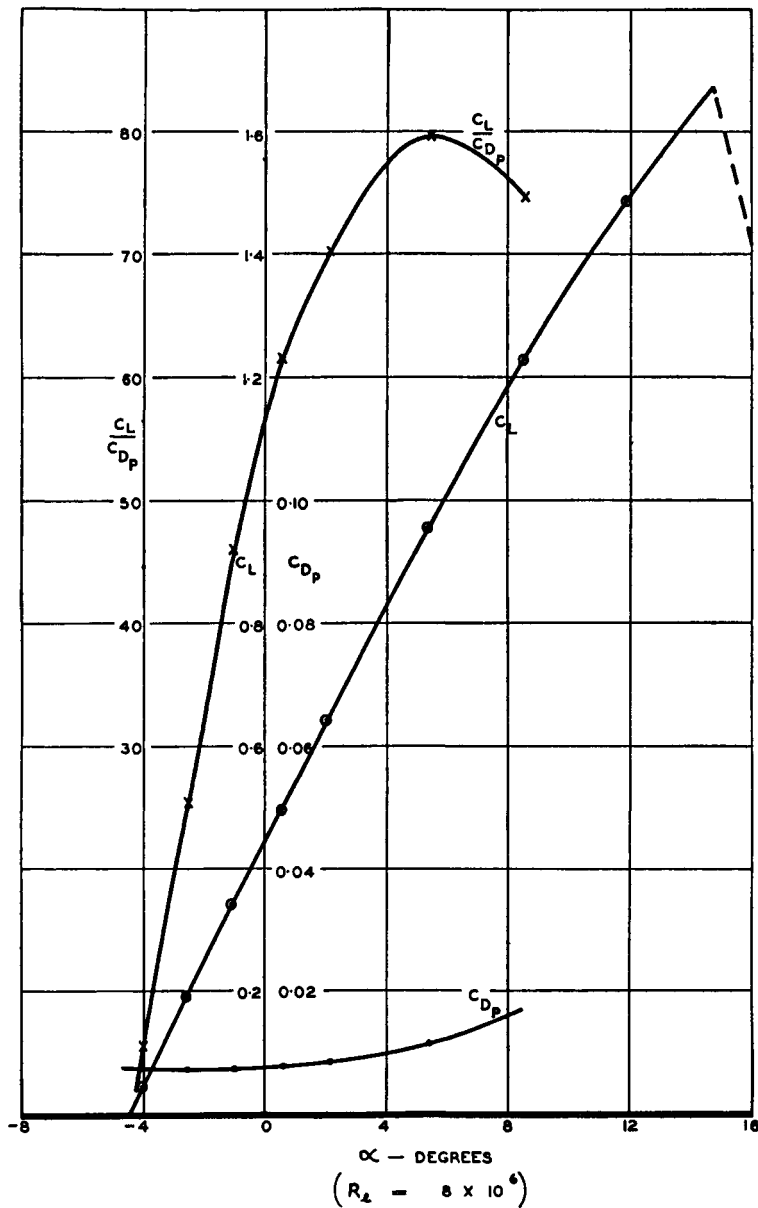


Fig. 4.5. Aerofoil characteristics of 10% thick Clark Y section  
(Reference 23)

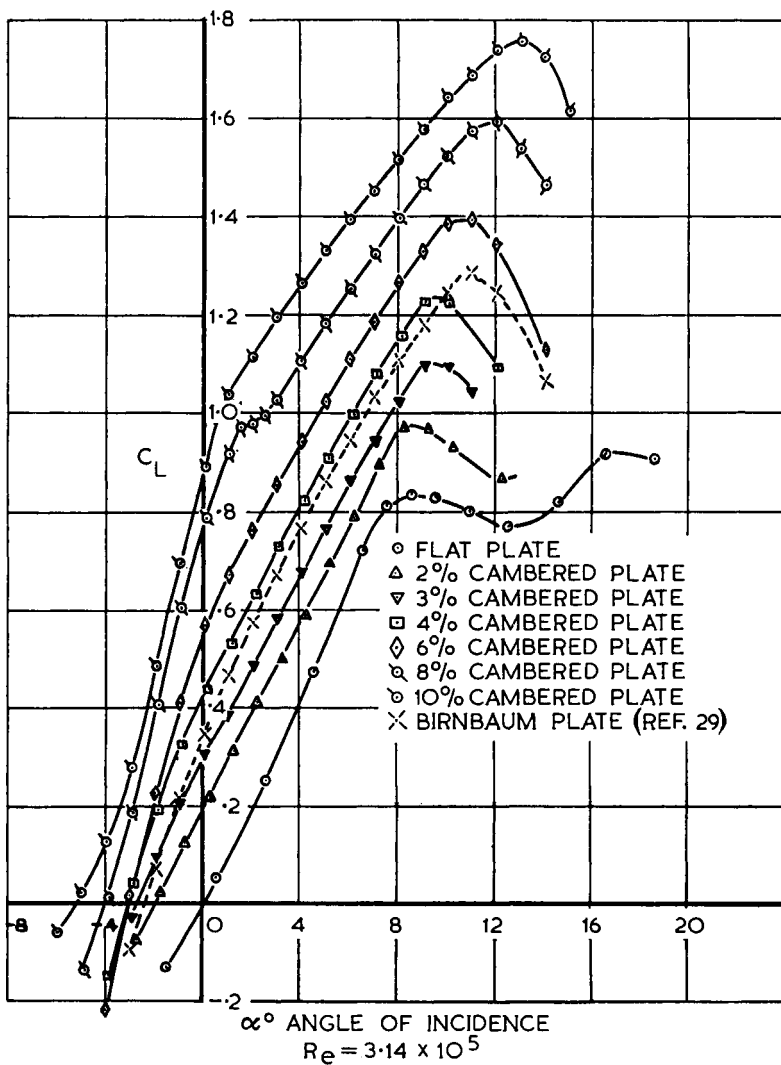


Fig. 4.6. Lift characteristics of cambered plates ( $\frac{t}{c} = 0.02$ ),  $R_e \approx 3 \times 10^5$   
(Reference 24)

In the more modern method of testing, the constant chord aerofoil is mounted between large end plates or, alternatively, the aerofoil is allowed to span the closed working section of the tunnel. Spanwise constancy of lift is thus achieved, in contrast to the previous type of test, where three-dimensional influences, such as tip vortices, cause a spanwise variation in lift.

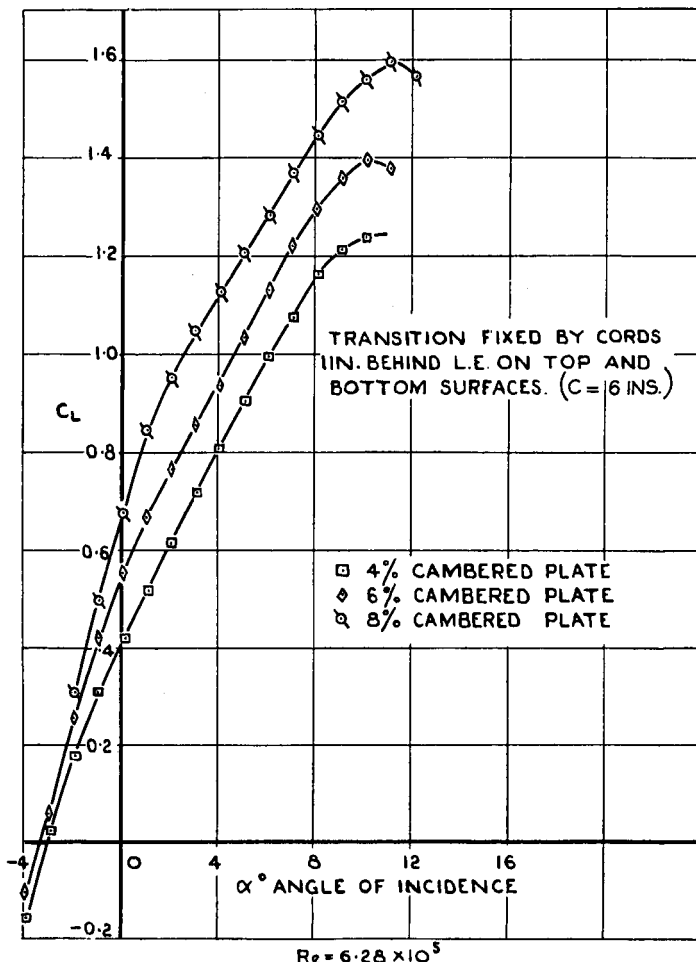


Fig. 4.7. Lift characteristics of cambered plates ( $\frac{t}{c} = 0.02$ ),  $R_e \approx 6 \times 10^5$   
(Reference 24)

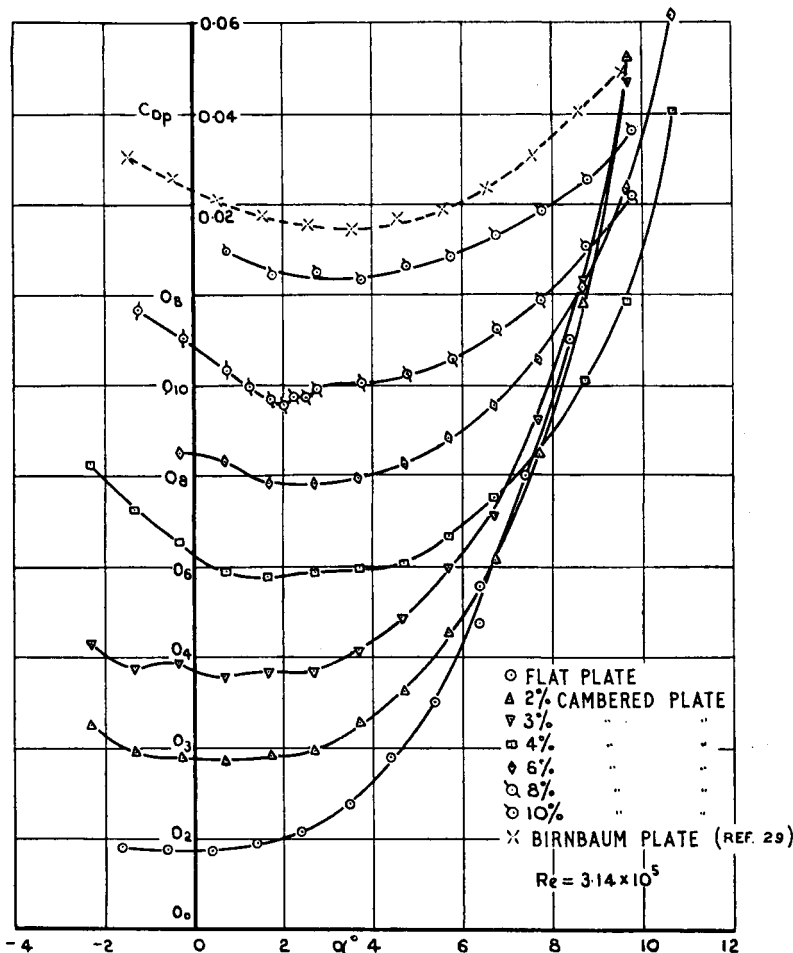


Fig. 4.8. Profile drag characteristics of cambered plates ( $\frac{t}{c} = 0.02$ ),  
 $R_e \approx 3 \times 10^5$  (Reference 24)

(Note zero lines are staggered so as to separate the curves)

After suitable corrections have been made for the influence of the test rig and tunnel constraint, the data are <sup>(22-24)</sup> presented as in Figs. 4.4 to 4.11. The three types of aerofoil sections (see Fig. 4.12) to which these data belong are very popular with fan designers and fulfil most needs.

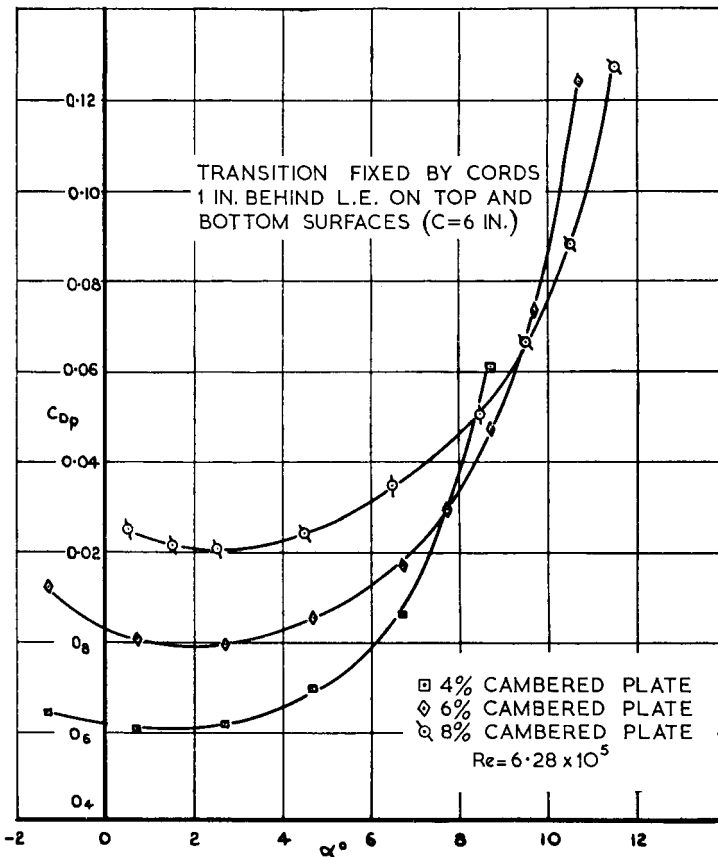


Fig. 4.9. Profile drag characteristics of cambered plates ( $\frac{t}{c} = 0.02$ ),  
 $R_e \approx 6 \times 10^5$  (Reference 24)

(Note zero lines are staggered so as to separate the curves)

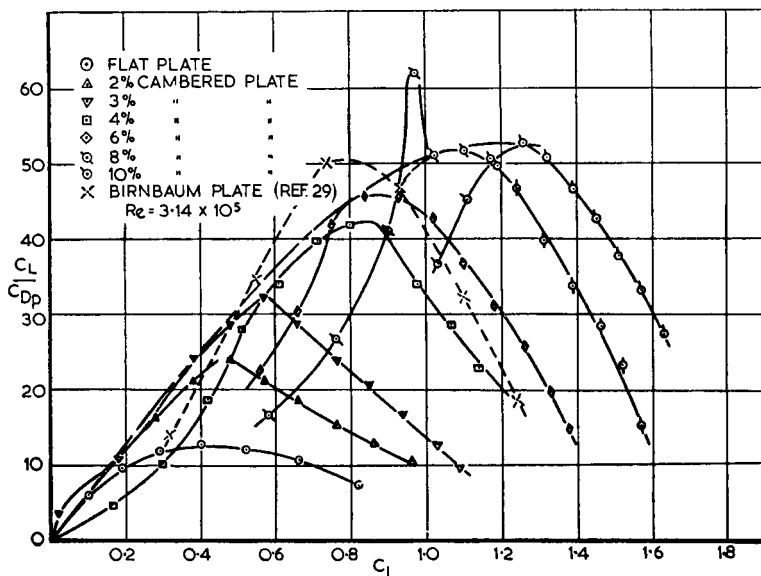


Fig. 4.10. Lift to profile drag ratios of cambered plates ( $\frac{t}{c} = 0.02$ ),  
 $R_e \approx 3 \times 10^5$  (Reference 24)

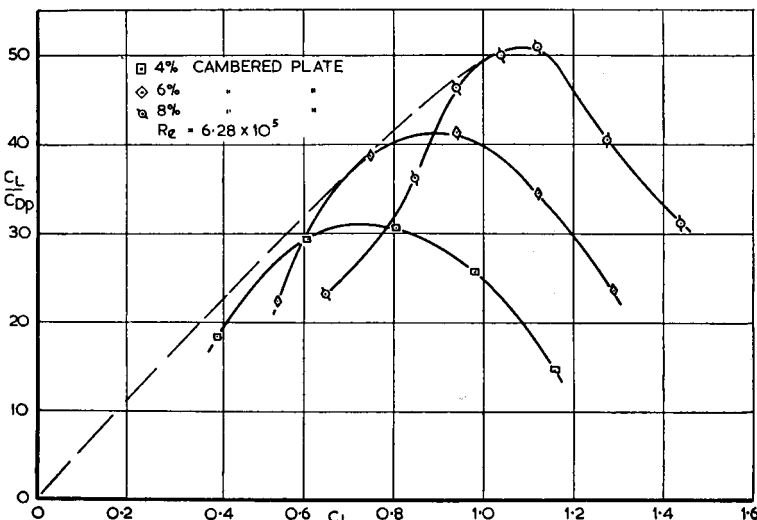


Fig. 4.11. Lift to profile ratios for cambered plates ( $\frac{t}{c} = 0.02$ ),  
 $R_e \approx 6 \times 10^5$  (Reference 24)

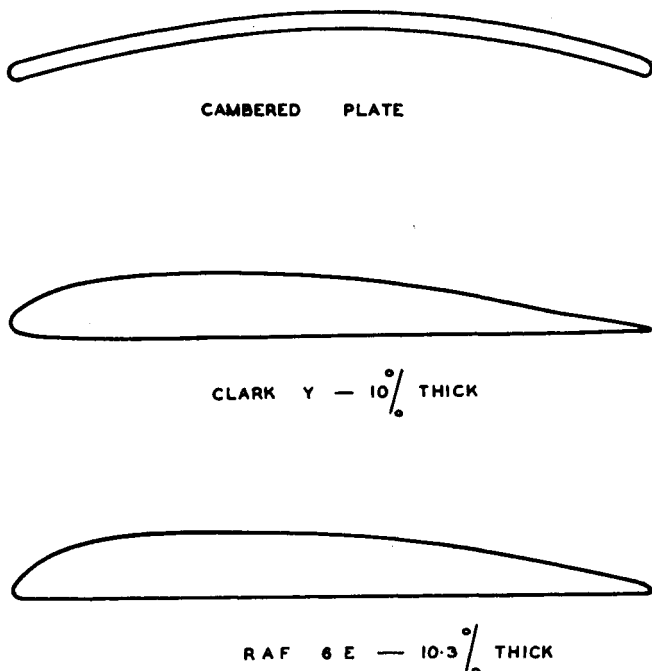


Fig. 4.12. Aerofoil sections suitable for fan design

#### 4.9. Cascade Aerofoil Data

As indicated previously, no direct use is made of the lift coefficient in the cascade method of design. The deflection data used in design are obtained from tests on cascades of deflecting aerofoils spanning the exit of a cascade wind tunnel. Aerofoils of many streamlined shapes and mean camber line contours have been tested in this manner; it was found<sup>(25)</sup> that a combination of the basic streamline shape, C4, with a circular arc camber line produced a very satisfactory blade section. Fig. 4.13 exemplifies how this 10 per cent thick symmetrical aerofoil is "bent" around a predetermined camber line.

The most important feature of the aerofoil is the camber line; flow deflections are, within reason, assumed to be independent of the streamlined shape adopted. A detailed discussion of the deflection data is presented in Section 9.3.

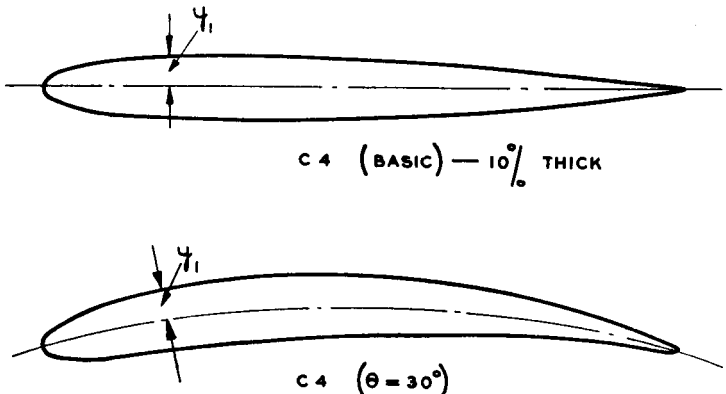


Fig. 4.13. Example of cascade aerofoil design method

#### 4.10. Effect of Reynolds Number on Aerofoil Data

The fundamental significance of Reynolds number has already been outlined in Section 2.4. As mentioned therein, the aerofoil force data are usually presented as functions of the chord Reynolds number.

From the data of Fig. 4.4 it will be seen that the major Reynolds number effects are confined to the high incidence cases, where flow separation is the dominant factor. The variations at lesser incidences can be explained in terms of the boundary layer growth. The decrease in skin friction with increasing Reynolds number produces a thinner boundary layer which reduces the profile drag as shown in Fig. 4.4. Moreover, the displacement effect of the boundary layer (Section 2.3.3) modifies the effective camber of the aerofoil; the thicker the layer on the suction surface, the greater is the loss in effective camber or, in other words, lift at a given incidence.

It is not wise, however, to place too much emphasis on having lift and drag data for the precise fan design Reynolds numbers since the boundary layer growth on an aerofoil is affected by factors such as surface roughness and free stream turbulence for which no exact correction can be made. Fortunately, the lift and drag changes which take place as a result of the above influences are not large enough to cause design difficulties for blades working under normal conditions. For special fans working at very low Reynolds numbers care is necessary as

large scale laminar separations can greatly modify the force data ; this problem is very rare and is therefore ignored in this presentation.

The Clark Y data are available for one Reynolds number only. In view of the similarity between this aerofoil and the RAF 6E, data on the latter can be used as a guide when predicting Reynolds number effects on the former.

Outside a limited incidence range, local flow separations of the type discussed in Section 4.2 occur on flat and cambered plates. As a result, Reynolds number effects are of lesser importance and hence the data given for a chord Reynolds number of  $6.28 \times 10^5$  (Figs. 4.7, 4.9, 4.11) should be representative of the higher Reynolds number cases.

When presenting test data on flow deflection angles and drag coefficients for cascades of aerofoils, it is usual to assume that flow deflection is independent of Reynolds number. An adjustment to the drag coefficient is, however, recommended ; details are presented in Section 10.4.

### 4.11. Wakes

As the flow leaves the trailing edge of an aerofoil at working incidences, the boundary layers from the two surfaces of the aerofoil join to form a wake or region of low velocity. Initially, the gradient of velocity across the wake is very large but as the flow progresses downstream this gradient is rapidly reduced under the influence of turbulent mixing. This process involves a progressive increase in the width of the wake until at an infinite distance downstream a uniform velocity field is again established and hence the wake ceases to exist. Incidentally, the profile drag of an aerofoil can be determined by measuring the momentum deficiency in the wake a little distance downstream of the trailing edge.

When turbulent boundary layer separation is present on the aerofoil, the wake is greatly widened ; the stall is characterized by large unsteady eddying motions (see Fig. 4.1) similar to those which are commonly observed downstream of a pier in a river. This phenomenon is, of course, indicative of a large force to which the aerofoil is subjected, mainly in the form of pressure drag (see Section 4.5).

A knowledge of the wake flow details is not required in fan design. A qualitative understanding is, however, useful when consideration is given to the problems of noise generation, instrumentation of test rigs, and blade vibration.

# 5

---

# VORTEX FLOWS IN DUCTING AND FAN

## 5.1. General

A vortex can be qualitatively described as a circulatory flow about an axis, OZ (see Fig. 5.1). When the fluid has a velocity component in the direction OZ, the air particles trace out helical flow paths.

There are at least two major types of vortices found in fan installations. The first is the general rotation of the entire flow in passing through a blade stage and the second is associated with blade extremity or wall boundary layer effects. These types of vorticity will be referred to hereafter as vortex and secondary flows respectively.

## 5.2. Condition for Radial Equilibrium

In connection with the vortex flow in a fan unit it is of interest to investigate the radial forces acting on the particle, P (Fig. 5.1). The centrifugal force acting radially must be countered by some other force if the particle is to remain at a constant radius with respect to the origin. Radial equilibrium

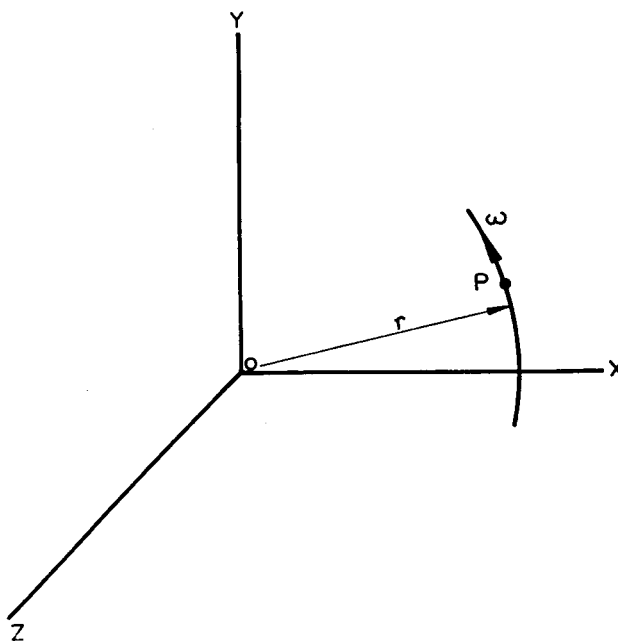


Fig. 5.1. Vortex flow

can be achieved when the pressure forces acting on the particle have an inward component equal to the centrifugal force. The problem is independent of the flow in the OZ direction, in other words, two-dimensional flow conditions can be assumed.

Take an element of fluid at radius,  $r$ , with unit length in the direction OZ, and rotating with angular velocity,  $\omega$ , about the axis OZ (Fig. 5.2).

The centrifugal force acting on the element is

$$\begin{aligned} \text{C.F.} &= \frac{mV^2}{r} \\ &= s \cdot dr \cdot \rho \frac{(\omega r)^2}{r} \end{aligned}$$

and the pressure force

$$\text{P.F.} = dp \cdot s$$

where  $dp$  is the pressure difference between the two faces of the element. Equating the two forces gives

$$\frac{dp}{dr} = \rho\omega^2 r \quad (5.1)$$

which is a universal requirement for radial equilibrium.

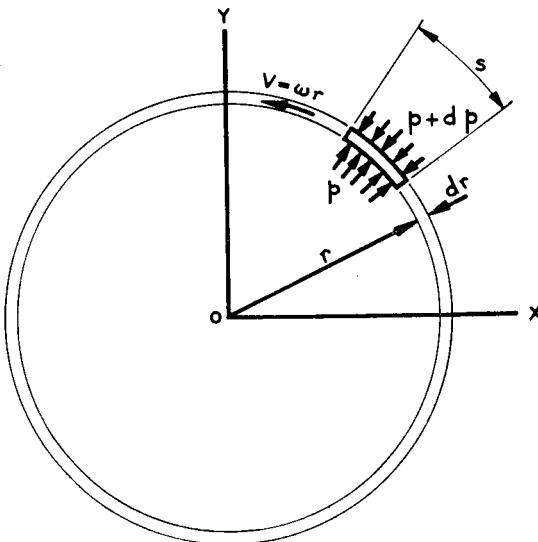


Fig. 5.2. Rotating element

### 5.3. General Relations for Vortex Flow

The term vortex flow is here used in the sense defined at the end of Section 5.1. When the flow has a velocity component along the axis the total head of a particle will be given by

$$H = p + \frac{1}{2}\rho U^2 + \frac{1}{2}\rho(\omega r)^2 \quad (5.2)$$

where  $U$  and  $\omega r$  are the axial and tangential velocity components respectively.

The contribution from the radial velocity component has been omitted on the assumption that it is small or zero.

Differentiating with respect to  $r$ ,

$$\frac{dH}{dr} = \frac{dp}{dr} + \frac{1}{2}\rho \frac{dU^2}{dr} + \frac{1}{2}\rho \frac{d(\omega r)^2}{dr} \quad (5.3)$$

When  $H$  and  $U$  are constant with radius,  $r$ , eq. (5.3) reduces to

$$\frac{dp}{dr} = -\frac{1}{2}\rho \frac{d(\omega r)^2}{dr} \quad (5.4)$$

Combining eqs. (5.1) and (5.4), in order to satisfy radial equilibrium requirements, it can be shown that

$$\omega r^2 = \text{constant} \quad (5.5)$$

i.e.  $\omega r$  is inversely proportional to  $r$ . A vortex flow with the above requirements regarding  $H$ ,  $U$  and  $\omega$  is commonly known as a "free vortex".

This type of flow is the one usually assumed when designing ducted axial flow fans. The greater part of the design theory given in this work utilizes this concept since it permits simple design methods and high fan efficiencies.

Some attention has, however, been devoted to fans which have an arbitrary, tangential velocity distribution of the form

$$\omega r = a + br \quad (5.6)$$

where  $a$  and  $b$  are constants.

Two well-known distributions which follow from this equation are

$$\omega r = a \quad (\text{where } b = 0) \quad (5.7)$$

and

$$\omega r = br \quad (\text{where } a = 0) \quad (5.8)$$

The first, of course, gives constant tangential velocity while the second is known as "solid rotation", so called because in this case the air would rotate as though it were a solid body.

When an arbitrary vortex of the above type is imparted to the air by means of fan blades or vanes, there is a radial displacement of the air particles. It has, however, been found in practice that radial equilibrium is quickly established; the flow then satisfies the equation

$$\frac{dH}{dr} = \rho \omega^2 r + \frac{1}{2}\rho \frac{dU^2}{dr} + \frac{1}{2}\rho \frac{d(\omega r)^2}{dr} \quad (5.9)$$

which is obtained by combining eqs. (5.1) and (5.3). This equation is a key one in developing design methods for fans with arbitrary vortex flow.

## 5.4. Secondary Flows

In Section 4.5.2, the secondary flow associated with finite aerofoils was discussed. Provided the tip clearances are small, this type of secondary flow is not the most important in fan performance. Before discussing secondary flow in fan units, it is instructive to consider the flow through a curved duct.

**5.4.1. Flow in a curved duct.** When air flows around a bend, vortices with streamwise axes are initiated by the side wall boundary layers. In order to establish the principle clearly, three initial assumptions are made: (i) that the duct is rectangular, (ii) that the boundary layers are thin, i.e. that the main body of the flow possesses a constant total head, and (iii) that no flow separation is present.

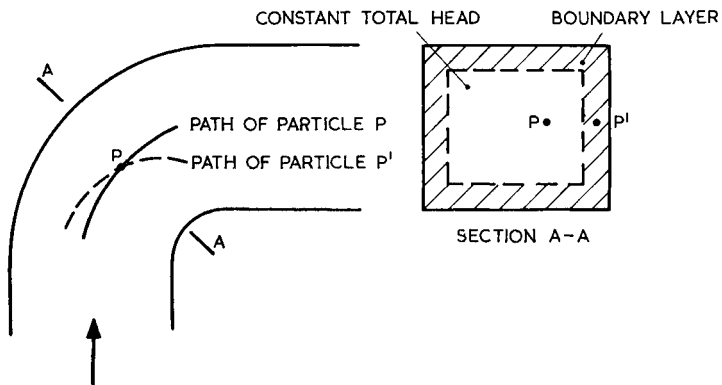


Fig. 5.3. Origin of secondary flow

It can be shown that radial equilibrium exists in any curved two-dimensional flow provided the total head is constant.<sup>(26)</sup> There must therefore be a static pressure gradient in the direction of the centre, O, in order to counter the centrifugal effects on the particle. This static pressure gradient, at a given radius, will remain virtually unchanged right up to side walls of the bend. The slow-moving air in the side-wall boundary layers, however, will not possess sufficient centrifugal force to balance the pressure gradient force imposed by the main stream, and, instead of conditions remaining as in Fig. 5.3, secondary flows, as illustrated in Fig. 5.4, will be created.

If one of the initial conditions is relaxed and the boundary layer assumed to be thick, it is obvious that in this situation the amount of fluid contained in the secondary flow will increase. The interaction of these secondary flows with flow separations in curved ducts will be discussed in Section 6.5.1.

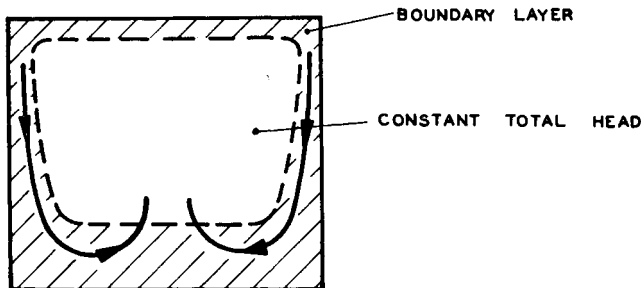


Fig. 5.4. Schematic presentation of actual flow conditions at Section A-A (Fig. 5.3.).

**5.4.2. Flow through a vanned corner.** Turning vanes are frequently fitted to corners as a means of reducing the separation losses. These vanes multiply the number of secondary flows present and reduce their individual magnitude (Fig. 5.5).

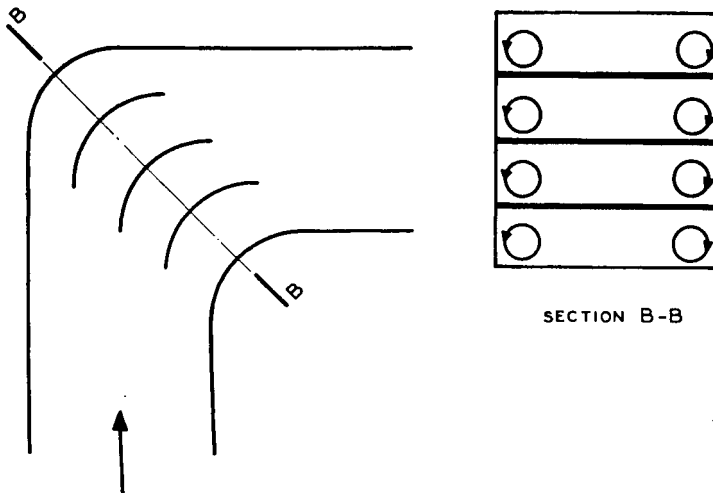


Fig. 5.5. Secondary flows in vaned corner

Hence although vanes are primarily employed as a method of reducing separation losses, their influence on the secondary flow problem is by no means negligible. Further reference to this subject will be made in Section 6.5.8.

**5.4.3. Flow through rotor or stator blades.** The function of a rotor or stator blade is similar to that of turning vanes in a corner. In the first place, the blades produce a deflection of the air, and secondly the extremities of the blades operate in the "wall" boundary layers of both the duct and the fan boss. Hence secondary flows appear on the surfaces of the blades at their extremities.

The axes of these flows will be of a curved, helical nature when main vortex flows of the types discussed in Section 5.3 are present. The complexity of the flow at the rotor blade extremities is further increased by tip clearance effects and by centrifugal influences on the boundary layer particles in contact with the rotating blades.

It is fortunately possible to carry out fan design using only main vortex flow considerations; the required pressure rise for a given fan output can be achieved with very good accuracy.

The problems of accurately analysing and assessing fluid momentum losses are, however, far more difficult and for this reason *ad hoc* methods are normally used in their solution.

# 6

---

## DUCTS

### 6.1. General

**6.1.1. Introduction.** The task of a fan is to increase the total head of the air for the purpose of overcoming all total head losses in a complete duct system. In some instances these losses may be known from experiments conducted before design of the fan commenced, but normally the losses have to be estimated from available data. Very often a specific fan design has to cover a range of operating conditions arising from modifications to the duct system; in estimating the high resistance end of the range it is advisable to work on moderately pessimistic assumptions, as a safeguard against the installation of an overloaded or stalled fan.

In general, the estimation of duct losses cannot be accomplished with anywhere near the degree of accuracy associated with the design of ducted axial flow fans. It will be appreciated therefore that the greatest care should be exercised in assessing the losses. There is in existence a considerable volume of experimental data which can be drawn on for assistance. A comprehensive review of this material is outside the scope of the present work; instead an attempt will be made to outline the important features of duct flow and to indicate the losses occurring in common duct elements.

**6.1.2. Duct components.** Any duct system can be subdivided into a number of elementary components such as:

- (a) Ducts of constant cross-sectional area
- (b) Contractions, of which the inlet is a special case
- (c) Diffusers, with the cross-sectional area increasing in the flow direction

- (d) Corners
- (e) Internal bodies such as obstructions, bracings, fairings, etc.

The above list embraces ducts of all cross-sectional shapes and also ducting whose shape is changing with distance along the duct. When data concerning a specific configuration are not available, an assessment based on equivalent units must be made.

**6.1.3. Definition of duct loss.** A duct loss can be defined as the mean loss of total head sustained by the stream in passing through the specific item of ducting. The losses are due to the following factors :

- (i) *Skin friction.* This parameter determines the losses due to fluid shear stresses, when the boundary layer is attached to the duct walls.
- (ii) *Eddying or separated flow.* These losses have their origin in the random large scale turbulence which rapidly absorbs more and more of the free stream energy as the region of separation rapidly expands.
- (iii) *Secondary flow.* Secondary flows, as defined in Section 5, lead to momentum losses. A portion of the streamwise momentum of the main flow is transferred to the secondary flow and finally dissipated as turbulence and heat.
- (iv) *Discharge losses.* In an open circuit duct system, the dynamic head of the air leaving the system is a loss which the fan must overcome.

The main concern is with the loss of total head in a streamwise direction. When the dynamic head associated with any cross flow is assumed to be small, this loss for a rectangular duct (Fig. 6.1) can be expressed in terms of the total head change as defined by the following relation :

$$\Delta H_1 = \frac{1}{ab} \int_0^a \int_0^b (\frac{1}{2}\rho v_a^2 + p)_A dy dx - \frac{1}{cd} \int_0^c \int_0^d (\frac{1}{2}\rho v_a^2 + p)_B dy dx \quad (6.1)$$

where  $v_a$  is the axial velocity component and  $p$  the static pressure.

When the duct has a circular cross-section, the relevant

equation is

$$\Delta H_1 = \frac{1}{\pi R_A^2} \int_0^{R_A} \int_0^{2\pi} (\frac{1}{2}\rho v_a^2 + p)_A r d\theta dr - \frac{1}{\pi R_B^2} \int_0^{R_B} \int_0^{2\pi} (\frac{1}{2}\rho v_a^2 + p)_B r d\theta dr \quad (6.2)$$

where  $R_A$  and  $R_B$  are the respective radii.

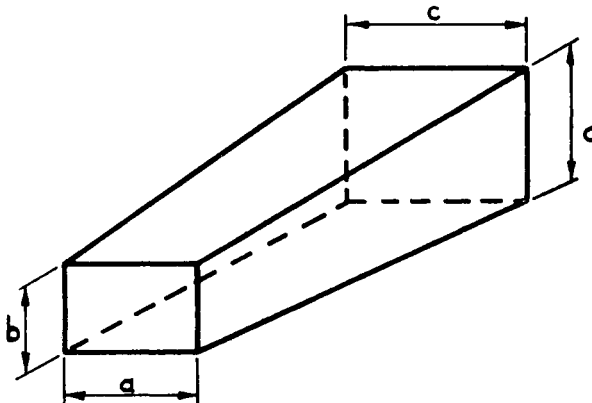


Fig. 6.1. Rectangular duct of changing cross-section

Flow in a straight duct of uniform cross-section, in which fully developed pipe flow is present, represents the simplest example of duct loss. The dynamic head integrations at the two stations are identical and the static pressure is constant throughout each of the two cross-sectional planes. The two expressions given above therefore reduce to

$$\Delta H_1 = p_A - p_B \quad (6.3)$$

When the flow is not fully developed, the pressure drop along the duct is not a true measure of the total head loss; estimates based on eq. (6.3) will, therefore, be only approximations.

In general, very little practical use can be made of eqs. (6.1) and (6.2) in estimating losses, since the distributions of velocity and static pressure at a given cross-section are usually unknown. It is therefore customary to assume that these quantities have a uniform distribution. This leads to the general equation

$$\Delta H_1 = \frac{1}{2} \rho V_A^2 \left[ 1 - \left( \frac{A_A}{A_B} \right)^2 \right] + (p_A - p_B) \quad (6.4)$$

where  $A_A$  and  $A_B$  are the respective cross-sectional areas at the two stations and  $V_A$  the mean velocity at station  $A$ . With a sweeping assumption of this nature, precision in assessing losses in non-uniform or curved ducting cannot be expected.

In this section on ducts the velocity notation used in the preceding sections has been altered. The symbol  $v$  denotes the local velocity at a point while  $V$  is the mean velocity of the air flowing past a given cross-sectional plane in the duct. In other words, the symbol  $\bar{U}$  of Section 3 has been replaced by  $V$ . Since the number of symbols suitable for use in designating velocities is limited, this step was taken in order to avoid confusion when dealing with combined duct and fan problems.

In computing mean values of velocity and total head from experimental data, the methods outlined in Section 22.4.5 may be employed after suitable adaptation.

**6.1.4. Non-dimensional treatment.** When the total head loss in an item of ducting is expressed in terms of some reference dynamic head, the parameter so obtained is a function of Reynolds number, namely,

$$K_1 = \frac{\Delta H_1}{\frac{1}{2} \rho V_A^2} = f(R_e) \quad (6.5)$$

The more fundamental Reynolds number is that based on the boundary layer at entry to the component but, since this is usually an unknown, the parameter

$$R_d = \frac{V_A d}{v}$$

is usually employed.

In general, duct losses are not a very pronounced function of this latter Reynolds number and in fact the small changes which occur are often well within the order of accuracy which can be expected when assessing the losses in a complex duct system. Entry and exit flow conditions from an item of ducting can be of greater importance than the duct Reynolds number just quoted.

**6.1.5. Method of estimating losses in a duct system.** It is usual and convenient to divide a duct system into a number of components (see Section 6.1.2), assess the loss in each component, and finally sum the losses arithmetically.

The measure of total loss so obtained is thus based on the assumption that there is no interaction between component parts. Unfortunately, however, interaction may in many instances grossly increase the total losses in a system. For example, separated flow in a wide-angle diffuser just upstream of a corner can increase the corner losses by a factor of 1 or 2; similarly, increased diffuser losses will occur when the corner is immediately upstream. In tabulating the component losses it is wise to provide a column for a multiplication factor, based on experience, to cover this eventuality.

The total head increase to be provided by the fan is then

$$\Delta H_T = K_1 \frac{1}{2} \rho V_1^2 + K_2 \frac{1}{2} \rho V_2^2 + \cdots + K_n \frac{1}{2} \rho V_n^2 \quad (6.6)$$

Since  $K_T = \Delta H_T / \frac{1}{2} \rho U^2$ , where  $U$  is mean axial velocity through fan annulus,

$$K_T = K_1 \left( \frac{A_f}{A_1} \right)^2 + K_2 \left( \frac{A_f}{A_2} \right)^2 + \cdots + K_n \left( \frac{A_f}{A_n} \right)^2 \quad (6.7)$$

where  $A_f$  is area of annulus swept by rotor blades and the number subscripts refer to specific duct components.

When a duct system consists of two or more branches from which the flows finally enter a common duct, the proportion of flow in each arm must be established on the assumption that the static pressure in the main duct, a little distance from the junction, is constant across the section. Such a system is very similar to an electrical network but, since the resistance is proportional to the square of the volume flow, the problem is less readily solved.

## 6.2. Straight Ducts of Constant Cross-sectional Area

The only loss in cylindrical ducting of this type is that due to skin friction. In square and rectangular ducts, small secondary flows are present in the corners but these can be ignored when assessing losses.

When the amount of straight ducting in a complex duct system is small, the skin friction losses associated with it are often less than the order of accuracy with which the losses in the diffuser or corner components can be estimated. Hence great precision is not required in computing the skin friction losses.

This does not hold good, of course, when the pressure drop along a lengthy pipe line is required.

Most industrial installations are relatively crude from the ultimate aerodynamic point of view. This, in conjunction with the fact that Reynolds numbers are very seldom low, results in the virtual elimination of laminar flow from the system.

**6.2.1. General methods of assessment.** In pipe lines, fully developed turbulent boundary layer flow exists for the major portion of the pipe line length, and hence skin friction data based on

$$R_d = \frac{Vd}{\nu}$$

can be used. When air is sucked into a duct from the surrounding atmosphere there is an initial entry length, prior to the establishment of fully developed flow, which is a very marked function of inlet conditions. The position of the transition point along the pipe is an important variable. With a carefully flared inlet and assuming that for large Reynolds numbers the boundary layer at inlet to the pipe is thin and turbulent, it is computed that fully developed flow should be established at a distance  $0.693dR_d^{1/4}$  downstream.<sup>(27)</sup> For a Reynolds number of  $9 \times 10^5$  the entry length is 21 diameters; an experimental value of 40 has, however, been reported by Nikuradse, at this Reynolds number, for disturbed inlet conditions. Even higher test values have been obtained; the explanation may depend on the length of the laminar flow régime upstream of transition in the pipe. At the other end of the scale, sharp edged unflared inlets will cause local flow separations and thus greatly reduce the entry length, to less than 10 diameters.

It is difficult to predict the entry length for any particular case but the above should provide a guide to the problem.

Downstream of transition, losses in the entry length will be greater than those in an equal length of pipe with fully developed flow. This is due to a smaller value of  $R_\theta$  which implies a higher skin friction. This fact is often ignored owing to the greater simplicity of computing skin friction losses from  $R_d$  data for all pipe flow. On the rare occasions when precision is required, a more refined approach along the lines indicated in Section 3 should be made.

Losses in square or rectangular ducts are assessed from cylindrical pipe data after an equivalent diameter has been established. The hydraulic radii for round and rectangular ducts are  $d/4$  and  $ab/2(a+b)$  respectively. Equating, the equivalent diameter of a rectangular duct is

$$d_{\text{equivalent}} = \frac{2ab}{(a+b)} \quad (6.8)$$

The most convenient method of expressing losses in a pipe is to specify the length to diameter ratio for which the static pressure loss is equal to one velocity head.

**6.2.2. Effect of duct irregularities.** The influence of roughness has been treated in Section 3.9, from which the appropriate increases in skin friction can be estimated.

Additional losses can result from poor jointing; these may reach considerable proportions when insufficient care is taken in fabricating and assembling the duct. Examples of common faults are illustrated in Fig. 6.2.

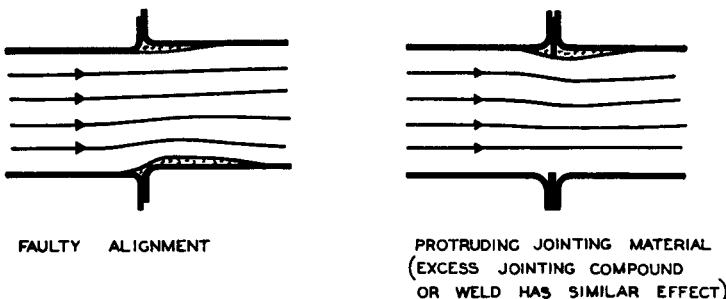


Fig. 6.2. Ducting faults

Leaks should be avoided as they also increase the total head losses. When the pressure inside the duct is higher than the surrounding pressure, air is forced out of the duct. The momentum lost in this manner is reflected in the subsequent diffusion which occurs immediately downstream of the leaking joint or hole; the resulting small static pressure rise increases the back pressure against which the fan is working.

Where there is imperfect sealing, air may issue into the duct when the static pressure inside is less than the external pressure.

This air disturbs the boundary layer, increases the momentum losses in the layer, and results in a static pressure drop. In diffusers and the like, separation may be initiated by the inflowing air. There is also the static pressure drop associated with the increased mass flow. Together they represent an increase in the total head which the fan must transfer to the air.

Ducting with a cross-section which is nominally constant may in practice possess large variations in area. This is particularly true of non-cylindrical ducts where insufficiently stiffened side walls may lead to local contractions and diffusions. In addition, certain forms of panel stiffening may produce surface irregularities on the interior walls. Usually, an increase in duct losses is the result.

**6.2.3. Details of losses.** The total head loss in a length of pipe,  $l$ , is given by

$$\Delta H_1 = \tau_0 A_w / A \quad (6.9)$$

where  $A_w$  and  $A$  are the wetted and cross-sectional areas respectively. Expanding,

$$\Delta H_1 = \frac{\gamma \frac{1}{2} \rho V_1^2 \cdot \pi d l}{\pi d^2 / 4}$$

or,

$$\frac{\Delta H_1}{\frac{1}{2} \rho V_1^2} = \frac{4 \gamma l}{d} \quad (6.10)$$

When  $\Delta H_1 = \frac{1}{2} \rho V_1^2$ ,

$$\frac{l'}{d} = \frac{0.25}{\gamma} \quad (6.11)$$

The number of diameters in which one velocity head is lost in smooth-walled pipes is plotted for turbulent layers in Fig. 6.3 as a function of Reynolds number.

When surface roughness exists, the friction coefficient can be obtained from Fig. 3.8 and then substituted in eq. (6.11). The value of  $\gamma$  for fully rough conditions has been used in preparing the appropriate curve on Fig. 6.3.

In addition to estimation of the equivalent roughness, some allowance has to be made for the expected standard of workmanship in the manufacture and assembling of the various lengths. Reductions of 20 per cent in the  $l'/d$  ratio are not

unusual for ducts of a poor standard. For a given smooth pipe and a constant kinematic viscosity it follows from eqs. (6.10) and (3.50) that the total head loss for turbulent flow is proportional to  $V_1^{1.8}$ . Hence, when the loss is known experimentally for a particular smooth pipe, this relation can be used to predict the loss at some other velocity. The resistance in fully rough pipes is proportional to the square of the velocity.

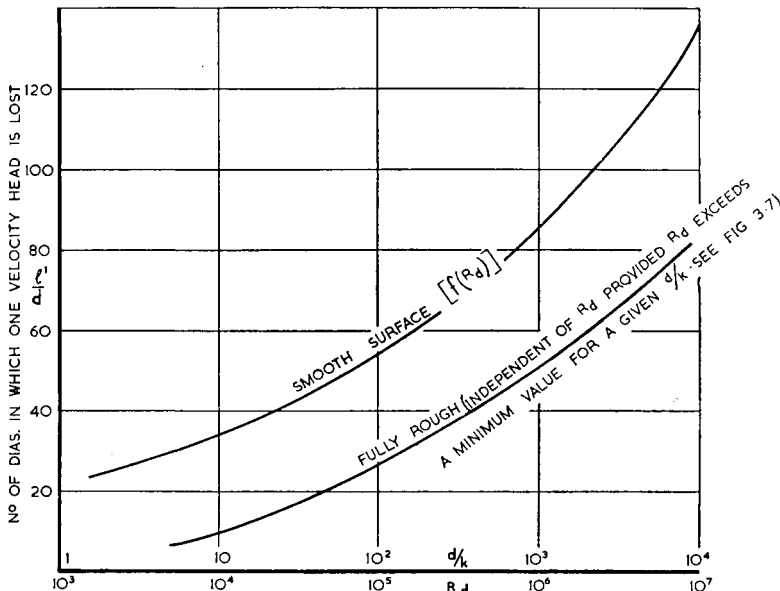


Fig. 6.3. Pipe loss data for smooth and fully rough conditions

### 6.3. Contractions

Contractions are, as a rule, comparatively short and hence skin friction losses are small and negligible.

In accelerating flows, pressure energy is converted into velocity head ; this process is usually free of undesirable features. However, with abrupt changes in cross-section, the air is over-speeded near the surface and the consequent retardation produces regions of eddying flow ; the larger these regions, the greater the losses.

**6.3.1. Contraction losses.** Contractions usually fall into one of the three categories listed in Fig. 6.4.<sup>(28)</sup>

Losses in the case of the conical contraction are a function of cone angle and area ratio and will vary between 5 and 10 per cent of the downstream mean velocity head.

High losses accompany sudden contractions, the area ratio being the main variable.

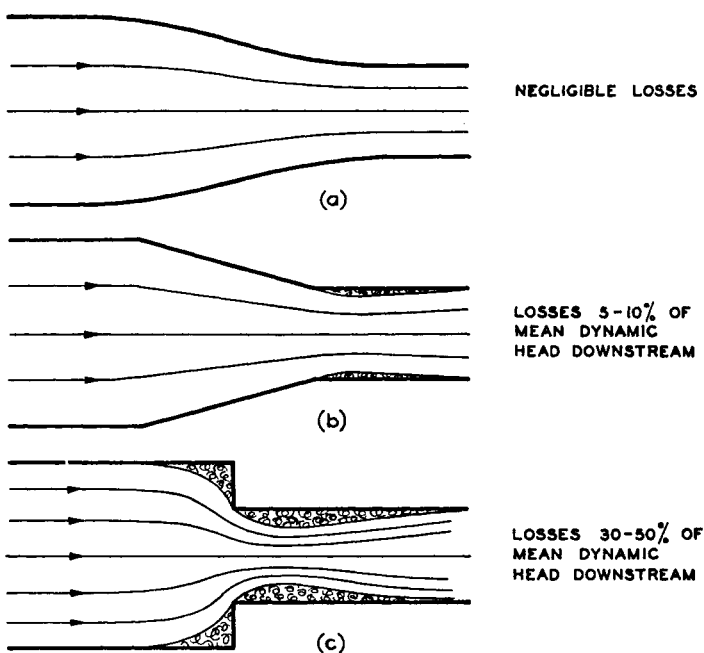


Fig. 6.4. Flow and losses in three types of contraction (Reference 28)

Provided the flow is turbulent upstream of the contraction, the variables of inlet velocity distribution and Reynolds number have very little influence on the duct losses.

**6.3.2. Inlet losses.** Inlet shapes vary, in a manner similar to contractions, from a streamlined type of entry to an abrupt, sharp edged variety (Fig. 6.5). It will be noted that the losses can be higher than those quoted in the previous sub-sections for the case of contractions. Two factors contribute to this state of affairs. The more important one is the greater curvature of

the inflowing streamlines which leads to larger regions of separation. The second factor is associated with the boundary layer, which is definitely laminar at the lip of the inlet; this results in a relatively large initial region of separation.

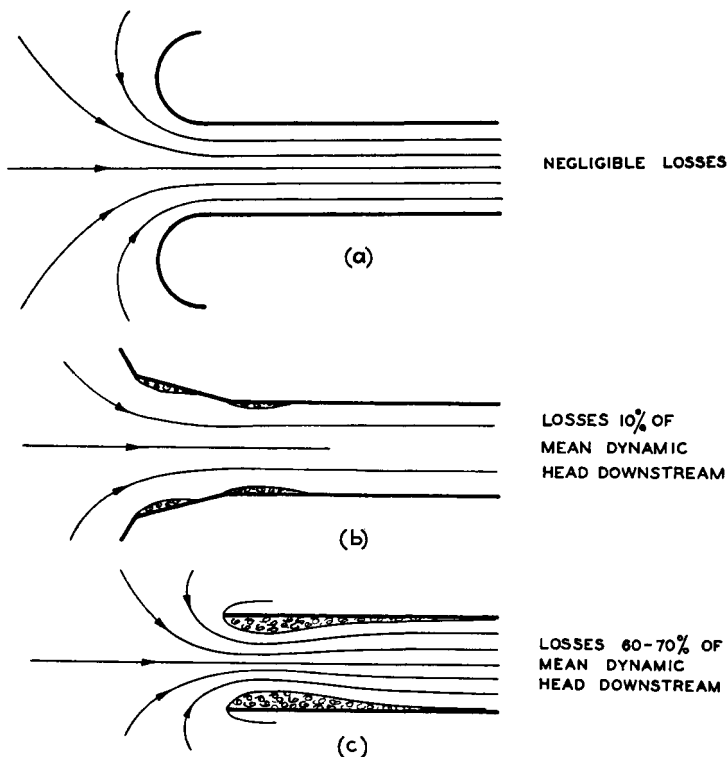


Fig. 6.5. Flow and losses in three types of inlet (Reference 28)

#### 6.4. Diffusers

When air is retarded in a diffuser, the static pressure increases as described in Section 2.3.8. Provided the diffusion angle is small, the losses are mainly skin frictional ones, but when the rate of diffusion is increased by employing wider angle diffusers the boundary layer is apt to separate from the duct walls; eddying flow then results.

It will be appreciated that extremely long diffusers of small

angle are undesirable, for skin friction reasons, while short wide-angle diffusers lead to separated flow conditions.

**6.4.1. Diffuser efficiency.** There is an ideal conversion of dynamic head into static pressure, when eq. (6.4) can be written

$$p_B - p_A = \frac{1}{2} \rho V_A^2 \left[ 1 - \left( \frac{A_A}{A_B} \right)^2 \right]$$

The diffuser efficiency can therefore be expressed as the ratio of the actual to the ideal pressure rise, namely,

$$\eta_D = \frac{p_B - p_A}{\frac{1}{2} \rho V_A^2 \left[ 1 - \left( \frac{A_A}{A_B} \right)^2 \right]} \quad (6.12)$$

or,

$$\eta_D = 1 - \frac{\Delta H_D}{\frac{1}{2} \rho V_A^2 \left[ 1 - \left( \frac{A_A}{A_B} \right)^2 \right]} \quad (6.13)$$

These equations are, of course, subject to the same approximations as those made in developing eq. (6.4).

The choice of station  $B$ , i.e. the downstream one, presents a little difficulty when the flow in the diffuser is separated. With a length of straight ducting of uniform cross-section fitted downstream of the diffuser outlet, pressure recovery usually continues up to a point just downstream of flow reattachment in this duct. This suggests that a diffuser containing separated flow and discharging direct to the atmosphere will be less efficient than a similar one fitted with a length of exit pipe.

**6.4.2. General flow in diffusers.** In small-angle diffusers, the flow at the exit is unseparated, but, owing to the greater relative retardation of the air adjacent to the surface, the cross-sectional velocity distribution, when compared with that of a constant area duct, is more peaked.

When separation occurs with increasing diffuser angle it is usually confined to one side of the diffuser at any particular instant. Given symmetrical inlet conditions, the separation will tend to flick from side to side or rotate around the duct. With non-uniform inlet or exit conditions, however, the separation may be confined to a specific region.

A further increase of angle produces a more general separation pattern on all walls of the diffuser. The severity of the separation at any particular time will not, in general, be identical on all sides; as a result, an unsteadiness similar to that just described will be present.

For very large diffusion angles, conditions approximating to a sudden expansion are experienced and, although the losses are high, the general flow in the duct system is steadier. Sudden expansions are characterized by a stable central core of high velocity fluid surrounded by regions of large and small scale turbulence which eventually produce a redistribution of the flow in the downstream ducting. The losses associated with a sudden expansion may approximate to an amount equal to the dynamic head at entry.

**6.4.3. Diffuser angle.** This parameter is probably the most important, as it is the major factor governing the static pressure

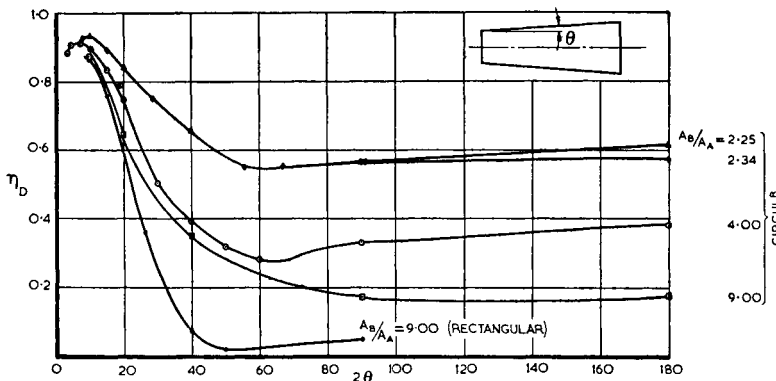


Fig. 6.6. Diffuser efficiency as function of included angle and area ratio

gradient along the diffuser. As suggested previously, there is an optimum angle for which the losses are minimal. The data of Fig. 6.6 suggest that the included angle should be in the range  $7^\circ$  to  $9^\circ$ .<sup>(29)</sup>

While these data may be used as a guide, the influence of other factors must not be ignored. Squire<sup>(30)</sup> has reported diffuser angles up to  $10^\circ$  without separation; on the other hand separation has been observed in the  $5^\circ$  diffusers of closed-return

type wind tunnels. In this type of tunnel great care is usually taken to avoid separation, in order to ensure a satisfactory velocity distribution in the test section. It is, therefore, a matter of some concern that separation should have been noted in diffusers which were thought to have a margin of safety.

Angles larger than  $9^\circ$  are permissible when a region of high resistance, e.g. a heat exchanger, is fitted to the diffuser exit. The resistance assists the diffuser to run "full"; use is now being made of this feature in some wind tunnels where the last diffuser is a wide-angled one fitted with one or more transverse wire screens. Owing to the low velocity through such screens, the total head loss is a very small part of the total losses in the tunnel circuit. Careful design<sup>(31)</sup> of such diffusers is urged since an arbitrary application of the principle may produce disappointing results.

**6.4.4. Area ratio.** Provided separation is avoided, diffuser efficiency tends to decrease slightly with increasing area ratio. When the diffuser angle is wide enough to initiate separation, a marked relation exists between area ratio and efficiency (see Fig. 6.6).

For diffusers with included angles in the neighbourhood of  $9^\circ$ , an increase in area ratio normally makes the diffuser more susceptible to separation. An area ratio of 16, without separation, has been achieved by Squire,<sup>(30)</sup> using a  $10^\circ$  diffuser; this, however, constitutes a rare exception to normal experience.

**6.4.5. Shape of diffuser.** As might be expected, the cross-sectional shape of the diffuser is of considerable importance. The variation of efficiency with included angle for three geometric types of diffuser is given in Fig. 6.7. For a given included angle the conical type diffuser is the most efficient. Although the rectangular type is not much inferior on this basis it should be remembered that since  $A_A/A_B$  is constant at 4 the length of the rectangular diffuser is somewhat greater. When the rectangular diffuser is compared with the other two, on a basis of constant rate of air diffusion, it is, with the exception of very small diffuser angles, inferior from a performance point of view.

The presence of a centre body in the duct decreases the efficiency; this annular type of diffuser is discussed more fully in Section 13.

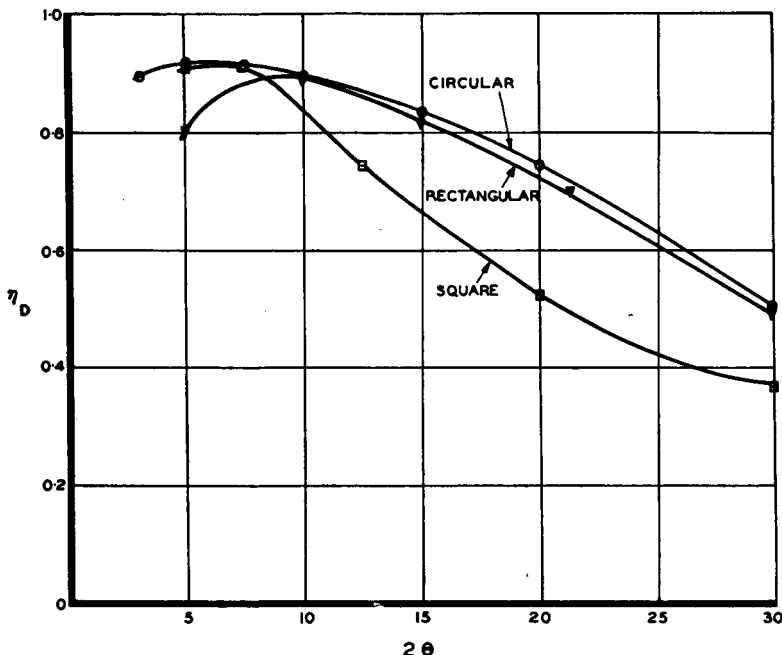


Fig. 6.7. Diffuser efficiency as function of section shape and included angle (Area ratio = 4)

**6.4.6. Reynolds number.** When skin friction is the dominant loss, as in small-angle diffusers, there is a small rise in efficiency as Reynolds number increases. For example, the efficiency of a  $6^\circ$  diffuser rises from 0.89 to 0.92 when the inlet Reynolds number is increased from  $10^5$  to  $10^6$ .<sup>(30)</sup> When separation is imminent or present, Reynolds number effects can be neglected provided the flow is turbulent at inlet to the diffuser.

These comments apply when the duct Reynolds number is used and the inlet flow is sensibly uniform. However, a true measure of Reynolds number effects can be obtained only by considering the parameter,  $R_\theta$ . Inlet conditions are recognized as having a major influence on diffuser performance and one of

the factors involved is undoubtedly the boundary layer Reynolds number. The thicker turbulent layer has a reduced skin friction but this is more than offset by the increase in pressure drag. As suggested in Section 3.6, the effect of adverse gradients on turbulent layers is not as yet clearly understood and hence a fundamental approach to diffuser flow is impossible. In view of these difficulties, there is no alternative to the present practice of dealing with these matters under the heading of inlet conditions.

**6.4.7. Upstream and downstream conditions.** The data presented so far on diffuser losses are applicable only when the inlet velocity distribution is approximately uniform. The quantitative information which follows will relate to conical type diffusers.

When the velocity distribution at inlet is of the fully developed pipe flow type there is<sup>(29)</sup> a drop of approximately 7 per cent in efficiency over the range of diffuser angles up to 30°; this reduces the peak efficiency to roughly 0.85.

The presence of a corner or some similar duct component upstream of a diffuser may lead to a non axisymmetric inlet velocity distribution. This will further reduce the efficiency of the diffuser; the amount will depend on the actual asymmetry of the flow. In such a case a factor based on personal experience must be applied.

In Section 6.4.1 an approximate efficiency relation, eq. (6.12), was developed. As stated therein, a length of uniform ducting may be necessary in order to obtain the maximum pressure recovery; when diffuser efficiency is computed from this relation this feature must be kept in mind. This point of maximum pressure may be from 2 to 6 outlet duct diameters downstream of the diffuser, depending on diffuser angle and inlet velocity distribution. Taking the case of fully developed pipe flow at the diffuser inlet, the difference in efficiency,<sup>(29)</sup> as computed by eq. (6.12) at diffuser exit and at the point of maximum pressure, will vary from 10 per cent for a diffuser angle of 5°, to 40 per cent for an angle of 25°. For uniform inlet conditions, the corresponding figures are approximately zero and 15 per cent at these two angles.

Complications also arise when a diffuser discharges into a

duct component with asymmetric tendencies, such as an unvaned corner. If separation were present in the diffuser, this downstream component could noticeably reduce the diffuser performance.

**6.4.8. Devices for improving diffuser flow.** There is a universal need for short, efficient diffusers. Long diffusers are costly to manufacture and often occupy valuable space. When they are erected vertically, the cost and magnitude of the supporting structure become considerable; horizontal installations absorb valuable floor space or ground area. Whether the application is industrial or scientific, the only virtue in a long small-angle diffuser is the insurance it generally provides against heavy total head losses and unsatisfactory flow characteristics.

It is not surprising, therefore, that many attempts have been made to improve the flow in wide-angle diffusers. Probably the most popular device is the resistance screen,<sup>(31)</sup> which was referred to in Section 6.4.3.

Another artifice consists in using full-length radial splitter vanes or annular dividing sleeves.\* Although the additional "wetted" surface increases the skin friction losses, some increase in cone angle can be achieved by such means prior to the onset of severe separation.

Separation is the result of a failure on the part of the boundary layer to transport sufficient momentum inwards in the direction of the surface to counter the effect of static pressure gradient on the velocity head (see Section 2.3.9). Many methods of "boundary layer control" have been evolved in an attempt to assist the boundary layer and these may, in general, be subdivided into three main classes:

- (i) Boundary layer suction where the low energy or "tired" air near the surface is removed, by means of a suction pump, through a porous or slotted wall (see Fig. 6.8).

\* A recent paper by Cockran and Kline (NACA Tech. Note 4309) dealing with rectangular diffusers has reported an efficiency of 72 per cent. for a diffuser of 42° included angle with an area ratio of 6·9. Five splitter vanes with leading edges just downstream of the inlet and extending approximately half way down the diffuser were employed. Two further reports by Kline on diffuser flow and design are now to hand and are available as Stanford University's Reports PD-4 and MD-4.

- (ii) Revitalization of the air near the surface by means of a high velocity jet issuing in the stream direction, from a spanwise tangential slot in the surface.

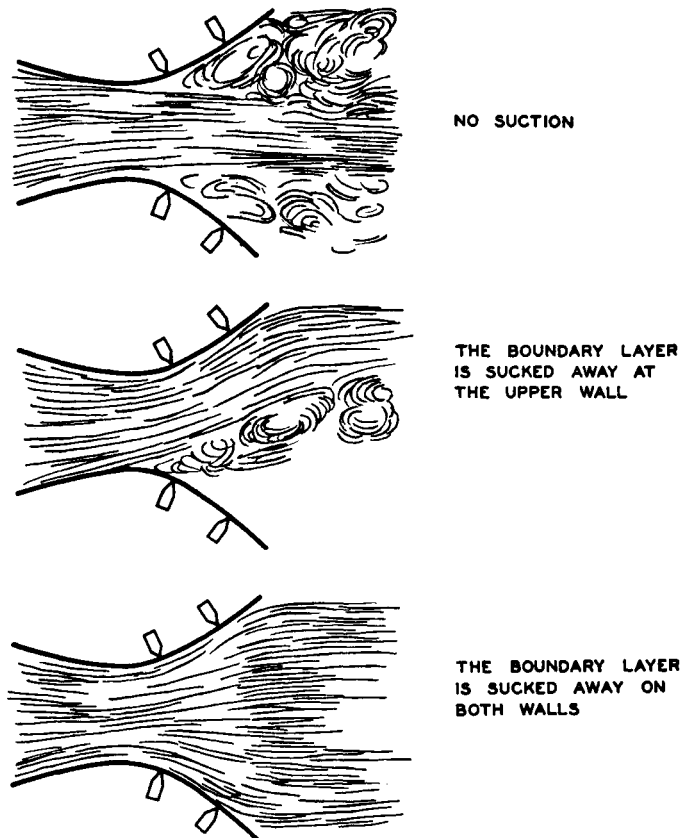


Fig. 6.8. Diffuser with boundary layer suction  
(line sketch of flow photograph by Tietjens)

- (iii) Augmentation of boundary layer mixing in order to increase the rate of momentum transfer towards the wall. Two devices which have proved successful are (a) large, distributed surface roughness<sup>(19)</sup> and (b) stub aerofoils<sup>(32)</sup> whose function is to generate streamwise vortices (see Fig. 6.9).

Experiment has shown that the introduction of a general swirl into the diffuser flow, by means of fixed vanes near the diffuser inlet, can delay flow separation.<sup>(29)</sup> It appears that the radial distribution of pressure has a favourable effect on the diverging flow. There must also be a beneficial increase in boundary layer mixing. This device is useful when flow steadiness is required, but, for reasons outlined in Section 6.1.3, appreciable declines in diffuser efficiency must be expected when the rotational flow is no longer small.

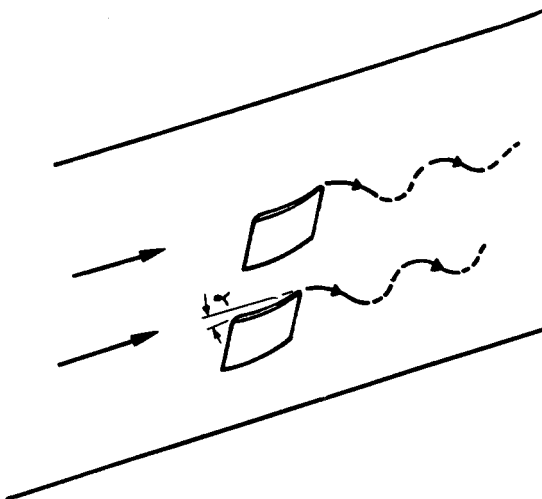


Fig. 6.9. Vortex generators

**6.4.9. Summary.** Sufficient data have been presented to facilitate the design of the most common types of diffuser. It will be apparent from the foregoing that good accuracy in estimation can be obtained only when separation is avoided and the inlet and outlet conditions are known in detail. Badly designed diffusers are a frequent source of trouble in industrial aerodynamic systems and hence the problem should not be considered too lightly.

## 6.5. Corners

In turning a flow by the medium of a curved duct, substantial changes in flow velocity can occur near the surface. The

retardations which follow local flow accelerations may lead to flow separations and hence heavy total head losses. Skin friction losses can in general be ignored.

Secondary flows, as described in Section 5.4.1, are always present in curved ducts. Such flows represent losses; unfortunately they also tend to increase the separation losses.

**6.5.1. Flow in a corner.** In the absence of boundary layers, the streamlined flow pattern, in a duct of rectangular cross-section, would resemble that illustrated in Fig. 6.10. On

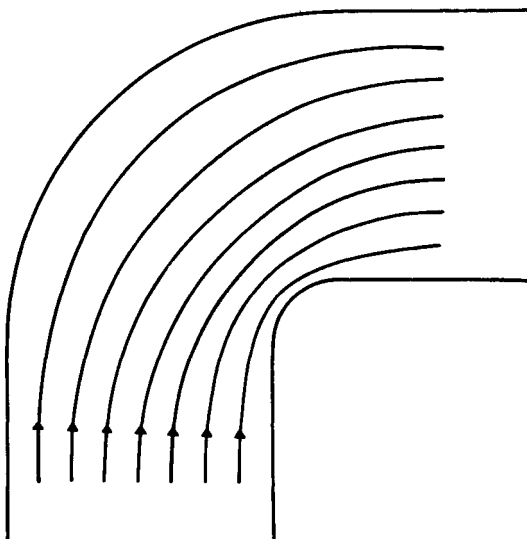


Fig. 6.10. Non-viscous flow in corner

the inside of the bend the streamlines first converge and then diverge whilst the reverse takes place around the outer wall. Since diverging streamlines signify flow retardation, the regions of rising pressure are self-evident.

The areas of boundary layer separation, forced by the adverse pressure gradients, are schematically presented in Fig. 6.11 for the case of an infinitely wide corner of rectangular cross-section. The presence of side walls, however, produces secondary flows and low energy air is swept from the side wall boundary layers into the inner wall region of separation. When the side wall boundary layers are thin, the out-of balance between centrifugal

and pressure forces is confined to a relatively small amount of fluid and the secondary flows are at a minimum. Since with fully developed pipe flow there are no fluid particles unaffected by an out-of-balance condition, higher losses can be expected.

The same arguments apply in the case of ducts of circular cross-section.

In the schematic diagram of Fig. 6.11 it can be seen that the flow does not re-attach to the inside duct wall until it has

90^\circ corner. Turning of the flow continues right up to this re-attachment point. It is clear therefore that undeturning will result if the corner discharges direct to the atmosphere.

Fig. 6.11. Regions of separation in right-angled corner

progressed an appreciable distance downstream of the  $90^\circ$  corner. Turning of the flow continues right up to this re-attachment point. It is clear therefore that undeturning will result if the corner discharges direct to the atmosphere.

**6.5.2. Assessment of losses.** When the inlet and outlet areas from a corner are identical, and when the inlet flow is fully developed and the outlet flow quickly reverts to a similar velocity distribution at station  $B$ , the total head loss is given by eq. (6.3), namely,

$$\Delta H_1 = p_A - p_B$$

The flow downstream of a corner in which boundary layers, eddying flow, secondary flow and a "free stream" are present is inevitably a complex one and hence no great accuracy can be expected in either measurement or estimation of the duct loss. A well-informed empirical approach to the problem is therefore

acceptable. The approximate relations of Section 6.1.3, i.e. eqs. (6.3) and (6.4), are usually employed; station *B* must not be chosen in a region of separated flow.

**6.5.3. Geometric parameters.** There are three major parameters associated with the geometry of the constant cross-sectional area bend commonly in use. These are:

(i) *Turning angle,  $\theta$*

(ii) *Radius ratio,* 
$$\frac{\text{mean rad. of curvature}}{\text{height or dia. of duct}} = \frac{R}{d}$$

(iii) *Aspect ratio,* 
$$\frac{\text{width of duct}}{\text{height of duct}} = \frac{W}{d}$$

The symbols are further defined in Fig. 6.12.

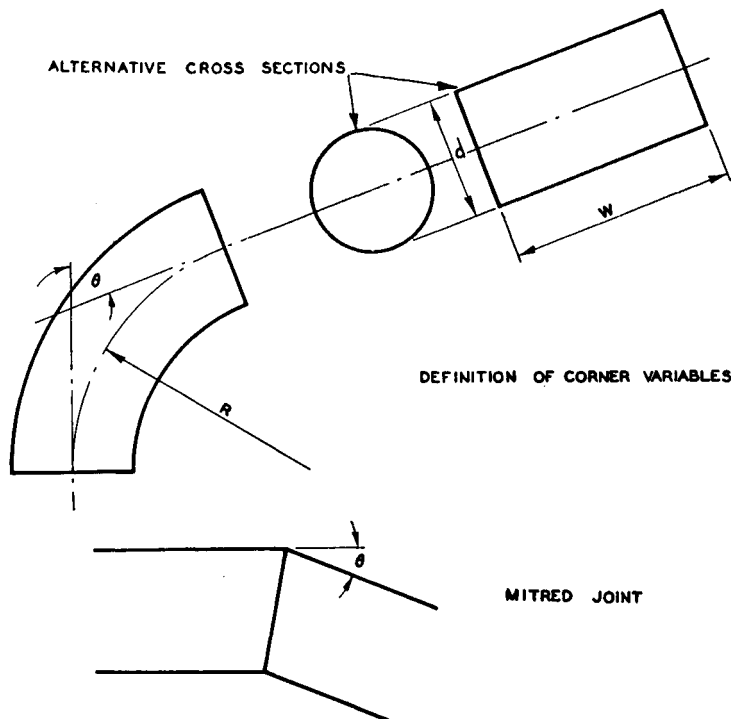


Fig. 6.12. Corner variables

The influence of  $\theta$  can be gauged from Table 6.1, where representative loss coefficients<sup>(33)</sup> are listed.

Table 6.1

$\theta$	<i>Square duct Mitred joint</i>	<i>Round duct Mitred joint</i>	<i>Round duct Radius ratio 3</i>
30°	0.15	0.10	0.02
60°	1.10	0.40	0.05
90°	1.60	1.05	0.20

This Table also provides an example of the importance of radius ratio. Quantitative data<sup>(33)</sup> on this point for different cross-sectional shapes are presented in Figs. 6.13 and 6.14, for 90° bends. By an increase in the radius ratio, the local flow accelerations and the magnitude of the subsequent adverse pressure gradient are reduced. As a result, eddying flow is minimized and the losses greatly reduced.

Aspect ratio effects in rectangular ducts are of a more complex nature. First, increasing aspect ratio provides the opportunity to obtain a more favourable radius ratio. Secondly, the secondary flows, which have their origin on the side walls, are restricted in strength and size, with beneficial results. On the other hand, with increasing aspect ratio, there is an increase in the ratio of wetted area to cross-sectional area and this leads to a rise in skin friction forces. There is, therefore, a limit to the benefits which can be obtained from aspect ratio increases. Detailed data for 90° bends are graphically presented in Fig. 6.14. Additional information on bends can be obtained from References 34 to 36.

**6.5.4. Reynolds number effects.** Tests on corners have failed to indicate any noticeable change in corner losses over the duct Reynolds number range usually encountered. Comments similar to those made in Section 6.4.6 are equally applicable in the present instance.

**6.5.5. Entry and exit conditions.** Duct losses increase when the inlet velocity distribution is changed from a sensibly uniform one. The author, however, is not in possession of any reliable quantitative data.

The performance of a corner will be greatly affected by the presence upstream of a wide-angle diffuser or some similar source of flow separation. Compound corners, that is, one corner adjoining another, can be considered in relation to this aspect; losses will depend on the orientation of the second corner with respect to the first and also on the length of straight ducting between them. In many cases, a compound corner must be treated as a single unit of ducting rather than as two separate corner units.<sup>(37)</sup>

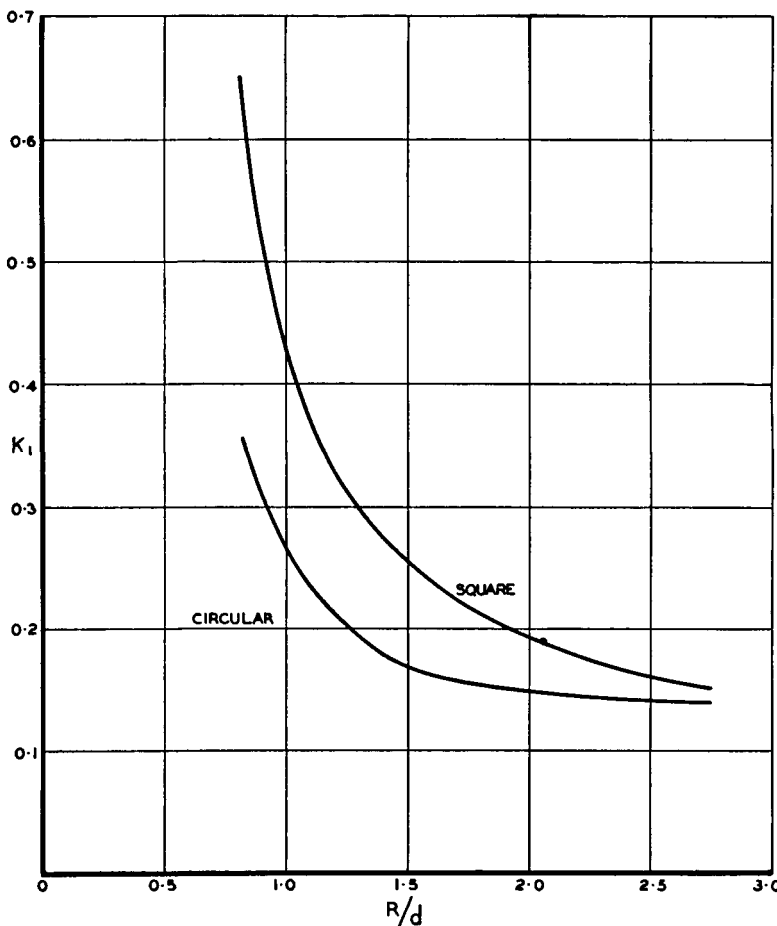


Fig. 6.13. Losses in right-angled corners

With a non-uniform distribution of velocity at inlet and with the higher velocity on the side adjoining the inner wall of the bend, losses may on occasion be greater than those outlined in Section 6.5.3. This is due to the greater loss of total head in the region of separated flow. If possible, this inlet condition should be avoided in design; if it is present in a particular installation, redesign should be considered.

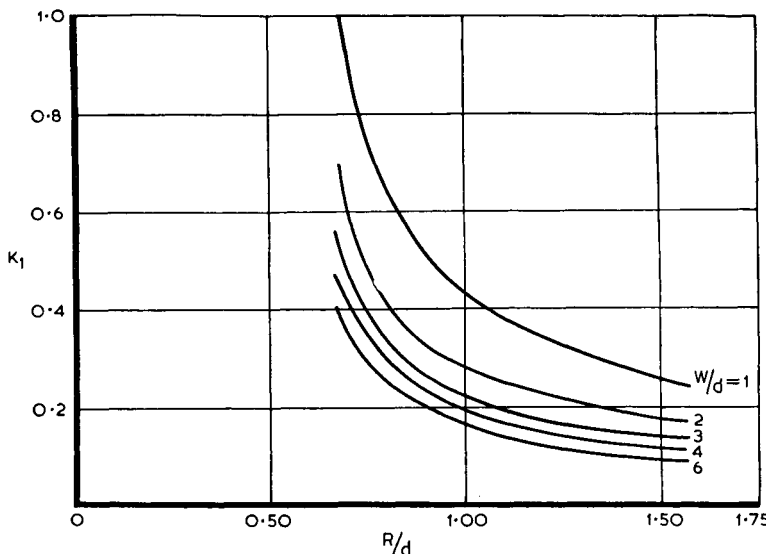


Fig. 6.14. Losses in rectangular right-angled corners

Experiment has shown<sup>(38)</sup> that the secondary motions initiated in a corner persist for large distances downstream; the influence of such vorticity on the flow in the subsequent portion of the duct system should be given some consideration.

With the re-attachment of the flow to the surface just downstream of the outlet, the velocity distribution fairly rapidly reverts to approximately that normally found in uniform ducting.

**6.5.6. Corners with special velocity distributions.** The foregoing has been confined to corners with a uniform cross-sectional area. When, however, the inner and outer walls of a corner of rectangular cross-section are suitably shaped, the

wall pressure gradients can be so adjusted as to keep separated flow to a minimum.<sup>(39)</sup> Since the inner wall is the more critical, an increase in the radius of curvature of this wall is beneficial. This leads to an expanded type of bend, as illustrated in Fig. 6.15. Tests on an expanded bend<sup>(40)</sup> having an

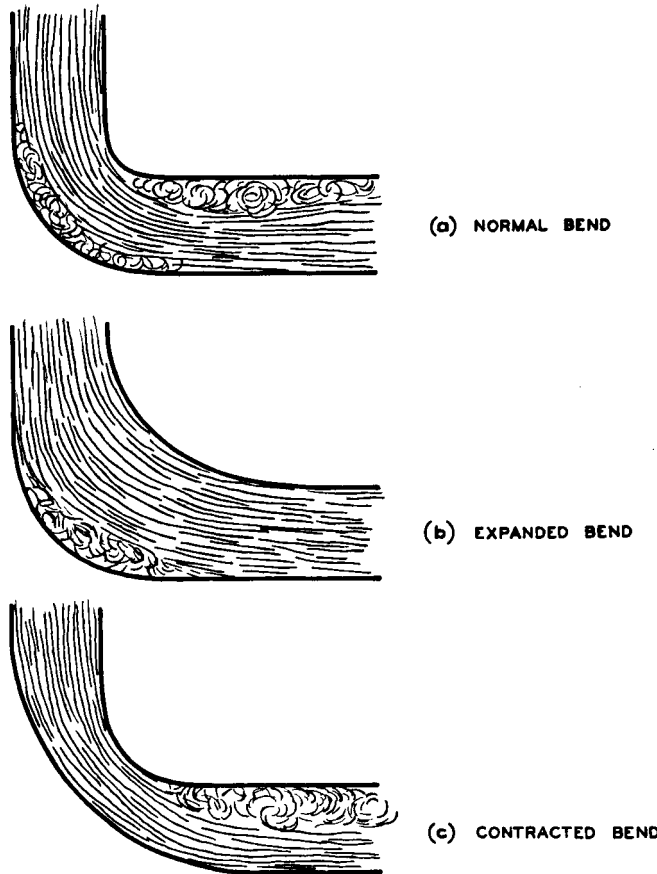


Fig. 6.15. Effect of varying corner shape in rectangular ducting  
(line sketch of flow photograph by Nippert)

inlet aspect ratio of 3 and of a design which eliminated streamwise pressure gradients on the inner wall, resulted in a loss coefficient of  $K_1 = 0.065$ . This compares more than favourably with the results presented in Fig. 6.14.

With a contracted type of bend, the streamwise pressure gradient on the outer wall can be removed, but while separation is eliminated on this wall, conditions on the inner wall are made more severe. The expanded type of bend is, therefore, the only one of practical value.

**6.5.7. Corners with boundary layer control.** Special bends employing boundary layer suction as a method of controlling the boundary layer have been designed and tested. From data available,<sup>(40)</sup> however, the performance of the well-designed expanded corner seems so little below that of a suction corner that the latter is unlikely to command much attention.

**6.5.8. Turning vanes.** From Fig. 6.14 it will be seen that low losses are attainable when relatively large values of aspect ratio and radius ratio are employed. For practical reasons, however, it is seldom possible to adopt such values. When a sharp corner of small aspect ratio is unavoidable, vanes may be fitted as a means of reducing the corner loss. These can be considered either as highly cambered aerofoils which deflect the flow or as solid surfaces which divide the corner into a number of air passages possessing favourable aspect ratios.

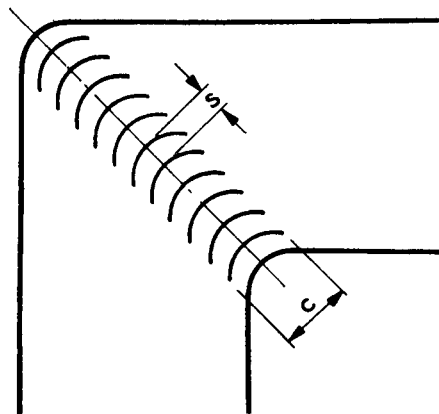


Fig. 6.16. Corner with turning vanes

Working on the assumption that the radial width of the passages between vanes should remain constant, Collar developed a relatively thick turning vane. It has been shown experimentally,<sup>(41)</sup> however, that equally good results can be obtained

with constant-thickness cambered plates (Fig. 6.16). These actually provide expanded bend conditions similar to those discussed in Section 6.5.6. When cambered plates are required to work over a range of inlet conditions, the performance of the vanes falls off, with the appearance of local regions of separation near the leading edge. The angle of the flow relative to the leading edge of a corner vane remains constant, however, and hence low losses can be expected when the local incidence of the vane is suitably adjusted to avoid leading edge separation and when there are sufficient vanes present to keep the lift coefficient to a reasonable value.

On the basis of the available data, therefore, further discussion will be confined to cambered plate vanes. The dependence of the loss coefficient on the gap/chord ratio is illustrated in Fig. 6.17. Salter's curve was obtained for inlet conditions where the boundary layer thickness was 10 per cent of the half duct width. When the turning losses are measured in the region outside the boundary layer, the dotted curve results; the presence of the boundary layer, therefore, doubles the minimum corner loss. It is clear from this result that the loss coefficient will be a very definite function of the inlet velocity distribution. The discrepancy between the Salter and the Klein curves may be due in some measure to differing inlet conditions. The loss coefficients measured by Klein are probably representative of corners with large inlet boundary layer thicknesses. Higher losses again can be expected for asymmetric inlet conditions. The increase in the loss coefficient with decreasing gap/chord ratio is due to the large total profile drag force acting on an excessive number of vanes.

When a set of corner vanes is to be designed, the aspect ratio of the passage at inlet should be at least 6. The distance between the vanes at inlet can now be established; the gap,  $s$ , then follows from the geometry of the corner. Reference to Fig. 6.17 gives the minimum loss for a gap/chord ratio of between 0.3 and 0.4. From this ratio the chord can be determined. When the foregoing leads to an impracticable arrangement, the dimensions can be changed provided the gap/chord ratio is maintained.

The detailed shape of the vane is not critical and hence the

form usually adopted is a circular arc possessing a camber angle equal to the required turning angle. For convenience in manufacture, small linear extensions to the leading and trailing edge tangents are usually incorporated.

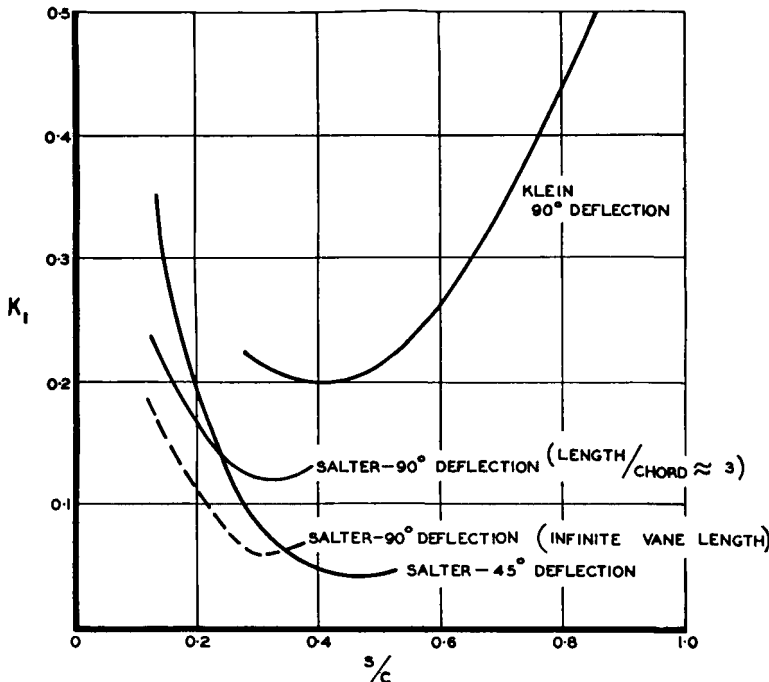


Fig. 6.17. Losses in vanned corner of rectangular cross-section (based on A.R.C. R. & M. 2469, and reproduced by permission of the Controller of H.M. Stationery Office)

Most of the experimental work is confined to corners of rectangular cross-section. The data so obtained have been applied to octagonal wind tunnel corners and even to circular corners. Some tests<sup>(42)</sup> have, however, been carried out with vanes on right-angled corners of circular cross-section. On the assumption that the inner portion of the bend is the more critical, the vanes have been arranged with a spacing approximating to an arithmetical progression. The geometric details of the best arrangement are presented in Fig. 6.18, along with the appropriate loss coefficient. The boundary layer thickness

at inlet was 30 per cent of the pipe radius and hence the loss measured is probably in the middle of a possible range of values, for varying inlet conditions.

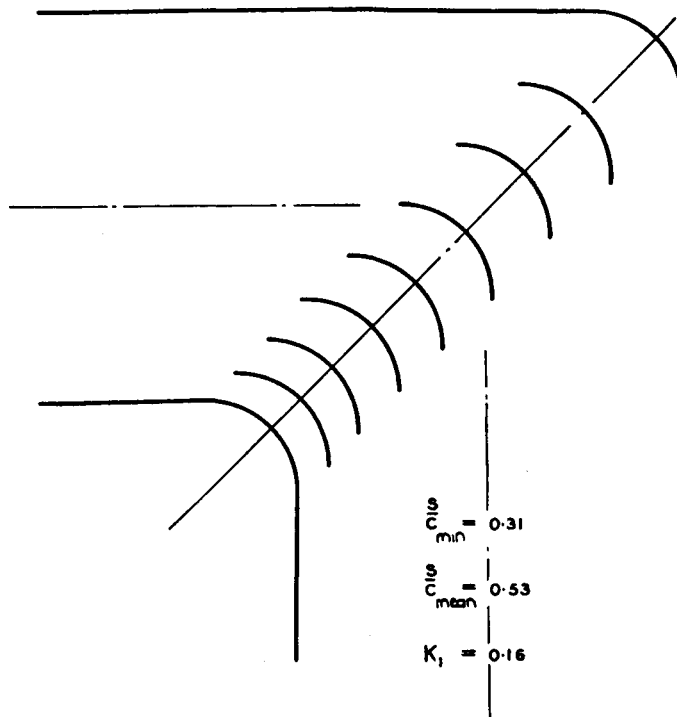


Fig. 6.18. Loss in vaned corner of circular cross-section

No comprehensive Reynolds number studies have been made but it is usually accepted that the above loss coefficients are fairly applicable to most duct systems. For any given corner installation, however, a small reduction in the loss coefficient may accompany a large increase in the mean duct velocity.

**6.5.9. Diffusing corners.** It is, generally speaking, bad practice to have the outlet cross-sectional area greater than the inlet value. Space and cost considerations, however, very often enforce the use of the diffusing corner in industrial installations. Tests<sup>(43)</sup> carried out on a vaned 90° diffusing bend of area ratio 1.45:1 gave loss coefficients which ranged

from 0.11 to 0.24 for a change in inlet boundary layer thickness from 2 per cent to 70 per cent of the half duct width; cambered aerofoils at a gap/chord ratio of 0.5 were employed as the turning vanes. Hence, provided the corner is vaned, a reasonable amount of diffusion can be obtained without additional loss since the above coefficients agree with those outlined for the non-diffusing bend.

In attempting an area ratio of 2.75:1, MacPhail<sup>(44)</sup> found separated flow downstream of the vanes. Insertion of a wire screen across the outlet duct gave a relatively uniform velocity distribution in the outlet duct. The results suggested that the resistance coefficient of the screen should lie somewhere between 1.4 and 3.0. When related to the mean velocity in the inlet duct, the corresponding loss coefficients are 0.19 and 0.40 respectively. These coefficients must be added to the actual corner losses in assessing the overall loss coefficient for a diffusing corner of this type. Unfortunately, MacPhail does not record the loss in the corner; since separation existed, however, the losses will be moderately high and it is suggested that  $K_1$  will be of the order 0.30 when the optimum use is made of the corner vanes. The total overall loss coefficient for the corner will then range upwards from 0.50. It should be remembered, however, that a considerable degree of diffusion has been achieved, with the consequent elimination of the losses in a separate diffuser.

## 6.6. Internal Bodies

Internal bodies cannot always be eliminated from the ducting. The losses associated with these obstructions must not be ignored, and this fact is illustrated by Fig. 6.19 which depicts the flow downstream of a rod.

It is possible to translate the drag of an obstruction into an equivalent total head loss coefficient. When  $D$  is the drag force,  $A_1$  the cross-sectional area of the duct and  $V_1$  the mean velocity,

$$K_1 = \frac{D}{\frac{1}{2} \rho V_1^2 A_1} \quad (6.14)$$

For the simple case of an obstruction of constant cross-sectional shape placed so that the longitudinal axis is at right angles to the air stream, the drag is obtained from the drag coefficient by the relation

$$D = C_D \frac{1}{2} \rho V_1^2 d l$$

where  $d$  is the diameter of a rod or the chord of an aerofoil and  $l$  is the length of the obstruction. Hence,

$$K_1 = \frac{C_D d l}{A_1} \quad (6.15)$$

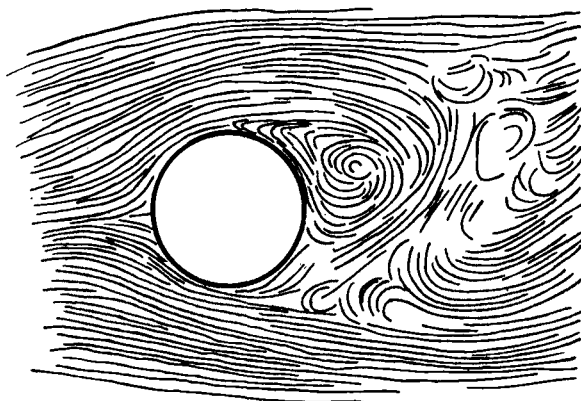


Fig. 6.19. Flow around cylinder

The appropriate coefficient for an axisymmetric body is

$$K_1 = \frac{C_D A}{A_1} \quad (6.16)$$

where  $A$  is the maximum cross-sectional area of the body. A wealth of information on the drag of various types of body is available in Reference 45. Some useful data on common types of obstruction are presented in Figs. 6.20 and 6.21 (References 45 to 47).

The use of wire screens has been previously mentioned as a method of improving the distribution of flow in diffusing passages. Available data on the resistance of such screens

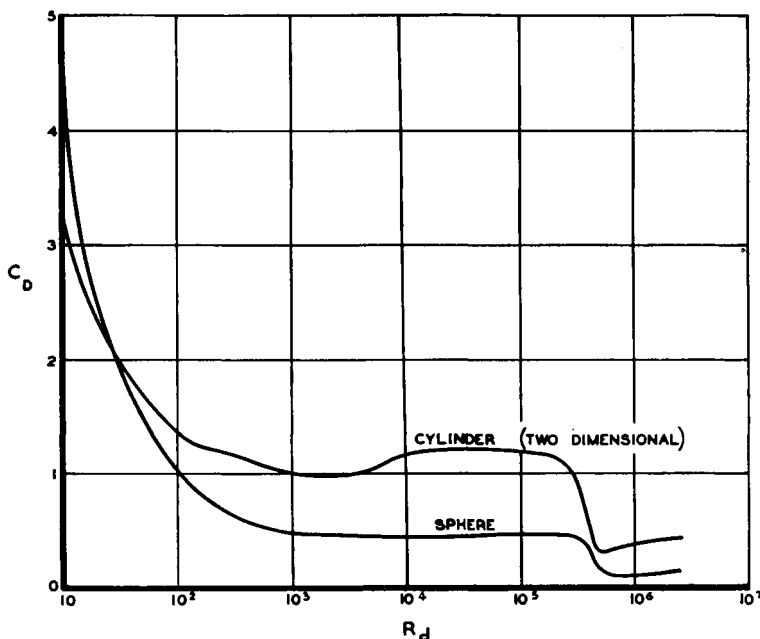


Fig. 6.20. Drag coefficients for cylinder and sphere

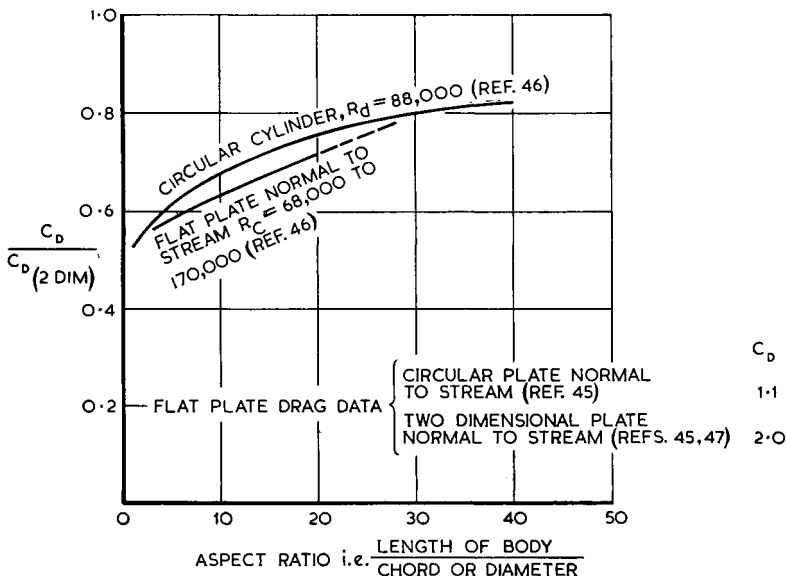


Fig. 6.21. Effect of aspect ratio on drag of bluff bodies

show some scatter; the Wieghardt expression<sup>(48)</sup> given below should, however, prove accurate enough for most purposes:

$$K_1 = \frac{6(1-\beta)}{\beta^{5/3} \left(\frac{Vd}{\nu}\right)^{1/3}} \quad (6.17)$$

where  $\beta$  is porosity (open area/total area),  $d$  is wire diameter and  $V$  is velocity just upstream of screen.

# 7

---

## INTRODUCTION TO FAN DESIGN METHODS

### 7.1. General

Fan design consists in designing two-dimensional blade sections at various radii; a moderate number of stations usually suffices, as additional information can be obtained by interpolation.

It is the purpose of this Section to provide an introduction to the various factors encountered in designing these blade sections and to set out in a concise manner the assumptions and limitations adopted.

While the basic equations and assumptions are often identical, design methods can vary in detail. The design method presented herein is one which has been evolved by the author from the original work by Patterson.<sup>(22)</sup> The most important feature claimed for it is *the expression of all design parameters in terms of two basic velocity ratios*. This, of course, permits a complete graphical representation of the design and performance equations. These ratios have clear physical significances which make them doubly suitable as the major design parameters.

### 7.2. Major Design Parameters

It can be shown that the ratio between the swirl velocity and the axial velocity component, denoted by  $\epsilon$ , at a given radius

is an important variable. As stated previously, the swirl imparted, or removed, by the rotor is a measure of the torque of the rotor. Assuming that for a given flow and pressure rise the efficiency remains constant, it is apparent that the amount of swirl for a given power input can be changed by altering the design speed of the rotor. This introduces a second parameter, the flow coefficient,  $\lambda$ , which is the ratio between the axial component and the rotational rotor speed at a given radius.

Rotor design is almost exclusively a function of the above coefficients of swirl and flow; stator design is largely a function of the former.

The quantity common to the above two coefficients is the axial velocity component and for consistency the axial velocity head has been used in reducing static pressure and total head changes to a non-dimensional form. In some existing design methods, the blade tip velocity is chosen as the reference velocity; it is felt, however, that the axial velocity is the more suitable quantity as it eliminates one variable.

### 7.3. Specific Speed

The idea of specific speed was first evolved in connection with water turbines as a means of classifying the wide range of hydrodynamic machines, from Pelton wheels, using small flows under heads of thousands of feet, to reaction turbines, using very large quantities under heads of a few feet.

The original conception was the unit machine, geometrically similar in all respects to the given machine, but of such a size that, under similar operating conditions, it would develop unit power on unit head. The speed of this unit machine was called the specific speed.

The phrase "similar operating conditions" means that the velocity vector diagrams for the flow through the rotors of the two machines are similar, assuming that the efficiency of the unit machine is identical with that of the given machine.

As a result of accumulated test experience, the turbine manufacturer was able to plot parameters relating to important design data against the specific speed; these data could then be used to assist in new designs. One of the main advantages was

the information provided concerning the most suitable types of turbine for specific duties.

The success obtained with turbines led to the use of specific speed in pump and fan design. The parameter, for fixed density, is usually expressed as

$$n_s = nQ^{1/2} \Delta H^{-3/4}$$

where  $n$  is fan speed (rev/sec),  $Q$  is rate of flow (cusec) and  $\Delta H$  is head rise ( $\text{lb}/\text{ft}^2$ ).

In the early days it proved a very useful guide to whether an axial flow or centrifugal fan should be used for a given task. Specific speed also provided a basis upon which empirical methods of design were evolved. With the development of more precise methods, and the evolution of the axial flow machine capable of doing work normally considered suitable only for a centrifugal fan, the use of specific speed as a parameter has lapsed to some extent.

There appears, however, to be a case for reintroducing specific speed for the following purposes:

- (a) indicating the type and general proportions of the most appropriate fan, number of stages, etc.
- (b) providing a guide to the most suitable rotor speed
- (c) assisting in the choice of the boss/fan ratio
- (d) suggesting suitable values of the two major design parameters for near optimum conditions.

This would result in a further simplification and speeding up of the initial stages of design since it would reduce the number of preliminary designs necessary.

For specific speed to be useful, the empirical presentation of the desired data, in terms of  $n_s$ , must be based on modern designs. The existing data are insufficient to warrant such a treatment in this book but the designer should not overlook specific speed as a possible future aid in further "streamlining" the design of axial flow fans.

## 7.4. Spanwise Load Distribution

It is usual for the flow and swirl coefficients to vary along the

blade span. Although there are numerous possibilities, the most common distributions of the flow and swirl coefficients are obtained by (a) assuming the axial velocity component to be constant everywhere, and (b) designing for a swirl velocity inversely proportional to the radius. This latter condition, which gives "free vortex" flow (see Section 5), ensures that there will be no radial displacement of the flow for the design condition, since the centrifugal forces are balanced by the forces due to the radial pressure gradient. If the swirl distribution differs from that given above, there is a radial component of flow preceding the re-establishment of radial equilibrium.

Departures from free vortex flow give what is commonly known as arbitrary vortex flow. Owing to its lower rotational speed, the blade root is the most critical design section and conditions here limit the work capacity of a rotor designed for free vortex flow. By increasing the swirl towards the tips, relative to the free vortex distribution, however, it is possible to increase the work capacity of the rotor, especially for small boss ratios. The ensuing axial velocity distributions for a particular arbitrary vortex flow can readily be calculated when suitable simplifying assumptions are made.

It is usual, therefore, to specify the loading along a blade by an assumed distribution of swirl. The effect of any subsequent radial flows on efficiency is, in most practical cases, assumed to be small.

## 7.5. The Blade Element

In the foregoing we have considered, in broad outline, overall flow changes without discussing the ability or otherwise of the fan blade to produce these changes.

A blade element at a given radius can be defined as an aerofoil section of vanishingly small span. It is assumed in design that each such element can be considered as a two-dimensional aerofoil, i.e. one which is completely independent of conditions at any other radius.<sup>(20)</sup> In addition, it can be assumed that flow conditions are steady over the whole area swept by the rotor blades. This is equivalent to assuming an infinite number of small chord blades. In practice, the above assumption

has proved satisfactory even when the number of blades is small. It applies equally to rotor and stator blades.

There is an upper limit to the amount of total head which rotor blades are capable of introducing into the flow. The total head rise, which is closely related to the lift on the blades, is dependent on four main factors: the dynamic head due to the relative velocity, the blade chord, the blade camber, and the angle of incidence which the velocity vector makes with the blade. An increase in each of these will, within limits, increase the attainable total head rise.

For a given mass flow, the relative velocity may be increased by increasing either the axial or the rotational component. The former is achieved by increasing the boss diameter and/or reducing the fan diameter. The subsequent diffusion which is often necessary downstream of the fan can, however, reduce the overall efficiency appreciably. The second expedient, that of increasing the rotor speed, also has its limitations as the loss in efficiency at small flow coefficients, i.e. large relative rotational speeds, can be appreciable. In addition, compressibility trouble may arise if the relative velocity at the tip exceeds 500–550 ft/sec.<sup>(22, 49)</sup> Noise is, of course, augmented with increasing tip speed.

It is more convenient to consider the solidity, which is the ratio of blade chord to circumferential gap between adjacent blade elements, than the blade chord. For solidities approaching unity and greater, there is an aerodynamic interference between adjacent blades which usually results in a marked reduction in lift for a given blade incidence. Hence for this and other obvious practical reasons, there is a limit to the amount which the chord can be increased for the purpose of obtaining higher pressure rises.

The maximum lift of a blade depends greatly on the cross-sectional shape of the aerofoil; increasing camber is, within limits, useful as a means of improving the load carrying capacity of a blade.

Lastly, there is a design limitation on the angle of incidence of the blade. Just prior to the stall of the blade element, the profile drag rises rapidly with a subsequent fall in the lift/drag ratio. This results in a reduced rotor efficiency.

Special consideration must also be given to the blade element of the stator. The swirl produced by the rotor in the case of the rotor-straightener unit must be removed by the stators. As the process is one of diffusion, i.e. an increasing static pressure in the direction of flow, the maximum angle through which the air can be deflected is  $45^\circ$  (see Section 11.3). Deflections of  $60^\circ$  or more are possible with the prerotator type of stator as in this case the air is accelerated. The greater the prerotation, however, the larger the static pressure rise across the rotor; rotor stalling may limit the amount of preswirl which can be used.

## 7.6. Multiplane Interference

When aerofoil sections are brought closer and closer to each other, there is mutual interference between the flow patterns around the aerofoils. This leads to a change of slope in the lift curve<sup>(25)</sup> and a decrease in the maximum lift.

For low solidities, no interference is experienced and the two-dimensional test data obtained for a single aerofoil can be used with confidence in design. On the basis of early experimental work, this design procedure was considered invalid for solidities greater than unity; an arbitrary limit of unity was also placed on the product of lift coefficient and solidity.<sup>(22)</sup> More recent work, however, has eliminated many of the uncertainties associated with these rules (see Sections 9.3 and 9.7).

Attempts have been made to extend the scope of the isolated aerofoil theory by the introduction of an interference factor such as the ratio of the actual lift of the blade to the lift it would exert in the absence of the other blades. These methods have, however, failed in general to produce consistent results. When the order of the interference factor is required, data given in Reference 50 for a series of flat plate aerofoils may be used as a guide.

Theoretical methods of calculating cascades of aerofoils, i.e. a number of aerofoils closely spaced, and the flow through them are given in such publications as References 51 and 52. While such methods are useful, most present day designs are based on experimental data obtained from two-dimensional cascade wind

tunnels. The main application of these data has been to axial flow compressor design. In the present work, British practice will be followed in designing high pressure rise fans.

## 7.7. Fan Efficiency

The efficiency of an axial flow fan depends greatly on the overall installation. Good inlet and outlet conditions are not always possible owing to space limitations, unavoidable obstructions, etc.; when this is the case, no accurate estimate of the losses can be made. These cases must be treated with caution. Some assistance may be obtained from published work, such as Reference 53, but actual experience is desirable. In design, every care should be taken in order to ensure a good layout.

Provided flow separation is avoided within a reasonable compass of the fan, the fan losses can be predicted with acceptable accuracy. It is now generally accepted that the losses may be subdivided arbitrarily into three components: profile drag, secondary drag and annulus drag.<sup>(54-56)</sup> The first, which is a two-dimensional loss, is fully understood but the two latter are still receiving considerable attention.

The profile drag is affected by Reynolds number and roughness. In general, the blade Reynolds number lies between  $2 \times 10^5$  and  $10^6$ ; in this range, fan efficiency tends to rise slowly with Reynolds number. When the Reynolds number magnitude is of the order  $0.9 \times 10^5$ , however, there is a sharp decline of efficiency with decreasing Reynolds number. In actual fact, this critical Reynolds number is a function of blade shape and stream turbulence. The effect of roughness is to increase the skin friction with a subsequent small loss in efficiency.<sup>(57)</sup> In some instances, however, severe roughness can modify the characteristics of the fan.<sup>(58)</sup>

The superimposed secondary motion near the extremities of the blades represents a loss since the motion is finally dissipated as turbulence and heat. This loss, known as secondary drag, is rather difficult to estimate. As shown in Section 5.4, the secondary flow depends on the air passage between the blades.<sup>(59, 60)</sup> Studies along these lines have, however, failed to

produce reliable quantitative data although qualitatively the losses are known to depend on the turning angle and the blade solidity.<sup>(61)</sup> Alternatively, Howell<sup>(54, 62)</sup> and Carter<sup>(56)</sup> have endeavoured to identify the motion with the normal trailing vortex system found downstream of finite wings. The loss is presented as an equivalent induced drag coefficient and although valid objections<sup>(61)</sup> can be raised to such a treatment it has nevertheless formed the basis of a quantitative estimate. It has been shown<sup>(56)</sup> that the real induced drag coefficient, due to a variation of lift along the blade (not including the sudden loss of lift at the extremities), is generally very small.

It has been assumed by Howell<sup>(62)</sup> that the annulus drag is associated with high skin friction on the boss and the wall swept by the blade tips. This explanation of its origin is not, however, completely acceptable since skin friction is decreased, not increased, by severe adverse pressure gradients.<sup>(11)</sup> These adverse gradients may nevertheless be expected to cause a deterioration of the boundary layers on the boss and wall. Mager<sup>(55)</sup> has investigated the flow deflections which accompany the sharp rise in pressure experienced by the boundary layers as they pass through the rotor, and has suggested a basis for future research.

Despite the uncertainty associated with the secondary and annulus losses, it is possible, on the basis of experimental work, to estimate these losses with sufficient accuracy for *design* purposes. Errors of a few per cent in fan efficiency have only a very minor influence on the final design parameters.

Since appreciable diffusion losses may occur over the tail fairing, this component of the fan unit must be given full consideration. Losses over the nose fairing, on the other hand, are smaller than the order of accuracy with which the major losses can be estimated, and hence can be neglected.

Finally, it is emphasized that the losses outlined above are the major ones, provided no flow separations exist in or near the fan.

## 7.8. Design Cases

Basically, the design theory presented is for the case of a rotor with both preswirl and afterswirl. The preswirl may be

supplied either by the first of a pair of contra-rotating rotors or by a set of stator blades, while the afterswirl may be removed by a contra-rotating rotor or by stators, or may be permitted to pass downstream unchanged. Provided attention is paid to the sign convention given in Section 8.3, the direction of the design swirl relative to the rotor direction can be adjusted as desired. When appropriate, the preswirl or afterswirl may be equated to zero; e.g. in a rotor-straightener unit the preswirl is zero.

The design theory will be developed for the case of free vortex flow through the rotor and stators. This design method, which is relatively simple, is used almost exclusively at the present time.

When, for the reason given in Section 7.4, designs for other than free vortex flow are undertaken, the linear swirl distribution given by eq. (5.6) proves adequate for design purposes and permits a simplified design procedure. Details of this method are given in Section 16.

## 7.9. Scope of Design

The design development will be confined to the case where inlet and outlet conditions promote relatively uniform flow. In Section 23, however, an attempt has been made to estimate the effect of minor departures from these design conditions. When the duct layout is designed, every effort should be made to ensure the best possible operating conditions for the fan.

From the data presented, it is possible to design for relatively high pressure rises. A limit, however, is reached when air compressibility invalidates the assumption of constant air density and when shock waves begin to appear on the blades. From experience it has been found that a limit of 550 ft/sec should be placed on the relative velocity between the air and the blade.

The isolated aerofoil method is the appropriate one in the majority of cases; the cascade method (see Section 7.6) is usually applicable only to fans of high solidity and boss ratios of the order 0.7. Design methods will be based exclusively on lift, drag and deflection data obtained from wind tunnel tests on isolated and cascade aerofoils.

## 7.10. Procedures

The general steps in the design methods used are now briefly outlined. Worked examples of slide rule accuracy given in Section 18 show the detailed procedure which it is suggested should be followed.

The required total head rise and capacity can be converted into suitable non-dimensional coefficients when the fan and boss diameters and the rotational speed are known or assumed. If a tentative estimate of efficiency is made, the swirl coefficients at selected spanwise stations can be provisionally established. Using the swirl and flow coefficients so obtained, a fairly accurate estimate of efficiency can be achieved; design values of swirl can then be determined at various radii for the appropriate values of flow coefficient.

Most design variables can be estimated as functions of the flow and swirl coefficients. Hence extensive use has been made of graphical representations in which the co-ordinates are the unknown and the flow coefficient, together with lines of constant swirl coefficient. The data from which the figures are plotted are tabulated at the end of the book in order to facilitate the preparation of graphs large enough for design purposes.

In computing and graphing the data, the following limits were used :

*Flow coefficient.* A lower limit of 0.2 fixed by efficiency considerations and an upper limit of 1.5, due to design difficulties.

*Swirl coefficient.* Upper limits of 1.5 and 1.0 for prerotators and straighteners respectively, fixed by blade stalling.

The first part of the design is of general application as it follows from momentum considerations and is hence independent of the type of blade used.

In the initial design steps the loss in efficiency for each component part of the fan unit is assessed separately. This procedure has the advantage that the designer, from a knowledge of the magnitude of the various losses, possesses valuable information which can be used with advantage in making the final choice of fan unit type and dimensions to ensure efficient and satisfactory operation. The time required to carry out

these separate estimations, with the aid of graphs, is negligible. It is considered that this procedure is therefore preferable to one which attempts to obtain a direct estimate of total efficiency by the use of one or two equations in which the losses are combined.

In choosing the notation, the continental system was passed over in favour of that employed by Patterson whose design methods are now widely known and used in English-speaking countries. The standard conventions of Reference 63 have been adopted where additional notation is required for the cascade method.

# 8

---

## ROTOR: MOMENTUM CONSIDERATIONS FREE VORTEX FLOW

### **8.1. General**

In this Section the development of simple design equations from momentum considerations is presented in detail. The total head relationships at each stage of a fan unit are given, the rise in total head is equated to the change in flow momentum through the rotor, the velocity vector diagrams are considered and finally the change in momentum is related to the forces exerted by the blades.

The design equations are extracted and presented in Section 8.6.

### **8.2. Design Assumptions**

It is assumed that both the total head rise and the axial velocity component remain constant along the blade length, and, further, that there is no radial component of flow. The latter condition is shown in Section 8.3 to be a consequence of the two former and is, of course, a requirement of free vortex flow.

Constant axial velocity is never fully achieved but it has been demonstrated in practice that moderate departures from it are relatively unimportant. This is supported by the analysis of Section 23 where it is shown that the action of an axial flow fan is to produce a relatively constant total head rise along the blade despite a gradient of axial velocity.

### 8.3. Pressure Relations and Velocity Vectors

Conditions in an elementary annulus of width,  $dr$ , and constant radius,  $r$ , are given in Fig. 8.1 at various stations in the fan unit. Air entering the prerotators axially is deflected tangentially in a direction opposite to the rotation of the fan. It is assumed that the air leaves the fan rotor with a swirl component in the direction of rotation, and that thus the straighteners are left the task of deflecting it back into the axial direction.

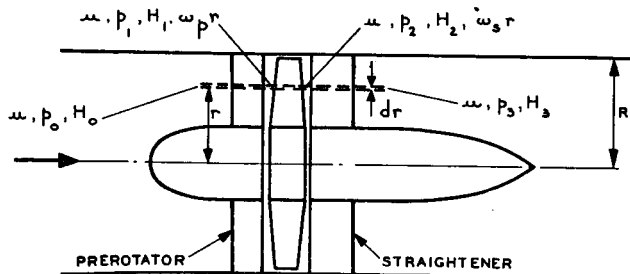


Fig. 8.1. Flow conditions in elementary annulus

It is convenient to take the *preswirl and afterswirl as both positive* although strictly they are of opposite sense. The equations to be developed will, however, be applicable to swirl of either sense provided this sign convention is observed.

The Bernoulli relationships at the four stations of Fig. 8.1 are :

$$H_0 = p_0 + \frac{1}{2}\rho u^2 \quad (8.1)$$

$$H_1 = p_1 + \frac{1}{2}\rho u^2 + \frac{1}{2}\rho(\omega_{pr}r)^2 \quad (8.2)$$

$$H_2 = p_2 + \frac{1}{2}\rho u^2 + \frac{1}{2}\rho(\omega_{sr}r)^2 \quad (8.3)$$

$$H_3 = p_3 + \frac{1}{2}\rho u^2 \quad (8.4)$$

where  $H$ ,  $p$ ,  $u$  and  $\omega r$  are the total head, static pressure, axial velocity component and swirl velocity component respectively.

The overall change in total head in the annulus can be written

$$H_3 - H_0 = \Delta h_{th} - \Delta h_R - \Delta h_P - \Delta h_S \quad (8.5)$$

where  $\Delta h_{th}$  is the theoretical total head rise, the other terms denoting the losses in the rotor, prerotators and straighteners respectively.

The following non-dimensional equation is obtained by dividing eq. (8.5) by  $\frac{1}{2}\rho U^2$ , where  $U$  is the mean axial velocity through the fan and, by virtue of the assumption in Section 8.2, equal to  $u$ :

$$\frac{H_3 - H_0}{\frac{1}{2}\rho U^2} = k_{th} - k_R - k_P - k_S \quad (8.6)$$

where  $k = \Delta h / \frac{1}{2}\rho U^2$ , for example  $k_{th} = \Delta h_{th} / \frac{1}{2}\rho U^2$ .

From eqs. (8.1) and (8.4) it follows that  $(H_3 - H_0) / \frac{1}{2}\rho U^2$  is also the non-dimensional static pressure rise for the unit. Defining  $\epsilon$ , the swirl coefficient as  $\epsilon = \omega r / u$ , the static pressure rise across the fan rotor at radius,  $r$ , is then given by

$$p_2 - p_1 = \Delta p = \frac{1}{2}\rho U^2(k_{th} - k_R + \epsilon_p^2 - \epsilon_s^2) \quad (8.7)$$

since

$$H_2 - H_1 = \Delta h_{th} - \Delta h_R$$

The Bernoulli relationships having been discussed, it is now appropriate to consider the work done by the rotor. The output of work from the rotor in the elementary annulus is

$$(H_2 - H_1)2\pi r \cdot dr \cdot u \quad (8.8)$$

and the input is  $\Omega dQ$ , where  $\Omega$  is the rotational speed of the rotor in radians per second and  $dQ$  is the element of torque. From the rate of change of angular momentum,

$$dQ = \rho \cdot u \cdot 2\pi r \cdot dr (\omega_s r + \omega_p r) r \quad (8.9)$$

when the sign convention adopted at the commencement of this sub-section is observed.

Replacing  $(H_2 - H_1)$  by the theoretical total head rise in eq. (8.8) and equating the new relation to  $\Omega dQ$ ,

$$(H_2 - H_1 + \Delta h_R)2\pi r \cdot dr \cdot u = \rho \cdot u \cdot 2\pi r \cdot dr (\omega_s r + \omega_p r) \Omega r \quad (8.10)$$

and therefore

$$\Delta h_{th} = \rho \cdot \Omega r (\omega_s r + \omega_p r) \quad (8.11)$$

Non-dimensionally,

$$k_{th} = \frac{2}{\lambda} (\epsilon_s + \epsilon_p) \quad (8.12)$$

where the flow coefficient is defined by  $\lambda = u/\Omega r$ .

The resultant velocity vector,  $w_r$ , which determines the lift on the blade element, is shown in Fig. 8.2, together with the velocity components at inlet and outlet from the blade element.

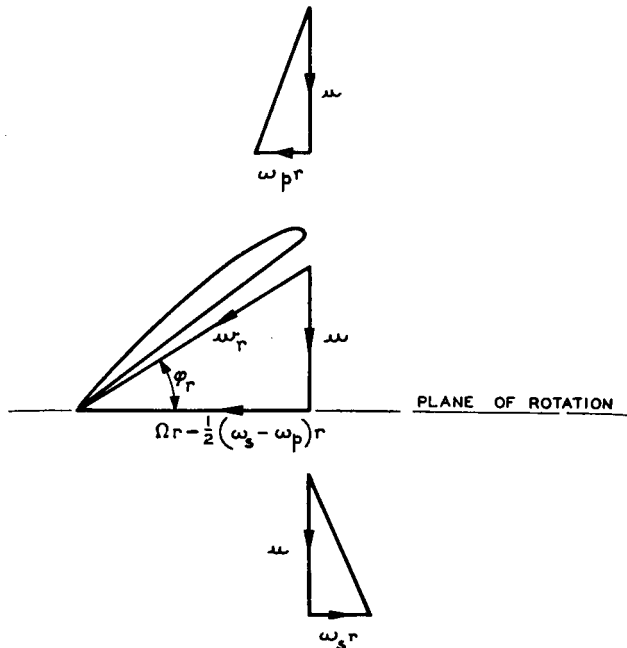


Fig. 8.2. Velocity vectors for rotor blade element

The tangential velocity component of the air relative to the blade is given by

$$\Omega r - \frac{1}{2}(\omega_s - \omega_p)r$$

where the second term is the mean swirl between the rotor inlet and outlet. The angle,  $\varphi_r$ , which the resultant velocity,  $w_r$ , makes with the plane of rotation is obtained from

$$\tan \varphi_r = \frac{u}{\Omega r - \frac{1}{2}(\omega_s - \omega_p)r} \quad (8.13)$$

or,

$$\tan \varphi_r = \frac{\lambda}{1 - \frac{1}{2}(\epsilon_s - \epsilon_p)\lambda} \quad (8.14)$$

Finally, it can be shown from eq. (8.11) that  $(\omega_s r + \omega_p r)$  is inversely proportional to the radius,  $r$ , when  $\Delta h_{th}$  is constant along the blade. It is usual to make one of these swirls zero or inversely proportional to the radius, and in this case the flow will satisfy the condition for free vortex flow (see Section 5.3).

#### 8.4. Blade Element Forces

From the force vector diagram, Fig. 8.3, it will be seen that the lift and drag may be expressed in terms of  $Y$  and  $X$ , the axial and tangential forces; these forces can be established from momentum changes.

The axial force,  $Y$ , is given by

$$Y = \Delta p \cdot s \cdot dr \quad (8.15)$$

where  $s$  is the gap defined by  $2\pi r/N$ , and  $N$  is the number of blades.

The rate of change of swirl momentum gives the tangential force,  $X$ , as

$$\begin{aligned} X &= s \cdot \rho \cdot u (\omega_s r + \omega_p r) dr \\ &= s \cdot \rho \cdot u^2 (\epsilon_s + \epsilon_p) dr \end{aligned} \quad (8.16)$$

From Fig. 8.3, the drag of a blade element is

$$D = X \cos \varphi_r - Y \sin \varphi_r \quad (8.17)$$

and substituting for  $X$  and  $Y$ ,

$$D = s \cdot \rho \cdot u^2 (\epsilon_s + \epsilon_p) dr \cdot \cos \varphi_r - s \cdot \Delta p \cdot dr \cdot \sin \varphi_r$$

Substituting for  $\Delta p$  from eq. (8.7), writing  $u/w_r$  as  $\sin \varphi_r$  (see Fig. 8.2) and dividing by  $\frac{1}{2}\rho w_r^2 c dr$ , in order to obtain a drag coefficient,

$$\begin{aligned} C_D &= \frac{s}{c} \sin^2 \varphi_r [2(\epsilon_s + \epsilon_p) \cos \varphi_r - (k_{th} - \epsilon_s^2 + \epsilon_p^2) \sin \varphi_r] \\ &\quad + \frac{s}{c} k_R \sin^3 \varphi_r \end{aligned}$$

Eliminating  $k_{th}$  by eq. (8.12) and using eq. (8.14),

$$C_D = 2 \frac{s}{c} \sin^2 \varphi_r (\epsilon_s + \epsilon_p) \left( \cos \varphi_r - \frac{\sin \varphi_r}{\tan \varphi_r} \right) + \frac{s}{c} k_R \sin^3 \varphi_r$$

and hence

$$C_D = \frac{s}{c} k_R \sin^3 \varphi_r \quad (8.18)$$

Similarly, the lift is

$$\begin{aligned} L &= X \sin \varphi_r + Y \cos \varphi_r \\ &= s \cdot \rho \cdot u^2 (\epsilon_s + \epsilon_p) dr \cdot \sin \varphi_r + s \cdot \Delta p \cdot dr \cdot \cos \varphi_r \end{aligned} \quad (8.19)$$

and hence

$$\begin{aligned} C_L &= \frac{s}{c} \sin^2 \varphi_r [2(\epsilon_s + \epsilon_p) \sin \varphi_r + (k_{th} - \epsilon_s^2 + \epsilon_p^2) \cos \varphi_r] \\ &\quad - \frac{s}{c} k_R \sin^2 \varphi_r \cos \varphi_r \end{aligned}$$

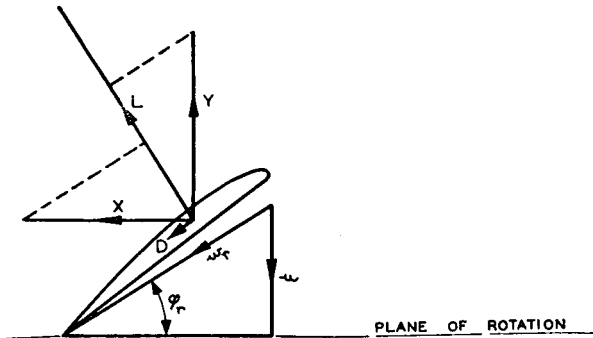


Fig. 8.3. Force vector diagram for rotor blade element

Making substitutions similar to the previous ones and using eq. (8.18),

$$C_L = 2 \left( \frac{s}{c} \right) (\epsilon_s + \epsilon_p) \sin \varphi_r - C_D \cot \varphi_r \quad (8.20)$$

or,

$$C_L \sigma = 2(\epsilon_s + \epsilon_p) \sin \varphi_r - \sigma C_D \cot \varphi_r \quad (8.21)$$

where  $\sigma = c/s$  = solidity.

## 8.5. Thrust and Torque Gradients

The element of thrust developed by the blade element due to the flow in the annulus is

$$dT = \Delta p \cdot 2\pi r \cdot dr$$

Defining a thrust coefficient,  $T_c$ , as

$$T_c = \frac{T}{\frac{1}{2}\rho U^2 \pi R^2} \quad (8.22)$$

where  $R$  is the tip radius,

$$dT_c = \frac{\Delta p}{\frac{1}{2}\rho U^2} \cdot 2x \cdot dx \quad (8.23)$$

where  $r/R = x$ .

Substituting from eq. (8.7),

$$\frac{dT_c}{dx} = 2x(k_{th} - k_R + \epsilon_p^2 - \epsilon_s^2) \quad (8.24)$$

The element of torque is given by eq. (8.9), and when a torque coefficient is defined as

$$Q_c = \frac{Q}{\frac{1}{2}\rho U^2 \pi R^3} \quad (8.25)$$

it follows that

$$\frac{dQ_c}{dx} = 4x^2(\epsilon_s + \epsilon_p) \quad (8.26)$$

## 8.6. Design Equations

In the foregoing, a number of simple design equations have been derived from momentum considerations. These are :

$$k_{th} = \frac{2}{\lambda} (\epsilon_s + \epsilon_p) \quad (8.12)$$

$$\tan \varphi_r = \frac{\lambda}{1 - \frac{1}{2}(\epsilon_s - \epsilon_p)\lambda} \quad (8.14)$$

$$C_L \sigma = 2(\epsilon_s + \epsilon_p) \sin \varphi_r - \sigma C_D \cot \varphi_r \quad (8.21)$$

The term  $\sigma C_D \cot \varphi_r$  is usually small and can often be ignored, giving

$$C_L \sigma = 2(\epsilon_s + \epsilon_p) \sin \varphi_r \quad (8.27)$$

The use of these equations is demonstrated in Section 18.

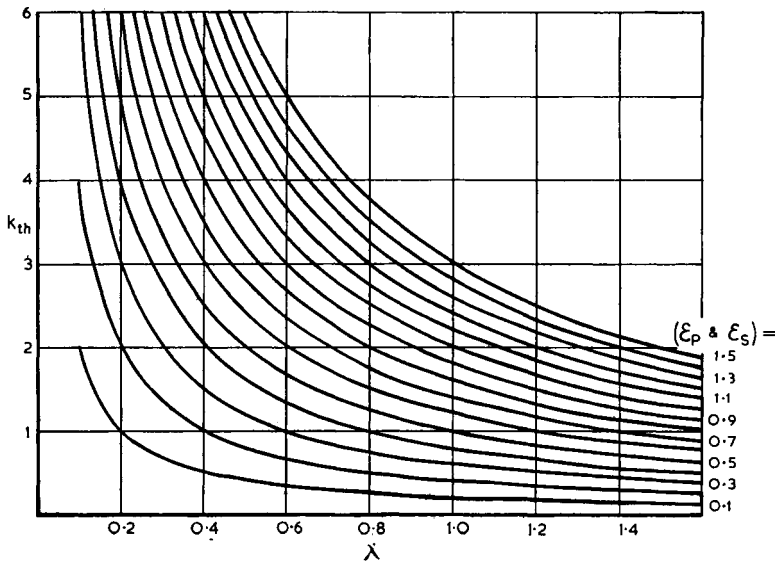


Fig. 8.4. Variation of  $k_{th}$  with  $\lambda$  and  $\epsilon$

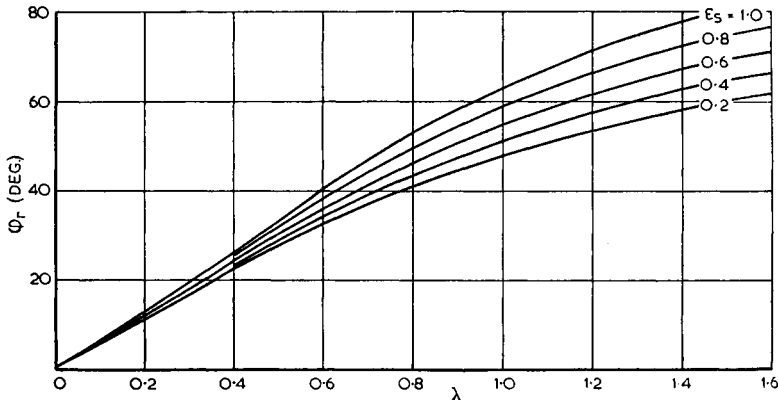
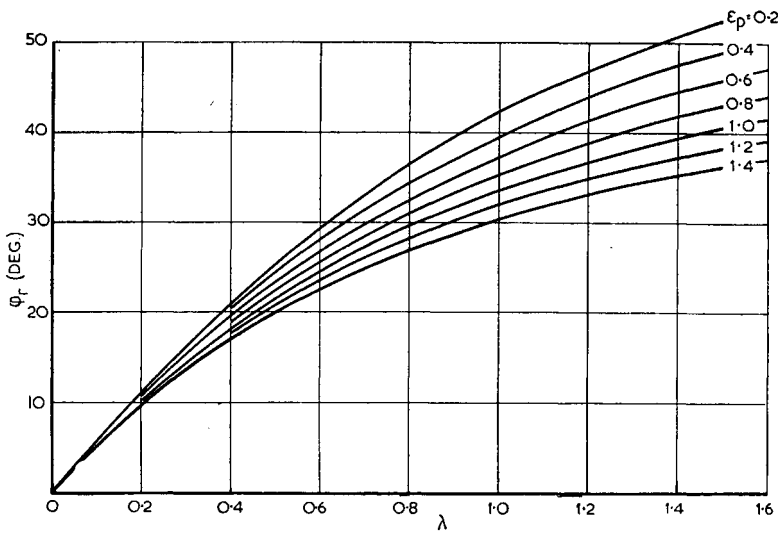
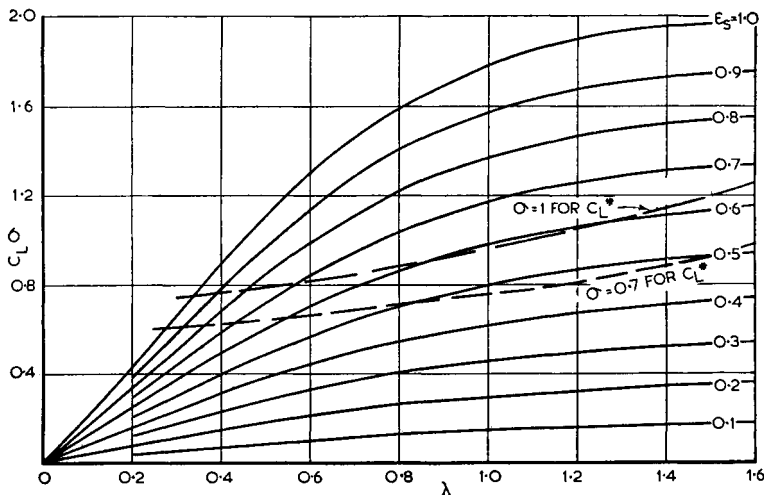


Fig. 8.5. Variation of flow angle  $\varphi_r$  with  $\lambda$  and  $\epsilon_s$ ,  $\epsilon_p = 0$

Fig. 8.6. Variation of flow angle  $\phi_r$  with  $\lambda$  and  $\epsilon_p$ ,  $\epsilon_s = 0$ Fig. 8.7. Product of  $C_L$  and  $\sigma$ ,  $\epsilon_p = 0$

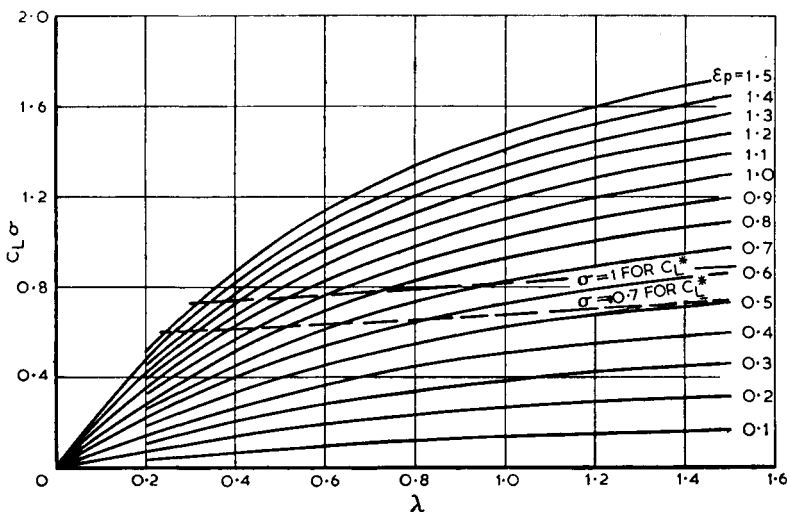


Fig. 8.8. Product of  $C_L$  and  $\sigma$ ,  $\epsilon_s = 0$

When either  $\epsilon_s$  or  $\epsilon_p$  is zero, these equations can be presented in simple graphical form (Figs. 8.4 to 8.8).

Equations (8.18), (8.24) and (8.26) are used subsequently in determining efficiency, thrust and torque respectively.

# 9

---

# ROTOR: BLADE ELEMENT CONSIDERATIONS FREE VORTEX FLOW

## 9.1. Introduction to Blade Element Design

Consideration can now be given to the blade element, whose function it is to produce the detailed flow changes discussed in the previous Section.

For low pressure rise fans, it is appropriate to consider each blade element as an isolated two-dimensional aerofoil (see Section 7.6). Production considerations often influence the choice of blade section. The RAF 6 and the Clark Y series of aerofoils are very popular as both possess a flat undersurface and are capable of high efficiency operation. When cheapness of construction is more important than the attainment of the highest possible efficiency, cambered plates of constant thickness, twisted from root to tip, are often used.

Because of its versatility and sound basis, the British cascade design method has been adopted for high pressure rise fans. The method predicts the optimum solidity and defines the blade camber line which is subsequently "clothed" with a symmetrical aerofoil section whose chord line is "bent" around the camber line.

The appropriate design method can be chosen according to the recommendations of Section 9.7.

## 9.2. Design of a Blade Element, Isolated Aerofoil Design Method

Provided the proposed design conforms with the recommendations of Section 9.7, a blade element can be designed in the following manner. When  $\epsilon_s$ ,  $\epsilon_p$  and  $\lambda$  are known,  $\varphi_r$  can be calculated and eq. (8.27) solved by assuming either  $C_L$  or  $\sigma$ . For a chosen aerofoil section, the angle of incidence,  $\alpha$ , corresponding to the design  $C_L$  can be obtained from aerofoil data (see Section 4.8). The aerofoil chord is given by

$$c = \frac{2\pi r}{N} \sigma \quad (9.1)$$

and sufficient data are now available to permit blade construction (see Fig. 9.1).

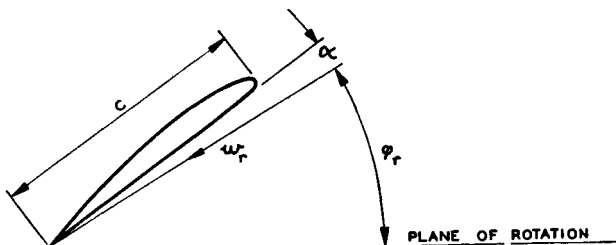


Fig. 9.1. Geometric details of blade element, isolated aerofoil method

In choosing the lift coefficient, it should be remembered that high efficiency is dependent on a large lift/drag ratio (see Section 10); the maximum ratio is reached just after the profile drag starts to rise appreciably with incidence. In addition, consideration must be given to the probable operating requirements. When the fan is designed for its maximum loading, a relatively large  $C_L$  may be used, while a conservative value is appropriate when some doubt exists concerning the magnitude of the maximum load. In this manner, the risk of blade stalling is minimized.

## 9.3. Optimum Loading, Cascade Design Method

In the cascade design method here employed, designing begins with a prediction of optimum conditions. With

increasing static pressure rise across the fan rotor, there is a sudden rapid increase in drag just prior to blade stalling. Maximum efficiency is obtained just before this rapid increase occurs.

Consider the relative velocity diagrams at inlet to and outlet from the blade element (Fig. 9.2).

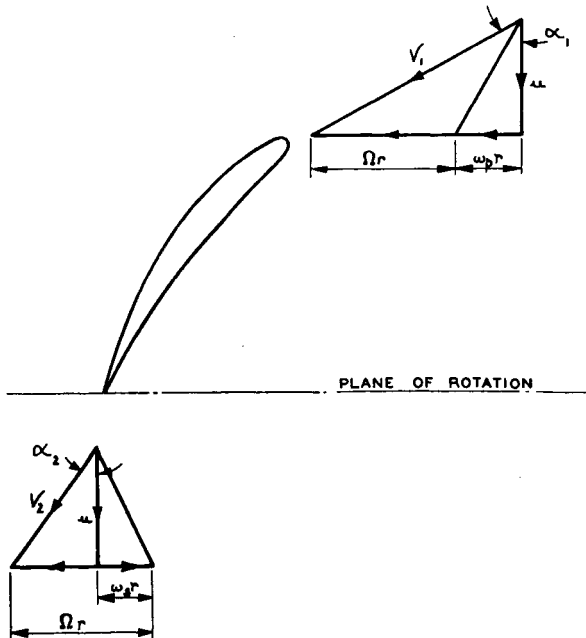


Fig. 9.2. Velocity vectors for rotor blade element

Optimum conditions are assumed to be reached when the deflection ( $\alpha_1 - \alpha_2$ ) for a given solidity is approximately 0.80 of the maximum, whose magnitude is dictated by blade stalling phenomena.

The inlet and outlet angles,  $\alpha_1$  and  $\alpha_2$  respectively, are two of the major variables. In determining the sign of the angles, the convention<sup>(63)</sup> that  $(\alpha_1 - \alpha_2)$  is always positive is accepted. It can be shown that  $\alpha_1$  is always positive for a retarding cascade and  $\alpha_2$  always negative for an accelerating one. For the type of rotor design considered here, the inlet angle is always positive, and provided  $(\epsilon_s \lambda)$  is less than unity  $\alpha_2$  will also be positive.

These angles are related to the swirl and flow coefficients (see Fig. 9.2) in the following manner :

$$\tan \alpha_1 = \frac{1 + \epsilon_p \lambda}{\lambda} \quad (9.2)$$

$$\tan \alpha_2 = \frac{1 - \epsilon_s \lambda}{\lambda} \quad (9.3)$$

$$\tan \alpha_1 - \tan \alpha_2 = \epsilon_s + \epsilon_p \quad (9.4)$$

From eq. (8.14) and the above it can also be shown that

$$\cot \varphi_r = \frac{1}{2}(\tan \alpha_1 + \tan \alpha_2) \quad (9.5)$$

Eq. (8.27) can then be rewritten

$$C_L = \frac{2}{\sigma} (\tan \alpha_1 - \tan \alpha_2) \sin \varphi_r \quad (9.6)$$

or,

$$C_L = \frac{2}{\sigma} (\tan \alpha_1 - \tan \alpha_2) \sin \cot^{-1} [\frac{1}{2}(\tan \alpha_1 + \tan \alpha_2)] \quad (9.7)$$

The remainder of this sub-section will be devoted to presentation of the recommended design relationships between  $C_L$ ,  $\sigma$ ,  $\alpha_1$  and  $\alpha_2$ .

Extensive experimental work on cascades of cambered aerofoils has shown that the optimum lift coefficient,  $C_{L^*}$ , can be expressed in terms of the inlet and outlet angles,  $\alpha_1$  and  $\alpha_2$ . Two such expressions, one from Howell<sup>(64, 65)</sup> and the other from Carter,<sup>(66)</sup> are :

$$C_{L^*} = 2 \left[ \frac{\cos \alpha_1}{\cos \alpha_2} \right]^{2.75} \quad (9.8)$$

and

$$C_{L^*} = 1.35 \left[ \frac{\cos \alpha_m}{\cos \alpha_2} \right]^2 \quad (9.9)$$

where  $\alpha_m$  is the complement of  $\varphi_r$ .

The first is based on the static pressure rise through a row of blades. Using Bernoulli's equation, it follows from Fig. 9.2 that the theoretical pressure rise is equal to the change in dynamic pressure, i.e.

$$\Delta p_{th} = \frac{1}{2} \rho V_1^2 - \frac{1}{2} \rho V_2^2 \quad (9.10)$$

(Alternatively, this relation can be obtained by combining eqs. (8.7) and (8.11) and using the vector diagrams of Fig. 9.2.) The expression from which eq. (9.8) was developed is therefore

$$C_L^* = 2 \left[ 1 - \frac{\Delta p_{th}}{\frac{1}{2} \rho V_1^2} \right]^{1.375} \quad (9.11)$$

The greater the static pressure rise, the smaller is the permissible  $C_L$ .

The relation (9.9) is obtained by assuming the lift coefficient, based on  $\frac{1}{2} \rho V_2^2$ , to be constant. This is roughly equivalent to assuming similar pressure distributions when the outlet velocity  $V_2$  is used in reducing them to non-dimensional form.

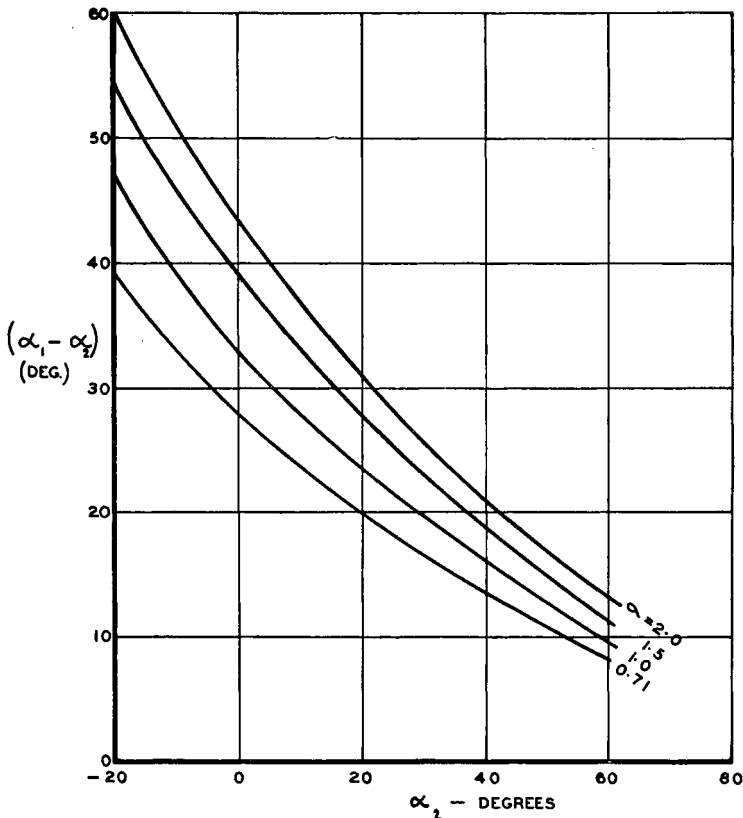


Fig. 9.3. Relations from Howell

When the optimum  $C_L$  is introduced into eq. (9.7), various relationships can be established between  $\alpha_1$ ,  $\alpha_2$  and  $\sigma$ . The one given by Carter is

$$\frac{1}{\sigma} \left( \frac{6/\sigma}{(6/\sigma) - 1} \right) (\tan \alpha_1 - \tan \alpha_2) \frac{\cos^2 \alpha_2}{\cos \alpha_m} = 0.675 \quad (9.12)$$

where allowances have been made for blade thickness.

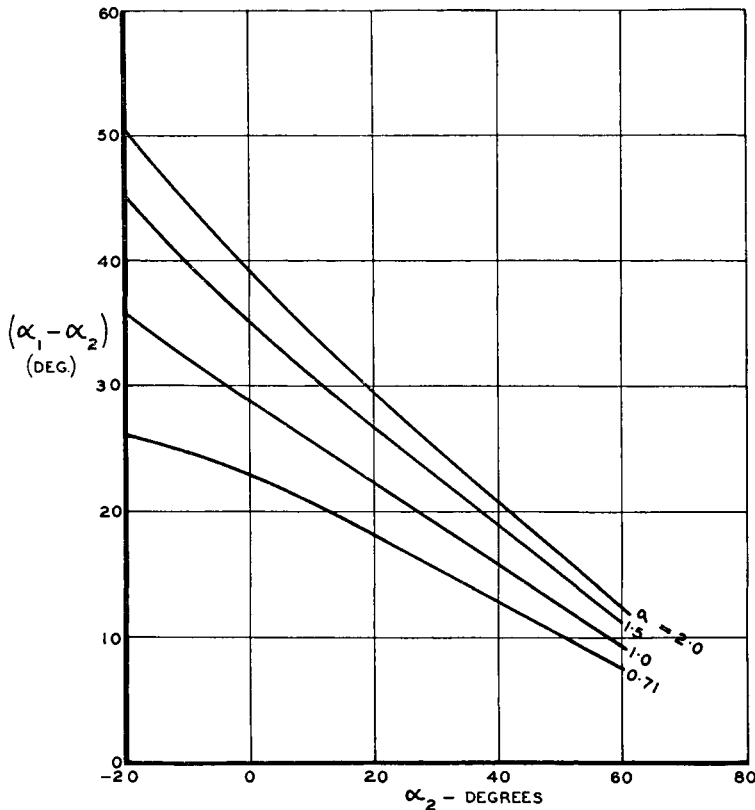


Fig. 9.4. Relations from Carter

One of the basic plots in the cascade design method is that giving the optimum solidity as a function of  $\alpha_2$  and  $(\alpha_1 - \alpha_2)$ . Three such graphs are presented in Figs. 9.3 to 9.5; the last-mentioned contains data supplied by a British firm engaged in designing and building jet engines. There are detailed differ-

ences which might be significant in compressor design but which are probably unimportant in relation to the high pressure rise fan provided it operates under reasonably favourable conditions. These relations, by fixing the solidity, suggest the lift coefficient at which the blade should operate. From Section 9.5 it will be seen that the blade camber line design is mainly dependent on relative flow angles and therefore small differences in design  $C_L$  will have only a minor influence on blade design details.

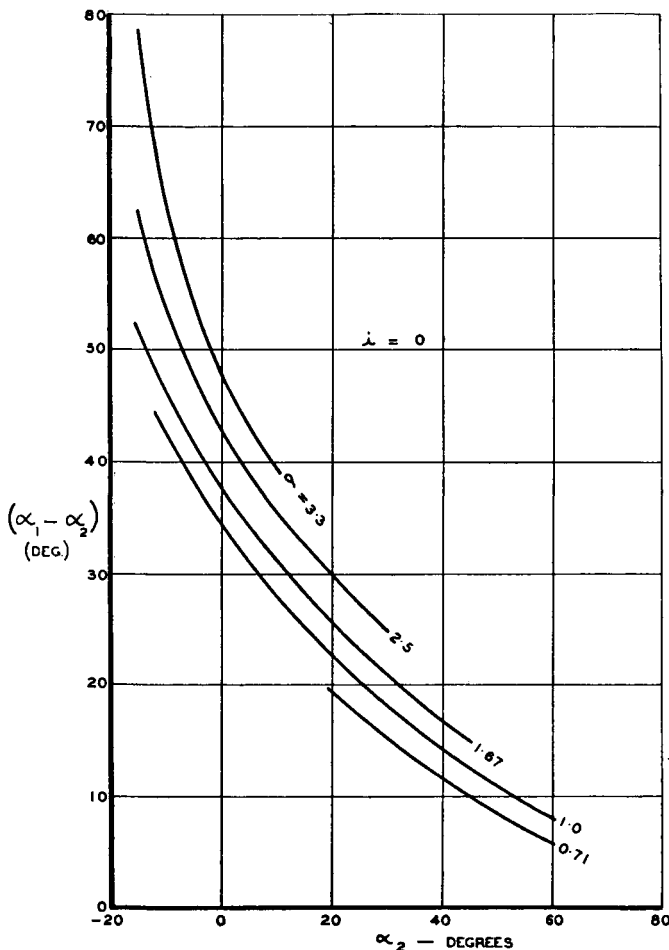


Fig. 9.5. Relations from a British engine firm

It is possible to plot  $C_L^*$  and  $(\tan \alpha_1 - \tan \alpha_2)$  as functions of  $\alpha_2$  and  $\sigma$ . Figs. 9.6 to 9.8 result from the use of the expression given in eq. (9.8).

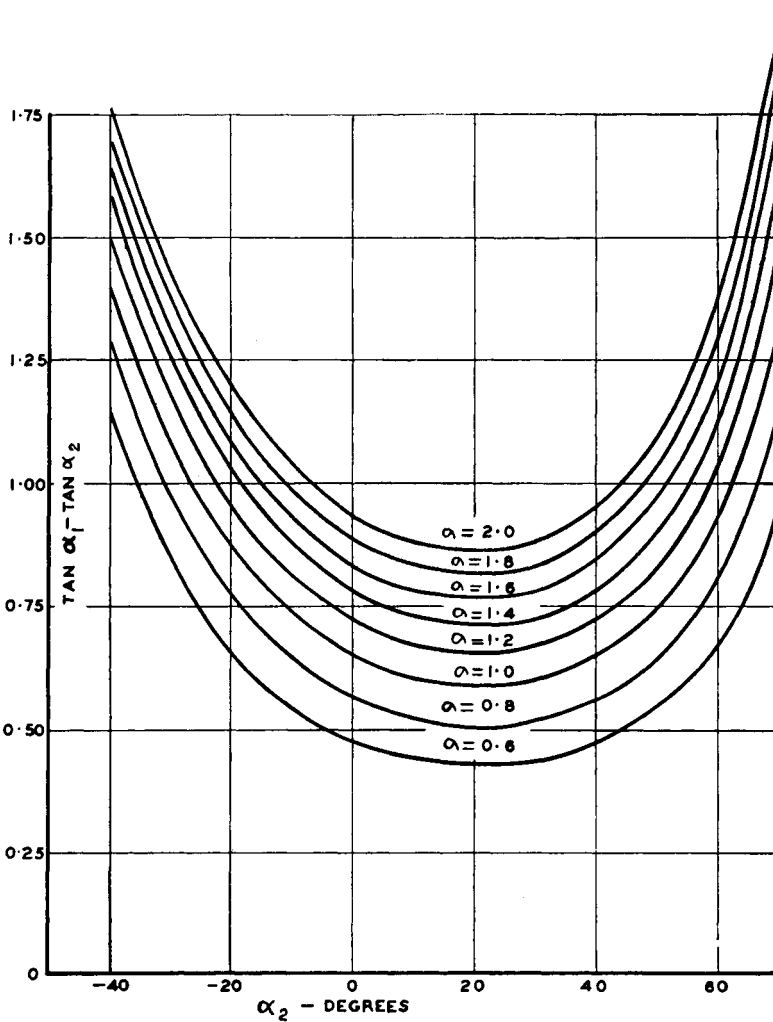


Fig. 9.6. Howell relations for optimum solidity

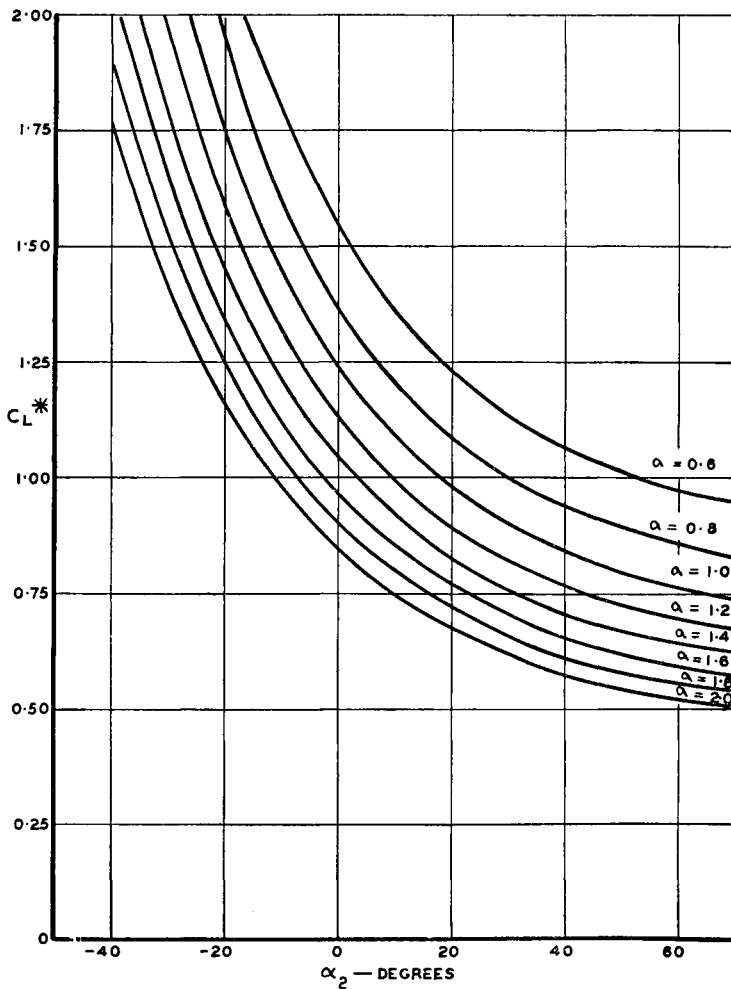


Fig. 9.7. Howell relations for optimum lift coefficient

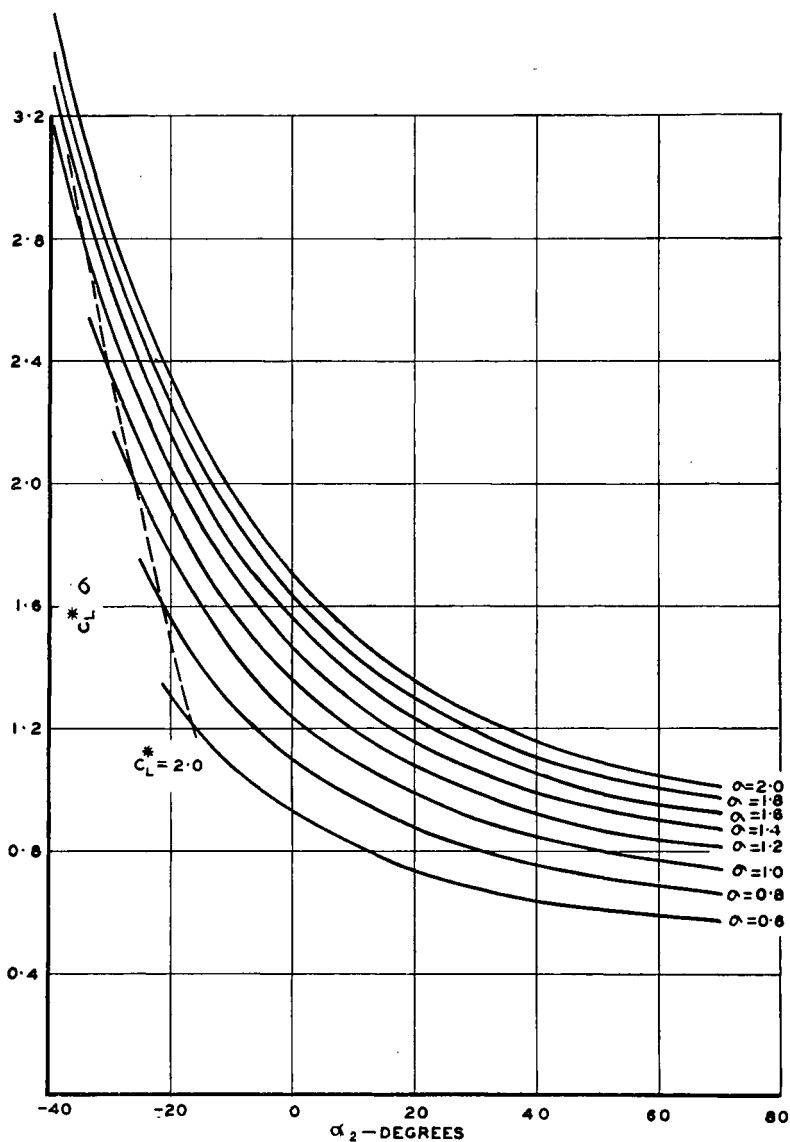


Fig. 9.8. Howell relations for product of  $C_L$  and  $\sigma$

## 9.4. Optimum Conditions in Terms of the Flow and Swirl Coefficients

Optimum values of  $C_L$  and  $\sigma$  can be expressed as functions of  $\epsilon$  and  $\lambda$  from the relations given in the previous sub-section. The following results have been obtained from use of the Howell relationship :

Eq. (9.8) can be written

$$C_L^* = 2 \left[ \frac{1 + \tan^2 \alpha_2}{1 + \tan^2 \alpha_1} \right]^{1.375}$$

and hence

$$C_L^* = 2 \left[ \frac{1 + \left( \frac{1 - \epsilon_s \lambda}{\lambda} \right)^2}{1 + \left( \frac{1 + \epsilon_p \lambda}{\lambda} \right)^2} \right]^{1.375} \quad (9.13)$$

When either  $\epsilon_p$  or  $\epsilon_s$  is zero, which is usually the case, eq. (9.13) reduces to

$$C_L^* = 2 \left[ \frac{1 + \left( \frac{1 - \epsilon_s \lambda}{\lambda} \right)^2}{1 + \left( \frac{1}{\lambda} \right)^2} \right]^{1.375} \quad (9.14)$$

and

$$C_L^* = 2 \left[ \frac{1 + \left( \frac{1}{\lambda} \right)^2}{1 + \left( \frac{1 + \epsilon_p \lambda}{\lambda} \right)^2} \right]^{1.375} \quad (9.15)$$

Optimum values of  $C_L$  and  $\sigma$  are plotted as functions of  $\epsilon$  and  $\lambda$  in Figs. 9.9 to 9.12. The limits of  $\sigma$  between which the design method is applicable are indicated.

It will be appreciated that the data given in Section 9.3 have been evolved with the express purpose of designing high efficiency axial flow compressors and that a relatively high  $C_L$  has therefore been used. Hence in designing fans care should be taken to ensure reasonable fan inlet and outlet conditions, and to avoid under-estimation of the pressure rise required. When any doubt exists, solidities in excess of the optimum should be chosen. If kept within limits, this will not affect the accuracy of the subsequent design.

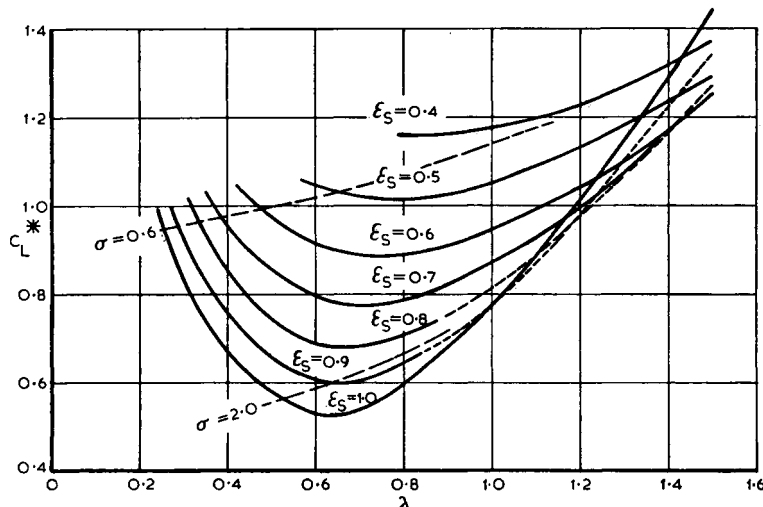


Fig. 9.9. Optimum lift coefficient,  $\epsilon_p = 0$ : cascade method

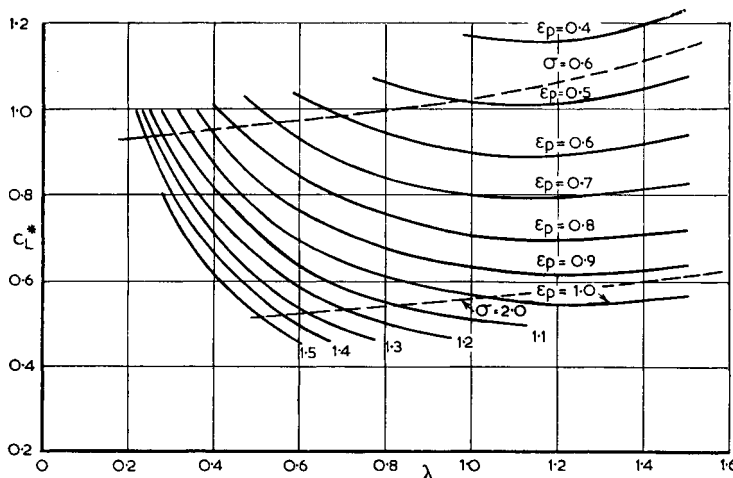


Fig. 9.10. Optimum lift coefficient,  $\epsilon_s = 0$  cascade method

**148 ROTOR: BLADE ELEMENT CONSIDERATIONS, FREE VORTEX FLOW**

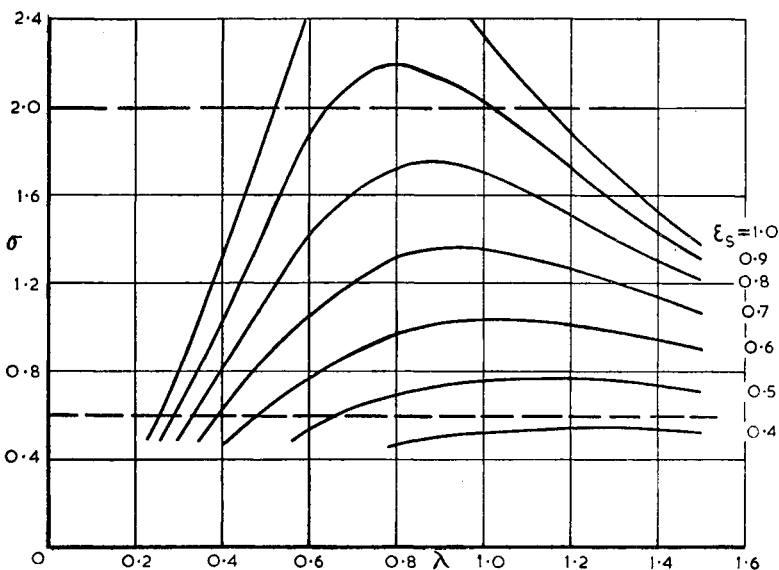


Fig. 9.11. Optimum solidity,  $\epsilon_p=0$ : cascade method

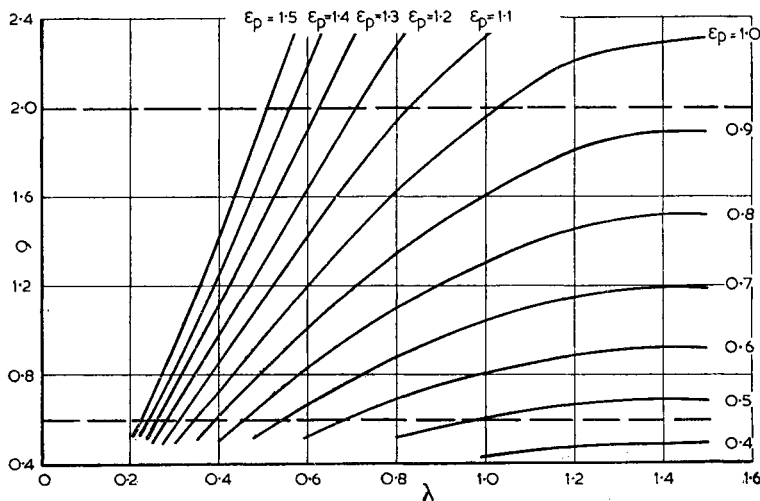


Fig. 9.12. Optimum solidity,  $\epsilon_s=0$ : cascade method

## 9.5. Design of a Camber Line, Cascade Design Method

The design method of this sub-section differs from that of 9.2 in that no direct use is made of the design  $C_L$  or of the usual aerofoil characteristics. Instead, once the optimum solidity is known, the design centres around the development of a camber line which will give the correct air deflection corresponding to the desired pressure rise. Circular arc type camber lines only will be treated here, as these are the most common variety.

The main variables involved in determining the blade shape are given in Fig. 9.13.

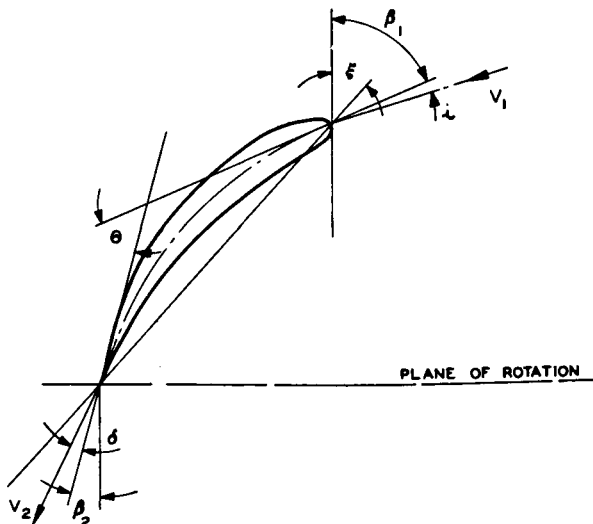


Fig. 9.13. Geometric details of blade element, cascade method

At the leading and trailing edges of the blade, the tangents to the camber line make angles of  $\beta_1$  and  $\beta_2$  respectively with the axial direction. The angle between the axial direction and the line joining the leading and trailing edges is known as the stagger angle,  $\xi$ .

When the inlet and outlet flows are assumed to make angles of  $i$  and  $\delta$  with the local tangents, the camber angle,  $\theta$ , is given by (see Figs. 9.2 and 9.13)

$$\theta = \beta_1 - \beta_2 = (\alpha_1 - i) - (\alpha_2 - \delta) \quad (9.16)$$

Provided the incidence,  $i$ , remains within the limits  $\pm 5^\circ$ , the outlet angle,  $\alpha_2$ , is not sensibly altered.<sup>(54)</sup> For this range of incidence, the angle of deviation,  $\delta$ , is given approximately by Constant's rule<sup>(67)</sup>

$$\delta = 0.26\theta \sqrt{\frac{s}{c}} \quad (9.17)$$

Substituting for  $\delta$  in eq. (9.16),

$$\theta = \frac{(\alpha_1 - \alpha_2) - i}{1 - 0.26\sqrt{(s/c)}} \quad (9.18)$$

In addition, the stagger angle is given by (see Fig. 9.13)

$$\xi = \beta_1 - \frac{\theta}{2} \quad (9.19)$$

In design, it is usually desirable and convenient to make  $i=0$ . When  $\epsilon_p$  or  $\epsilon_s$  is zero, and the relations of eqs. (9.2) and (9.3) are used, the camber and stagger angles are given by

$$\epsilon_p = 0 \quad \left\{ \begin{array}{l} \theta = \frac{\tan^{-1} \frac{1}{\lambda} - \tan^{-1} \left( \frac{1 - \epsilon_s \lambda}{\lambda} \right)}{1 - 0.26\sqrt{(s/c)}} \\ \xi = \tan^{-1} \frac{1}{\lambda} - \frac{\theta}{2} \end{array} \right. \quad (9.20)$$

$$\epsilon_s = 0 \quad \left\{ \begin{array}{l} \theta = \frac{\tan^{-1} \left( \frac{1 + \epsilon_p \lambda}{\lambda} \right) - \tan^{-1} \frac{1}{\lambda}}{1 - 0.26\sqrt{(s/c)}} \\ \xi = \tan^{-1} \left( \frac{1 + \epsilon_p \lambda}{\lambda} \right) - \frac{\theta}{2} \end{array} \right. \quad (9.22)$$

$$(9.23)$$

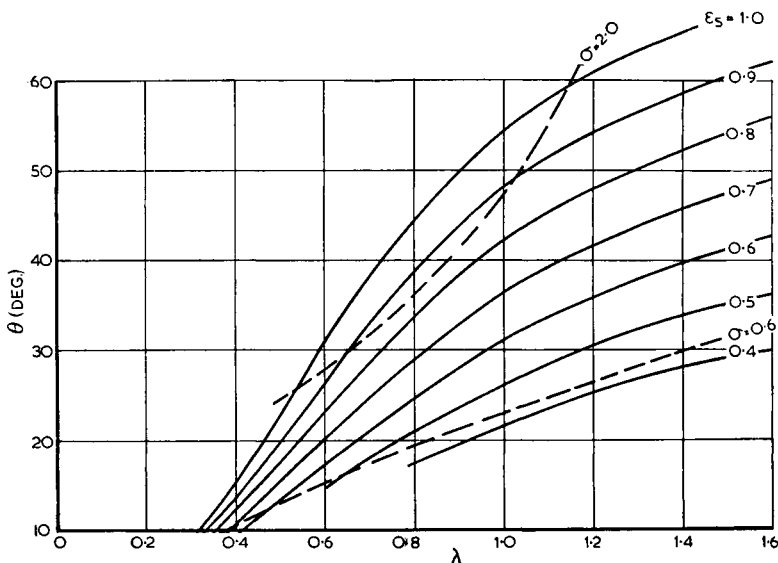
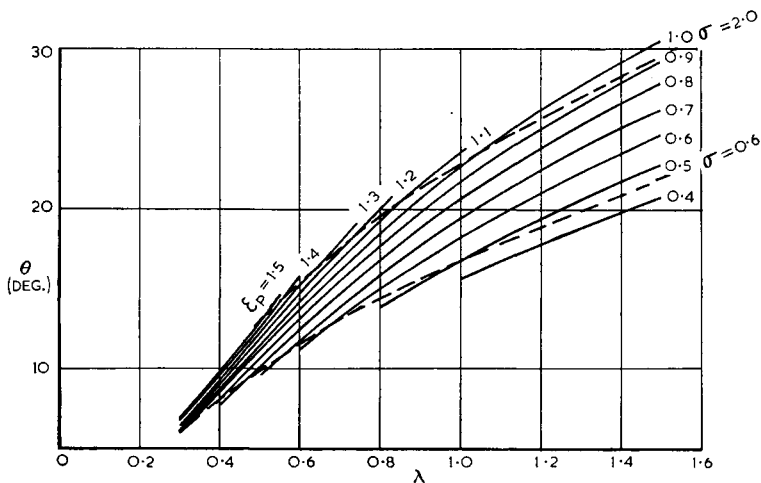
When the optimum solidity is used in design, these angles can be expressed in terms of the swirl and flow coefficients (Figs. 9.14 to 9.17).

The camber,  $\theta$ , can be expressed alternatively as

$$\frac{\text{Rad. of curvature}}{c} = \frac{1}{2 \sin \frac{\theta}{2}} \quad (9.24)$$

or

$$\frac{b}{c} = \frac{1}{2} \tan \frac{\theta}{4} \quad (9.25)$$

Fig. 9.14. Camber angle for cascade aerofoil,  $\epsilon_p = 0$ Fig. 9.15. Camber angle for cascade aerofoil,  $\epsilon_s = 0$

**152 ROTOR: BLADE ELEMENT CONSIDERATIONS, FREE VORTEX FLOW**

where  $b$  is the camber height measured from the chord line.

For the range,  $\theta = 0$  to  $50^\circ$ , eq. (9.25) can be approximated by

$$\frac{b}{c} = 0.00221\theta \quad (9.26)$$

For example, if  $\theta = 40^\circ$ ,  $\frac{b}{c} = 0.0884$ .

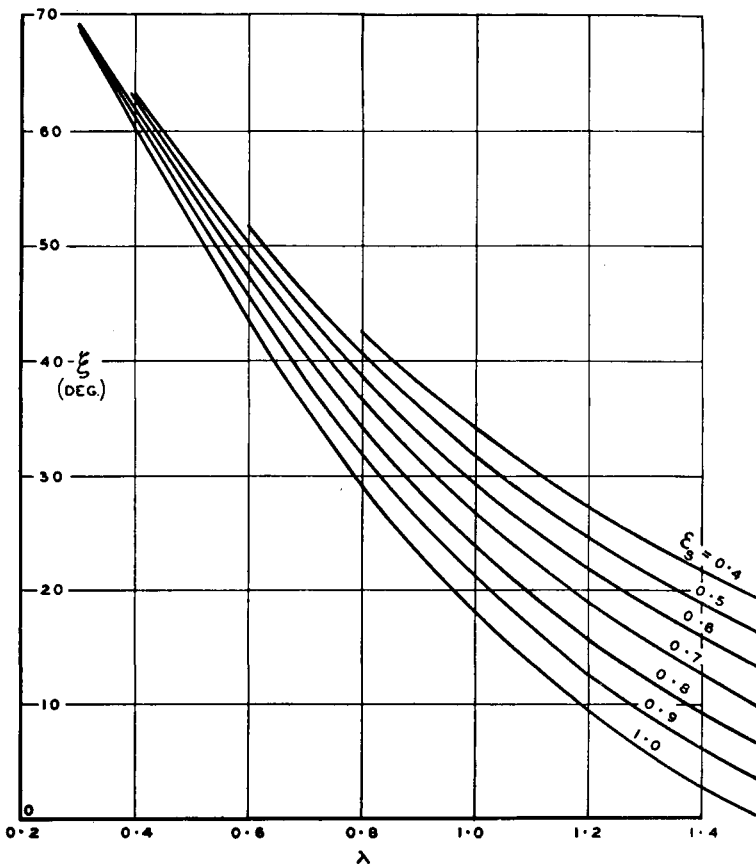
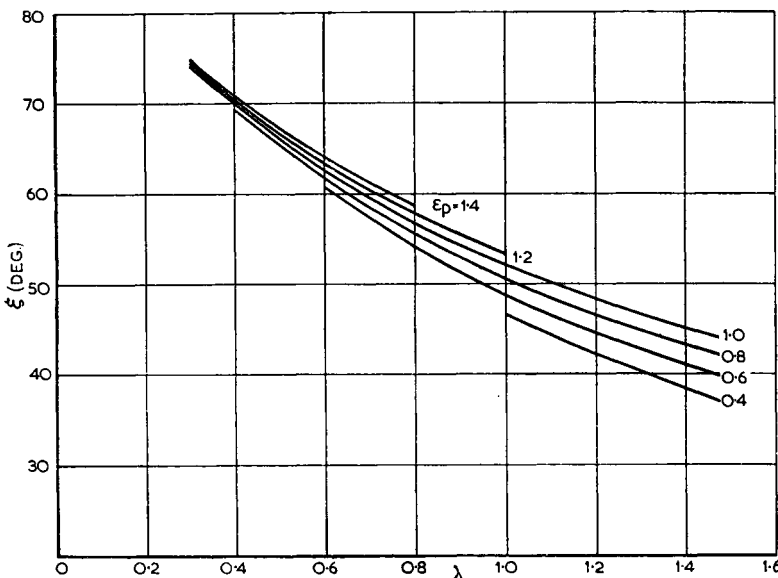


Fig. 9.16. Stagger angle for cascade aerofoil,  $\epsilon_p = 0$

Fig. 9.17. Stagger angle for cascade aerofoil,  $\epsilon_s = 0$ 

## 9.6. Clothing the Camber Line, Cascade Design Method

It is normal practice to choose a symmetrical aerofoil section and set out the co-ordinates along the curved camber line. A popular section is the C4, which is the fourth of a series of aerofoils developed for compressor work; details of the section are given in the Tables at the end of the book.

As an alternative, a constant thickness plate, rounded at the leading and trailing edges (Fig. 4.12), can be bent around the camber line. Although not as efficient as the C4 aerofoil section, cambered plate blades are simple and cheap to manufacture. They are usually assumed to behave in a fashion similar to orthodox aerofoils with the same camber, provided the inlet flow is approximately tangential to the leading edge of the blade. When the angle of incidence,  $i$ , exceeds  $\pm 3^\circ$ , local flow separations at the leading edge will reduce efficiency and lead to possible "underturning" of the air. These effects are, however, not serious enough to restrict the usefulness of such fans in industrial installations.

## 9.7. Choice of Appropriate Design Method

It is apparent that, in view of the limited experimental data available, no single design method can cover the entire range of ducted axial flow fans. Multiplane interference prevents the use of the isolated aerofoil design method for solidities much above unity, while the cascade design method cannot be used for solidities much less than 2/3. The problem which arises, therefore, is the fixing of a nominal boundary between the two methods.

Information available concerning multiplane interference is not completely satisfactory. Collar<sup>(50)</sup> suggests, however, that when  $\varphi_r$  is approximately 40° and the solidity less than unity, the interference between adjacent blades is small. For a given solidity, the actual lift coefficient for a  $\varphi_r$  greater than 40° is liable to be less than for the isolated aerofoil and vice versa.

It is difficult to say how much importance should be attached to these assumptions. Detailed experiments<sup>(68)</sup> on a fan designed by the isolated aerofoil method showed satisfactory agreement with theory although the values of  $\sigma$  and  $\varphi_r$  at the blade root were in excess of those given above. With a much larger boss ratio than the 0.5 which was used in the experiments, however, appreciable discrepancies might arise.

Observance of the following general rule should ensure a satisfactory design: if the product of the lift coefficient and solidity for a given blade element lies above the lines of unit solidity given in Figs. 8.7 and 8.8, the cascade method of design should be employed; below the lines of  $\sigma=0.7$ , the isolated aerofoil method is the appropriate one. These lines of constant solidity were obtained by using the optimum lift coefficients as determined from the cascade method. Between the lines  $\sigma=1$  and  $\sigma=0.7$ , either method may be employed; in the case of straighteners only, i.e.  $\epsilon_p=0$ , the cascade method is preferable for values of  $\lambda$  greater than 0.8, as in this region  $\varphi_r$  may exceed 40° (Fig. 8.5) and loss of lift may result, as previously indicated.

The above recommendations apply to a specific blade element. When the rotor as a whole is considered, modifications may be necessary. The case of a rotor with a moderate boss ratio of 0.5 and high local loading at the root will be considered as an example. The greater portion of the blade can

be designed on the basis of the isolated aerofoil theory, but special attention must be paid to the root. Two alternatives suggest themselves :

- (i) The use of the cascade method near the blade root and the blending of the sections so obtained with a similar cambered aerofoil for which the two-dimensional characteristics are known. For example, the 10 per cent thick C4 and Clark Y sections both have similar ordinates and differ mainly in the shape of the camber line (see Figs. 4.12 and 4.13). A blending is therefore readily achieved.
- (ii) The use of the isolated aerofoil design method with suitable modifications at the root. These modifications may include (a) a small increase of blade angle relative to the plane of rotation in order to counter a possible loss of design lift at the root, and (b) a limitation on the lift coefficient used ; the optimum values given by the cascade method can be used as a guide.

As mentioned previously, rotors designed entirely by the cascade method tend to be high pressure rise fans with large boss ratios.

# 10

## ROTOR LOSSES

### 10.1. General

In Section 8, the rotor design method was developed in terms of the pressure coefficient  $k_{th}$ . Before this coefficient can be determined, however, rotor losses, among others, must be assessed.

The various sources of loss have already been introduced in Section 7.7; it is clear that the distribution of losses along the blade span will be far from regular. To overcome this difficulty, it is normal practice to ascertain the mean value of the losses and to assume a uniform distribution of these losses along the blade. As was indicated earlier, small inaccuracies are not critical in calculating efficiency in rotor design.

The rotor efficiency is given by

$$\eta_R = \frac{K_{th} - K_R}{K_{th}} \quad (10.1)$$

where  $K_R$  is the mean total head loss coefficient in the rotor as a whole.

An efficiency relationship in terms of the major parameters  $\lambda$  and  $\epsilon$  will now be developed for an elementary annulus.

### 10.2. Momentum Considerations

The drag relation obtained in Section 8 from momentum considerations is

$$C_D = \frac{s}{c} k_R \sin^3 \varphi_r \quad (8.18)$$

or

$$\frac{k_R}{C_D} = \frac{\sigma}{\sin^3 \varphi_r} \quad (10.2)$$

Multiplying by  $C_L/k_{th}$  and writing  $\gamma$  for  $C_L/C_D$ ,

$$\gamma \frac{k_R}{k_{th}} = \frac{C_L \sigma}{k_{th} \sin^3 \varphi_r}$$

Substituting for  $C_L \sigma$  (eq. 8.21) and  $k_{th}$  (eq. 8.12),

$$\gamma \frac{k_R}{k_{th}} = \frac{\lambda}{\sin^2 \varphi_r} - \frac{\sigma C_D \cot \varphi_r}{k_{th} \sin^3 \varphi_r}$$

and substituting for  $C_D$  (eq. 8.18),

$$(\gamma + \cot \varphi_r) \frac{k_R}{k_{th}} = \frac{\lambda}{\sin^2 \varphi_r} \quad (10.3)$$

Normally  $\cot \varphi_r$  will be small compared to  $\gamma$ , and eq. (10.3) may be written

$$\gamma \frac{k_R}{k_{th}} = \frac{\lambda}{\sin^2 \varphi_r} \quad (10.4)$$

For a given lift/drag ratio, therefore, the efficiency  $(1 - k_R/k_{th})$  of a blade element is a function of  $\lambda$  and  $\epsilon$ , since  $\varphi_r$  can be expressed in terms of these parameters (eq. 8.14). Figs 10.1 and 10.2 illustrate simple relationships which exist for the prerotorator-rotor and rotor-straightener design cases.

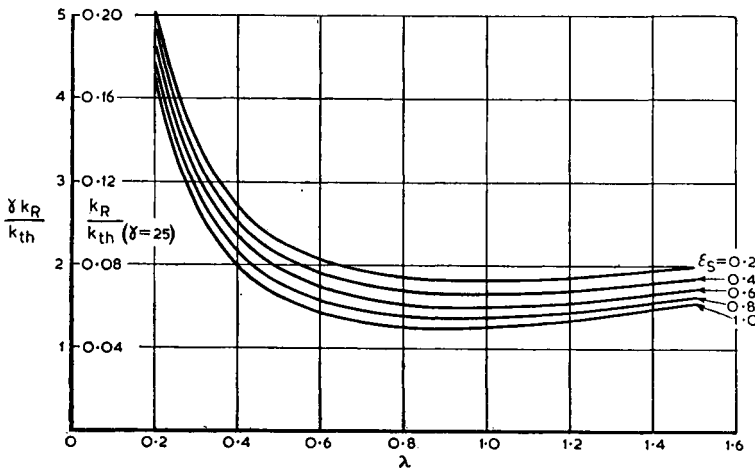


Fig. 10.1. Loss of efficiency in rotor blade element,  $\epsilon_p = 0$

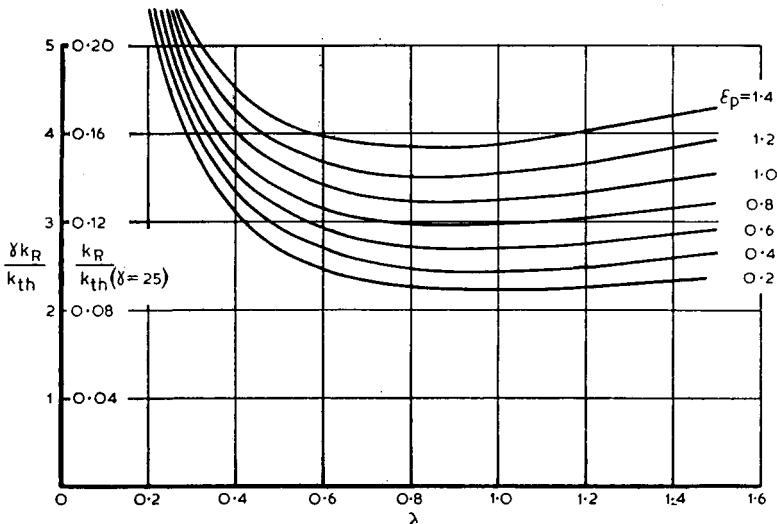


Fig. 10.2. Loss of efficiency in rotor blade element,  $\epsilon_s = 0$

### 10.3. Component Losses

A simple method of treating the various losses will now be outlined. The mean combined loss coefficient  $K_R$  can be written

$$K_R = K_{R_P} + K_{R_S} + K_{R_A} \quad (10.5)$$

where the coefficients refer to profile, secondary and annulus losses respectively.

Similarly,

$$C_D = C_{D_P} + C_{D_S} + C_{D_A} \quad (10.6)$$

It can readily be shown that eq. (10.4) may be written

$$\left( \frac{K_{R_P}}{K_{th}} + \frac{K_{R_S}}{K_{th}} + \frac{K_{R_A}}{K_{th}} \right) = \left( \frac{C_{D_P}}{C_L} + \frac{C_{D_S}}{C_L} + \frac{C_{D_A}}{C_L} \right) \frac{\lambda}{\sin^2 \varphi_r} \quad (10.7)$$

that is, each component loss can be considered independently and then summed. For example, the loss of efficiency due to profile drag is

$$\frac{K_{R_P}}{K_{th}} = \frac{C_{D_P}}{C_L} \frac{\lambda}{\sin^2 \varphi_r} \quad (10.8)$$

Since we are concerned only with the mean loss for the rotor as a whole, the values of  $\lambda$  and  $\epsilon$  at the midspan station are chosen as representative of the rotor. Estimates of the drag/lift ratios in eq. (10.7) will now be considered.

#### 10.4. Profile Drag

The estimation of efficiency loss due to profile drag will depend on whether the fan is designed by the isolated aerofoil or the cascade design method. In the former case, the drag coefficient can be ascertained from the experimental aerofoil data once the design midspan lift coefficient has been chosen (e.g. see Fig. 4.4). From the value of  $C_L/C_{D_p}$  thus obtained the loss in efficiency can be computed from eq. (10.8).

Limited data available on the drag of aerofoils in cascade<sup>(67)</sup> indicate that, for design conditions, the coefficient varies between 0.014 and 0.018 for  $s/c = 1.5$  and 0.5 respectively, at chord Reynolds numbers  $R_e > 3 \times 10^5$  (see Fig. 10.3). For  $R_e < 1 \times 10^5$ , the drag rises and it is suggested that the above values should be increased by 0.007.

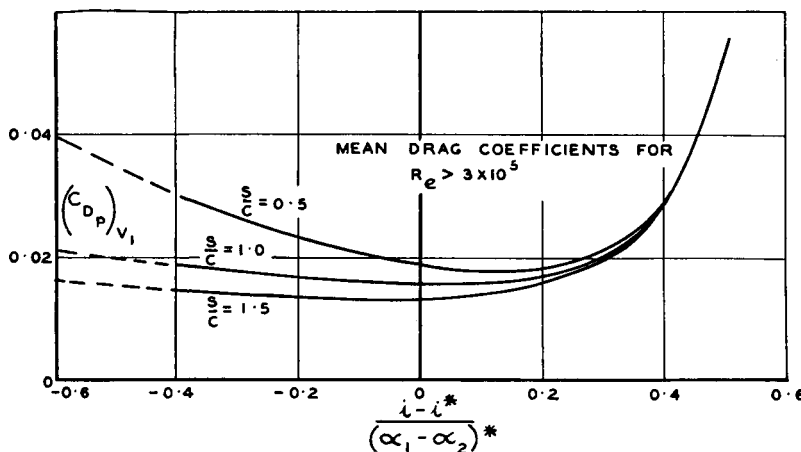


Fig. 10.3. Drag data for cascade aerofoils where asterisk refers to design values of variables

(Based on A.R.C. R. & M. 2095, and reproduced by permission of the Controller of H.M. Stationery Office)

These drag coefficients are with respect to the dynamic head at inlet to the blade, namely  $\frac{1}{2}\rho V_1^2$ . When the deflection of the air is small, the velocity  $V_1$  approximates to the mean relative velocity  $w_r$ . For convenience in comparing the relative merits of alternative designs it will be assumed in subsequent developments that the drag coefficients are with respect to  $\frac{1}{2}\rho w_r^2$ .

When both blade chord and thickness are held constant and the gap,  $s$ , is reduced, the flow suffers a constriction at the point of maximum thickness and this is followed by an increased diffusion as the flow approaches the trailing edge. This gives rise to the increase in drag with solidity as noted above.

When the blade has a rough surface, allowance must be made for the increase in profile drag.

### 10.5. Secondary Drag

From the comments of Section 7.7 it will be seen that very little is known quantitatively about the secondary losses. Howell<sup>(62)</sup> made efforts to correlate experimental  $C_{D_s}$  data with blade aspect ratio and gap/chord ratio as well as with  $C_L$ . The best results were obtained from the following relation :

$$C_{D_s} = a C_L^2 \quad (10.9)$$

where  $a$  is a function of chord Reynolds number only, and  $C_L$  is a mean value for the blade. The coefficient  $a$  varies from 0.019 at  $R_e = 1 \times 10^5$  to 0.015 at  $5 \times 10^5$ . As in the preceding subsection,  $C_{D_s}$  and  $C_L$  were determined with respect to  $\frac{1}{2}\rho V_1^2$ . The value of  $a$  most commonly used is 0.018,<sup>(67)</sup> that is,

$$C_{D_s} = 0.018 C_L^2 \quad (10.10)$$

Subsequent efforts by Carter<sup>(56, 69)</sup> using wall boundary layer parameters in addition to the variables investigated by Howell have not proved particularly successful. It is suggested, therefore, that, until the position is clarified, eq. (10.10) be adopted when conventional aerofoil sections are employed, and the following equation

$$C_{D_s} = 0.025 C_L^2 \quad (10.11)$$

when constant thickness sheet metal blades are used.<sup>(70)</sup> These equations appear to give results which are of the right order when  $C_{D_s}$  and  $C_L$  are assumed to be based on  $\frac{1}{2}\rho w_r^2$ . From eq. (10.7) it then follows that

$$\frac{K_{R_s}}{K_{th}} = \frac{aC_L\lambda}{\sin^2 \varphi_r} \quad (10.12)$$

When the cascade design method is used and the optimum lift coefficient,  $C_L^*$ , adopted, the loss in efficiency can be expressed directly as a function of  $\epsilon$  and  $\lambda$ .

## 10.6. Annulus Drag

This aspect of fan design is completely arbitrary (see Section 7.7). In cascade practice<sup>(54, 62)</sup> the equivalent drag coefficient is expressed as

$$C_{D_A} = 0.020 \frac{s}{c} \cdot \frac{c}{h} \quad (10.13)$$

where  $h$  is blade span and  $s$  is mean gap.

The constant, 0.020, is based on a skin friction coefficient of 0.010; this appears to be much too high, particularly in an adverse pressure gradient, where skin friction is greatly reduced. The flow deflections mentioned in Section 7.7, however, constitute losses which, added to the skin friction, could produce losses of the above order.

Owing to the arbitrary nature of eq. (10.13) this expression is not suitable for application to fan design in general. As an alternative, it will be assumed that the magnitude of annulus drag does not vary greatly from fan to fan and hence it is suggested that

$$\frac{K_{R_A}}{K_{th}} = \text{constant} = 0.02 \quad (10.14)$$

for fans with conventional aerofoil sections, and

$$\frac{K_{R_A}}{K_{th}} = 0.03 \quad (10.15)$$

for blades employing constant thickness aerofoil sections.<sup>(70)</sup> These figures appear to be of the right order.

## 10.7. Tip Clearance Losses

Provided tip clearance is small, e.g. less than 1 per cent of the blade height, no separate allowance need be made as the losses are incorporated in the estimates of secondary and annulus drag.

The limited data available<sup>(71, 72)</sup> on the effect of tip clearance are plotted in Fig. 10.4. These results all agree concerning the rate at which design efficiency falls off as the clearance is increased, i.e.

$$\text{additional loss in eff.} = 3 \times \frac{\text{additional clearance}}{\text{blade height}}$$

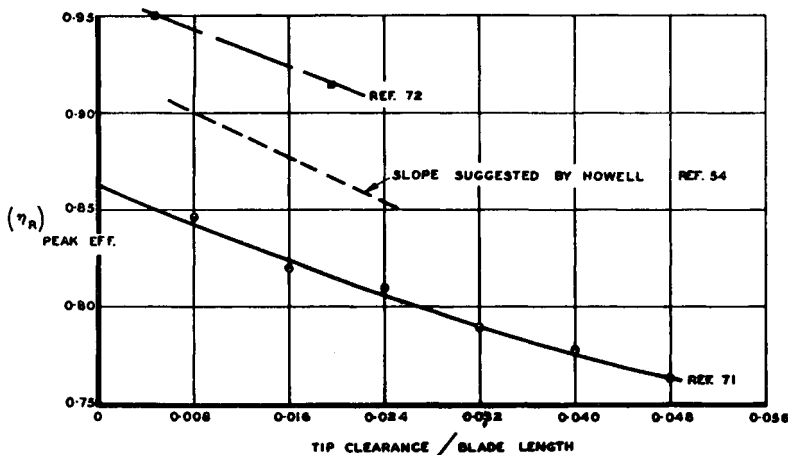


Fig. 10.4. Effect of tip clearance on rotor efficiency

Excessive tip clearance will also lead to a reduction in the actual pressure rise when compared with the design value (see Section 22.4.5).

## 10.8. Total Drag

In addition to the rotor losses already mentioned, there is a disk drag associated with the rotor surfaces internal to the flow annulus. Provided, however, that the clearances between the rotor boss and the fairings are small and that there is no leak through the disk due to lightening holes, the losses are negligible.

When the annulus drag is assumed to be constant, it follows that the rotor efficiency depends mainly on the ratio  $C_L/(C_{D_p} + C_{D_s})$ . This ratio is plotted in Fig. 10.5 as a function of  $C_L$  and  $C_{D_p}$  on the assumption that  $C_{D_s} = 0.018C_L^2$ . Hence design values of  $C_L$  approaching unity appear to give optimum performance when profile drag remains constant. Profile drag will, however, usually increase slightly with  $C_L$  and hence the

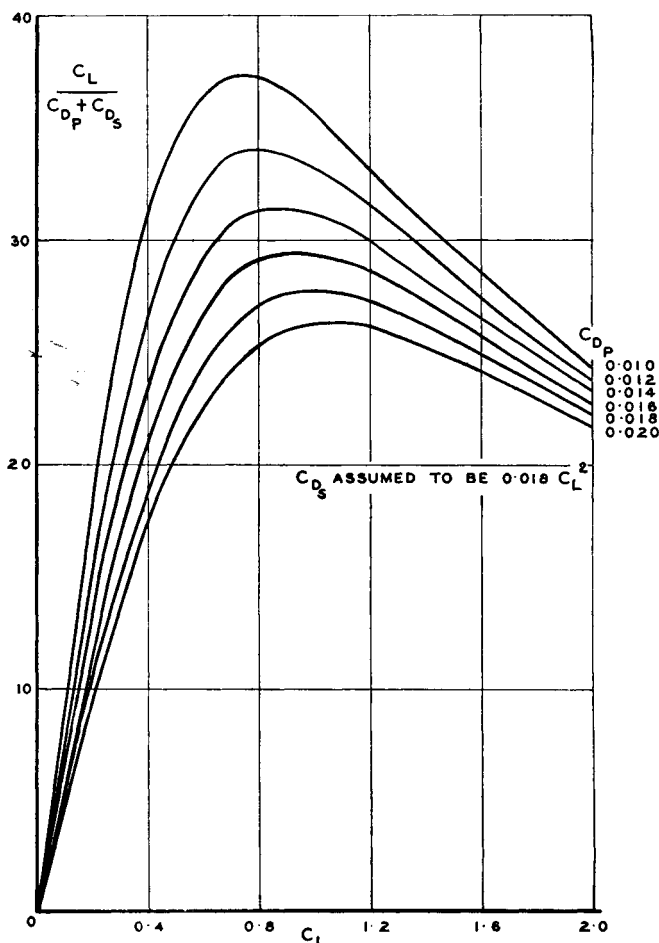


Fig. 10.5. Influence of lift coefficient on efficiency

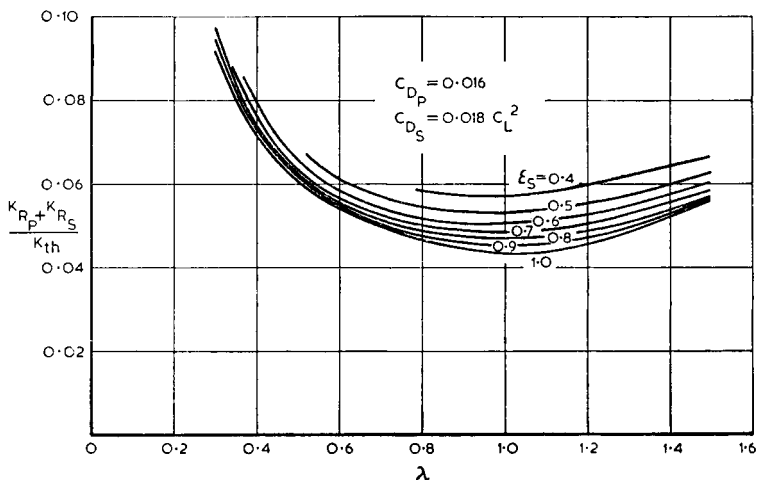


Fig. 10.6. Loss in efficiency due to profile and secondary drag.  $\epsilon_p = 0$ : cascade method

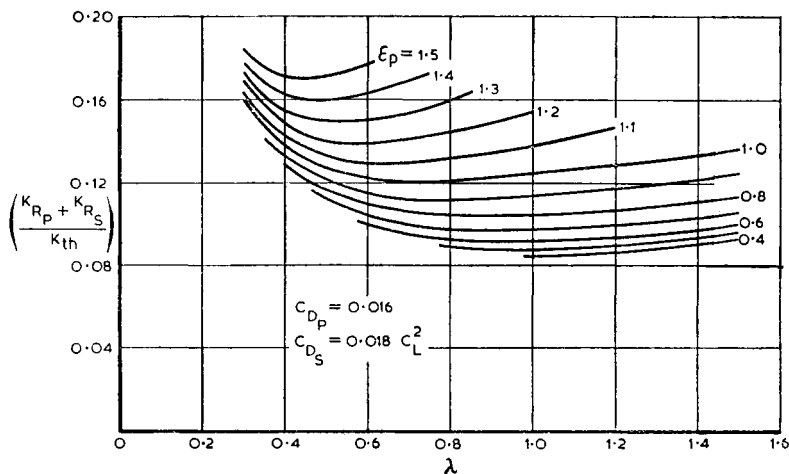


Fig. 10.7. Loss in efficiency due to profile and secondary drag,  $\epsilon_s = 0$ : cascade method

true optimum  $C_L$  may be slightly less than 0.8. The above applies to the low pressure rise type of fan.

Taking a mean value of 0.016 for the profile drag of aerofoils in cascade (see Section 10.4), and using the optimum values of  $C_L$  given in Section 9.4, the efficiency losses due to profile and secondary drags have been presented in Figs. 10.6 and 10.7 for the two cases, i.e.  $\epsilon_p$  or  $\epsilon_s$  equal to zero. The greater efficiency of the rotor-straightener unit is at once apparent. For cambered plate aerofoils, the loss in efficiency will be up to 50 per cent greater than that recorded in these figures. The values of  $\epsilon$  and  $\lambda$  used are, of course, those at the representative station.

# STATOR DESIGN

## III. General Momentum Considerations

Prerotators and straighteners can be treated in a manner similar to that used for rotor blades. For a stator blade element at radius  $r$ , we have the diagrams given in Figs. 11.1 and 11.2, where the effective swirl component is assumed, as before, to be the mean of the inlet and outlet swirl.

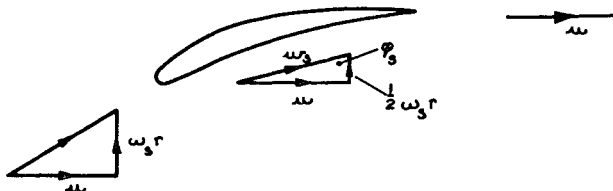


Fig. 11.1. Velocity vectors for straightener blade element

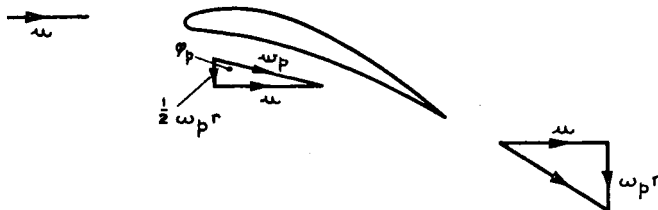


Fig. 11.2. Velocity vectors for prerotator blade element

Applying the method of Section 8.4, the following relations are obtained :

*Straighteners*

$$C_L = 2 \frac{s}{c} \epsilon_s \sin \varphi_s - C_D \frac{\epsilon_s}{2} \quad (11.1)$$

$$C_D = \frac{s}{c} k_s \sin^3 \varphi_s \quad (11.2)$$

where  $\varphi_s = \cot^{-1} (\epsilon_s/2)$ .

*Prerotators*

$$C_L = 2 \frac{s}{c} \epsilon_p \sin \varphi_p - C_D \frac{\epsilon_p}{2} \quad (11.3)$$

$$C_D = \frac{s}{c} k_p \sin^3 \varphi_p \quad (11.4)$$

where  $\varphi_p = \cot^{-1} (\epsilon_p/2)$ .

The lift coefficient has been plotted in Fig. 11.3 as a function of  $\epsilon$  and  $s/c$  on the assumption that  $C_D \epsilon / 2$  is small.

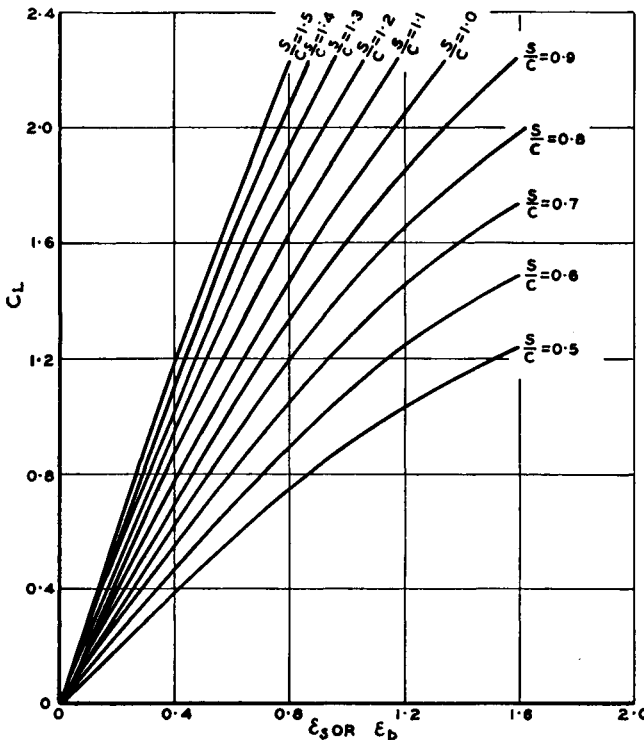


Fig. 11.3. Lift coefficient as function of swirl

## 11.2. Straightener Design, N.P.L. Type

When the swirl velocity is small, a simple solution<sup>(50)</sup> evolved at the N.P.L. is often employed. This consists in using stators with a gap/chord ratio of unity, the stators being so arranged that in a purely axial flow there is no lift on the stators, i.e. the "no-lift" line of the section is parallel with the fan axis. Provided the stators are not stalled, all swirls can be removed with a single stator setting. Although absolutely speaking this is only approximately true, it is for all practical purposes an adequate solution, particularly in wind tunnel installations where a symmetrical section such as the N.A.C.A. 0012 (see Table section) is often used. The flow diagram for such a section is given in Fig. 11.4.

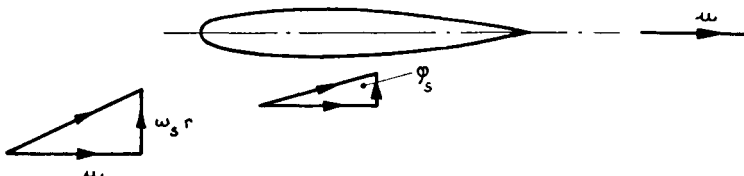


Fig. 11.4. Flow past N.P.L. type straightener

From Fig. 11.4, the angle of incidence, i.e. the angle between the chord line and the mean relative velocity vector, is

$$\alpha = 90^\circ - \varphi_s \quad (11.5)$$

Assuming that the two-dimensional N.A.C.A. 0012 aerofoil commences to stall at  $14^\circ$  incidence, we have  $\epsilon_s = 0.5$  as a limiting value. Allowance should, however, be made for the fact that  $\epsilon_s$  at the blade root is, owing to secondary flows, greater than the design value. Accordingly, this type of straightener can be considered satisfactory<sup>(73)</sup> for the design range

$$\epsilon_s = 0 \text{ to } 0.4$$

Although this method of design can be extended to higher values of  $\epsilon_s$  by the use of cambered sections, it is not advisable or desirable to do so; the cascade design method is the better approach to this problem.

It may be mentioned in passing that modifications to the above type of stator are possible in cases where small residual swirls are of little consequence. Structural features, space limitations or other practical considerations may make such modifications desirable. For free vortex flow, small inlet swirls and constant  $C_L$  along the vane, it can readily be shown from eq. (11.1) that the chord remains constant with radius. Eq. (9.17) indicates that the angle of deviation,  $\delta$ , will increase with  $s/c$  but the resulting increase in residual swirl from the above modification may, from an efficiency point of view, be unimportant (see Section 14.1). When the fan unit is designed for free vortex flow, no trouble with stator stalling will occur, provided  $C_L$  does not increase with radius,  $s/c$  at the stator root is no greater than unity, and  $\epsilon_{s_b}$  is less than 0.4.

### 11.3. Straightener Design, Aerofoils in Cascade

When the value of  $\epsilon_s$  exceeds 0.4, the cascade method of design is to be preferred. The design details of the vanes can be found in a manner similar to that employed for rotor blades in Section 9.5.

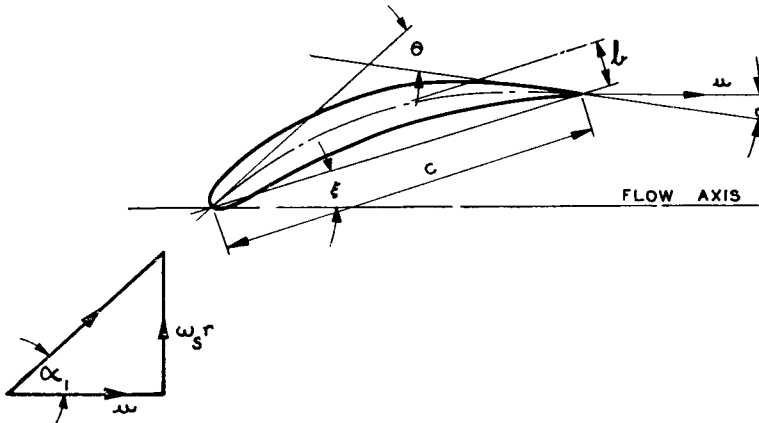


Fig. 11.5. Geometric details of straightener blade element

Fig. 11.5 gives the important details of the flow and the main parameters involved in designing a circular arc camber line aerofoil. The normal design assumption that the angle of

incidence,  $i$ , is zero has been made (see Section 9.5); when the stator is not working at the design condition, the outlet angle will remain constant provided the incidence,  $i$ , does not exceed the limits  $-5^\circ$  to  $+5^\circ$  mentioned previously. This is in substantial agreement with the assumed behaviour of the N.P.L. type of straightener.

From Fig. 11.5 we have the following relationship:

$$\theta = \alpha_1 + \delta \quad (11.6)$$

and substituting for  $\delta$  from eq. (9.17)

$$\theta = \frac{\alpha_1}{1 - 0.26\sqrt{(s/c)}} \quad (11.7)$$

The radius of curvature and percentage camber follow from eqs. (9.24) and (9.26).

The stagger angle,  $\xi$ , is given by

$$\xi = \alpha_1 - \frac{\theta}{2} \quad (11.8)$$

Since  $\tan \alpha_1 = \epsilon_s$  and  $\alpha_2 = 0$ , the optimum  $s/c$  can be determined from Fig. 9.6 as a function of  $\epsilon_s$ . This relationship is plotted in Fig. 11.6 and compared with the approximate expression given in Reference 54, that is,

$$\tan \alpha_1 - \tan \alpha_2 = \frac{1.55}{1 + 1.5(s/c)} \quad (11.9)$$

The recommended values of  $s/c$  for  $\epsilon_s$  approaching unity are becoming excessively small and hence  $\epsilon_s = 1.0$  has been arbitrarily chosen as the practical design limit. For values of  $\epsilon_s$  less than 0.5 it is desirable to maintain  $s/c$  at 1.5, as experimental data do not at present exist for higher values of  $s/c$ ; the working  $C_L$  is then less than the optimum.

The lift coefficient corresponding to the above values of  $s/c$  can be obtained from the approximate form of eq. (11.1), i.e.

$$C_L = 2 \frac{s}{c} \epsilon_s \sin \varphi_s \quad (11.10)$$

For  $\epsilon_s > 0.5$ , and with optimum values of  $C_L$  derived from Fig. 9.7, the following approximate relationship is obtained:

$$C_L^* = 2.18 - 1.43\epsilon_s \quad (11.11)$$

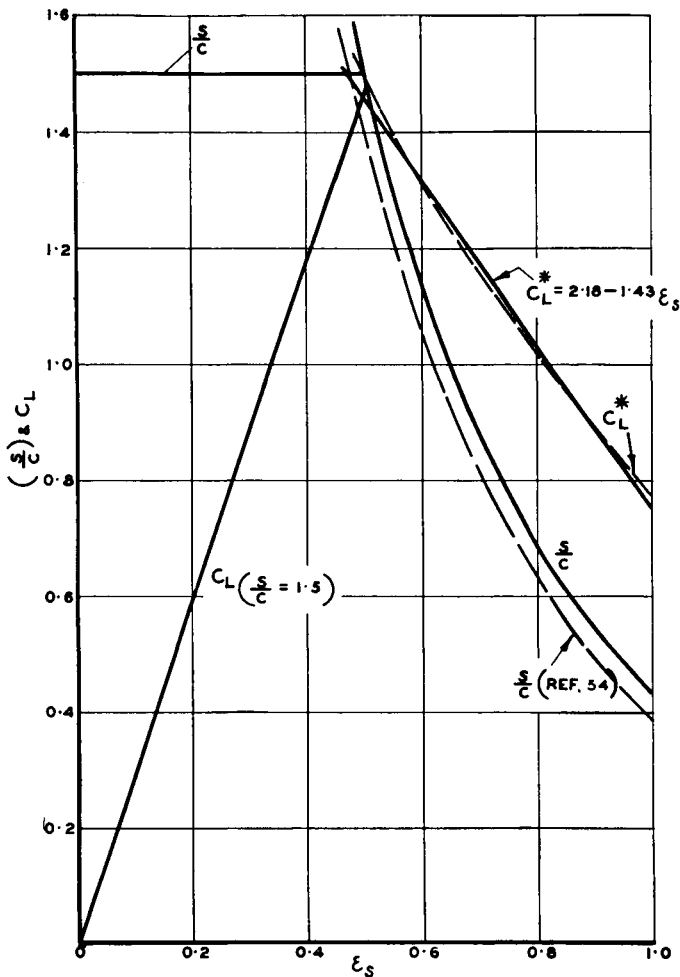


Fig. 11.6. Recommended values of  $C_L$  and  $\frac{s}{c}$  for cascade type straighteners

The camber angle,  $\theta$ , and stagger angle,  $\xi$ , as expressed by eqs. (11.7) and (11.8) respectively, are presented in Fig. 11.7 as functions of  $\epsilon_s$  and  $s/c$ ; when optimum  $s/c$  is used, the angles depend only on  $\epsilon_s$ , in the manner shown.

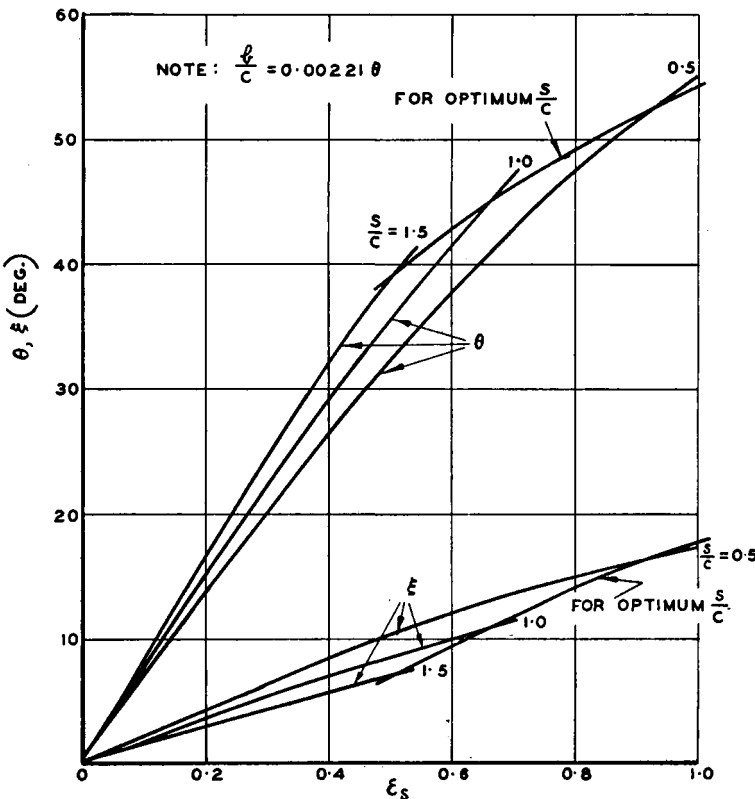


Fig. 11.7. Camber and stagger angles for cascade type straighteners

#### 11.4. Prerotator Design, Aerofoils in Cascade

A prerotator accelerates the air since it introduces a tangential velocity component, thus producing a static pressure drop across the stator. It is thus less critical in design than the straightener vane, and therefore lower solidities and higher lift coefficients are possible.

From Fig. 11.8, and the assumption that  $i=0$ ,

$$\theta = \alpha_2 + \delta \quad (11.12)$$

For accelerating cascades and optimum design conditions, the angle of deviation,  $\delta$ , is given approximately by

$$\delta = 0.20 \frac{s}{c} \cdot \theta \quad (11.13)$$

where 0.20 is a mean value of  $m$  as obtained from Reference 74 for accelerating flow stators. Substituting for  $\delta$  in eq. (11.12),

$$\theta = \frac{\alpha_2}{1 - 0.20(s/c)} \quad (11.14)$$

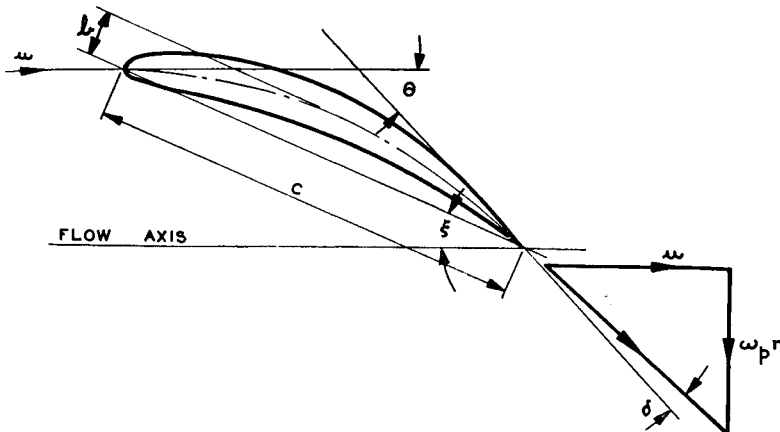


Fig. 11.8. Geometric details of prerotor blade element

The radius of curvature and camber/chord ratio are, as before, given by eqs. (9.24) and (9.26).

The stagger angle,  $\xi$ , is,

$$\xi = \frac{\theta}{2} \quad (11.15)$$

It can be shown from Section 9.3 that, owing to the accelerating flow, the angle  $\alpha_2$  is negative. Hence, from Fig. 9.6, it can be seen that gap/chord ratios in excess of 1.5 appear permissible. As no experimental and design data are available for greater values, however, this value will be accepted as the maximum.

For  $s/c = 1.5$ , the design lift coefficient reaches a value of 2 at  $\epsilon_p = 0.7$ . Since secondary drag is a function of  $C_L^2$  (see Section 10.5), it is obvious that some limit should be placed on  $C_L$ . Hence it is suggested that, for  $\epsilon_p > 0.7$ , a constant  $C_L$  of 2 should be adopted; this reduces  $s/c$  to 0.84 at the arbitrarily

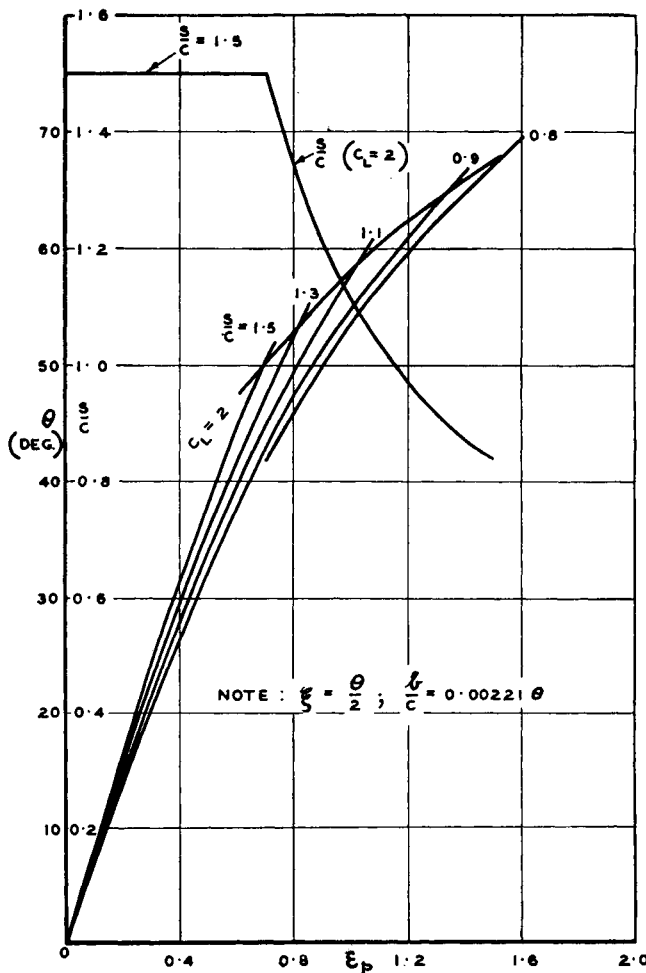


Fig. 11.9. Design data for prerotators

chosen limit of  $\epsilon_p = 1.5$  (Fig. 11.9). The above recommendations are in agreement with Reference 75 where satisfactory turning and low losses resulted from similar values of gap/chord ratio.

The change in camber angle,  $\theta$ , with  $s/c$  and  $\epsilon_p$  is given in Fig. 11.9

# I2

---

## STATOR LOSSES

Stator losses are, of course, similar in nature to those occurring in rotor blading. The decrease in fan efficiency due to the loss in total head as the air passes through the stators is, for an average case, of the order of 3 per cent. Great accuracy in estimating the losses is therefore not essential. In the light of this, some simplifying assumptions can be made.

Before the composition of the drag coefficients is discussed, the essential features of the general equations will be outlined.

### I2.I. Momentum Considerations

When a procedure similar to that adopted in Section 10.2 is followed, and the appropriate equations chosen, it can be shown that the straightener loss coefficient,  $k_s$ , is given by the expression

$$\left(\gamma + \frac{\epsilon_s}{2}\right) \frac{k_s}{k_{th}} = \frac{\lambda}{\sin^2 \varphi_s} \cdot \frac{\epsilon_s}{\epsilon_s + \epsilon_p} \quad (12.1)$$

or

$$\gamma \frac{k_s}{k_{th}} = \frac{\lambda}{\sin^2 \varphi_s} \cdot \frac{\epsilon_s}{\epsilon_s + \epsilon_p} \quad (12.2)$$

since  $\gamma \gg \epsilon_s/2$ .

Straighteners may sometimes be installed downstream of a prerotator-rotor design arrangement for the express purpose of removing the residual swirl resulting from off-design operation. In such a case eq. (11.2) reduces to

$$\frac{k_s}{k_{th}} = \frac{C_D}{(s/c)k_{th}} \quad (12.2a)$$

for the design condition.

With a similar development for prerotators,

$$\gamma \frac{k_p}{k_{th}} = \frac{\lambda}{\sin^2 \varphi_p} \cdot \frac{\epsilon_p}{\epsilon_p + \epsilon_s} \quad (12.3)$$

When zero-preswirl vanes are installed in the fan annulus for structural or other reasons, then

$$\frac{k_p}{k_{th}} = \frac{C_D}{(s/c)k_{th}} \quad (12.3a)$$

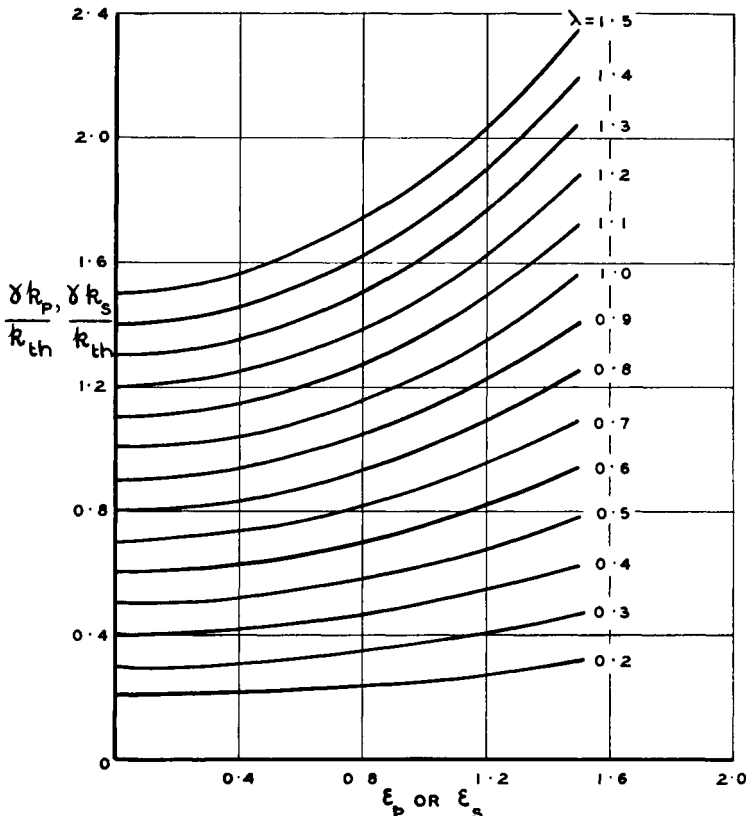


Fig. 12.1. Loss of efficiency in stator blade element for either  $\epsilon_p$  or  $\epsilon_s = 0$

For the normal prerotorator-rotor or rotor-straightener designs, the loss in efficiency, e.g.  $k_P/k_{th}$ , is a function of  $\gamma$ ,  $\lambda$  and  $\epsilon$  (Fig. 12.1) since  $\sin \varphi$  is related to  $\epsilon$  (see Section 11.1).

With the adoption of the various recommendations of Section 11, the following relations are obtained when either  $\epsilon_p$  or  $\epsilon_s$  is zero, which is normally the case:

(i) *N.P.L. type of straightener.* In this instance  $s/c = 1$  and hence eq. (11.10) reduces to

$$C_L = 2\epsilon_s \sin \varphi_s$$

Substituting in eq. (12.2),

$$\frac{k_s}{C_D k_{th}} = \frac{\lambda}{2\epsilon_s \sin^3 \varphi_s} \quad (12.4)$$

The value of the coefficient,  $C_D$ , will approximate to 0.020 for normal operating conditions (Fig. 12.2).

(ii) *Straightener, cascade method of design.* For the range  $0.5 < \epsilon_s < 1.0$ , the optimum lift coefficient is given by eq. (11.11) while for  $\epsilon_s < 0.5$  a constant gap/chord ratio of 1.5 is assumed. Hence:

for  $0.5 < \epsilon_s < 1.0$

$$\frac{k_s}{C_D k_{th}} = \frac{\lambda}{(2.18 - 1.43\epsilon_s) \sin^2 \varphi_s} \quad (12.5)$$

for  $\epsilon_s < 0.5$

$$\frac{k_s}{C_D k_{th}} = \frac{\lambda}{3\epsilon_s \sin^3 \varphi_s} \quad (12.6)$$

(iii) *Prerotorator, cascade method of design.* The relevant equations are

for  $0.7 < \epsilon_p < 1.5$  ( $C_L = 2$ )

$$\frac{k_p}{C_D k_{th}} = \frac{\lambda}{2 \sin^2 \varphi_p} \quad (12.7)$$

for  $\epsilon_p < 0.7$  ( $s/c = 1.5$ )

$$\frac{k_p}{C_D k_{th}} = \frac{\lambda}{3\epsilon_p \sin^3 \varphi_p} \quad (12.8)$$

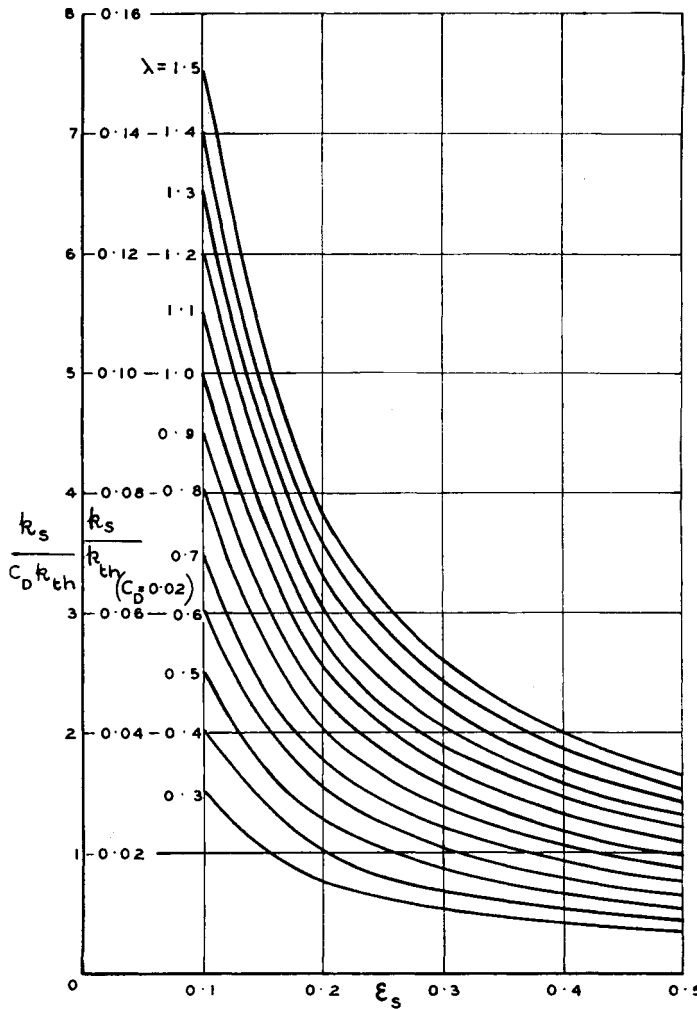


Fig. 12.2. Efficiency losses in N.P.L. type straighteners,  $\epsilon_p = 0$

## 12.2. Drag Coefficient

The data which have been published on the drag of accelerating and decelerating stators,<sup>(54, 75, 76)</sup> that is prerotators and straighteners, differ somewhat in their method of presentation. Secondary drag is, however, proportional to  $C_L^2$  in both cases. In view of the relative unimportance of the precise value of the

drag, and since the total drag coefficients are of the same order of magnitude in each case, a common set of data have been adopted.

Tip clearance losses can be avoided with proper sealing; as a result the annulus drag component will probably be smaller than the accuracy with which efficiency can be estimated. It is suggested, therefore, that only the profile and secondary drag

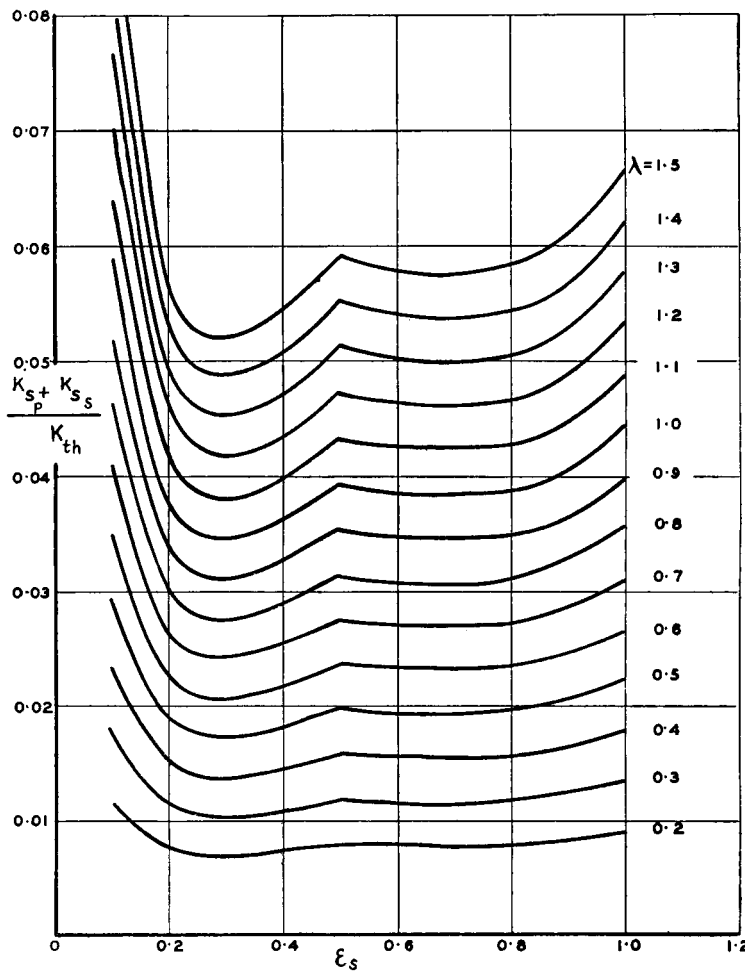


Fig. 12.3. Efficiency losses in cascade type straighteners for design recommendations,  $\epsilon_p = 0$

components need be considered. The recommended values for cascaded aerofoils of orthodox section are those given in Section 10.8, namely:

$$C_{D_p} = 0.016$$

$$C_{D_s} = 0.018 C_L^2$$

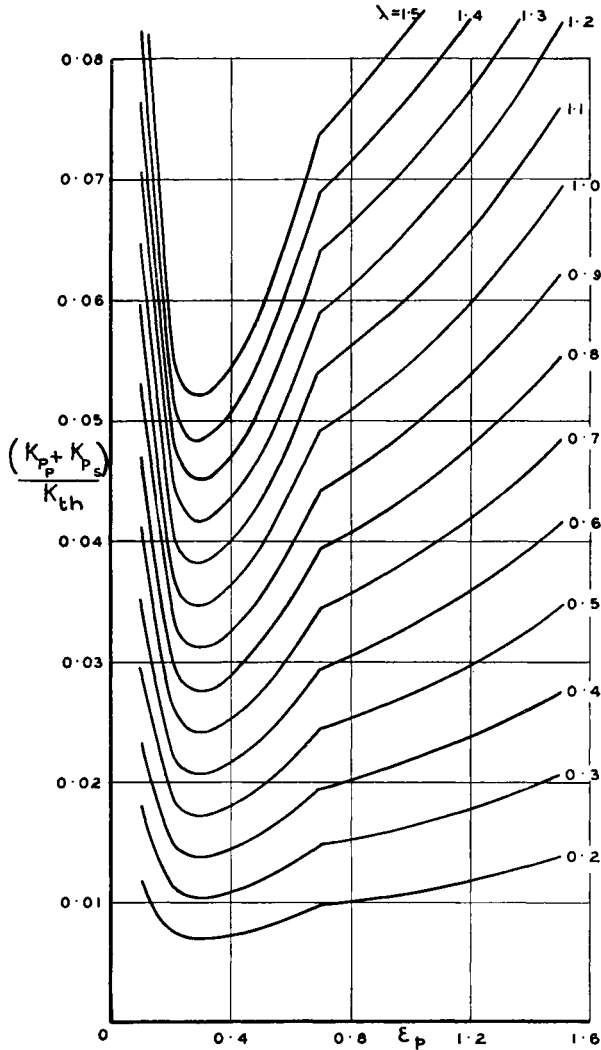


Fig. 12.4. Efficiency losses in prerotators for design recommendations,  
 $\epsilon_a = 0$

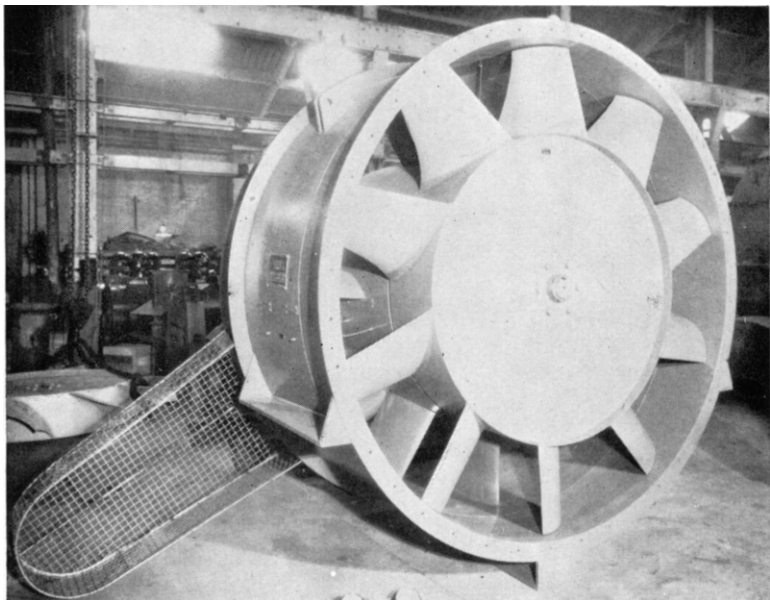
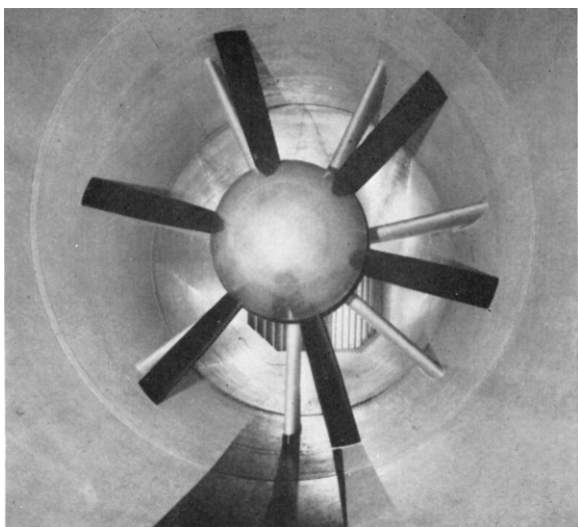
When the design recommendations of Section 11 are followed, it is possible to express the approximate efficiency loss, due to stator drag, as a function of  $\epsilon$  and  $\lambda$ . The loss coefficients,  $K_S/K_{th}$  and  $K_P/K_{th}$ , for cascaded aerofoils of orthodox section, are illustrated in Figs. 12.3 and 12.4. An increase of up to 50 per cent is appropriate for vanes of cambered plate design.

As in Section 10.3, the values of  $\epsilon$  and  $\lambda$  at the midspan station can be chosen as representative of the stators when assessing the mean efficiency loss. The above treatment should be satisfactory for fan design purposes.

PLATE 1

(a) Fan unit of  
9 ft x 7 ft wind  
tunnel at A.R.L.  
(Melb.)

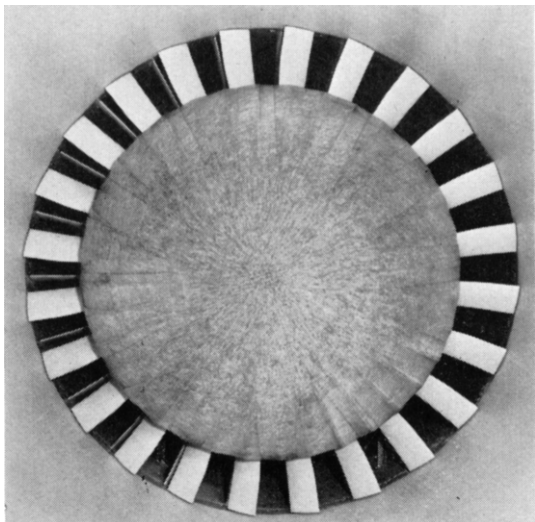
*(By courtesy of  
Dept. of Supply,  
Commonwealth of  
Australia)*



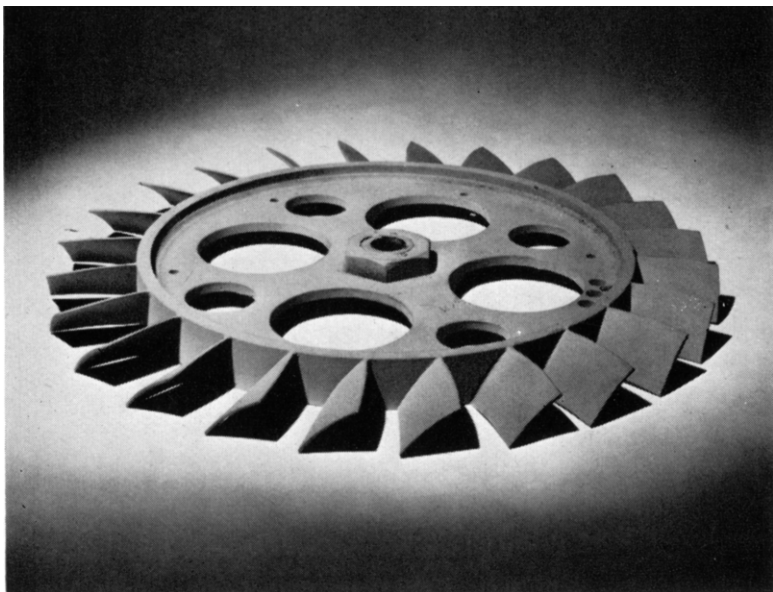
(b) Industrial air-moving fan unit

*(By courtesy of Aerex Co.)*

PLATE 2

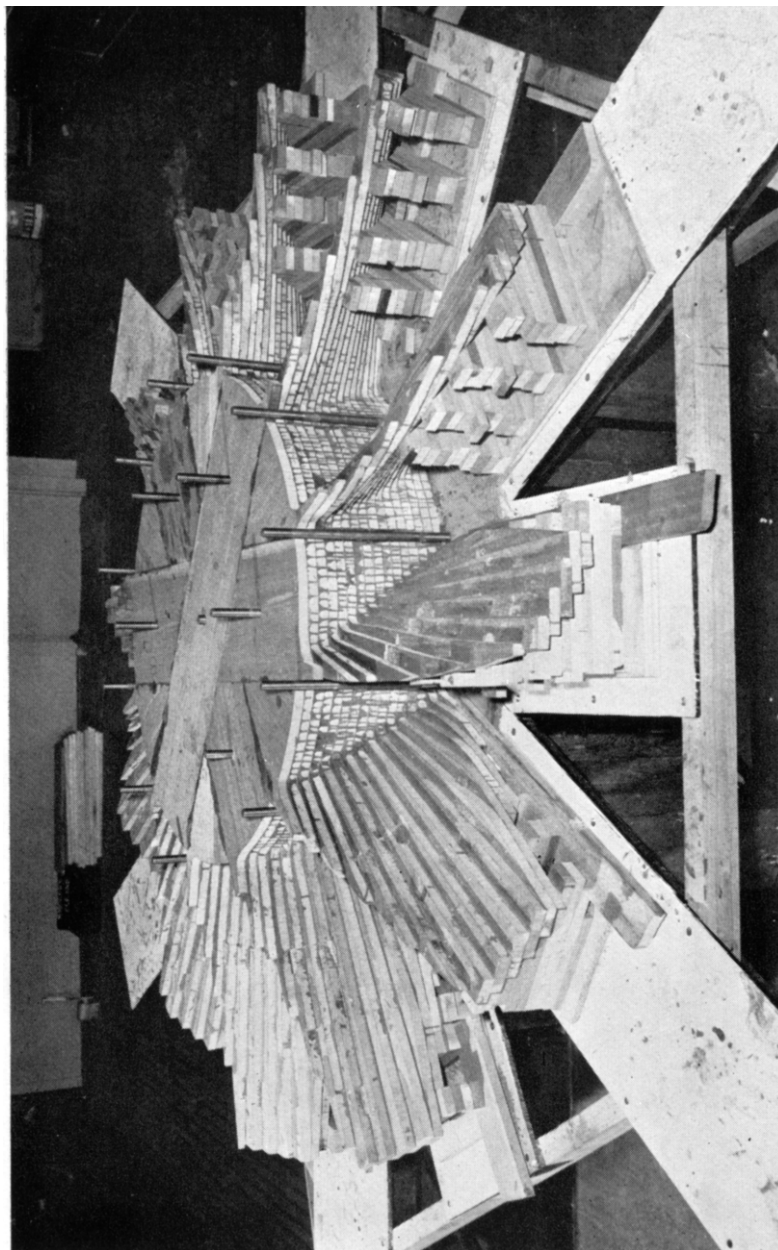


(a) Wind tunnel  
fan unit employ-  
ing cambered  
sheet metal blades  
*(By courtesy of  
Dept. of Supply,  
Commonwealth of  
Australia)*



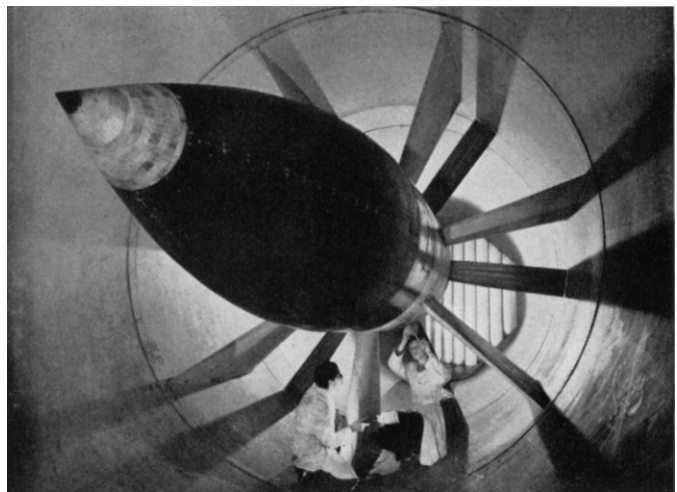
(b) Sheet metal blade rotor  
*(By courtesy of Dept. of Supply, Commonwealth of Australia)*

PLATE 3



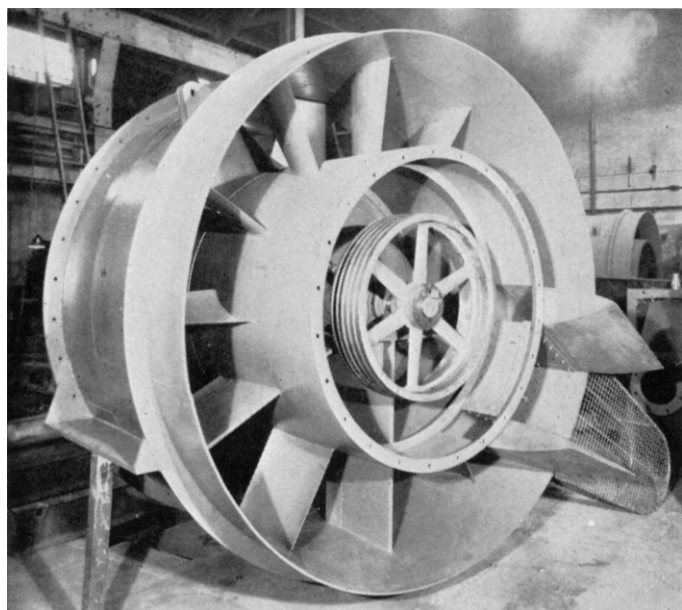
Construction of 12-bladed fan from wooden laminations  
*(By courtesy of Dept. of Supply, Commonwealth of Australia)*

PLATE 4



(a) Straighteners and tail fairing of A.R.L. (Melb.) wind tunnel fan

*(By courtesy of Dept. of Supply, Commonwealth of Australia)*



(b) Straighteners and drive fairings of industrial fan unit

*(By courtesy of Aerex Co.)*

---

# TAIL FAIRING DESIGN AND ASSOCIATED LOSSES

## 13.1. Fairing Shape

As the boss diameter in normal fan installations constitutes an appreciable proportion of the fan diameter, considerable diffusion occurs in the downstream section of the duct enclosing the tail fairing. The subsequent loss in fan unit efficiency can be very high, particularly when flow separation occurs. To

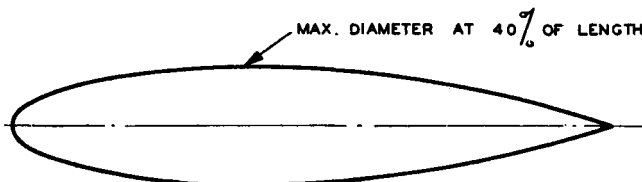


Fig. 13.1. Streamlined body of revolution

avoid unnecessary losses, the tail fairing should have a streamlined form and be of sufficient length to ensure a reasonable rate of diffusion. The aft portion of any efficient streamlined body of revolution can be used. One such shape<sup>(77)</sup> is illustrated in Fig. 13.1; the co-ordinates are given in the Tables Section.

### 13.2. Diffusion Efficiency

From Section 6.4.1 the diffuser efficiency is given by

$$\eta_D = 1 - \frac{\Delta H_D}{\frac{1}{2} \rho U^2 [1 - (A_A/A_B)^2]} \quad (6.13)$$

where  $\Delta H_D$  is mean total head loss

$U$  is mean axial velocity through rotor

$A_A, A_B$  are the rotor annulus and duct areas respectively.

In design,  $\Delta H_D$  is obtained by assuming the diffusion efficiency. Unfortunately, very little experimental information is available but from the existing evidence<sup>(70, 78)</sup> it appears that  $\eta_D = 0.80$  to  $0.85$ , provided flow separation is avoided. This is less than the efficiency associated with ordinary small-angle diffusers (Section 6.4.3) and this result is due in some measure to the additional "wetted" surface which is provided by the fairing.

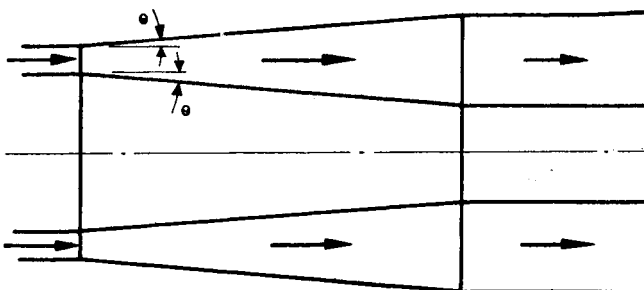


Fig. 13.2. Annular diffuser

Some interesting data on annulus type diffusers are available in Reference 78 (see Fig. 13.2). First, the peak efficiency is less than that given in Fig. 6.6 and secondly, departure from a uniform inlet velocity causes drastic reductions in efficiency; both these features are illustrated in Fig. 13.3. When allowance is made for the likely velocity distribution downstream of the last blade row, it follows that the efficiencies suggested above are of the right order. Although the diffusion angle (Fig. 13.3) has been defined in a manner similar to that employed in Section 6.4, the diffusion on inner and outer walls effectively

doubles the diffuser angle. In other words, an annular diffuser in which  $2\theta = 6^\circ$  is approximately equivalent to a conical diffuser of included angle  $12^\circ$ .

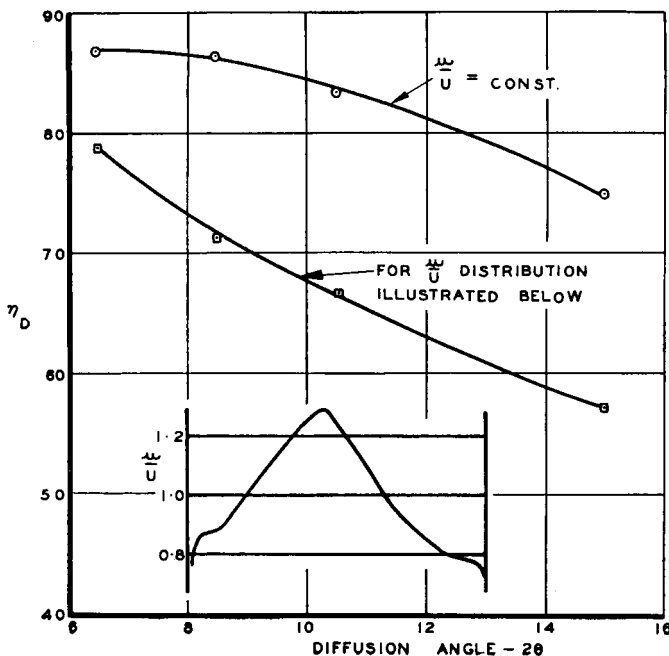


Fig. 13.3. Annular diffuser efficiency  
(Based on A.R.C. C.P. 178, and reproduced by permission of  
the Controller of H.M. Stationery Office)

### 13.3. Loss Coefficient

The loss of total head,  $\Delta H_D$ , can be expressed non-dimensionally as

$$K_D = \frac{\Delta H_D}{\frac{1}{2} \rho U^2} \quad (13.1)$$

and hence eq. (6.13) can be written

$$K_D = (1 - \eta_D) \left[ 1 - \left( \frac{A_A}{A_B} \right)^2 \right] \quad (13.2)$$

When the duct diameter of the fan unit remains constant, we have

$$K_D = (1 - \eta_D)[x_b^2(2 - x_b^2)] \quad (13.3)$$

This expression is presented in Fig. 13.4 for various efficiencies; the curve for  $\eta_D = 0$  gives the order of losses to be expected when no tail fairing is used.

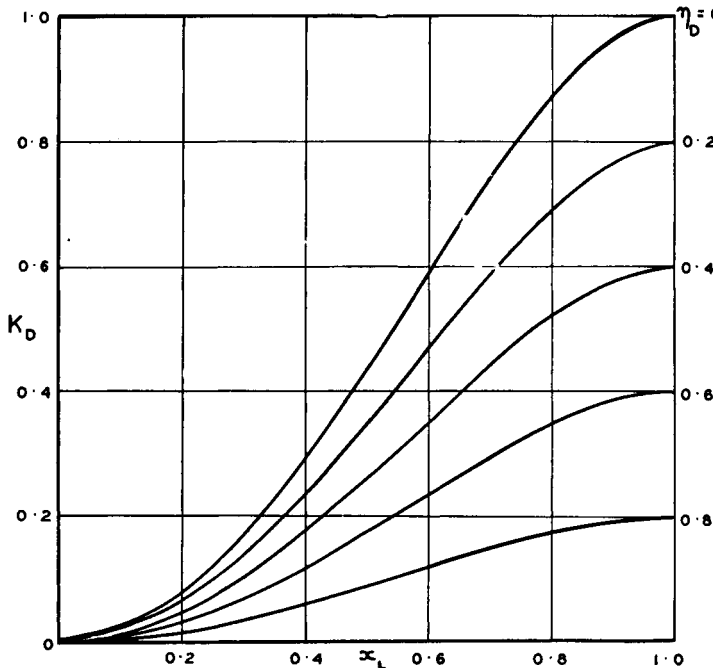


Fig. 13.4. Tail fairing loss coefficient

The component loss in the fan unit efficiency can be written in the form

$$\frac{K_D}{K_{th}}$$

This parameter has been plotted in Fig. 13.5 as a function of  $x_b$  and  $K_{th}$  for  $\eta_D = 0.80$  and constant duct diameter. For small values of  $K_{th}$ , the boss ratio must be small if large losses in efficiency are to be avoided.

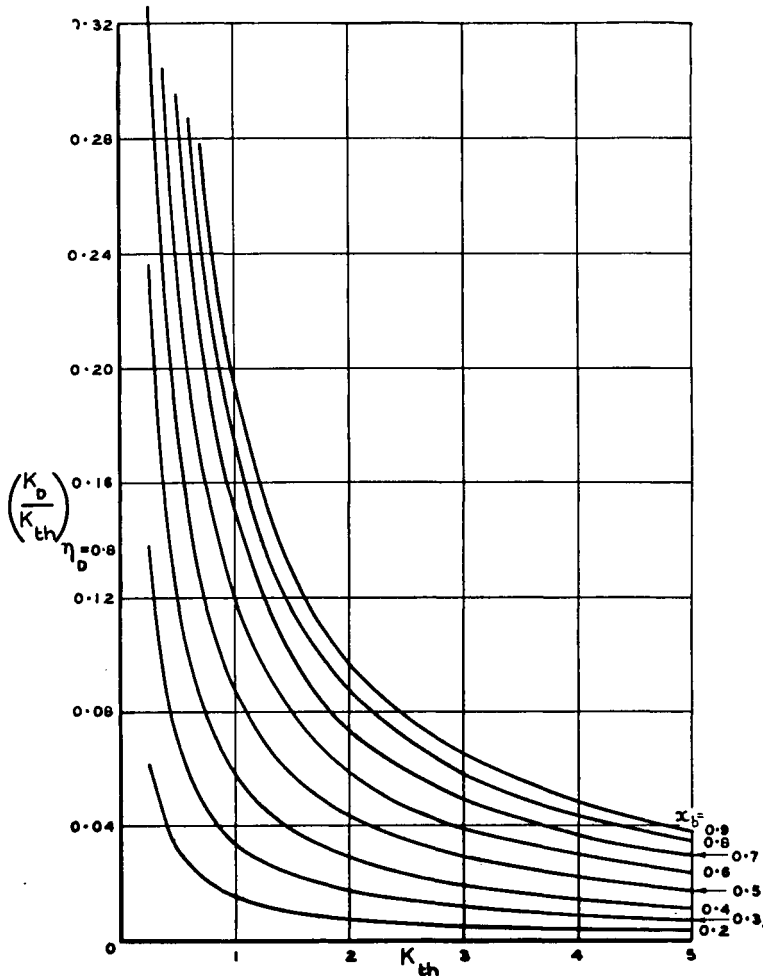


Fig. 13.5. Loss in fan efficiency for  $\eta_D = 0.8$

### 13.4. Fineness Ratio

Since the tail fairing length governs the rate of diffusion, some design rule concerning length is obviously required. Insufficient data are available, however, to indicate the minimum fairing length which can be used for a given boss ratio without inviting the risk of flow separation.

Owing to the relatively small area ratios involved, diffuser angles larger than those indicated in Section 6.4.3 can be employed. To simplify the problem, use will be made of an equivalent diffuser angle which can be defined as the included angle,  $2\theta$ , made by a cone which opens from an area  $A_A$  to  $A_B$  in a length,  $l$ . This length is given by

$$l = \frac{R - R\sqrt{(1 - x_b^2)}}{\tan \theta}$$

or non-dimensionally by the fineness ratio

$$f = \frac{l}{2r_b} = \frac{1 - \sqrt{(1 - x_b^2)}}{2x_b \tan \theta} \quad (13.4)$$

This expression applies only when the duct diameter of the fan unit remains constant.

The fineness ratio is presented in Fig. 13.6 as a function of boss ratio and equivalent diffuser angle. For small boss ratios it is more appropriate to consider the tail fairing as one in a stream unbounded by duct walls. Experiment has shown that streamlined shapes with a total length to diameter ratio of 3 are the most efficient.<sup>(79)</sup> Assuming that the maximum diameter occurs at the 40 per cent length position, the fineness ratio of the tail fairing will be

$$f = 1.8$$

As indicated previously, the lack of experimental data imposes the necessity of making tentative suggestions concerning the choice of fineness ratio. Use of the  $8^\circ$  curve in Fig. 13.6 should ensure a conservative design; this is supported by the downstream experimental velocity traverses given in Reference 70. For most design cases, an equivalent diffuser angle of  $10^\circ$  will probably be safe while  $12^\circ$  may be suspect. When separation is present, difficulty must be anticipated in estimating the efficiency.

Shorter fairings can be used in a fan unit consisting of a rotor only, since the unremoved swirl improves the flow over the tail fairing. An experimental example of this can be seen in Reference 70 where, for a boss ratio of 0.6, a fairing corresponding to an equivalent diffuser angle of  $14^\circ$  was successfully employed.

The flow over the same tail fairing was badly separated when the swirl was removed by the addition of straighteners.

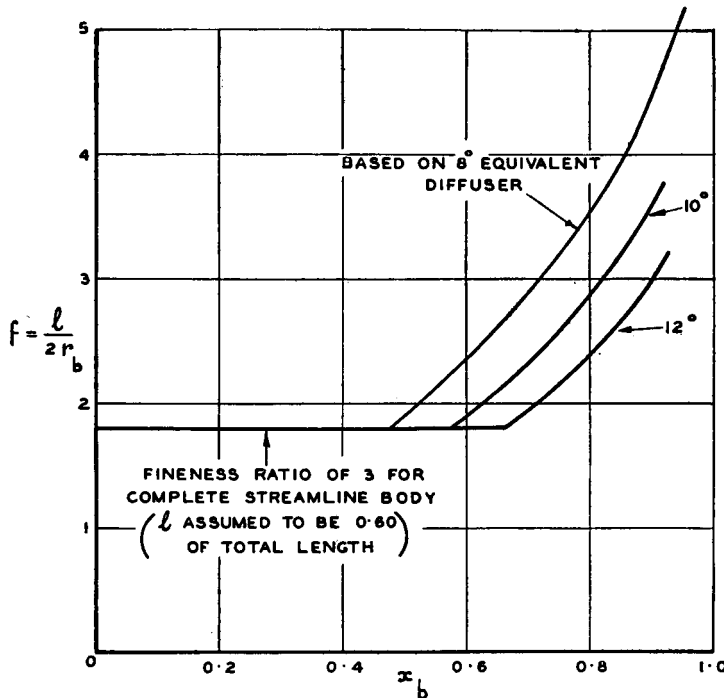


Fig. 13.6. Fineness ratio

In conclusion, despite some uncertainty due to the lack of extensive test results, sufficient information has been presented to permit confidence in designing efficient tail fairings. The suggested value of  $\eta_D$ , namely 0.8, should prove accurate for attached flow conditions. With large Reynolds numbers, good outlet conditions from the last blade row and optimum tail fairing length, efficiencies up to 0.85 may be expected.

# | 4

## OVERALL EFFICIENCIES

In Sections 10, 12 and 13, blade element losses were analysed and recommendations made concerning the mean loss in total head as the flow passes through each component of the fan unit. After a discussion on the effect of residual swirl, the use of these data in fan design will be considered.

### I4.1. Losses due to Swirl

In a fan unit which consists of a rotor only (see Section 1.6), attention must be paid to the losses associated with the downstream swirl. Assuming the flow to be axial on entry to the rotor, the total head loss can be related to the tangential velocity component imparted by the rotor. It follows that the loss in efficiency is

$$\frac{\frac{1}{2}\rho(\omega_s r)^2}{\Delta h_{th}}$$

or

$$\begin{aligned} \frac{k_{\text{swirl}}}{k_{th}} &= \frac{\epsilon_s^2}{k_{th}} \\ &= \frac{1}{2}\epsilon_s\lambda \end{aligned} \tag{14.1}$$

The coefficient,  $k_{\text{swirl}}$ , varies along the blade; when free vortex flow exists, the mean loss coefficient,  $K_{\text{swirl}}$ , can be obtained from values of  $\epsilon$  and  $\lambda$  at the midspan station. Arbitrary vortex flow need not be considered since fans so designed are usually high pressure rise units and hence will

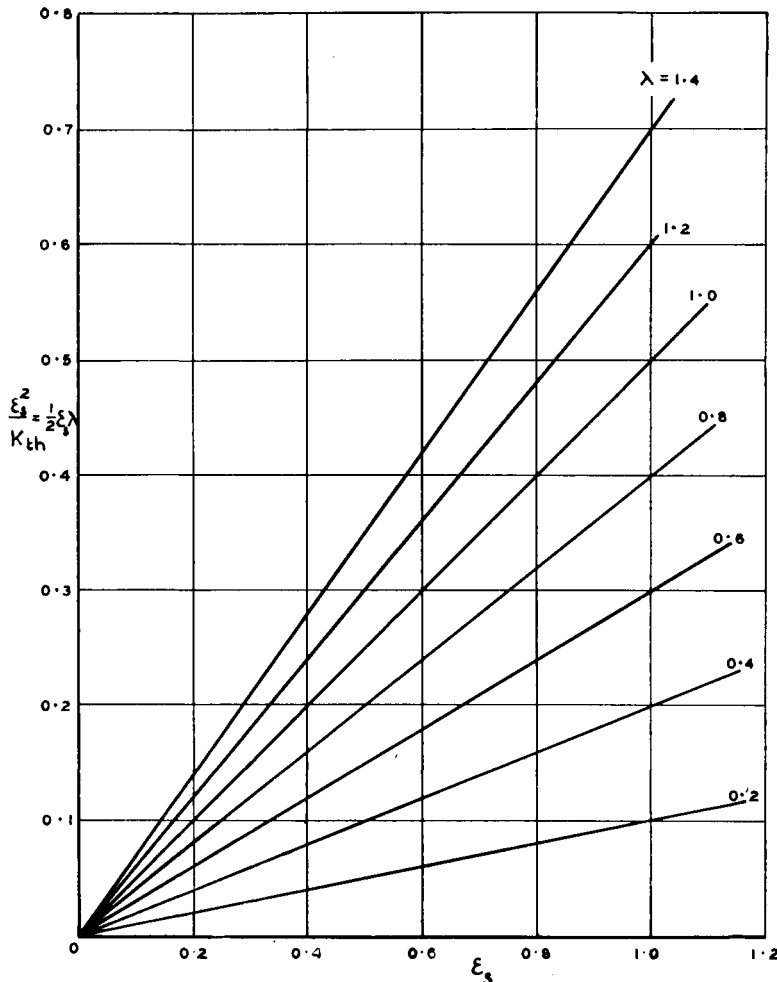


Fig. 14.1. Loss in fan efficiency due to swirl, in the absence of straighteners

possess stators. It will be seen from Fig. 14.1 that substantial efficiency losses can result.

If inadvertent swirl exists downstream of the last row of blading in a fan unit, the efficiency loss will be

$$\frac{\epsilon_{R.S.}^2}{K_{th}}$$

where  $\epsilon_{R.S.}$  is the residual swirl coefficient and equal to the tangent of the angle which the outlet flow makes with the axial direction. Angles of a few degrees magnitude can be shown to be unimportant from an efficiency point of view.

## 14.2. Overall Fan Unit Efficiency Relations

The total head rise required of the fan unit can be expressed by

$$K_{T_v} = \frac{\Delta H_T}{\frac{1}{2}\rho V^2} \quad (14.2)$$

where  $\Delta H_T$  is the duct loss (excluding the fan unit losses) and  $V$  is the mean axial velocity in the constant area duct just upstream of the nose fairing.

Total efficiency of the fan unit is

$$\eta_T = \frac{\Delta H_T}{\Delta H_{th}}$$

or

$$\eta_T = \frac{K_{T_v}(1-x_b^2)^2}{K_{th}} \quad (14.3)$$

when the velocity,  $V$ , is related to the mean annulus velocity,  $U$ , by means of the fan boss ratio,  $x_b$ . For free vortex flow,  $K_{th}$  is equal to  $k_{th}$ , owing to the condition of constant total head rise along the blade.

Alternatively, the total efficiency may be expressed by the general equation

$$\eta_T = \frac{K_{th} - K_R - K_P - K_S - K_{swirl} - K_D}{K_{th}} \quad (14.4)$$

which reduces to the following relations for the cases listed in Section 1.6:

*Rotor unit*

$$\eta_T = \frac{K_{th} - K_R - K_{swirl} - K_D}{K_{th}} \quad (14.5)$$

*Rotor-straightener unit*

$$\eta_T = \frac{K_{th} - K_R - K_S - K_D}{K_{th}} \quad (14.6)$$

*Prerotor-rotor unit*

$$\eta_T = \frac{K_{th} - K_R - K_P - K_D}{K_{th}} \quad (14.7)$$

*Prerotor-rotor-straightener unit*

$$\eta_T = \frac{K_{th} - K_R - K_P - K_S - K_D}{K_{th}} \quad (14.8)$$

*Contra-rotating rotors*

$$\eta_T = \frac{K_{th} - K_{R_1} - K_{R_2} - K_D}{K_{th}} \quad (14.9)$$

Swirl is known to have a beneficial effect on diffuser efficiency owing to its suppression of flow separation. Hence the addition of stators to a rotor unit with a short, streamlined tail fairing may not always result in the expected gain (see Section 13.4). In such an instance,  $K_{swirl}$  and  $K_D$  are interrelated.

For a given flow, duct loss and fan diameter, the value  $K_{T_v}$  can be computed. A choice of boss diameter and an assumed value of  $\eta_T$  then permit an estimate of  $K_{th}$  to be obtained from eq. (14.3). With the further choice of a rotor speed, the values of  $\epsilon$  and  $\lambda$  at the midspan station can be established, thus permitting an estimate of the various loss coefficients given in eqs. (14.5) to (14.9). By the use of these equations, a computed value of  $\eta_T$  is obtained which when substituted in eq. (14.3) gives the value of  $K_{th}$  to be used in design. An iteration of the above process will not give any noticeable increase in accuracy if the initial choice of efficiency has been a reasonable one.

A study of the individual loss coefficients allows assessment of the relative merits of alternative designs as well as indicating where the heaviest losses are occurring. Design modifications, aimed at improving efficiency, can then be undertaken at this early stage.

### **14.3. Factors Affecting Overall Fan Unit Efficiency**

The absolute drag acting on a blade varies as the square of the mean relative velocity,  $w_r$ , between the rotor blades and the air. The greater rotor efficiency of a rotor-straightener unit in comparison with a prerotor-rotor unit can be traced to this

feature. Moreover, for a given  $\lambda$ , increasing values of  $\epsilon$  will respectively reduce and increase the mean relative velocities of the two units above mentioned, and this tends to enlarge the difference in rotor efficiency.

A reduction in the design value of  $\lambda$  for a given fan configuration means increased rotor speed and hence an increase in  $w_r$ . Rotor efficiency is therefore a very definite function of  $\lambda$ ; the optimum  $\lambda$  is in the vicinity of unity, depending on the design method employed. The loss coefficient,  $k_R/k_{th}$ , tends to increase rapidly as  $\lambda$  decreases and approaches values of the order 0.2.

Tail fairing losses often constitute a major part of the total losses, with the result that the optimum efficiency for the complete fan unit may be obtained at values of  $\lambda$  somewhat less than unity. A further limitation on the value of  $\lambda$  exists for fans having relatively high pressure rises; to avoid blade overloading, the rotational speed of the rotor must be increased, thus reducing the design value of  $\lambda$ .

A large lift/drag ratio is, of course, an essential for high efficiency fans. The above generalities should be given consideration during the initial design stages.

#### **14.4. Aerodynamic Efficiency of Complete Duct and Fan System**

Fan design is often influenced by the wider objective of achieving the highest possible overall efficiency for the complete duct and fan installation; in this discussion only aerodynamic aspects will be considered. It is the task of the designer of air moving equipment to discover the least-power arrangement by carrying out a number of preliminary designs of various possible duct and fan unit configurations. The effect of such considerations on the design of fan units will be discussed.

In the case of a fan unit which exhausts air from a duct system, the property called "static efficiency" must be taken into consideration. This variable is the ratio of the power absorbed by the air in the duct system to that absorbed by the rotor, or alternatively, the ratio of the fan static pressure head

to the theoretical total head input to the air. Hence for an exhausting unit,

$$\text{Static efficiency} = \frac{\Delta H_T - \text{downstream losses}}{\Delta H_{th}} \quad (14.10)$$

$$= \eta_T - \frac{K_{\text{downstream losses}}}{K_{th}} \quad (14.11)$$

where both pressure coefficients are with respect to  $\frac{1}{2}\rho U^2$ . Hence, the requisites for high static efficiency are high total head efficiency, low discharge losses and a relatively large total head rise coefficient. It is easy therefore to see that static efficiency is closely related to system efficiency when due attention is paid to the aerodynamic merit of the duct system. In other words, if the duct system absorbs a minimum power, consistent with practical design considerations, then the design of the fan unit to achieve the highest possible static efficiency will ensure a maximum aerodynamic efficiency for the complete system.

The first term in eq. (14.11) has already been extensively discussed in previous subsections but some pertinent comments regarding the second term are of interest. The magnitude of the term can be lessened by reducing the discharge losses and/or by decreasing the axial velocity in the fan unit. With an efficient diffuser the first objective is readily obtained but there is a practical limit to the amount by which reduced velocity can increase static efficiency. The blade loading, as expressed by  $C_{Lc}$ , increases with reducing  $U$  and if blade stalling is to be avoided then a substantially lower value of  $A$  may have to be used, as discussed in the previous subsection. This tends to reduce  $\eta_T$ , particularly when prerotation is introduced to relieve blade loading. It will be seen, therefore, that designing for the highest possible static efficiency is a relatively complex matter and one which can be resolved only by carrying out a number of preliminary designs.

Peak static efficiency is situated on the operating curve somewhere between the point of peak total head efficiency and the stall; assuming that the non-dimensional downstream losses remain constant, the effect on static efficiency of the small loss in  $\eta_T$  as the stall is approached is more than offset by the increase in  $K_{th}$  (see eq. (14.11)). The necessity for accuracy in

duct and fan design when designing for high static efficiency cannot be over-emphasized in view of the proximity of the design point to the point at which blade separation commences.

Fan units of high static efficiency tend to be relatively large owing to the desirability of keeping axial velocity low. Available space, size limitations or capital cost may sometimes place a restriction on the maximum static efficiency for which it is possible to design.

Ducted fan units are quite often employed when a jet of air is required for cooling or other purposes. In this instance both fan static pressure head and static efficiency are zero; for this and other obvious reasons it is meaningless to consider these variables when assessing the fan unit performance. For the fan unit not fitted with a special nozzle, it can be shown that

$$H.P. = \frac{\text{cu. ft/min.} \times \text{exit velocity head}}{33,000 \times \eta_T}$$

For a particular operation, however, it will usually be found that there is a combination of volume flow and exit velocity which, for a given power, will result in the greatest effectiveness. Hence before commencing the fan design this relationship should be determined. Provided  $\eta_T$  is high, it can then be said that the operational efficiency of the unit is completely acceptable. When a special nozzle is fitted every effort should be made to keep duct losses low.

By applying arguments similar to those just outlined the dependence of the fan design on system efficiency considerations can be readily established for any specific installation. Sufficient has been said about this phase of the design problem to emphasize the importance of a co-ordinated approach to duct and fan design problems.

# 15

---

## TORQUE, THRUST AND POWER

### 15.1. Torque

The torque acting on the rotor shaft can be expressed in terms of the swirl momentum added to the stream. For free vortex flow it follows from eq. (8.26) that

$$Q_c = \int_{x_b}^1 4(\epsilon_s + \epsilon_p)x^2 \, dx \quad (15.1)$$

Substituting for  $(\epsilon_s + \epsilon_p)$  from eq. (8.12) and remembering that  $k_{th}$  is a constant

$$Q_c = k_{th}A(1 - x_b^2) \quad (15.2)$$

The torque then follows from eq. (8.25). Alternatively, when the power is known, torque can be obtained from the relation

$$\text{Shaft h.p.} = \frac{2\pi Q \times \text{rev/min}}{33,000} \quad (15.3)$$

### 15.2. Thrust

In fan design, the main interest in the thrust produced by the rotor is in relation to the design of thrust bearings and supports. For these purposes, an estimate based on the pressure rise across the rotor and the swept area is usually adequate.

When more detailed information is required, the equations of

Section 8.5 must be developed. From eq. (8.23),

$$T_c = \int_{x_b}^1 \frac{\Delta p}{\frac{1}{2}\rho U^2} 2x \, dx \quad (15.4)$$

For free vortex flow, where  $u$  and  $k_{th}$  are constant along the blade,

$$T_c = k_{th} \int_{x_b}^1 2x \left( \eta_R - \frac{\epsilon_s^2}{k_{th}} + \frac{\epsilon_p^2}{k_{th}} \right) dx \quad (15.5)$$

This expression can readily be integrated for the following three conditions :

$$\epsilon_s = \epsilon_p, \quad T_c = k_{th} \eta_R (1 - x_b^2) \quad (15.6)$$

$$\epsilon_p = 0,$$

$$\begin{aligned} T_c &= k_{th} \int_{x_b}^1 \left( 2x \eta_R - k_{th} \frac{A^2}{2x} \right) dx \\ &= k_{th} \eta_R (1 - x_b^2) + \frac{1}{2} k_{th}^2 A^2 (\log_e x_b) \end{aligned} \quad (15.7)$$

$$\epsilon_s = 0,$$

$$T_c = k_{th} \eta_R (1 - x_b^2) - \frac{1}{2} k_{th}^2 A^2 (\log_e x_b) \quad (15.8)$$

The total thrust follows from eq. (8.22).

### 15.3. Power

Although it is possible to define a power coefficient similar to the above torque and thrust coefficients, it is more practical to determine the power from the relation

$$\text{Shaft h.p.} = \frac{\Delta H_T \times \text{cu. ft/min}}{33,000 \times \eta_T} \quad (15.9)$$

where  $\Delta H_T$  is in lb/ft<sup>2</sup>.

This expression can readily be developed from the fundamental definition of power when it is remembered that  $\Delta H_T$  multiplied by the swept area represents a pressure force.

When  $\Delta H_T$  is expressed in inches of water

$$\text{Shaft h.p.} = \frac{5.2 \times \text{in. water} \times \text{cu. ft/min}}{33,000 \times \eta_T} \quad (15.10)$$

Alternatively, if the torque is given, power can be obtained from eq. (15.3).

Setting aside Reynolds number effects, the resistance to flow of a turbulent fluid in a given duct varies as the flow velocity squared and hence power varies as the velocity cubed. Since the non-dimensional coefficient  $A$  remains unchanged, it also follows that the power will vary as the cube of the rotational speed. The index would be slightly less than three if noticeable Reynolds number effects were present in the ducting.

# 16

---

## DESIGN OF FAN UNIT WITH ARBITRARY VORTEX FLOW

### 16.1. General

The free vortex method of design for ducted axial flow fans is simple and adequate for most purposes. Such a method is, however, seldom used in compressor design, where maximum work per stage of blading is required.

Because of the greater relative blade speed at the tip, increased work can be done if the total head rise is allowed to increase towards the tip. Since the total head rise is now no longer constant along the blade, the axial velocity component will also vary with radius.

Initially it was thought that inefficiency would result from such a step since the existence of a total head gradient increases the mixing losses. Moreover the radial flows necessary to establish equilibrium were expected to result in a further loss in efficiency. These fears have been shown by experiment to be unfounded, and in fact very high efficiencies<sup>(72)</sup> have been obtained from rotors designed to have increasing work capacity towards the tip.

There are, however, very well-defined limits to the amount by which arbitrary vortex blading, as opposed to free vortex

blading, will increase the mean total head rise of a given fan unit. As the boss ratio decreases the potential gain will, on a percentage basis, be increased.

Arbitrary vortex flow may also find an application where, for aesthetic or practical reasons, a very small boss ratio is desirable. Since the swirl and flow coefficients for a free vortex are inversely proportional to the radius,  $\epsilon$  and  $\lambda$  tend to infinity as the axis is approached. It is clear, therefore, that design and manufacturing difficulties are inevitable when the design of a free vortex fan having a boss ratio of the order of 0.2 is attempted. In the case of low pressure rise fans, the high tail fairing losses indicated in Fig. 13.5 for low  $k_{th}$  may impose the necessity of using very small boss ratios, in which case consideration should be given to a design based on arbitrary vortex flow.

At first sight, a linear swirl distribution approximating to the free vortex one for values of  $x$  in excess of 0.4 might appear logical. In the majority of cases, however, advantage should be taken of the greater work potential of the blade tips, therefore the designer should arrange for a regular increase in  $k_{th}$  from boss to tip. A reduced number of blades and an improved blade planform are probable advantages of such a design.

Despite the large number of variables present in arbitrary vortex flow, a direct approach to the design problem can be made when simplifying assumptions based on experimental evidence are employed.

## 16.2. General Design Steps

Detailed rotor design falls into three general sections :

- (i) Choice of fan and boss diameters, fan speed and swirl distribution to give the required flow and pressure rise.
- (ii) Solution of flow equations for the purpose of establishing the axial velocity component distribution.
- (iii) Use of the above data in computing the blade element details.

In designing stators steps (ii) and (iii) are necessary. When

prerotators are used, the axial velocity distribution downstream of these stators must be determined before the rotor design can be attempted.

### 16.3. Basic Pressure Relations

The fan configuration described and illustrated in Section 8.3 will be adopted in developing the theory. Since the axial velocity component is now a variable in both the radial and axial directions, the relations at the four stations for an elementary annulus are :

$$H_0 = p_0 + \frac{1}{2}\rho u_0^2 \quad (16.1)$$

$$H_1 = p_1 + \frac{1}{2}\rho u_1^2 + \frac{1}{2}\rho(\omega_p r)^2 \quad (16.2)$$

$$H_2 = p_2 + \frac{1}{2}\rho u_2^2 + \frac{1}{2}\rho(\omega_s r)^2 \quad (16.3)$$

$$H_3 = p_3 + \frac{1}{2}\rho u_3^2 \quad (16.4)$$

In the above relations, the velocity heads associated with the small radial flows have been ignored as being of second order magnitude.

Continuing with the policy of rejecting second order terms in order to limit the number of variables, we have from Section 8.3

$$H_2 - H_1 = \Delta h_{th} = \rho \Omega r (\omega_s r + \omega_p r) \quad (16.5)$$

which involves the assumption of no radial displacement of the flow and no rotor losses.

Finally it is assumed that radial equilibrium is very quickly established downstream of a particular blade row. The condition for such equilibrium was established in Section 5.2 and is expressed as follows :

$$\frac{dp}{dr} = \rho \frac{(\omega r)^2}{r} \quad (5.1)$$

At stations 1 and 2 the equations are respectively

$$\left. \begin{aligned} \frac{dp_1}{dr} &= \rho \frac{(\omega_p r)^2}{r} \\ \frac{dp_2}{dr} &= \rho \frac{(\omega_s r)^2}{r} \end{aligned} \right\} \quad (16.6)$$

All the above assumptions find justification in the close

agreement which has been established between theory and experiment (see Section 22.4.4).

## 16.4. Initial Design Considerations

To facilitate a simple analytical approach to the design problem, the swirl distribution given in Section 5.3 will be adopted. Therefore,

$$\left. \begin{aligned} \bar{\epsilon}_p &= a_p + b_p x \\ \bar{\epsilon}_s &= a_s + b_s x \end{aligned} \right\} \quad (16.7)$$

where  $\bar{\epsilon} = \omega r / U$  and  $a$  and  $b$  are constants to be chosen. When  $\omega r$  is constant along the span it follows from eq. (16.5) that  $\Delta h_{th}$  is also a linear function of  $x$ .

In solving for the axial velocity distribution downstream of a row of blading, a knowledge of the radius at which  $u = U$  removes the need for a trial and error method of solution. In most instances, the relation between the axial component and the radius is approximately linear and this feature simplifies the problem.

The total flow through the fan is given by

$$\text{Vol. flow/sec} = 2\pi \int_{r_b}^R u r \, dr$$

Dividing throughout by  $\pi(R^2 - r_b^2)$ ,

$$U = \frac{2}{1 - x_b^2} \int_{x_b}^1 u x \, dx \quad (16.8)$$

Eq. (16.8) can be integrated by writing

$$u = C_1 + nx$$

giving

$$U = \left[ (u - nx) + \frac{2}{3} n \left( \frac{1 - x_b^3}{1 - x_b^2} \right) \right]$$

Defining the radial position at which  $u = U$  by  $x_U$ ,

$$x_U = \frac{2}{3} \left( \frac{1 + x_b + x_b^2}{1 + x_b} \right) \quad (16.9)$$

Therefore the point at which the local velocity is equal to the mean velocity is independent of the constants,  $C_1$  and  $n$ .

An exception to the above linear rule may occur downstream of the last row of blading when all swirl has been removed. Here the air particles follow a truly axial direction and hence the static pressure will be constant throughout a given cross-section. Hence the radial variation in the axial velocity head will be identical to the assumed change in total head. A simple design relation which is approximately true for the case of constant swirl is

$$u = C_2 + m\sqrt{x}$$

The parameter  $x_U$  is then given by

$$x_U = \frac{1}{2^5} \left( \frac{1 - x_b^{5/2}}{1 - x_b^2} \right)^2 \quad (16.10)$$

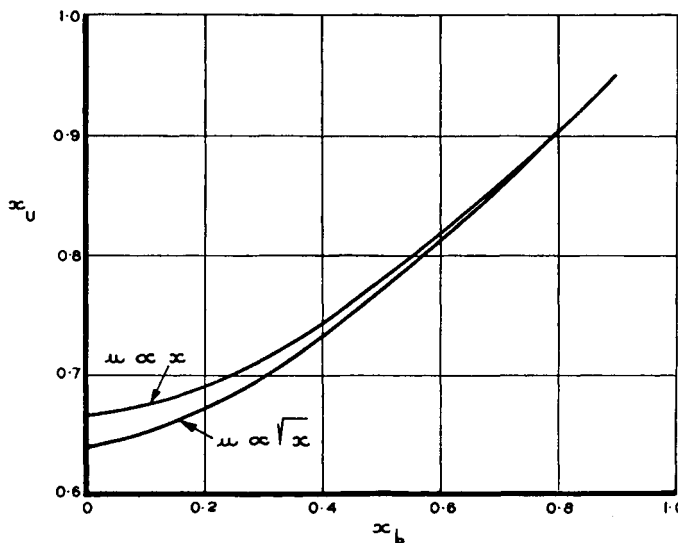


Fig. 16.1. Radial position at which local axial velocity equals mean value

From the graphical presentations of eqs. (16.9) and (16.10) given in Fig. 16.1, it will be seen that the difference in  $x_U$  is negligible except for small values of  $x_b$ .

The mean total head rise is given by

$$\Delta H_{th} = \frac{1}{\pi(R^2 - r_b^2)} \int_{r_b}^R 2\pi \Delta h_{th} r \, dr \quad (16.11)$$

Assuming the distribution  $\Delta h_{th}$  to be approximately linear with  $x$ , the mean coefficient  $K_{th}$  is obtained from eq. (8.12) in the form

$$K_{th} = \frac{2x_U}{\bar{A}} (\bar{\epsilon}_s + \bar{\epsilon}_p)_{x_U} \quad (16.12)$$

where  $\bar{A} = U/\Omega R$ , and  $k_{th} = K_{th}$  at  $x_U$ , computed from eq. (16.9).

[In developing the free vortex design method of Section 8, the flow and swirl coefficients were defined in terms of the local velocity,  $u$ , while the pressure coefficients were based on  $U$ , the mean axial velocity. Since  $u = U$  for this design condition, the universal use of the mean velocity in all coefficients might at this stage appear to be more logical, but in dealing with the various requirements of design, and of analytical and test procedures, some flexibility is of distinct advantage.]

## 16.5. Axial Velocity Distribution for Rotor

Subtracting eq. (16.2) from eq. (16.3), substituting for  $(H_2 - H_1)$  in eq. (16.5), and dividing throughout by  $\frac{1}{2}\rho U^2$

$$\frac{p_2 - p_1}{\frac{1}{2}\rho U^2} + \left(\frac{u_2}{U}\right)^2 - \left(\frac{u_1}{U}\right)^2 + \bar{\epsilon}_s^2 - \bar{\epsilon}_p^2 = \frac{2}{\lambda} (\bar{\epsilon}_s + \bar{\epsilon}_p) \quad (16.13)$$

This is the basic equation which must be satisfied at all radii. When eqs. (16.6) are integrated, the above pressure term can be replaced by inertia terms. Since the flow parameters at station  $x_U$  are known in detail, this radial position is chosen as an integration limit. It then follows that

$$p_1 - (p_1)_{x_U} = \rho \int_{x_U}^x \frac{(\omega_p r)^2}{x} \, dx$$

$$p_2 - (p_2)_{x_U} = \rho \int_{x_U}^x \frac{(\omega_s r)^2}{x} \, dx$$

Hence

$$\frac{p_2 - p_1}{\frac{1}{2}\rho U^2} = 2 \int_{x_U}^x \bar{\epsilon}_s^2 \frac{dx}{x} - 2 \int_{x_U}^x \bar{\epsilon}_p^2 \frac{dx}{x} + \left[ \frac{p_2 - p_1}{\frac{1}{2}\rho U^2} \right]_{x_U} \quad (16.14)$$

Solving eq. (16.13) at  $x_U$ ,

$$\left[ \frac{p_2 - p_1}{\frac{1}{2} \rho U^2} \right]_{x_U} = \left[ (\bar{\epsilon}_p + \bar{\epsilon}_s) \left( \bar{\epsilon}_p - \bar{\epsilon}_s + \frac{2}{\lambda} \right) \right]_{x_U} \quad (16.15)$$

Finally, by combining eqs. (16.13), (16.14) and (16.15),

$$\begin{aligned} \left( \frac{u_2}{U} \right)^2 &= \left( \frac{u_1}{U} \right)^2 + \left[ (\bar{\epsilon}_p + \bar{\epsilon}_s) \left( \bar{\epsilon}_p - \bar{\epsilon}_s + \frac{2}{\lambda} \right) \right] - \left[ (\bar{\epsilon}_p + \bar{\epsilon}_s) \left( \bar{\epsilon}_p - \bar{\epsilon}_s + \frac{2}{\lambda} \right) \right]_{x_U} \\ &\quad + \left[ 2 \int_{x_U}^x \bar{\epsilon}_p^2 \frac{dx}{x} - 2 \int_{x_U}^x \bar{\epsilon}_s^2 \frac{dx}{x} \right] \end{aligned} \quad (16.16)$$

The desired velocity,  $u_2$ , is now expressed in terms of known quantities when it is assumed that conditions downstream of the prerotators have already been established. The latter terms can be integrated as follows:

$$\begin{aligned} 2 \int_{x_U}^x \bar{\epsilon}^2 \frac{dx}{x} &= 2 \int_{x_U}^x (a + bx)^2 \frac{dx}{x} = [2a^2 \log_e x + b^2 x^2 + 4abx] \\ &\quad - [2a^2 \log_e x + b^2 x^2 + 4abx]_{x_U} \end{aligned} \quad (16.17)$$

## 16.6. Axial Velocity Distribution for Prerotators

Assuming no total head loss in the blading the subtraction of eq. (16.1) from eq. (16.2) gives

$$\frac{p_1 - p_0}{\frac{1}{2} \rho U^2} + \left( \frac{u_1}{U} \right)^2 - \left( \frac{u_0}{U} \right)^2 + \bar{\epsilon}_p^2 = 0 \quad (16.18)$$

Assuming zero swirl upstream of the stators, integration of eq. (5.1) at the upstream and downstream stations gives

$$p_0 = \text{const.}$$

$$\text{and } p_1 - (p_1)_{x_U} = \rho \int_{x_U}^x \frac{(\omega_p r)^2}{x} dx$$

and hence

$$\frac{p_1 - p_0}{\frac{1}{2} \rho U^2} = 2 \int_{x_U}^x \bar{\epsilon}_p^2 \frac{dx}{x} + \left[ \frac{p_1 - p_0}{\frac{1}{2} \rho U^2} \right]_{x_U} \quad (16.19)$$

Solving eq. (16.18) at  $x_U$ ,

$$\left[ \frac{p_1 - p_0}{\frac{1}{2} \rho U^2} \right]_{x_U} = -[\bar{\epsilon}_p^2]_{x_U} \quad (16.20)$$

Hence, finally,

$$\left(\frac{u_1}{U}\right)^2 = \left(\frac{u_0}{U}\right)^2 - 2 \int_{x_U}^x \bar{\epsilon}_p^2 \frac{dx}{x} - \bar{\epsilon}_p^2 + [\bar{\epsilon}_p^2]_{x_U} \quad (16.21)$$

When the integral is solved by means of eq. (16.17), the distribution of  $u_1$  along the blade can readily be computed. The velocity  $u_0$  can usually be taken as constant and equal to  $U$ .

## 16.7. Axial Velocity Distribution for Straighteners

Downstream of the straightener vanes there is no radial gradient of static pressure. There is, however, a change in axial velocity which may be determined when  $H_2$  is assumed to equal  $H_3$ , and eq. (16.3) is subtracted from eq. (16.4), i.e.

$$\frac{p_3 - p_2}{\frac{1}{2} \rho U^2} + \left(\frac{u_3}{U}\right)^2 - \left(\frac{u_2}{U}\right)^2 - \bar{\epsilon}_s^2 = 0 \quad (16.22)$$

When  $p_3$  is assumed to be constant and the pressure term treated in a manner similar to that used for previous ones, the required equation is :

$$\left(\frac{u_3}{U}\right)^2 = \left(\frac{u_2}{U}\right)^2 + 2 \int_{x_U}^x \bar{\epsilon}_s^2 \frac{dx}{x} + \bar{\epsilon}_s^2 - [\bar{\epsilon}_s^2]_{x_U} \quad (16.23)$$

All terms on the right-hand side of the equation will be known from the rotor computations.

## 16.8. Blade Element Design Parameters

The mean relative velocity,  $w_r$  is affected by the change in the axial component as the air passes through the rotor. In line with the procedure adopted with the swirl component (Section 8.3) the effective axial component is taken to be the mean of  $u_1$  and  $u_2$ . Therefore in order to make use of the design equations and graphs developed for the free vortex case, the swirl and flow coefficients must be re-defined in the following terms :

$$\lambda_{12} = \frac{u_1 + u_2}{2Q_r} \quad (16.24)$$

$$\epsilon_{p_{01}} = \frac{2\omega_p r}{u_0 + u_1} \quad (16.25)$$

$$\epsilon_{p_{12}} = \frac{2\omega_p r}{u_1 + u_2} \quad (16.26)$$

$$\epsilon_{s_{12}} = \frac{2\omega_s r}{u_1 + u_2} \quad (16.27)$$

$$\epsilon_{s_{23}} = \frac{2\omega_s r}{u_2 + u_3} \quad (16.28)$$

where the velocity  $u$  has been replaced by the appropriate local mean axial velocity. This development introduces an exception to the rule that all pressure coefficients are expressed in terms of the mean axial velocity,  $U$ . Eq. (8.12) must be rewritten

$$k_{th}' = \frac{\Delta h_{th}}{\frac{1}{2}\rho \left( \frac{u_1 + u_2}{2} \right)^2} = \frac{2}{\lambda_{12}} (\epsilon_{s_{12}} + \epsilon_{p_{12}}) \quad (16.29)$$

Since the total head distribution in arbitrary vortex flow design is expressed in terms of  $\bar{\epsilon}$ , this equation will not be required for design. A limited use for it exists, however, in the case of rotor analysis.

The original expression (eq. (9.11)) on which the data of Figs. 9.6 to 9.12 are based gives the optimum lift coefficient as a function of the velocities,  $V_1$  and  $V_2$ . In order to reduce eq. (9.11) to eq. (9.8), which is in terms of the inlet and outlet angles,  $\alpha_1$  and  $\alpha_2$ , a constant axial velocity through the rotor at a given radius must be assumed. The mean axial velocity, which has just been defined, is normally adopted in compressor work.

In the design of any type of arbitrary vortex flow fan, therefore, the design equations and graphs developed for free vortex flow can be used, provided the coefficients of eqs. (16.24) to (16.28) replace  $\lambda$ ,  $\epsilon_s$  and  $\epsilon_p$ .

## 16.9. Limitations of Design Method

If the addition of total head to the air were the only consideration involved, arbitrary vortex flow would result in a substantial increase over and above that obtainable with the

usual free vortex configuration. The useful total head rise is, however, equal to the static pressure increase across the fan unit, and some thought should therefore be given to this aspect of the problem.

Downstream of the last blade row of a fan unit designed to have zero residual swirl, the static pressure at any cross-section will be constant. Therefore the design increase in total head towards the tip will be limited by axial velocity considerations; as the radial gradient in  $\Delta h$  is increased, the axial velocity at the root is diminished, with undesirable consequences. First, the reduction in the effective axial velocity at the blade roots will reduce the work potential in this region. Secondly, separation over the tail fairing will be precipitated when the dynamic head in this region is low.

The author is unaware of any detailed experimental data on arbitrary vortex units employing both straighteners and a tail fairing; hence the limit to be suggested must be regarded as tentative only, pending experimental confirmation. With this qualification, it is suggested that the design difference in total head between root and tip should not exceed 1.5 times  $\frac{1}{2}\rho U^2$ . Using eq. (16.5) in a non-dimensional form, this condition can be expressed by

$$\frac{2}{A}[(\bar{\epsilon}_s + \bar{\epsilon}_p)_t - x_b(\bar{\epsilon}_s + \bar{\epsilon}_p)_b] < 1.5 \quad (16.30)$$

The amount by which the mean total head rise coefficient can exceed the local value at the root will, for a linear total head distribution, be approximately half this value, i.e. 0.75. Since arbitrary vortex flow tends to reduce the work capacity at the blade root, the possible increase in  $K_{th}$  when free vortex flow is departed from may be significantly less than 0.75.

With a suitable rearrangement of eqs. (16.1) to (16.5) a spanwise distribution of  $\omega r$  can be computed to give, in the design case, an approximately linear radial variation in  $u_3$ . However, any ensuing design improvements at the blade root will in most cases be small. Provided care is taken in such circumstances to use the equations for the general case, no design difficulties will be encountered.

The gradient,  $dk/dx$ , increases with load on an arbitrary vortex rotor, an extreme example of which is available in Fig. 22.18. Therefore, in operating this type of fan at appreciably higher loads than design, a decrease in  $u_3/U$  at the boss, attended by flow problems, must be anticipated.

When the swirl distribution approximates to a free vortex one, the axial velocity can be assumed to be constant throughout the unit.

### 16.10. Design Procedures

The designer now possesses sufficient information for design purposes. The choice of fan and boss diameters and rotor speed precedes the conversion of the flow and head requirements into the non-dimensional coefficients,  $K_{th}$  and  $\bar{A}$ . The swirl coefficients at  $x_V$  can then be determined from eq. (16.12) and the distribution of swirl adjusted so that the limit suggested in eq. (16.30) is not exceeded.

The axial velocity distributions are obtained from the solution of eqs. (16.16), (16.21) and (16.23). Conversion of the flow and swirl coefficients, based on the velocity,  $U$ , into the required form for blade element design follows from the relations

$$\lambda_{12} = \bar{\lambda} \frac{u_1 + u_2}{2U} \quad (16.31)$$

$$\epsilon_{p_{01}} = \bar{\epsilon}_p \frac{2U}{u_0 + u_1} \quad (16.32)$$

$$\epsilon_{p_{12}} = \bar{\epsilon}_p \frac{2U}{u_1 + u_2} \quad (16.33)$$

$$\epsilon_{s_{12}} = \bar{\epsilon}_s \frac{2U}{u_1 + u_2} \quad (16.34)$$

$$\epsilon_{s_{23}} = \bar{\epsilon}_s \frac{2U}{u_2 + u_3} \quad (16.35)$$

The design of the blade elements is possible when the above parameters are used in the manner illustrated in Sections 18.5 and 18.6.

## 16.11. Efficiency Estimates

For free vortex flow, the midspan station was chosen as being representative of the fan in estimating the mean total head losses. With the increase in load towards the tip which normally occurs for arbitrary vortex flow, it is suggested that  $x_U$  be adopted as the representative station (see Fig. 16.1); at this station the axial velocity is constant and equal to the mean value for the fan. Hence the appropriate values of  $\bar{\epsilon}_p$ ,  $\bar{\epsilon}_s$  and  $\bar{\lambda}$  can be used in assessing the losses in efficiency when the methods outlined in Sections 10 and 12 are employed. It is assumed that arbitrary vortex flow does not involve total head losses additional to those listed therein.

## 16.12. Torque and Thrust

The equations given in Sections 15.1 and 15.2 for free vortex flow must now be modified. Instead of eq. (8.9) we can write

$$dQ = \rho \left( \frac{u_1 + u_2}{2} \right) 2\pi r \, dr (\omega_s r + \omega_p r) r \quad (16.36)$$

and when eq. (8.25) is used the torque coefficient is given by

$$Q_c = \int_{x_b}^1 \frac{2(u_1 + u_2)}{U} (\bar{\epsilon}_s + \bar{\epsilon}_p) x^2 \, dx \quad (16.37)$$

Eq. (15.4) can be used as a starting point in developing the thrust coefficient equation. The value of  $(p_2 - p_1)$ , as obtained from eqs. (16.2) and (16.3) is substituted for  $\Delta p$  to give

$$T_c = \int_{x_b}^1 2x \left( \eta_R k_{th} + \bar{\epsilon}_p^2 - \bar{\epsilon}_s^2 + \frac{u_1^2 - u_2^2}{U^2} \right) dx \quad (16.38)$$

The values of thrust and torque then follow from eqs. (8.22) and (8.25) respectively.

### 17.1. Introduction

The axial flow fan has, in general, gained the reputation of being a relatively noisy type of air-moving unit. Too often, owing to bad design or installation of the fan concerned, unnecessary noise is introduced. A short section on noise is therefore appropriate.

The scientific study of fan noise is still in its infancy and hence no comprehensive findings can be given here. There are, however, many known aspects of the problem which should be kept in mind.

Periodic changes in air pressure are transmitted through the air in the form of sound waves. These changes may originate at the surface of a vibrating body or may arise from certain types of air turbulence. The frequency with which the periodic changes take place is of considerable importance as the notes arising from certain frequency bands can be most distressing. When the sound being transmitted at any time covers a wide range of frequencies the result is usually known as noise.

Tolerance of noise varies greatly from individual to individual and hence it is difficult to specify an acceptable level. It is safer, therefore, to assume that all fan noise is undesirable. There are two distinct stages in the task of minimizing fan noise :

- (i) The elimination, in the design stage, of as many potential noise sources as possible and the use of good design principles in minimizing any unavoidable noise.
- (ii) The absorption of a large proportion of the residual noise by appropriate means, e.g. by the use of porous materials.

The second stage has received much attention in textbooks dealing with sound and will therefore receive only passing mention here. Since the first is closely allied to the aerodynamic design, this aspect of noise suppression will be considered more fully.

## 17.2. Noise Sources

Noise in axial flow fans may be attributed to three main, and interdependent, sources. These are:

- (a) the periodic pressure field created by the rotor blades
- (b) vortex noise associated with the turbulence present in shear flows
- (c) mechanical vibrations which may or may not be aerodynamically excited.

The main aspects of these various sources will be considered qualitatively.

**17.2.1. Rotation noise.** At any point in the neighbourhood of a rotor, the air pressure will vary with a frequency given by the product of the number of blades and the rotational speed of the rotor. Normally the contribution from this source is small except near the plane of rotation, in which the sound intensity is at a maximum. Other factors can, however, cause an amplification of the disturbances.

It is usually assumed<sup>(80)</sup> that this form of sound is not associated with a longitudinal wave motion. The author has, however, obtained experimental evidence which suggests that the column of air contained by the duct is vibrated at a forced frequency by the rotor with a nodal pattern similar to that found in organ pipes; the plane of the rotor is, of course, an antinode. When the applied frequency is identical with a multiple of the natural frequency of the air column, resonance occurs. A forced vibration of the duct structure at this frequency can then occur, giving rise to a large increase in the noise intensity. A change in the duct length is often desirable as a means of avoiding organ pipe resonance.

When the flow field through which the rotor blades are moving is non-uniform, a strong note is produced. For example,

the wakes from prerotor vanes produce very noticeable increases in the noise level. At the trailing edge of an aerofoil, the velocity gradients across the wake are large but diminish quickly as the flow passes downstream. Hence the distance between the stator and rotor blades is of considerable importance from a noise point of view. When the distance is small, the noise can be very intense and even painful. The same, of course, applies when plate or rod systems are used upstream of the rotor as mechanical supports. Even in the absence of a wake, some increase in noise, occasioned by the rotor blades cutting the non-uniform pressure field created by the stators while deflecting the flow, might be expected. To minimize the noise intensity, the number of evenly spaced supports or stators and the number of rotor blades should not possess a common factor.

An argument very similar to the above can be applied in the case of the fan fitted with straightener vanes; here, however, the noise intensity is usually lower. The lower relative velocity between the air and the stators is a possible contributing factor. Since the stators can be rigidly supported at each end, restraint can be placed on aerodynamically excited blade vibrations, thus minimizing the noise level.

In the foregoing, it has been tacitly assumed that the wakes are those which normally arise downstream of aerofoils having attached boundary layers. When flow separation is present, the general flow becomes less steady and the wake widens appreciably; a marked increase in noise intensity is at once apparent. An increase in vortex noise can account for quite a large proportion of the additional noise. For low pressure rise fans, an irregular low frequency rumble may be set up, while severe surging can accompany the stall in high pressure rise units. A fan exhibiting the above noise features should be investigated with a view to the possibility of blade stalling.

**17.2.2. Vortex noise.** The aeolian tone was probably the first form of vortex noise to receive attention. When a bluff body is placed in an airstream, boundary layer separation leads to a vortex shedding in which a vortex is shed first from one side of the body and then from the other in an alternating

manner. The body need not necessarily vibrate with the shedding frequency for sound to be propagated. Theories have recently been advanced in an attempt to explain the dynamics of sound arising from an aerodynamic origin. For present purposes, however, it is sufficient to accept that a turbulent mixing flow is capable of producing audible and undesirable sounds. The noise level will, of course, rise with increasing turbulence in the stream.

The turbulence in an attached boundary layer produces noise which is barely noticeable at the stream velocities usually encountered in industrial installations. Separated flow, whether of a general type or of the kind which produces the aeolian note, causes a sharp increase in noise level, often to a quite objectionable point. This leads to the axiom that the lower the drag or total head losses in a duct system, the quieter the unit.

With the exception of the aeolian type of phenomenon, aerodynamic noise is of complex structure and spread over a wide band of frequencies. This is due to the wide range of eddy sizes found in turbulent mixing flow. The greatest energy, however, is usually found in the vicinity of 1000 cycles per second.

**17.2.3. Mechanical noise.** The vibration of solid bodies can arise from either mechanical or aerodynamic sources. Since such bodies are very efficient noise transmitters, particularly when resonant, every endeavour should be made to avoid excitation or, failing that, to damp the oscillations of the body. Separated or fluctuating flows can create a considerable nuisance by forcing the vibration of rods, supports or sheet metal ducting.

**17.2.4. Compressibility effects.** In the design theory, incompressible flow is assumed since a restriction is placed on the tip speed of the blade (Section 7.9). One of the major reasons for this limitation is the large increase in noise which accompanies the approach to sonic velocities locally near the blade surface. It is therefore customary to limit the rotational velocity of the blade tip to 550 ft/sec which is approximately half the speed of sound for the standard atmosphere.

The increase in noise level with tip speed is related to the

local increase in air density and the possibility of severe shock-induced boundary layer separations.

### 17.3. Noise Investigations

A considerable proportion of the total noise emitted by present day fan installations can be eliminated. The origin of the noise must be investigated as a preliminary to applying corrective measures. Instruments capable of analysing sound and vibration are of great assistance in such an investigation.

A sound analyser, which contains filters, measures the sound energy in a narrow band of frequencies, a process which is repeated for each band of the complete noise spectrum. When the frequency of maximum energy coincides with the rotational frequency, or a multiple thereof, the major source is obvious. If, however, this frequency is not dominant, and the energy is instead distributed over a wide range of frequencies in the neighbourhood of 1000 c/s, vortex noise is at once suspected.

Features which tend to amplify the noise, e.g. separated flow or improper location of stator blades, should receive priority in a noise suppression programme. The next phase of the work involves a reduction in the forced and resonant vibration of solid surfaces; reflecting surfaces should also receive consideration.

### 17.4. Absorption of Noise

A similarity which has been established between electrical and acoustical energies permits treatment of the noise suppression problem in a manner analogous to the use of electrical filters.<sup>(81)</sup> This similarity aids the design of devices which will absorb low frequencies and pass high ones or vice versa. Resonators can also be designed to absorb acoustic energy at a particular frequency; such selective devices are, however, of limited use as in most cases the noise is spread over a wide range of frequencies.

When air velocities are low and the total head losses are in consequence unimportant, very efficient silencing systems can be built; the silencer on a motor vehicle is an example of such

a system. The design of a "filter" system for the normal duct installation, on the other hand, is a difficult problem on account of the desirability of minimizing total head losses. There are, nevertheless, many cases where resonators or filters have produced remarkable reductions in noise level for negligible increases in flow resistance.

Most noise-absorbing devices must be specially designed for each specific case. When high frequencies are the only troublesome ones, sheets of porous materials on the duct walls give noise attenuation over a wide frequency range.

### 17.5. Conclusions

If serious thought is given to the matters outlined above, a number of the mistakes which are often made in the fan design stage can be avoided. As more and more quantitative data become available, a design estimate of noise level will become a possibility.

The author is of the opinion that, with an adequate research effort, large improvements in noise-absorbing techniques are possible. The design of silencing devices will eventually be integrated into the general aerodynamic design problem.

The subject matter presented here, when used in conjunction with the given references, should prove of value to the engineer concerned with noise suppression. It is recommended that each problem be diagnosed along the lines indicated in order to eliminate unnecessary sources of sound and to design effective absorption devices. In the latter connection, the reader is advised to study modern textbooks dealing with sound in a comprehensive manner.

---

# DESIGN EXAMPLES

## 18.1. Introduction

Fan design is not inherently a difficult problem. The design equations are relatively few and simple and can be expressed graphically in most cases. Free vortex type fans involve a minimum amount of work and can, with experience, be designed aerodynamically in three to four hours total time.

There are, however, certain aspects of fan design which may cause the prospective designer some anxiety. The main difficulty is probably associated with the large number of variables which play either a major or minor part in the design procedure. After a little practical experience has been gained, however, the numerous variables can be mentally sorted into a few major groups.

Difficulties of decision may also arise in the early stages of a design. The type of unit, the method of design, the size and speed of the fan, are all matters demanding attention; a decision on one is capable of affecting one or more of the others. At this point the design is very fluid and preliminary procedures can become extremely tedious. A graphical approach at this stage cannot be too highly recommended.

For a given operating condition, two designers could produce fan units so vastly different in appearance that it would prove somewhat difficult to accept them as alternative solutions. On refinement, however, the two designs should tend to converge towards a single optimum solution in which a careful balance between various conflicting requirements is attained. As in

other branches of engineering, however, individual differences will still be present and these will tend to stamp the final product with the designer's "trade mark".

The design examples presented in this Section have been planned to give a fairly wide coverage of the design data presented in previous Sections; the emphasis has been placed on designs where one or more of the blade limitations previously discussed is involved. In the initial stages, the design procedure is relatively independent of the blade design method which must eventually be chosen. Preliminary procedures are illustrated in the next sub-section and the results of this investigation are followed up in Section 18.3 with the design of a cambered plate fan employing the isolated aerofoil method.

## 18.2. Preliminary Design Procedures

Very often the type of fan unit, fan speed, fan diameter and possibly boss diameter are fixed by circumstances outside the designer's control. When the design is similar to an existing fan, or when the designer has the necessary experience, the detailed design problem can be tackled directly since the designer is confident that the flow requirements can readily be met in a satisfactory manner.

A possible specification for a fan unit could read as follows:

*A ducted axial flow fan fitted with flow straighteners is required to deliver 12,000 cu. ft/min through a duct system in which the total head loss is 2.0 in. of water. It is desirable to limit the fan diameter to 30 in. Rotor and stator blades are to be of a cambered plate type. The free vortex type rotor, which is to operate at sea level ( $\rho = 0.002378$  slug/ft<sup>3</sup>), is to be directly coupled to an electric motor (1430 rev/min) enclosed in the tail fairing.*

In the above specification, the type of unit and the rotor speed have been fixed, thus leaving only the fan and boss diameters to be determined. The choice of these latter variables will influence the blade design and the overall efficiency. It is therefore customary to carry out preliminary designs for the purpose of establishing the best overall dimensions of the unit.

For five different combinations of fan and boss diameters, the results given in Table 18.1 have been obtained.

Table 18.1. Preliminary Designs

Design	A	B	C	D	E
$2R$ Fan dia. (in.)	30	30	30	27	27
$2r_b$ Boss dia. (in.)	20	18	16	20	18
$x_b = r_b/R$	0.667	0.6	0.533	0.741	0.667
$u = \text{cu. ft/min}/60\pi R^2(1-x_b^2)$	73.4	63.6	57.0	111.1	90.6
$\frac{1}{2}\rho u^2$	6.41	4.81	3.86	14.7	9.76
$K_{th} = (\Delta H_T / \frac{1}{2}\rho u^2) \times (1/\eta_T)$	2.10	2.81	3.51	0.91	1.38
$\Omega R = \text{rev/min. } 2\pi R/60$	187	187	187	168	168
$A = u/\Omega R$	0.392	0.340	0.305	0.663	0.540
$\lambda_b = A/x_b$	0.588	0.567	0.572	0.894	0.811
$\epsilon_b$ Fig. 8.4	0.61	0.80	1.00	0.40	0.56
$(C_L \sigma)_b$ Fig. 8.7	0.72	0.94	1.24	0.61	0.81
$C_{Lb}^*$ Fig. 9.9	0.90	0.70	0.54	1.14	0.94
$\sigma_b = (C_L \sigma)/C_L^*$	0.79	1.34	> 2	0.54	0.87
$\lambda_m = A/x_m$	0.471	0.425		0.761	0.649
$\epsilon_m$ Fig. 8.4	0.50	0.60		0.36	0.44
$\gamma K_R/K_{th}$ Fig. 10.1	2.12	2.21		1.75	1.78
$(K_{Rp} + K_{Rs})/K_{th}$ see text	0.103	0.108		0.085	0.087
$K_{RA}/K_{th}$ eq. (10.15)	0.03	0.03		0.03	0.03
$\eta_R$ eq. (10.1)	0.867	0.862		0.885	0.883
$\gamma K_S/K_{th}$ Fig. 12.1	0.50	0.465		0.78	0.68
$K_S/K_{th}$ see text	0.024	0.023		0.038	0.033
$K_D/K_{th}$ Fig. 13.5	0.066	0.042		0.176	0.100
$\eta_T$ eq. (14.6)	0.777	0.797		0.671	0.750

Notes: In estimating  $K_{th}$ ,  $\eta_T$  was assumed to be 0.77 in all cases. All quantities are expressed in standard units unless otherwise indicated.

It will be noted that the tabulations are sub-divided into three main sections:

- (i) reduction of the given data to a non-dimensional form suitable for detailed design purposes
- (ii) study of loading on the rotor and stator blades at the blade root which is the most critical section
- (iii) estimates of component losses in the fan unit and a prediction of overall efficiency.

The designer, on the basis of previous experience, is often able to assess the chances of a successful design at the conclusion of the first sub-section. Although very little effort is required in carrying out the above tabulated computations, a graphical method can be used as an alternative in the early stages of the preliminary design. The non-dimensional

coefficients,  $A$  and  $K$ , are related to the dimensional quantities by the expressions

$$A = \frac{\text{cu. ft/min}}{2\pi^2(1-x_b^2)R^3 \times \text{rev/min}} \quad (18.1)$$

$$K = \frac{R^4(\Delta H(\text{in. of water}))(1-x_b^2)^2 \times 60^2 \times 5.2 \times \pi^2}{\frac{1}{2}\rho(\text{cu. ft/min})^2} \quad (18.2)$$

The nomogram presentation of these relations, as given in Figs. 18.1 and 18.2, provides a rapid and simple method for selecting configurations suitable for further investigation.

A measure of the severity of stator loading is at once apparent from the value of  $\epsilon_b$  given in Table 18.1; except for design C, the values are below the recommended upper limit of unity. In assessing the rotor blade loading, use has been made of the cascade data on optimum lift in order to set an upper limit to the design lift coefficient at the critical station. (When the blade loading is low and overloading at the blade root no longer a factor,  $C_L$  is of interest in preliminary design procedures only for the purpose of assessing efficiency. The choice of lift coefficient is usually arbitrary, being influenced by the factors discussed in Sections 4.8, 10.4 and 10.8.) At this stage, design C can be discarded on the grounds of excessive rotor and stator loading.

From the values of  $\epsilon$  and  $\lambda$  at the midspan station, combined with blade data, the loss coefficients can be computed in the manner shown. Provided the design lift coefficients are above 0.7, the lift/drag ratio, as presented in Fig. 18.3, is relatively independent of  $C_L$ ; the drag coefficients quoted therein should produce conservative estimates of the fan efficiency. For the rotor, the values of  $C_{L\sigma}$  and  $C_{L*}$  at the root suggest the use of lift coefficients not less than 0.7. A similar state of affairs exists in the case of the straighteners when the lift coefficients, for the values of  $\epsilon_m$  tabulated above, are obtained from Fig. 11.6. In view of these considerations, a constant value of 20.5, for  $C_L/(C_{D_P} + C_{D_S})$ , has been assumed in all cases. The third place of decimals, to which the loss coefficients are given, is not significant and has been included for comparative purposes only.

The highest overall efficiency was obtained with design B. A

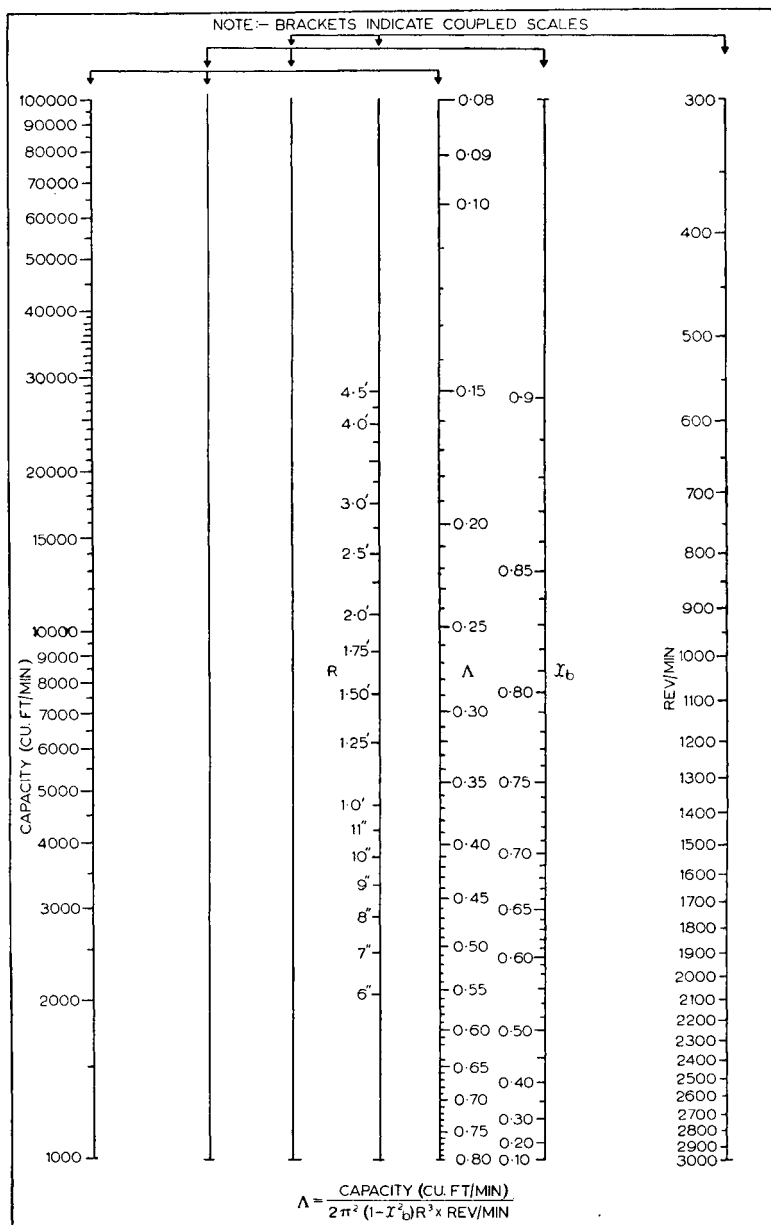


Fig. 18.1. Nomogram involving the flow coefficient

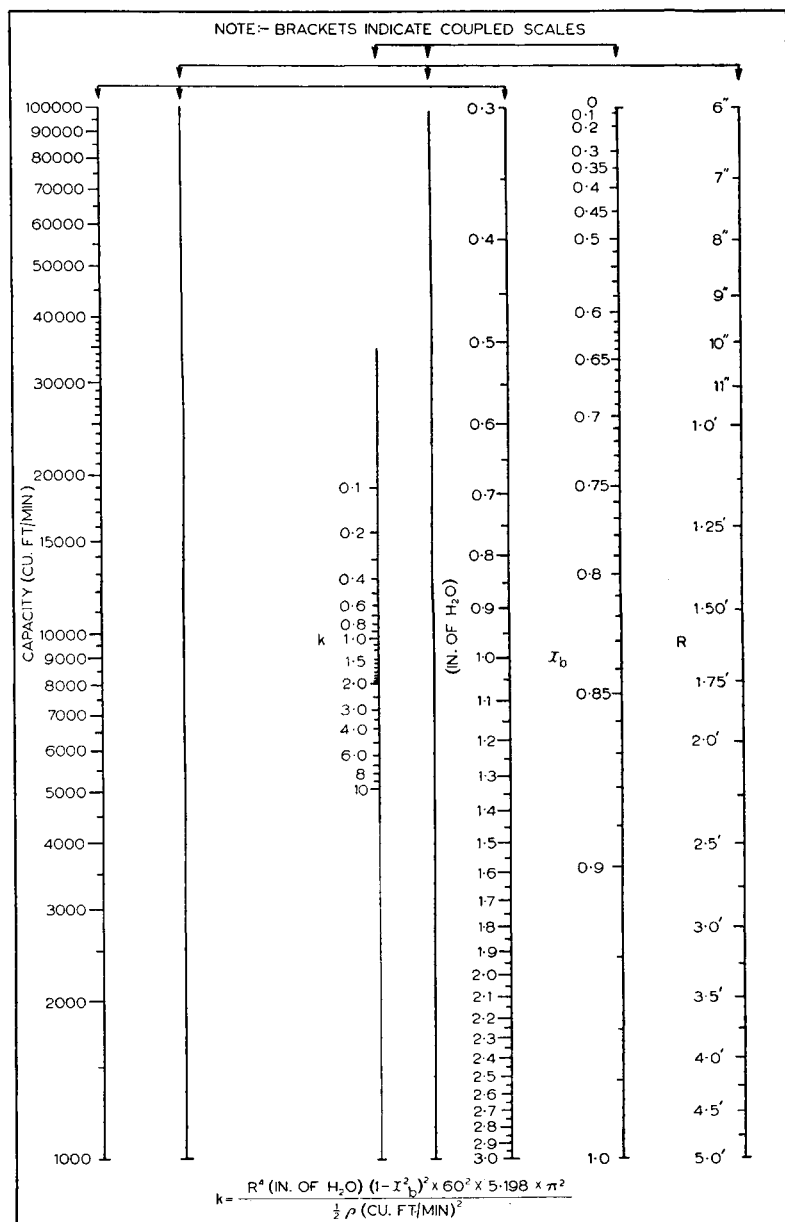


Fig. 18.2 Nomogram involving the total head rise

study of the rotor loading of this design suggests that the blade root details, as computed by the isolated aerofoil method, may have to be modified to allow for multiplane interference effects. The stators can readily be designed by the cascade method.

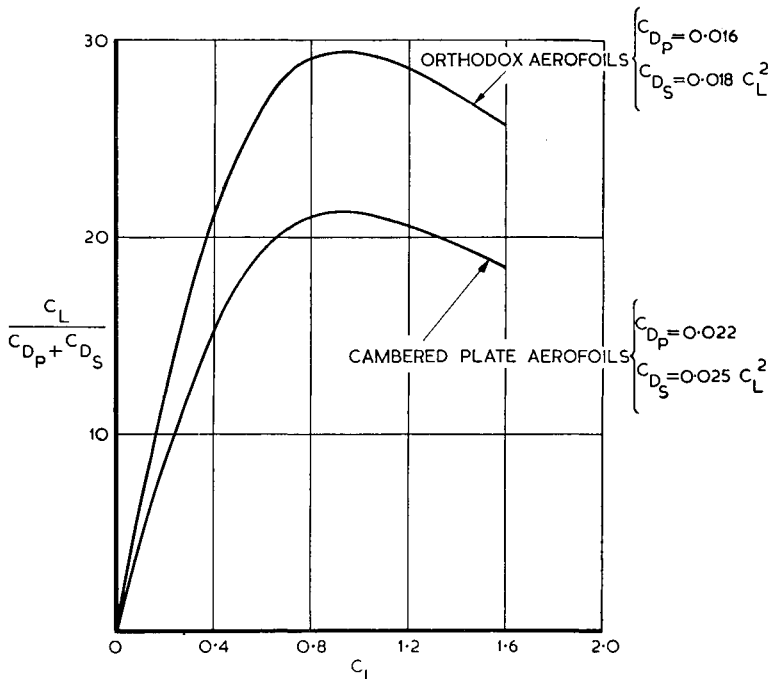


Fig. 18.3. Lift to drag ratios for preliminary design purposes

Assuming the efficiency is 0.80, the shaft power is given by eq. (15.10), i.e.

$$\begin{aligned} \text{h.p.} &= \frac{12,000 \times 2 \times 5.2}{33,000 \times 0.80} \\ &= 4.73 \end{aligned}$$

Housing such a relatively small motor in the 18 in. o.d. rear fairing should not prove difficult.

In all respects, therefore, design B can be made to fulfil the specification requirements; detailed design procedures will be given in the next sub-section.

Returning to a comparison of the designs, it will be seen that the tail fairing loss constitutes a very important factor influencing the overall efficiency of the units. In addition, a casual inspection of the trends in blade loading and efficiency as outlined in Table 18.1 indicates that a choice of fan and boss diameters of 27 in. and 16 in. respectively would also lead to a practical design configuration.

In the foregoing example it has been assumed that the total head rise requirement is independent of fan diameter. When, however, the fan units exhaust direct to the atmosphere the discharge loss for the 27 in. fan will be 23 per cent greater than that for the larger 30 in. unit. Given the same upstream duct losses, the  $\Delta H_T$  requirement for the smaller unit will then be greater than 2 in. of water; the preliminary designs just described would, under these circumstances, be carried out for the appropriate values of  $\Delta H_T$ .

Irrespective of the initial data supplied to a designer, a layout similar to that employed in Table 18.1 should meet all requirements.

When static efficiency is of vital importance, provision should be made for adding this quantity, as determined from eq. (14.11), to the table.

### 18.3. Free Vortex Design, Isolated Aerofoil Method

As mentioned previously, design B has been chosen for detailed design. Since the total efficiency was 3 per cent greater than originally assumed,

$$K_{th} = 2.81 \times \frac{0.77}{0.80} = 2.71$$

This small change in  $K_{th}$  will not noticeably alter the efficiency just computed and hence there is no necessity for a new calculation.

Making the free vortex design assumptions that the total head rise coefficient,  $k_{th}$ , and the axial velocity component,  $u$ , are both constant along the blade span, the design follows readily from eqs. (8.12), (8.14) and (8.27). The results of these computations are set out in Table 18.2.

Table 18.2. Rotor Blade Details from Momentum Considerations

$x = r/R$	0.6	0.7	0.8	0.9	1.0
$\lambda = A/x$	0.567	0.486	0.425	0.378	0.340
$\epsilon$ eq. (8.12)	0.768	0.658	0.576	0.512	0.461
$1 - \frac{1}{2}\epsilon\lambda$	0.782	0.840	0.878	0.903	0.921
$\tan \varphi_r$ eq. (8.14)	0.725	0.578	0.484	0.418	0.369
$\varphi_r$	35.9	30.0	25.8	22.7	20.3
$\sin \varphi_r$	0.586	0.500	0.435	0.386	0.347
$C_L\sigma$ eq. (8.27)	0.900	0.658	0.501	0.395	0.320

The next design phase concerns the detailed design of the blade elements at the chosen radii. First, the appropriate Reynolds number can, when  $c$  is assumed to equal half the blade span (see Section 18.7), be determined for the midspan station from the relation

$$R_e = w_r c / \nu = \frac{uc}{\sin \varphi_r \nu} \\ = 280,000$$

where  $\nu = 1.564 \times 10^{-4}$  ft<sup>2</sup>/sec at s.t.p. Hence the lift and drag data of Figs. 4.6 and 4.8 ( $R_e = 3.14 \times 10^5$ ) are suitable for design use. Secondly, design lift coefficients in excess of 0.7 have been assumed in the preliminary design; from Fig. 4.10 it would appear that a 6 per cent plate with its high lift/drag ratio is the most efficient in this range.

The root condition will be re-examined for the modified value of  $K_{th}$ , namely 2.71. From Fig. 9.9 for  $\lambda_b = 0.567$  and  $\epsilon_b = 0.768$ ,

$$C_L^* = 0.74$$

and hence,

$$\sigma_b = 1.215$$

An attempt can now be made to determine the planform of the blade. Many possibilities exist. Patterson's design methods, considering only the efficiency loss due to profile drag, were aimed at keeping either the blade element efficiency or the lift coefficient constant along the blade. Linear radial variations of either  $C_L$  or  $c$  are among other attractive possibilities. Constant chord can also on occasions produce a satisfactory design. In the present instance, however, constant chord will,

for  $C_L = 0.74$  at the root, result in a tip lift coefficient of 0.44. A glance at the curve in Fig. 4.10 for 6 per cent camber immediately suggests an unsatisfactory efficiency.

Since the  $C_L$  range over which acceptable efficiency can be obtained with cambered plates is less than that for more orthodox aerofoils, a constant design  $C_L$  of 0.8 has been adopted for stations  $x = 0.7$  to 1.0. The number of blades employed will in this case be governed by a desire to keep the blade aspect ratio approximately 2 (see Section 18.7).

Blade element details can now be computed, as in Table 18.3.

Table 18.3. Rotor Blade Element Design Details

$x = r/R$	0.6	0.7	0.8	0.9	1.0
$C_L$	0.74	0.80	0.80	0.80	0.80
$\sigma$	1.215	0.822	0.626	0.494	0.400
$Nc = 2\pi x R \sigma$ (in.)	68.7	54.2	47.2	41.9	37.7
$c$ ( $N=16$ ) (in.)	4.29	3.39	2.95	2.62	2.36
$\alpha$ Fig. 4.6	1.9	2.6	2.6	2.6	2.6
$\varphi_r + \alpha$	37.8(38.7)	32.6	28.4	25.3	22.9

It will be noted that the solidity at the root is in excess of that normally used in the isolated aerofoil method. Hence a check at this station along the lines of the cascade theory appears warranted.

The optimum camber angle,  $\theta$ , and the stagger angle,  $\xi$ , for the values of  $\epsilon$  and  $\lambda$  at  $x_b$  were obtained from Figs. 9.14 and 9.16 respectively, being :

$$\theta = 20.5^\circ$$

$$\xi = 50.3^\circ$$

These values give

$$\begin{aligned} (\varphi_r + \alpha) &= 90^\circ - 50.3^\circ \\ &= 39.7^\circ \\ \alpha &= 39.7^\circ - 35.9^\circ \\ &= 3.8^\circ \end{aligned}$$

and

$$\begin{aligned} b/c &= 0.00221 \times 20.5 \\ &= 0.045 \end{aligned}$$

The camber of the aerofoil at the root is, however, 6 per cent and hence a conversion from a 4.5 per cent to a 6 per cent plate must be made. From Fig. 4.6 it will be seen that the  $C_L$  of an isolated 4.5 per cent plate at  $3.8^\circ$  of incidence is 0.82 and that a 6 per cent plate attains this lift at  $\alpha = 2.8^\circ$ . It is suggested therefore that the new setting at the root should be,

$$\begin{aligned}\varphi_r + \alpha &= 35.9^\circ + 2.8^\circ \\ &= 38.7^\circ\end{aligned}$$

This is equivalent to assuming an interference factor of  $0.74/0.82 = 0.90$ . This new value of blade setting at the root has been added, as an amendment, to Table 18.3. However, owing to the fairly local nature of the correction, no very noticeable reduction in the fan output would be expected with a rotor employing the original root setting.

The torque and thrust on the rotor are given as follows:

$$\begin{aligned}Q_c &= K_{th}A(1 - x_b^2) \\ &= 0.59 \\ Q &= Q_c \frac{1}{2} \rho U^2 \pi R^3 \\ &= 17.4 \text{ ft lb}\end{aligned}$$

$$\begin{aligned}T_c &= K_{th} \eta_R (1 - x_b^2) + \frac{1}{2} K_{th}^2 A^2 (\log_e x_b) \\ &= 1.292 \\ T &= T_c \frac{1}{2} \rho U^2 \pi R^2 \\ &= 30.5 \text{ lb}\end{aligned}$$

Two further portions of the unit remain to be designed. These are the straighteners and the fairings.

As mentioned previously, the cascade design method will be used for the stators. When it is assumed that the flow enters the vane along the tangent at the leading edge, this being the most favourable condition for cambered plates, the optimum design is a function of one variable only, i.e.  $\epsilon_s$ .

Taking the values of  $\epsilon_s$  from Table 18.2 for the various radial stations, the data of Table 18.4 are obtained.

The number of stator vanes, 15, differs by one from that used in the rotor design; this is to reduce the beat noise (Section 17.2.1).

Table 18.4. Straightener Design Details

$x = r/R$	0.6	0.7	0.8	0.9	1.0
$\epsilon$ Table 18.2	0.768	0.658	0.576	0.512	0.461
$s/c$ Fig. 11.6	0.74	0.98	1.22	1.46	1.50
$\theta$ Fig. 11.7	48.3	44.9	41.9	39.5	36.7
% camber eq. (9.26)	10.7	9.9	9.3	8.7	8.1
$\xi$ Fig. 11.7	13.4	10.8	8.9	7.5	6.7
$c (N=15) = 2\pi x R c/s N$ (in.)	5.09	4.49	4.12	3.88	4.19

When the above design is set out geometrically, it will be seen that the blade differs only slightly from a conical shape. Hence, for practical purposes, the design may be adjusted in order to utilize this simple geometric form. Such adjustments involve small modifications to the chord and tangent angles at inlet to and outlet from the stator blade. Increases rather than decreases in blade chord are recommended since the latter will increase the local lift coefficient. So far as blade angles are concerned, the angle of incidence,  $i$ , for the design case should be maintained within the limits  $\pm 3^\circ$ ; small deviations from the design outlet angle are not serious, the residual downstream swirls so obtained being usually of little consequence.

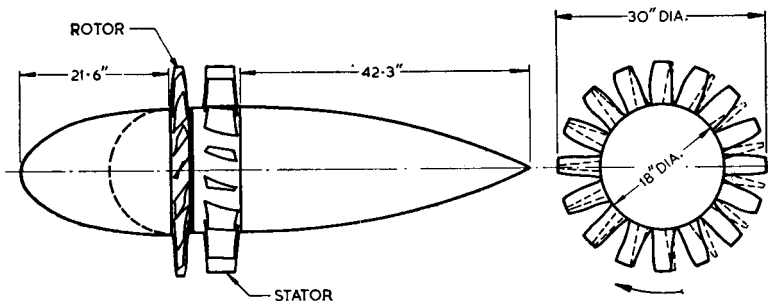


Fig. 18.4. Fan unit designed in Section 18.3

The nose and tail fairings should preferably be good streamlined shapes (see Section 13.1). The diameter of the streamlined body illustrated in Fig. 13.1 reaches a maximum at the 40 per cent length position; the forward and rearward portions of the body can be considered separately when designing the nose

and tail fairings. Nose fairings should be kept relatively short, while tail fairings may have to be long if flow separation is to be avoided. For the conservative included angle of  $8^\circ$ , the appropriate fineness ratio is obtained from Fig. 13.6 as 2.35. A suitable fineness ratio for the nose fairing is 1.2 as this provides a good entry to the fan. This ratio, however, can be reduced without any noticeable penalties. Hemispheres are frequently employed as nose spinners and are generally satisfactory.

The aerodynamic design of the fan unit is illustrated in Fig. 18.4.

#### 18.4. Free Vortex Design, Cascade Design Method

In the remaining design examples, the complete computations will not be given. The emphasis will be on illustrating features associated with the particular method of design.

As an illustration of the cascade aerofoil method, a 6 ft diameter prerotator-rotor unit delivering 110,000 cu. ft/min against a total head loss in the duct system of 12 in. of water has been chosen. The preliminary design, in which the boss ratio and fan speed were assumed to be 0.7 and 920 rev/min respectively, is tabulated in Table 18.5. The efficiency used in estimating  $K_{th}$  was arranged to equal the computed value in this instance.

Table 18.5. Preliminary Design

$u = \text{cu. ft/min}/60\pi R^2(1 - x_b^2)$	127	$\lambda_m = \Lambda/x_m$	0.52
$\frac{1}{2}\rho u^2$	19.2	$\epsilon_m = K_{th}\lambda_m/2$	1.08
$K_{th} = (\Delta H_T/\frac{1}{2}\rho u^2)(1/\eta_T)$	4.16	$(K_{RP} + K_{RS})K_{th}$ Fig. 10.7	0.13
$\Omega R = \text{rev/min } 2\pi R/60$	289	$K_{RA}/K_{th}$ eq. (10.14)	0.02
$\Lambda = u/\Omega R$	0.44	$K_R/K_{th}$	0.15
$\lambda_b = \Lambda/x_b$	0.63	$K_P/K_{th}$ Fig. 12.4	0.03
$\epsilon_b = K_{th}\lambda_b/2$	1.31	$K_D/K_{th}$ Fig. 13.5	0.04
$\sigma_b$ Fig. 9.12	2.06	$\eta_T$ eq. (14.7)	0.78

Stator loading is acceptable since the value of  $\epsilon_b$  is below the limit of 1.5 fixed in Section 11.4. The loading at the rotor blade root is, however, more critical but the value of solidity determined in the above preliminary design is acceptable as it approximates to the recommended upper design limit of 2. The rotor efficiency is not as high as in the previous design

example although the blading is of a more orthodox and efficient type. This apparent anomaly is due to the lower efficiency of a rotor with preswirl (see Section 14.3). When efficiency is the major consideration, a rotor-straightener configuration must be adopted. However, before a fan of this type can be designed to carry out the same task, rotor speed must be increased for the purpose of reducing rotor and stator blade loading. In the present instance, the preswirl condition was chosen in order to illustrate prerotor design.

The rotor blade element design is simplicity itself when optimum conditions are assumed and graphical methods employed. The procedure is illustrated in Table 18.6. Once again the chord has been chosen with a view to keeping the blade aspect ratio approximately 2. From these data, and with the aid of Figs. 4.13 and 9.13, the blade section and setting at each radius can be drawn out.

Table 18.6. Rotor Blade Design Details

$x=r/R$	0.7	0.76	0.82	0.88	0.94	1.0
$\lambda = A/x$	0.629	0.579	0.537	0.500	0.468	0.440
$\epsilon_p = k_{th}\lambda/2$	1.308	1.203	1.118	1.04	0.973	0.915
$\sigma$ Fig. 9.12	2.06	1.59	1.27	1.04	0.86	0.73
$\theta$ Fig. 9.15	16.3	14.2	12.6	11.2	10	9.3
$\xi$ Fig. 9.17	62.9	64.2	65.3	66.3	67.1	68.0
$c(N=48) = 2\pi x R \sigma/N$ (in.)	6.78	5.69	4.91	4.31	3.80	3.44

The development of the prerotor sections follows in a similar manner from the design data tabulated in Table 18.7.

Table 18.7. Prerotor Vane Design Details

$x=r/R$	0.7	0.76	0.82	0.88	0.94	1.0
$\epsilon_p$ Table 18.6	1.308	1.203	1.118	1.04	0.973	0.915
$s/c$ Fig. 11.9	0.92	0.97	1.02	1.08	1.14	1.20
$\theta$ Fig. 11.9	64.6	62.6	60.8	59.0	57.4	55.8
$\xi = \theta/2$	32.3	31.3	30.4	29.5	28.7	27.9
$c(N=37) = 2\pi x R c/sN$ (in.)	4.64	4.78	4.91	4.98	5.03	5.09

In choosing the number of stator blades the main factors taken into consideration were the avoidance of a common

multiple in the number of rotor and stator blades and the choice of a reasonable stator chord without excessive multiplicity of vanes.

### 18.5. Arbitrary Vortex Design, Cascade Design Method

In this illustration, a fan possessing a constant swirl velocity along the blade will be designed to meet the same specification as the previous design example. Since conditions at  $x_U$  will closely approximate to those which are listed in Table 18.5 for  $x_m$ , the efficiency can be assumed to be the same, that is, 0.78.

From eq. (16.9) for  $x_b = 0.7$

$$x_U = 0.859$$

and hence for constant  $\bar{\epsilon}_p$ , eq. (16.12) gives

$$\begin{aligned}\bar{\epsilon}_p &= \frac{4.16 \times 0.44}{2 \times 0.859} \\ &= 1.066\end{aligned}$$

Checking in eq. (16.30)

$$\frac{2\bar{\epsilon}_p}{\bar{\lambda}} (1 - x_b) = 1.45$$

which satisfies the limitation tentatively suggested in Section 16.9.

For the present set of conditions, eqs. (16.16) and (16.21) reduce respectively to

$$\left(\frac{u_2}{U}\right)^2 = 1 + 2\bar{\epsilon}_p \left(\frac{1}{\bar{\lambda}} - \frac{1}{\bar{\lambda}_U}\right)$$

and

$$\left(\frac{u_1}{U}\right)^2 = 1 - 2\bar{\epsilon}_p^2 (\log_e x - \log_e x_U)$$

Table 18.8 provides details of the prerotor vane design procedure.

The distribution of  $u_1/U$  is illustrated in Fig. 18.5 from which it will be noted that the linear design approximation is accurate.

Table 18.8. Prerotator Vane Design Details

$x = r/R$	0.859	0.70	0.76	0.82	0.88	0.94	1.00
$\lambda = \bar{A}/x$	0.512	0.629	0.579	0.537	0.500	0.468	0.440
$\log_e x$	-0.152	-0.357	-0.275	-0.199	-0.128	-0.062	0
$\log_e x - \log_e x_U$	0	-0.205	-0.123	-0.047	0.024	0.090	0.152
$(u_1/U)^2$ eq. (16.21)	1	1.465	1.279	1.106	0.945	0.795	0.655
$u_1/U$	1	1.211	1.131	1.054	0.973	0.891	0.810
$(u_1 + u_0)/2U$	1	1.106	1.066	1.027	0.987	0.946	0.905
$\epsilon_{p01}$ eq. (16.32)	0.964	1	1.039	1.080	1.127	1.178	
$s/c$ Fig. 11.9		1.14	1.11	1.08	1.05	1.02	0.99
$\theta$ Fig. 11.9	57.3	58.1	59.0	60.0	61.0	62.0	
$\xi = \theta/2$	28.7	29.1	29.5	30.0	30.5	31.0	
$c (N=43)$ $= 2\pi x R c / s N$ (in.)	3.23	3.60	3.99	4.41	4.85	5.31	

If the distribution were to differ appreciably from that assumed, then, by rewriting eq. (16.8) in the form

$$\frac{2}{1-x_b^2} \int_{x_b}^1 \frac{u}{U} x \, dx = 1$$

the calculations could be repeated for new values of  $x_U$  until this expression was satisfied.

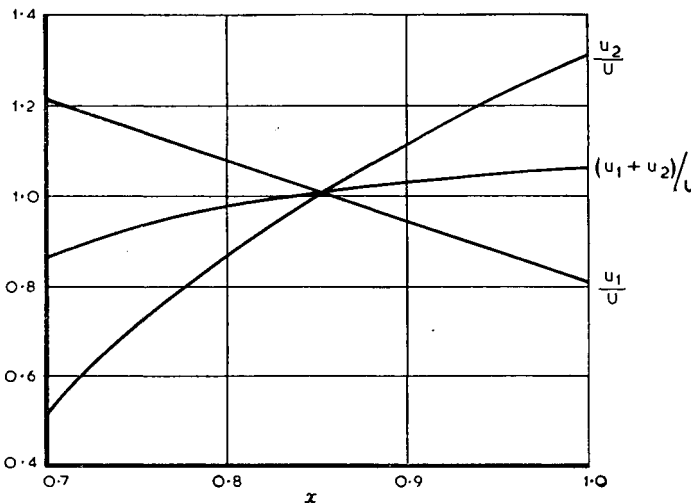


Fig. 18.5. Axial velocity distributions  
for design of Section 18.5

Following this procedure for the rotor, it was found that  $x_U = 0.85$  gave the best result. From a practical point of view, however, it is doubtful whether this refinement is really warranted. Details of the rotor design are listed in Table 18.9.

Table 18.9. Rotor Blade Design Details

$x = r/R$	0.85	0.70	0.76	0.82	0.88	0.94	1.00
$1/\bar{\lambda} = x/\bar{A}$	1.933	1.590	1.727	1.862	2.00	2.137	2.273
$2\bar{\epsilon}_p(1/\bar{\lambda} - 1/\bar{\lambda}_U)$	0	-0.731	-0.439	-0.151	0.143	0.435	0.725
$(u_2/U)^2$ eq. (16.16)	1	0.269	0.561	0.849	1.143	1.435	1.725
$u_2/U$	1	0.518	0.750	0.922	1.07	1.20	1.316
$(u_1 + u_2)/2U$	1	0.865	0.942	0.988	1.022	1.046	1.063
$\epsilon_{p12}$ eq. (16.33)		1.232	1.131	1.078	1.043	1.02	1.002
$\lambda_{12}$ eq. (16.31)		0.670	0.617	0.572	0.533	0.499	0.469
$\sigma$ Fig. 9.12		1.96	1.53	1.29	1.12	1.00	0.90
$\theta$ Fig. 9.15	16.8	14.9	13.4	12.2	11.2	10.3	
$\xi$ Fig. 9.17	61.5	62.7	64.0	65.2	66.5	67.5	
$c$ ( $N = 48$ ) $= 2\pi x R \alpha / N$ (in.)	6.45	5.47	4.99	4.64	4.42	4.27	

On comparing the rotor blade details with those listed in Table 18.6 for the free vortex blade, it will be noted that the reduction in blade chord at the root is relatively small. Therefore, although the total head rise at this blade element has been reduced by nearly 20 per cent, the lower effective axial velocity (see Fig. 18.5) has reduced the work potential.

It can be concluded, therefore, that the use of arbitrary vortex flow produces small but probably worthwhile gains in the load carrying capacity of fans with boss ratios of the order of 0.7. In the foregoing, a conservative outlook has been maintained; when the absolute maximum work is required from a given fan configuration, the design must be supported by a test and development programme.

In this question of large pressure rises, it should be noted that emphasis so far has been on design for high efficiency. Thus the maximum useful total head rise will exceed the design value and can best be ascertained experimentally.

## 18.6. Arbitrary Vortex Design, Isolated Aerofoil Method

This example illustrates the use of arbitrary vortex flow for

fans with small boss ratios. The preliminary design procedure will be dispensed with, and instead the design requirements for a rotor-straightener unit will be stated as follows:

$$K_{th} = 1.2$$

$$\bar{A} = 0.4$$

$$x_b = 0.2$$

From eq. (16.9)

$$x_U = 0.689$$

Taking  $\bar{\epsilon}_s$  as constant, eq. (16.12) gives

$$\begin{aligned}\bar{\epsilon}_s &= \frac{1.2 \times 0.40}{2 \times 0.689} \\ &= 0.348 \text{ say } 0.35\end{aligned}$$

The change in the total head rise coefficient along the blade is, from eq. (16.30),

$$\frac{2\bar{\epsilon}_s}{\bar{A}}(1-x_b) = 1.40$$

which appears satisfactory. Eqs. (16.16) and (16.23), for the given configuration, reduce to

$$\left(\frac{u_2}{U}\right)^2 = 1 + 2\bar{\epsilon}_s\left(\frac{1}{\bar{\lambda}} - \frac{1}{\bar{\lambda}_U}\right) - 2\bar{\epsilon}_s^2(\log_e x - \log_e x_U)$$

and

$$\left(\frac{u_3}{U}\right)^2 = 1 + 2\bar{\epsilon}_s\left(\frac{1}{\bar{\lambda}} - \frac{1}{\bar{\lambda}_U}\right)$$

The design computations for the rotor are presented in Table 18.10.

Constant chord blades of RAF 6E section provide a convenient solution for a low pressure fan of this type. The solidity, which is inversely proportional to  $x$  in these circumstances, has been chosen so that  $C_L$  at the tip is equal to 1.1. The resulting lift coefficient distribution should ensure a high rotor blade efficiency (see Figs. 4.4 and 18.3).

In the previous design examples, the rotor blade aspect ratio was in the vicinity of 2. Since the blade length is now 80 per cent of the fan radius, a greater aspect ratio is consequently more appropriate.

Table 18.10. Rotor Blade Design Details

$x = r/R$	0.689	0.2	0.3	0.4	0.6	0.8	1.0
$\log_e x$	-0.375	-1.61	-1.203	-0.916	-0.511	-0.223	0
$\log_e x - \log_e x_U$	0	-1.235	-0.828	-0.541	-0.136	-0.152	0.375
$2\bar{\epsilon}_s^2(\log_e x - \log_e x_U)$	0	-0.303	-0.203	-0.133	-0.033	0.037	0.092
$1/\bar{\lambda} = x/A$	1.721	0.50	0.75	1.00	1.50	2.00	2.50
$2\bar{\epsilon}_s(1/\bar{\lambda} - 1/\bar{\lambda}_U)$	0	-0.855	-0.678	-0.505	-0.155	0.195	0.545
$(u_2/U)^2$ eq. (16.16)	1	0.448	0.525	0.628	0.878	1.158	1.453
$u_2/U$	1	0.67	0.725	0.793	0.937	1.078	1.206
$(u_1 + u_2)/2U$	1	0.835	0.863	0.897	0.969	1.039	1.103
$\lambda_{12}$ eq. (16.31)		1.67	1.15	0.897	0.645	0.519	0.442
$\epsilon_{12}$ eq. (16.34)		0.419	0.406	0.390	0.362	0.337	0.317
$1 - \frac{1}{2}(\epsilon_{12}\lambda_{12})$		0.650	0.764	0.825	0.883	0.912	0.930
$\tan \varphi_r$ eq. (8.14)		2.57	1.505	1.087	0.733	0.569	0.475
$\varphi_r$		68.7	56.4	47.4	36.2	29.6	25.4
$\sin \varphi_r$		0.932	0.833	0.736	0.591	0.494	0.429
$C_L \sigma$ eq. (8.27)		0.78	0.676	0.575	0.426	0.333	0.272
$C_L$		0.63	0.82	0.93	1.03	1.08	1.1
$\sigma$		1.23	0.825	0.618	0.412	0.309	0.247
$\alpha$ Fig. 4.4		1.7	3.7	4.8	6.0	6.5	6.7
$\varphi_r + \alpha$		70.4	60.1	52.2	42.2	36.1	32.1

It can be shown that, for constant chord,

$$\text{Aspect ratio} = \frac{(1-x_b)N}{2\pi\sigma_t}$$

and when the number of blades,  $N$ , is equal to 10, a.r. = 5.15.

Since the straighteners are the last row of blading, and constant  $\bar{\epsilon}_s$  gives a linear variation of total head rise, the radial distribution of the downstream axial velocity will approximate the square root law given in Section 16.4. The value of  $x_U$  is therefore given by eq. (16.10). (From Fig. 16.1 it will be seen that there is a significant difference at low boss ratios between the values of  $x_U$  given by the linear and square root distributions). The design calculations are listed in Table 18.11.

Although the root value of  $u_3/U$  is relatively small, trouble with separation over the rather small tail fairing is not anticipated.

For convenience, the recommended values of  $s/c$  (Fig. 11.6) at the root and tip were adopted and a straight line distribution assumed for intermediate values. This procedure gives a conservative design in the present instance.

Table 18.11. Straightener Design Details

$x=r/R$	0.67	0.2	0.3	0.4	0.6	0.8	1.0
$1/\bar{\lambda}=x/\bar{A}$	1.675	0.50	0.75	1.00	1.50	2.00	2.50
$2\bar{\epsilon}_s(1/\bar{\lambda}-1)/\bar{\lambda}_v$	0	-0.823	-0.648	-0.473	-0.123	0.228	0.578
$(u_3/U)^2$ eq. (16.23)	1	0.177	0.352	0.527	0.877	1.228	1.578
$u_3/U$	1	0.421	0.593	0.725	0.937	1.110	1.257
$(u_2+u_3)/2U$	1	0.546	0.659	0.759	0.937	1.094	1.232
$\epsilon_{23}$ eq. (16.35)		0.641	0.531	0.461	0.374	0.320	0.284
$s/c$		1.02	1.08	1.14	1.26	1.38	1.5
$\alpha_1=\tan^{-1} \epsilon_{23}$	32.7	28.0	24.7	20.5	17.7	15.9	
$\theta$ eq. (11.7)	44.3	38.4	34.2	29.0	25.5	23.4	
$\xi$ eq. (11.8)	10.5	8.8	7.6	6.0	4.9	4.2	

## 18.7. Miscellaneous Design Features

While as many features as possible have been illustrated in the design examples given, a few more are worthy of note.

The design of fans for peak static efficiency (see Section 14.4) will involve some degree of blading analysis since the blade loading which must be used will be higher than that recommended in the foregoing design procedures. Such a design should be undertaken only by an experienced designer and should preferably be supported by a test programme in the case of a major installation.

When fans operate in regions where atmospheric conditions differ from the I.C.A.N. standard, the correct pressure and density (see Section 2.1) must be used when carrying out calculations dealing with any aspect of fan work.

A simple method of producing cambered plate fan blades has been described in Reference 82. The procedure consists of setting the blade out so that the line joining the root and tip mid-chord points makes a predetermined angle with the axis of a right cylinder out of which the blades will be cut. In this manner the correct amount of twist between root and tip can be obtained from a metal sheet of single curvature. By a suitable spanwise shaping of the leading and trailing edges the correct rate of change of twist along the blade can also be achieved. This method of production is very suitable for fans with boss ratios in excess of 0.6 but practical difficulties arise for free vortex designs when  $x_b$  is less than 0.5. With the aid of trial

and error methods of either a graphical or computational nature, this production procedure can be extended to right cones.

The choice of blade aspect ratio is influenced by a number of factors. With the object of keeping annulus and secondary drags to a reasonable level it is generally accepted that the aspect ratio should be at least 2. From the practical point of view, increasing the aspect ratio reduces the axial dimension of the boss to which the blades are attached. Very large aspect ratios are undesirable for reasons of blade multiplicity, lack of blade stiffness and decreased aerodynamic efficiency due to the low blade Reynolds numbers which follow from small chord blades.

Close control should be exercised over tip clearances if the penalties outlined in Sections 10.7 and 22.4.5 are not to be incurred.

The tensile stress due to the centrifugal effect constitutes the major stress component in rotor blades. Bending moments due to aerodynamic loads increase the tensile stresses by a small but significant amount, while shear stresses and torsional moments are, on the whole, negligible. When the centroid of each blade element lies along a radial line perpendicular to the axis of rotation, bending stresses due to centrifugal forces are eliminated. It is therefore advisable to arrange the blade geometry with this requirement in mind.

In the mechanical design of rotor blades the question of metal fatigue should not be overlooked. Variations in stress level occur during starting and stopping procedures; the greatest danger, however, is from fluctuating loads acting on the blades during running. The latter may arise from unsteady airflow conditions created by flow separations in the duct system.

In addition, obstructions or vanes upstream of the rotor may, owing to the ensuing pressure fluctuations (see Section 17.2.1), incite blade vibration. For the simple case of evenly spaced vanes, such as prerotators, each rotor blade experiences a pulsation which occurs with a frequency determined by the rotational speed of the rotor and the number of vanes. When any harmonic of natural blade frequency coincides with the forced frequency, resonance and possibly flutter will result. Some mechanical and/or aerodynamic redesign of the relevant parts of the installation is then imperative. The possibility of

straightener vibration and resonance due to rotor excitation is also worthy of investigation, if only from a noise point of view.

The very low Reynolds number design case has been excluded from the foregoing subject matter, mainly because it is rarely encountered in practice, but also because an accurate mathematical approach to the problem is difficult. When the laminar layer encounters the region of rising pressure on a fan blade it separates from the surface and very often fails to re-attach itself at some downstream position. In regions of rising pressure this re-attachment can occur only when the separated shear layer undergoes complete transition to turbulence. As the Reynolds number is progressively reduced, a stage is reached when viscous forces completely prohibit the formation of turbulent flow. The lift which can be obtained from a blade is then greatly restricted: this state of affairs is accompanied by high drag coefficients.

In circumstances such as these it is advisable to carry out the design in conjunction with a test programme. Highly cambered aerofoils make the best blade sections since the extent of the favourable pressure regions on the suction surface can be increased by camber. In this manner the laminar separation point will be pushed as far downstream as possible.

### 18.8. Fan Layout Design

The structural, mechanical and aerodynamic requirements of a fan unit are not usually incompatible with one another. The aim should be freedom from encumbrances within the fan unit. The elimination of all unnecessary obstructions, the avoidance of flow separation and the use of stators as structural members and/or fairings for belt or shaft drives are important objectives.

In the wind tunnel fan installation shown in Plates 1(a) and 4(a) the straighteners support the fan and motor and in addition provide ducts for the electrical leads and motor cooling air. The industrial unit of Plate 4 (b) illustrates the fairings around the belt drive and also the addition of local upstream camber to the structural support plates for the purpose of providing good inlet flow conditions so that the plates may be more effective as straighteners.

When large swirls are present and the fan is supported independently of the straighteners, it is advisable to locate the support plates downstream of the stators in order to avoid serious separation losses. If the plates or related items possess a distinct bluffness, a streamlined fairing should be added as a housing. In the absence of straighteners in the unit any small increase in the duct system resistance will increase the swirl and hence increase the separation losses due to the support plates. The process is therefore a cumulative one which causes a sharp rise in fan power.

Similar comments apply equally well to the problem of housing shaft or belt drives.

In the absence of prerotators, the best type of nose fairing is one which is attached to the rotor, namely a spinner. This arrangement eliminates noise-producing supports as well as providing a simpler design.

The general rules outlined above apply equally to the installation of stators, supports and drive fairings upstream of the rotor.

Before the layout of the various components of the fan unit is completed, serious consideration should be given to the subject of noise suppression, as discussed in Section 17.

The positioning of the unit in the duct system is almost as important as a good fan unit layout. If it is too close to the exit from a corner, the efficiency and work capacity of the unit can be greatly impaired by non-uniformity in the inlet flow to the rotor. With few exceptions, the outlet flow from a corner possesses an appreciable mean velocity gradient between the inner and outer walls. Upstream and downstream ducting should be designed on the principles outlined in Section 6, the complete suppression of separation being a most desirable requisite.

It is appreciated that the ideal arrangement is, owing to space and cost limitations, very often impossible. The author has, however, seen many instances where failure to apply the above principles has resulted in an unnecessarily bad design. In fact the potential gain from good layout design is greater when space and other limitations are most stringent. An informed aerodynamic approach to all duct and fan problems is essential for subsequent satisfactory operation.

# 19

## ROTOR ANALYSIS

### 19.1. General

A knowledge of the performance of a fan for off-design conditions is often desirable, the variable pitch fan being a case in point. Again, it may be that an actual fan is available but its performance may be unknown. In such circumstances it is a positive advantage to have a method for analysing a fan.

It has already been indicated in the course of this work that most design variables can be expressed in terms of the major parameters  $\epsilon$  and  $\lambda$ . The relationship sought, therefore, is one which connects  $\epsilon$  and  $\lambda$  with the blade characteristics.

As before, the blade element will be examined first and the application of such data to the fan as a whole will be indicated.

### 19.2. Analysis of a Rotor Blade Element, Isolated Aerofoil Case

The general configuration of a rotor with prerotators and straighteners as outlined in Section 8.3 will be considered.

The rotor velocity vector diagram of Fig. 8.2 is modified in the manner illustrated in Fig. 19.1. When the axial velocity changes owing to any alteration in the resistance of the duct system, the tangential velocity vector,  $\omega_p r$ , will also vary; the non-dimensional relation  $\epsilon_p$ , however, should remain constant, since it represents a deflection angle.

The axial velocity component has been assumed to remain constant from inlet to outlet; thus free vortex flow is implied.

An essential part of the analysis problem is the rotor no-work case. For such a condition the velocity vector diagram is EBG, where

$$\text{Mean resultant velocity} = (w_r)_{N.L.} = EB$$

$$\text{Axial component} = u_{N.L.} = BG$$

$$\text{Tangential component} = \Omega r + (\omega_p r)_{N.L.} = EG$$

Since no work is done, the swirl will pass through the rotor unchanged and hence

$$\epsilon_s = -\epsilon_p,$$

when the sign convention of Section 8 is applied.

With increasing load, the point D will move away from B and the velocity vectors will then be given by:

$$\text{Mean resultant velocity} = w_r = ED$$

$$\text{Axial component} = u = CG$$

$$\text{Tangential component} = \Omega r + \frac{1}{2}(\omega_p - \omega_s)r = EG - CD$$

The relationship between  $\epsilon_s$  and  $\lambda$  will now be established in terms of the no-lift and lift curve characteristics of the aerofoil section. From Fig. 19.1

$$u = BG - BC$$

$$= [\Omega r + (\omega_p r)_{N.L.}] \tan \Phi - \left[ \frac{(\omega_p r)_{N.L.} - \frac{1}{2}(\omega_p - \omega_s)r}{\tan \psi} \right]$$

Dividing by  $\Omega r$

$$\lambda = [1 + \epsilon_p \lambda_{N.L.}] \tan \Phi - \left[ \frac{\epsilon_p \lambda_{N.L.} - \frac{1}{2}\lambda(\epsilon_p - \epsilon_s)}{\tan \psi} \right] \quad (19.1)$$

where

$$\begin{aligned} \lambda_{N.L.} &= \left( \frac{u}{\Omega r} \right)_{N.L.} \\ &= [1 + \epsilon_p \lambda_{N.L.}] \tan \Phi \\ &= \frac{1}{\cot \Phi - \epsilon_p} \end{aligned} \quad (19.2)$$

Eq. (19.1) can be rewritten

$$\epsilon_s = 2 \tan \psi \left[ \frac{\lambda_{N.L.}}{\lambda} - 1 \right] - \epsilon_p \left[ 2 \frac{\lambda_{N.L.}}{\lambda} - 1 \right] \quad (19.3)$$

in which the only remaining unknown is  $\psi$ .

From eq. (8.27) we have

$$C_L = 2 \left( \frac{s}{c} \right) (\epsilon_p + \epsilon_s) \sin \varphi_r$$

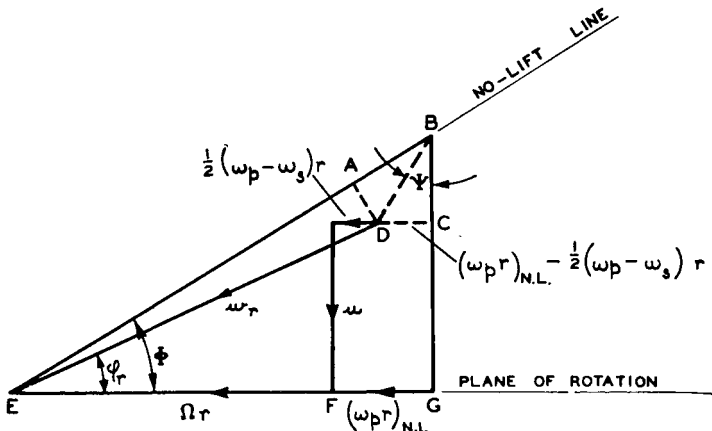


Fig. 19.1. Velocity vectors for rotor blade element (for reference, see Fig. 8.2)

Assuming a linear lift curve for an isolated aerofoil blade section, over the working range of the rotor, we obtain the relation

$$C_L = m \sin (\Phi - \varphi_r) \quad (19.4)$$

where  $m$  is a constant and  $(\Phi - \varphi_r)$  is the incidence with respect to the no-lift line (see Fig. 19.1). For the RAF 6 type of blade section and similar aerofoils

$$m = 5.7$$

An expression for  $\sin (\Phi - \varphi_r)$  can be obtained as follows:

$$\begin{aligned} AD &= wr \sin (\Phi - \varphi_r) \\ &= BD \cos (\Phi + \psi) \\ &= DC \cos (\Phi + \psi) / \sin \psi \end{aligned}$$

Therefore

$$wr \sin (\Phi - \varphi_r) = [(\omega_p r)_{N.L.} - \frac{1}{2}(\omega_p - \omega_s)r] \frac{\cos (\Phi + \psi)}{\sin \psi} \quad (19.5)$$

Equating the lift coefficient relationships of eqs. (8.27) and

(19.4) and making use of eq. (19.5)

$$\tan \psi = \frac{\cos \Phi}{\frac{4(\epsilon_p + \epsilon_s)}{m\sigma} \left[ \frac{1}{\epsilon_p \left( \frac{2\lambda_{N.L.}}{\lambda} - 1 \right) + \epsilon_s} \right] + \sin \Phi} \quad (19.6)$$

It will be noted that the equation contains the unknown  $\epsilon_s$  and hence eqs. (19.3) and (19.6) must be combined in order to obtain a solution, namely,

$$\begin{aligned} \epsilon_s &= \frac{2 \cos \Phi \left[ \frac{\lambda_{N.L.}}{\lambda} - 1 \right]}{\frac{4(\epsilon_p + \epsilon_s)}{m\sigma} \left[ \frac{1}{\epsilon_p \left( \frac{2\lambda_{N.L.}}{\lambda} - 1 \right) + \epsilon_s} \right] + \sin \Phi} - \epsilon_p \left[ \frac{2\lambda_{N.L.}}{\lambda} - 1 \right] \\ &= \frac{2 \cos \Phi \left( \frac{\lambda_{N.L.}}{\lambda} - 1 \right) - \frac{4\epsilon_p}{m\sigma} - \epsilon_p \sin \Phi \left( \frac{2\lambda_{N.L.}}{\lambda} - 1 \right)}{\frac{4}{m\sigma} + \sin \Phi} \end{aligned} \quad (19.7)$$

When there is no prerotation, eq. (19.3) reduces to

$$\epsilon_s = \frac{2 \tan \psi}{\lambda} [\tan \Phi - \lambda] \quad (19.8)$$

eq. (19.6) to

$$\tan \psi = \frac{\cos \Phi}{\frac{4}{m\sigma} + \sin \Phi} \quad (19.9)$$

and eq. (19.7) to

$$\epsilon_s = \frac{2 \cos \Phi \left[ \frac{\tan \Phi}{\lambda} - 1 \right]}{\frac{4}{m\sigma} + \sin \Phi} \quad (19.10)$$

The desired relationships between  $\lambda$  and  $\epsilon$  have now been developed and hence the total head rise,  $k_{th}$ , can be obtained from eq. (8.12), i.e.

$$k_{th} = \frac{2}{\lambda} (\epsilon_s + \epsilon_p)$$

For the case of zero preswirl it will be noted that  $\tan \psi$ , as

given by eq. (19.9), is a constant for a particular blade element; in consequence there is a linear change in  $\omega_s r$  with  $u$  (Fig. 19.1).

The variation of  $\tan \psi$  with  $\Phi$  and  $\sigma$ , for  $\omega_p r = 0$  and  $m = 5.7$ , has been presented in Fig. 19.2. For increasing design flow coefficients, i.e.  $\Phi$  large, the variation of  $u$  with pressure rise across the rotor becomes greater. Increasing the solidity reduces the variation. These trends are, in general, fairly well known from practical experience.

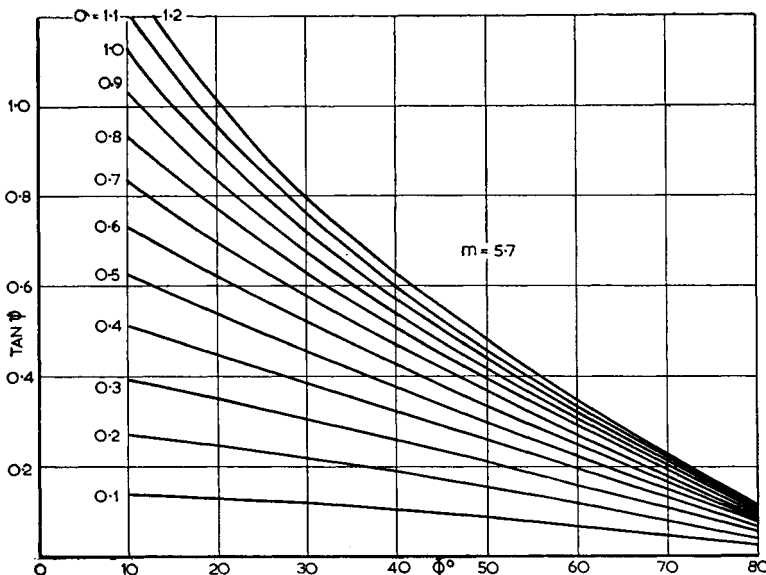


Fig. 19.2. Measure of rate of change of swirl as through-flow varies,  
 $\epsilon_p = 0$

When prerotators are employed, the performance characteristics of the fan can be changed by using variable pitch preswirl vanes.

The swirl coefficient,  $\epsilon_p$ , will normally, according to the convention adopted in Section 8.3, be positive but  $\epsilon_s$  can be negative. These negative values occur when a lightly loaded rotor is supplied with positive preswirl from stators or a contra-rotating rotor.

### 19.3. Rotor Characteristic, Isolated Aerofoil Case

The relationship which exists between the pressure rise and the capacity of a rotor at a given speed is known as the characteristic curve. Non-dimensionally, the mean total head rise through the rotor can be expressed by

$$K = \frac{\Delta H}{\frac{1}{2}\rho U^2} \quad (19.11)$$

and the capacity by

$$\bar{A} = \frac{U}{\Omega R} \quad (19.12)$$

Plotting one parameter against the other results in a unique curve except at very low Reynolds numbers where the characteristic is a marked function of Reynolds number. The total head rise coefficient,  $K$ , can be expressed by

$$K = K_{th} \left( 1 - \frac{K_R}{K_{th}} \right) \quad (19.13)$$

and hence it remains only to determine  $K_{th}$  and  $K_R$ , as functions of  $\bar{A}$ , from the data of the preceding sub-section.

The present development will be used almost exclusively for free vortex flow rotors. There are, however, many low pressure rise fans in existence which do not conform with free vortex conditions and hence an approximate approach, based on the foregoing analysis, will also be outlined. For the general case, eqs. (16.11) and (16.29) are used in obtaining the relation

$$K_{th} = \frac{2}{1-x_b^2} \int_{x_b}^1 k_{th}' \left( \frac{u_1 + u_2}{2U} \right)^2 x \, dx \quad (19.14)$$

**19.3.1. Characteristic for free vortex flow.** Since  $u_1 = u_2 = U$  at all radii, the values of  $\lambda$  for a given value of  $\bar{A}$  can be computed from

$$\lambda = \frac{\bar{A}}{x} \quad (19.15)$$

At each radius, therefore,  $k_{th}$  can be calculated, for a given  $\bar{A}$ , by the methods outlined in Section 19.2. Eq. (19.14) can then be solved by graphical integration.

The lift coefficient distribution along the blade is often of

interest as it provides information from which the onset of blade stalling can be roughly predicted. From the appropriate values of  $\epsilon$  and  $\lambda$ , the angle  $\varphi_r$  can be obtained from eq. (8.14) which leads to the solution of eq. (8.27) for  $C_L$ .

In most cases, a simplified approach is both accurate and adequate. When the flow is nominally of the free vortex type, the off-design variation of  $k_{th}$  along the blade is not usually large and hence  $k_{th}$  at the midspan section approximates to  $K_{th}$ . This reduces the problem to the solution of the equations for one radius only.

Before eq. (19.13) can be solved, the loss coefficient,  $K_R$ , must be known or assumed. Following previous procedure, an estimate is made, based on conditions at the midspan station. First, by rearranging eq. (10.7) we obtain

$$\frac{K_R}{K_{th}} = \frac{K_{R_A}}{K_{th}} + \left[ \frac{C_{D_P} + C_{D_S}}{C_L} \cdot \frac{\lambda}{\sin^2 \varphi_r} \right] \quad (19.16)$$

When the lift coefficient is computed by the method just outlined,  $C_{D_S}$  can be calculated from eq. (10.10) or eq. (10.11) and  $C_{D_P}$  obtained from aerofoil data. Substitution of the appropriate value of  $K_{R_A}/K_{th}$  (eqs. (10.14) and (10.15)) then leads to the solution of eqs. (19.16) and (19.13).

For near-design conditions, the accuracy with which  $K_R/K_{th}$  can be computed should be acceptable; errors may arise, however, when the extremes of the operating range are being investigated. As the volume of experimental data grows it may become possible to make suitable adjustments to the drag coefficients in order to obtain an improved accuracy over the whole range of operation.

**19.3.2. Characteristic for arbitrary vortex flow.** Significant departures from free vortex flow are suspected when the procedure of the previous sub-section gives a large variation of  $k_{th}$  along the blade for a given  $\bar{A}$ . In addition, a visual inspection of the rotor will often indicate to the experienced eye the type of flow to be expected, since an arbitrary vortex flow rotor has a lesser rate of twist between root and tip than is the case in a corresponding free vortex design.

When the flow is of an arbitrary vortex nature, the assumption made in Section 16.8 in respect of the average axial velocity

must be adopted. The relation (19.15) is no longer valid and it is necessary to replace it by

$$\lambda_{12} = \frac{\bar{A}}{x} \left( \frac{u_1 + u_2}{2U} \right) \quad (19.17)$$

before the distribution of  $\lambda_{12}$  for a given  $\bar{A}$  can be computed. Assuming that conditions upstream of the rotor have been established, we are still left with the unknown  $u_2$ , a distribution of which must now be assumed. With the tentative values of  $\lambda_{12}$  so obtained, eq. (19.7) can be solved for  $\epsilon_{s_{12}}$  at each spanwise station.

When the flow and swirl coefficients are converted by the relations given in eqs. (16.31) and (16.33), the velocity  $u_2$  is computed from eq. (16.16); a more accurate distribution of  $u_2$  can now be assumed. By such trial and error methods, a satisfactory solution is obtained.

The mean theoretical total head follows from eq. (19.14) when  $k_{th}'$  is determined from eq. (16.29) for values of  $\epsilon_{p_{12}}$ ,  $\epsilon_{s_{12}}$  and  $\lambda_{12}$  at a given radius.

When an estimate of  $K_{th}$  is the only requirement, a simpler approach can be made. In Section 16.11 it was suggested that an estimate of the mean properties of the rotor could be obtained from local parameters at  $x = x_U$  (see eqs. (16.9) and (16.10)). A solution of eq. (16.16) is not required as  $u_1 = u_2 = U$ .

If it can be taken that the rotor has been designed by conventional aerodynamic methods, the foregoing assumptions are, within the main operating range of the rotor, not unreasonable. For a given  $\bar{A}$ , the flow coefficient at this representative spanwise station can be obtained from eq. (19.15), the corresponding swirl coefficient from the appropriate equations in Section 19.2, and  $K_{th}$  from eq. (8.12), since at this station  $k_{th} = K_{th}$ .

When either method is used in analysing the rotor for arbitrary vortex flow, an estimate of  $K_R$  can be obtained, for the spanwise station chosen above, when the relevant parameters have been evaluated by the method outlined in the free vortex case.

Eq. (19.13) may then be solved for each of the desired values of  $\bar{A}$ .

Substituting the appropriate values of  $\epsilon_{12}$  and  $\lambda_{12}$  in eqs. (8.14) and (8.27) will give an approximate lift coefficient distribution, from which the onset of blade stalling conditions can be roughly predicted.

#### 19.4. Rotor Characteristic, Cascade Aerofoil Case

Rotors designed by the cascade aerofoil method could be analysed by the foregoing treatment if the lift curve slope and no-lift angle were known, but generally speaking these quantities are not available.

It has been found<sup>(67)</sup> that when the ratio of the actual flow deflection to the optimum deflection is plotted against the ratio  $(i - i^*)/(\alpha_1 - \alpha_2)^*$  the curve so obtained is fairly unique for all cascade results (Fig. 19.3).

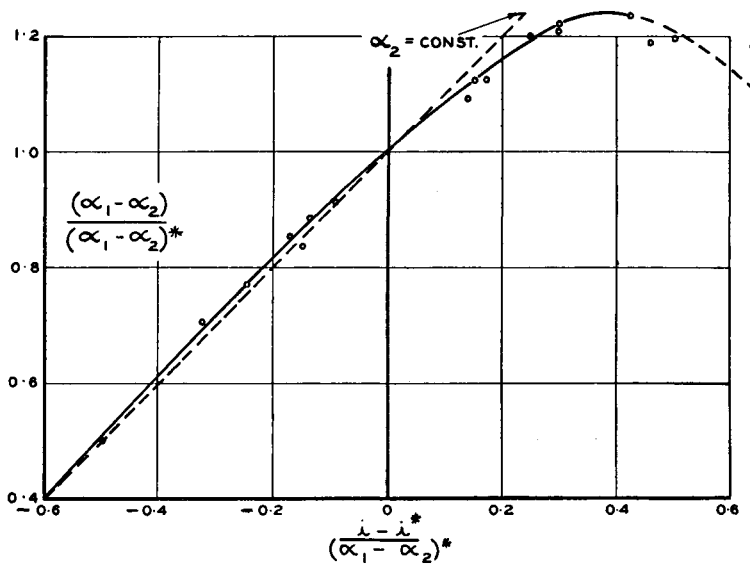


Fig. 19.3. Deflection data for cascade aerofoils  
(Based on A.R.C. R. & M. 2095, and reproduced by permission of the Controller of H.M. Stationery Office)

The angle of incidence,  $i^*$ , is the angle at which the optimum deflection  $(\alpha_1 - \alpha_2)^*$ , defined by  $0.80 (\alpha_1 - \alpha_2)_{\max}$ , is obtained; the choice of  $i^*$  does not appear to be critical and hence the

design assumption,  $i=0$  (Section 9.5), will in general be accepted. Denoting the design value of  $\alpha_1$  by  $\alpha_1^*$ ,  $(i-i^*)$  can be replaced by  $(\alpha_1 - \alpha_1^*)$ .

The method of analysis to be outlined is mainly applicable to rotors with circular arc blades designed for optimum or near-optimum conditions by the British cascade method. The aerodynamic design data must either be known or be established from the blade geometry. In the latter case, the variables  $\sigma$ ,  $\theta$  and  $\xi$  at each chosen spanwise station can be obtained by measurement and then inserted in the design equations

$$\xi = (\alpha_1^* - i^*) - \frac{\theta}{2} \quad (9.19)$$

and

$$\theta = \frac{(\alpha_1 - \alpha_2)^* - i^*}{1 - 0.26\sqrt{(s/c)}} \quad (9.18)$$

When the above recommendation for the incidence,  $i^*$ , is accepted, these equations can be solved for  $\alpha_1^*$ , and  $(\alpha_1 - \alpha_2)^*$ .

It should be borne in mind that the estimates of the angles  $\alpha_1^*$  and  $\alpha_2^*$  are based on blade geometry. Some of the implications of this approach will now be considered.

The angles are, in the case of free vortex flow, related to the flow and swirl coefficients by means of eqs. (9.2) and (9.3), i.e.

$$\tan \alpha_1 = \frac{1 + \epsilon_p \lambda}{\lambda} \quad (9.2)$$

$$\tan \alpha_2 = \frac{1 - \epsilon_s \lambda}{\lambda} \quad (9.3)$$

When  $\epsilon_p$  is zero, eq. (9.2) reduces to

$$\tan \alpha_1 = \frac{1}{\lambda}$$

and, since  $u = U$ , the values of  $\tan \alpha_1$  obtained by the use of eq. (9.19) should be directly proportional to the radius,  $r$ , for design conditions. Large deviations from this relationship will raise doubts concerning the design method used; in view of the method of estimating  $\alpha_1$ , such discrepancies can be explained only in terms either of a non-uniform inlet velocity or of a change in design incidence,  $i^*$ , along the blade.

When preswirl is employed, the deflection angle represented by  $\epsilon_p$  will remain constant at a given radius and be independent of  $\bar{\lambda}$ . On substitution in eq. (9.2),  $\tan \alpha_1$  is no longer proportional to  $r$ , but if the design method is to be free of doubt the variation of  $\lambda$  obtained from eq. (9.2) should, for free vortex flow, be inversely proportional to the radius, in order to ensure a uniform inlet axial velocity distribution (see eq. (19.15)).

For arbitrary vortex flow, the coefficients,  $\epsilon_{p12}$ ,  $\epsilon_{s12}$  and  $\lambda_{12}$  should be substituted for  $\epsilon_p$ ,  $\epsilon_s$  and  $\lambda$  in eqs. (9.2) and (9.3). On rewriting these equations we have

$$\tan \alpha_1 = \left( \frac{1 + \bar{\epsilon}_p \bar{\lambda}}{\bar{\lambda}} \right) \frac{2U}{u_1 + u_2} \quad (19.18)$$

and

$$\tan \alpha_2 = \left( \frac{1 - \bar{\epsilon}_s \bar{\lambda}}{\bar{\lambda}} \right) \frac{2U}{u_1 + u_2} \quad (19.19)$$

Trial and error methods must be employed in the solution of the above equations. The variables associated with inlet conditions, namely  $\bar{\epsilon}_p$  and  $u_1$ , can be established from a prerotorator analysis. In the case of zero preswirl,  $u_1$  may be assumed to equal  $U$  provided the inlet to the fan unit is in conformity with good design practice. The unknowns in eq. (19.18) are now  $\bar{\lambda}$  and  $u_2$  and one of these must be assumed before the equation can be tentatively solved.

At  $x = x_U$ ,  $\bar{\lambda}$  can be computed from eq. (19.18). The design coefficient,  $\bar{\lambda}$ , follows immediately from eq. (19.15) and hence  $\bar{\lambda}$  at each chosen station can be determined. Eq. (19.18) is then solved in order to obtain the corresponding values of  $u_2$ . When the radial variation of  $u_2$  is small, it can be assumed that the flow is of a free vortex type. If the distribution appears unreasonable, e.g. grossly irregular, the method of estimating  $\alpha_1^*$  becomes suspect, so further analysis by this method is unwise.

The above discussion is intended to serve as a guide when an attempt is made to analyse a rotor of uncertain design origin; when aerodynamic design data are available a number of the problems treated do not arise.

**19.4.1. Characteristic for free vortex flow.** On the assumption that a satisfactory solution of eq. (9.2) has been

achieved for design conditions, the design deflection  $(\alpha_1 - \alpha_2)^*$  can be computed from eq. (9.18). Since  $\alpha_2^*$  is now known, the variation of  $\epsilon_s$  along the blade can be established from eq. (9.3). The theoretical total head coefficient,  $k_{th}$ , follows from eq. (8.12); this should be approximately constant along the blade for free vortex flow. If large variations are present, the initial assumption concerning the type of flow may have to be revised.

The mean total head coefficient,  $K_{th}$ , can be obtained from eq. (19.14) by substituting unity for the velocity ratio, or from the value of  $k_{th}$  at the midspan station, when the simplified approach discussed in Section 19.3.1 is adopted. The design value of  $K_{th}$  for a given  $\bar{A}$  is now known.

For an off-design value of  $\bar{A}$ , the distribution of the coefficient,  $\lambda$ , along the blade is calculated from eq. (19.15). Substitution of  $\lambda$  in eq. (9.2) establishes the inlet angle,  $\alpha_1$ , at these stations. The value  $(\alpha_1 - \alpha_1^*)/(\alpha_1 - \alpha_2)^*$  is then computed and  $(\alpha_1 - \alpha_2)$  follows from Fig. 19.3. From the appropriate values of  $\alpha_2$  and  $\lambda$ , the swirl coefficient  $\epsilon_s$  is calculated from eq. (9.3). The subsequent procedure is similar to that just outlined for the design case.

It will be noted in Fig. 19.3 that the maximum deflection is reached for

$$\frac{\alpha_1 - \alpha_1^*}{(\alpha_1 - \alpha_2)^*} \approx 0.4$$

Blade stalling can be assumed when the computed value of this parameter exceeds the above figure.

In determining  $K_R$ , a procedure similar to that outlined in Section 19.3.1 can be followed. The profile drag coefficient is given in Fig. 10.3 in terms of the inlet velocity,  $V_1$ , which is related to  $w_r$  by the expression

$$\frac{V_1}{w_r} = \frac{\sin \varphi_r}{\cos \alpha_1}$$

Hence, when accuracy is required, the value extracted from Fig. 10.3 should be multiplied by

$$\frac{\sin^2 \varphi_r}{\cos^2 \alpha_1}$$

in order to obtain the appropriate profile drag coefficient. Eq. (19.13) can then be solved for each chosen value of  $\bar{A}$ .

**19.4.2. Characteristic for arbitrary vortex flow.** As before, either the complete or the simplified method of analysis can be used. The latter is generally adequate, particularly when, for various reasons, the expected order of accuracy is not such as to warrant the longer complete analysis. Once the representative station has been chosen (see Section 19.3.2), the procedure follows lines identical with those outlined in the previous subsection.

The more complete analysis is similar to that outlined for the free vortex case, except that trial and error methods must be adopted in solving eqs. (19.18) and (19.19). For example, the values of  $u_2$  obtained, for design conditions, from the approximate treatment of eq. (19.18), may be used in the solution of eq. (19.19);  $\epsilon_s$  then follows once  $\alpha_2^*$  has been estimated from eq. (9.18). By substituting the appropriate values of  $\epsilon_s$  in eq. (16.16) a computed distribution of  $u_2$  can be obtained. An attempt should now be made to satisfy all three equations by successive approximations to the velocity distribution. This may involve an adjustment to the assumed design distributions of  $\alpha_1^*$  and  $\alpha_2^*$ . When an off-design value of  $\bar{A}$  is chosen, eq. (19.18) must first be satisfied for tentative distributions of  $\alpha_1$  and  $u_2$ , and when  $\alpha_2$  is obtained from the use of Fig. 19.3,  $\epsilon_s$  can be assessed from eq. (19.19) as before. After eq. (16.16) has been solved for the velocity distribution, a trial and error procedure similar to that just described can be carried out.

In the above manner the distributions of  $\epsilon_{s_{12}}$  and  $\lambda_{12}$  for a given  $\bar{A}$  can be established. The coefficient,  $k_{th}'$ , then follows from eq. (16.29) and  $K_{th}$  from eq. (19.14).

The subsequent steps which have to be taken in order to establish the characteristic curve,  $K$  versus  $\bar{A}$ , are similar to those just described in the preceding sub-section except that estimates of the total head losses are based on conditions at  $x = x_U$ .

# 20

---

## STATOR ANALYSIS AND OVERALL FAN UNIT PERFORMANCE

The problem of analysing stators is a relatively simple one since there is only one major variable, the swirl coefficient.

In most cases all that is required is an assurance that stator stalling is not likely to occur. Nevertheless, a method of analysis which will permit detailed studies to be undertaken will be outlined.

### 20.1. Prerotators

When the aerodynamic design data are known, a prerotator analysis is unnecessary owing to a constancy in the non-dimensional outlet conditions while  $\bar{A}$  is changing. The two main occasions on which an analysis is required are, first, when design information is not available and second, when variable pitch prerotators are installed.

By actual measurement, the variables  $i$ ,  $\theta$ ,  $\xi$  and  $\beta_2$  can be established at the various radial stations. The angle,  $\alpha_2$ , can

be estimated from the more general form of eq. (11.14) which is obtained by combining eqs. (9.16) and (11.13) to give

$$\theta = \frac{\alpha_2 - i}{1 - 0.20s/c} \quad (20.1)$$

It should, however, be pointed out that the procedure of estimating  $\alpha_2$  from eq. (20.1) is valid only when the stators conform approximately to the design recommendations of Section 11.

### 20.1.1. Free vortex flow.

Assuming that  $\alpha_1$  is zero

$$\tan \alpha_2 = \epsilon_p$$

which gives the desired information concerning the swirl when  $\alpha_2$  is either known or estimated from eq. (20.1).

The flow as a whole is accelerated when passing through a prerotator stage and hence the designer is not concerned with general separation from the stators. However, with appreciable increases or decreases in the angle of incidence,  $i$ , local regions of separation may appear, in the vicinity of the leading edge, on the convex and concave surfaces respectively. These separations will (a) increase the noise level of the fan unit, and (b) lead to a decrease in the overall efficiency.

The above features must be borne in mind when variable pitch stators are employed. Provided  $i$  is within the limits  $\pm 5^\circ$ , no difficulty should be encountered; an estimate of the angle  $\alpha_2$  and hence  $\epsilon_p$  is obtainable from eq. (20.1).

**20.1.2. Arbitrary vortex flow.** When the stators are designed to give a departure from free vortex conditions, the radial static pressure gradients are modified in accordance with equilibrium requirements. The axial velocity component then possesses a radial gradient which must be considered when analysing the stators. The major variable is the swirl coefficient expressed by

$$\epsilon_{p_{01}} = \frac{2\omega_p r}{u_0 + u_1} \quad (16.25)$$

or

$$\epsilon_{p_{01}} = \bar{\epsilon}_p \frac{2U}{u_0 + u_1} \quad (16.32)$$

In addition, when  $\alpha_1$  is zero, we have from the point of view of using cascade design data

$$\epsilon_{p_{01}} = \tan \alpha_2$$

Provided inlet conditions to the fan unit are such as to promote a uniform flow,  $u_0$  will equal  $U$  and the distribution of  $u_1$  can be tentatively assumed. The value of  $\epsilon_p$  for a given  $\alpha_2$  then follows from eq. (16.32). A computed distribution of  $u_1$  is then established from eq. (16.21); by an iterative process, acceptable distributions of  $\epsilon_{p_{01}}$  and  $u_1$  can be obtained.

When variable pitch stators are used, comments similar to those made in relation to the case of free vortex flow are equally applicable.

**20.1.3. Estimate of loss in fan efficiency.** The efficiency loss is a function of the flow coefficient as well as of the swirl coefficient, and can be obtained from eq. (12.3):

$$\frac{K_P}{K_{th}} = \left( \frac{C_{D_P} + C_{D_S}}{C_L} \right) \frac{\lambda}{\sin^2 \varphi_p} \cdot \frac{\epsilon_p}{\epsilon_p + \epsilon_s} \quad (20.2)$$

This equation can be solved when  $\epsilon_s$  is known and the following relations are evaluated for a given  $\epsilon_p$  at a representative radial station:

$$2 \cot \varphi_p = \epsilon_p \quad (\text{see Section 11.1}) \quad (20.3)$$

$$C_L = 2 \frac{s}{c} \epsilon_p \sin \varphi_p \quad (\text{see Section 11.1}) \quad (20.4)$$

$$C_{D_S} = 0.018 C_L^2 \quad (10.10)$$

The profile drag coefficient is obtained from relevant experimental data. Provided  $i$  does not exceed  $\pm 5^\circ$ ,  $C_{D_P}$  may be taken as 0.016 in estimating the efficiency loss in prerotators of orthodox design.

When the recommendations of Section 11 are used in design,  $K_P/K_{th}$ , i.e.  $(K_{P_P} + K_{P_S})/K_{th}$ , can be extracted from Fig. 12.4 as a function of  $\lambda$  since  $\epsilon_p$  will, for fixed pitch stators, remain constant at the design value.

Since at the representative station  $u_0 = u_1 = U$ , it follows that  $\epsilon_p = \bar{\epsilon}_p = \epsilon_{p_{01}}$ , and hence no difficulty arises concerning the appropriate coefficient to be used.

## 20.2. Straighteners

From Fig. 19.3 it will be seen that  $\alpha_2$  remains reasonably constant for negative values of  $i$  while for increasing positive values there is a progressive trend towards undeturning as the stall is approached. Unless truly axial flow at outlet is required, these small changes in  $\alpha_2$  away from its design value of zero are, from an efficiency point of view, of little consequence (see Section 14.1).

The inlet conditions to the straighteners are dictated by the rotor and hence the main concern in analysing these stators is associated with predicting the onset of stator stalling. A knowledge of the aerodynamic design data is very helpful in this connection. When the design calculations are not available, estimates of the essential parameters can be derived from the measured angles,  $\theta$ ,  $\xi$ ,  $\beta_1$  and  $\beta_2$ , at each radial station. Provided the stators are of the general type discussed in Section 11, it is possible to employ the more general form of eq. (11.7), which is obtained from the combination of eqs. (9.16) and (9.17), that is,

$$\theta = \frac{\alpha_1 - i}{1 - 0.26\sqrt{(s/c)}} \quad (20.5)$$

If  $i$  were assumed to be zero,  $\alpha_1^*$  could be estimated immediately. For design values of  $\epsilon_s$  greater than 0.5, the cascade method of design is based on design deflections which are 80 per cent of the maximum obtainable. Hence

$$(\alpha_1 - \alpha_2)_{\max} = 1.25(\alpha_1 - \alpha_2)^*$$

and since  $\alpha_2$  remains reasonably constant and normally has a design value of zero, the limiting value of  $\alpha_1$  is given by the expression

$$\alpha_{1, \text{stall}} \approx 1.25\alpha_1^* \quad (20.6)$$

The value of  $\alpha_1$  estimated from the rotor data should therefore be less than  $1.25\alpha_1^*$  if the stators are to function properly.

In the absence of design data, a check on the outlet angle,  $\alpha_2$ , is sometimes useful. For  $\alpha_2$  to be zero, the blade outlet angle,  $\beta_2$ , should equal the angle of deviation,  $\delta$ , which for optimum

design conditions is given by eq. (9.17), i.e.

$$\delta = 0.26\theta \sqrt{\frac{s}{c}} \quad (9.17)$$

Features peculiar to the type of vortex flow present will now be considered.

**20.2.1. Free vortex flow.** The angle,  $\alpha_1$ , is obtained from

$$\tan \alpha_1 = \epsilon_s$$

since the swirl coefficient is known from the analysis of the rotor. Sufficient information is now available to permit a check on stator effectiveness.

**20.2.2. Arbitrary vortex flow.** When the swirl is removed by the straighteners there is no radial static pressure gradient; owing to a gradient in total head, however, there must be a spanwise axial velocity gradient. Hence we have

$$\tan \alpha_1 = \epsilon_{s_{23}}$$

Sufficient data are available from the rotor analysis to permit the solution of eq. (16.23) for the distribution of  $u_3$  and also to allow computation of the above swirl coefficient from

$$\epsilon_{s_{23}} = \bar{\epsilon}_s \frac{2U}{u_2 + u_3} \quad (16.35)$$

**20.2.3. Estimate of loss in fan efficiency.** The relevant expression is derived from eq. (12.2)

$$\frac{K_S}{K_{th}} = \left( \frac{C_{D_p} + C_{D_s}}{C_L} \right) \frac{\lambda}{\sin^2 \varphi_s} \cdot \frac{\epsilon_s}{\epsilon_s + \epsilon_p} \quad (20.7)$$

In evaluation of the variables contained in the above equation, the procedure and recommendations are identical with those given for the prerotor case;  $\varphi_s$  and  $\epsilon_s$  are, of course, substituted for  $\varphi_p$  and  $\epsilon_p$  in the relationships.

When the operating  $\bar{A}$  of the fan varies, both  $\epsilon_s$  and  $\lambda$  change and hence the loss in efficiency as the air passes through the stators is a function of both these variables; an estimate of the loss is obtainable from Fig. 12.3 when the stators have been appropriately designed (see Section 11).

### 20.3. Overall Fan Unit Performance

For the general configuration which has been used in the design and analysis methods, the overall efficiency of the fan unit is given by eq. (14.8), that is,

$$\eta_T = \frac{K_{th} - K_R - K_P - K_S - K_D}{K_{th}}$$

The method of analysis has provided estimates of all these coefficients except  $K_D$ , which can be derived from the data of Section 13.

Employing eq. (14.3), i.e.

$$\eta_T = \frac{K_{T_v}(1 - x_b^2)^2}{K_{th}}$$

the coefficient  $K_{T_v}$ , which is defined in eq. (14.2), can be obtained as a function of  $\bar{A}$  from the analytical procedures of Sections 19 and 20.

The desired fan characteristic is now known. Despite the large number of assumptions which has been made, the order of accuracy which can be achieved is quite acceptable. As the designer accumulates practical experience, it should eventually become possible to achieve a very high order of accuracy in all cases; such improvements will, in part, be the result of more refined methods of estimating the various drag coefficients.

# 21

---

## VARIABLE PITCH ROTORS AND EXAMPLES OF FAN ANALYSIS

### 21.1. General

There are various disadvantages in the operation of fixed pitch fans. When a fan is bought "off the shelf", the rotor must be run at a certain rotational speed, specified by the makers, if the desired values of pressure rise and capacity are to be realized. This usually involves the utilization of V belt drives since most motors are of the constant speed, a.c. type.

The use of variable pitch fan blades has introduced an era of greater flexibility in the operation of ducted axial flow fans. A given pressure rise and the accompanying capacity can now be achieved with the aid of an additional variable. For example, the rotor speed of a particular configuration can be changed to a more convenient value and the blade pitch altered so as to keep the operating requirements unchanged. A large increase in the non-dimensional duct resistance, due to additional duct elements, can also be dealt with by the expedient of reducing the blade setting angle relative to the plane of rotation; an increase in rotor speed will then permit the original capacity to be reproduced.

The overall efficiency with which a fan executes a specific task is often unimportant since the shaft horsepower may be quite small. However, for large installations, such as mine ventilating fans, the question of efficiency is of paramount importance; an increase of 2 or 3 per cent in efficiency can represent an extremely worthwhile reduction in the mine running expenses. Variable pitch greatly extends the operating range over which high efficiency can be obtained and it is in this respect that such fans attract most attention. The additional capital cost is soon offset by the savings effected through increased efficiency.

The advantages inherent in variable pitch are becoming more widely understood and as a result increasing use is being made of the principle. Three types of configuration, in ascending order of complexity, are listed below:

(i) A "standard" blade is designed for a rotor of given boss and fan diameters. For a specific task, the correct number of blades is permanently fixed to the boss at the desired pitch angle. When a change in fan duty occurs, the blade pitch is altered by substituting a different rotor. This method avoids the mechanical complication of adjustable pitch and may provide a cheap solution if the replaced rotor is returned to a stock pool for re-use at a subsequent date. The root setting and the number of blades used are sufficient to specify a particular variant.

Sheet metal bladed fans are probably the most suitable for this particular treatment since the blades can readily be welded to the boss.

(ii) As an alternative to a permanent root fixing, the pitch can be altered manually, by remote control or otherwise, when the fan is inactive. The blade root is usually provided with a screwed attachment by which the blade is secured to the boss.

(iii) In some instances it may not be practical to stop the fan in order to change pitch, in which case suitable manual or automatic mechanisms must be provided.

The second type of unit is the most popular, since the mechanical complications are by no means excessive. A discussion of the

many interesting mechanical features of variable pitch designs is outside the scope of the present work.

The aerodynamic advantages of this device will be discussed and methods presented by which acceptable designs can be speedily computed.

## 21.2. Design Procedure

Generally speaking, fan analysis is the mainstay of variable pitch designs. First, a fan unit is designed for a chosen condition, and then an analysis is carried out over the desired range of operating conditions. As a result of this it may be found that a redesign of the fan for some other operating condition is likely to produce a better compromise design.

Sufficient design data have been presented in preceding sections and hence the remainder of this section will be devoted to examples of fan analysis.

## 21.3. Effects of Rotor Blade Pitch Variation

The upstream rotor of the free vortex contra-rotating fan arrangement described in Reference 68 has been analysed according to the approximate, midspan method described in Section 19.3.1. The test data available on this rotor constitute a check on the accuracy of the recommended analysis method. As the rotor was tested in a wind tunnel rig, results are available for very low values of the pressure rise coefficient and these provide a check at this end of the range.

Design details of the rotor are set out in Table 21.1.

Table 21.1. Details of Front Rotor

$x$	0.5	0.625	0.75	0.875	1.0
$\varphi_r + \alpha$	56.6	48.1	41.5	36.8	33.0
$\sigma$	1.237	0.886	0.633	0.462	0.350
$\Phi = \varphi_r + (\alpha - \alpha_{N.L.})$	61.1	52.6	46.0	41.3	37.5

Blade section—RAF 6E ( $m = 5.7$ ,  $\alpha_{N.L.} = -4.5$ )  
 Fan diameter—1 ft  
 Boss diameter—6 in.  
 Reynolds number— $(w_r c / \nu)$  midspan  $\approx 1.5 \times 10^5$  at 3300 rev/min

A suggested procedure for analysing the rotor is presented for the design pitch case in Table 21.2.

Table 21.2. Analysis of Rotor at  $x=0.75$  over Operating Range  
0° Pitch Change

$\Lambda = u/\Omega R$	0.45	0.50	0.55	0.60	0.65	0.70
$\lambda = \Lambda/x$	0.6	0.667	0.733	0.8	0.867	0.933
$\tan \Phi - \lambda$ see Table 21.1	0.436	0.369	0.303	0.236	0.169	0.103
$2 \tan \psi/\lambda$ eq. (19.9)	1.270	1.145	1.040	0.953	0.880	0.817
$\epsilon_s$ eq. (19.8)	0.553	0.420	0.314	0.225	0.149	0.083
$k_{th}$ eq. (8.12)	1.84	1.27	0.86	0.56	0.34	0.18
$\varphi_r$ eq. (8.14)	35.8	37.8	39.6	41.6	42.8	44.2
$C_L$ eq. (8.27)	1.02	0.82	0.63	0.47	0.32	0.18
$C_{DS}$ eq. (10.10)	0.019	0.012	0.007	0.004	0.002	0.001
$C_{DP}$ Fig. 4.4.	0.019	0.015	0.014	0.015	0.017	0.021
$\gamma K_R/K_{th}$ eq. (10.4)	1.75	1.77	1.81	1.82	1.88	1.93
$K_R/K_{th}$ eq. (19.16)	0.085	0.078	0.080	0.094	0.132	0.252
$K$ eq. (19.13)	1.68	1.17	0.79	0.51	0.30	0.14

The rotor has also been analysed, in a manner similar to the above, for blade angles which vary by  $-8^\circ$ ,  $-4^\circ$ ,  $4^\circ$  and  $8^\circ$  from the design values; the results are graphically presented in Figs. 21.1 and 21.2.

Comparison of the computed characteristic and efficiency curves for the design pitch with the experimental ones shows reasonable agreement between the two. It will be noticed that two of the experimental values of efficiency appear to be unduly large. On reassessing the experimental techniques used, it appears that the most likely source of error is in the measurement of  $K$ . The close proximity of the measuring instrument to the rotor blades could lead to a slight over-estimation of the total head rise (see Section 22.4.3) and the rotor efficiency. If this were so the true value of  $K$  would be closer to the computed characteristic curve. Notwithstanding the above minor points, the agreement can be considered as being completely satisfactory, thus justifying the use of this method of analysis in the design of variable pitch fans.

The representative distributions of  $k_{th}$  given in Fig. 21.3 show that the error involved in assuming  $k_{th}$  at  $x_{\text{midspan}}$  to be equal to  $K_{th}$  is within acceptable limits (see also Section 22.4.4).

Lines of constant rotor efficiency have been superimposed

on the characteristic curves (Fig. 21.1). While satisfactory estimates of efficiency can be made for decreasing pressure rise conditions, difficulties arise in predicting the manner in which efficiency will decrease as the stall approaches with increasing fan loading. Flow separation on the blade may first appear at

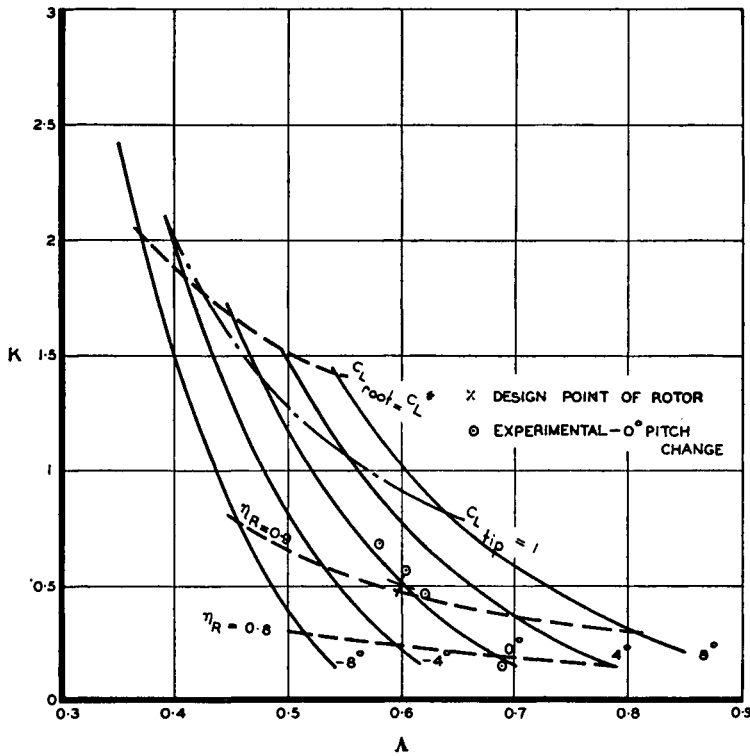


Fig. 21.1. Rotor characteristics for various blade settings

either extremity of the blade and will then move slowly or rapidly along the blade with an increase in the duct resistance. Normally, the onset of these phenomena cannot be predicted with precision as they depend on a large number of factors whose effect cannot be accurately assessed. Nevertheless, the importance of the problem imposes the necessity of devising ways and means of setting limits for the safe and efficient operation of the fan.

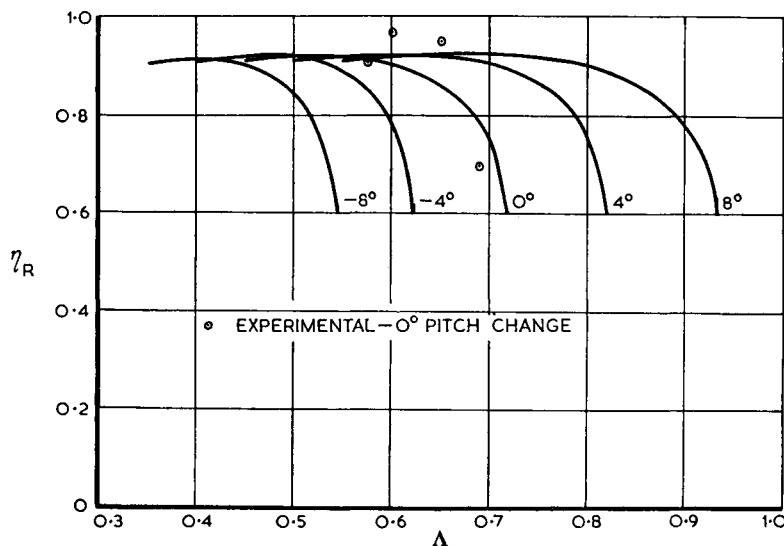


Fig. 21.2. Rotor efficiency for various blade settings

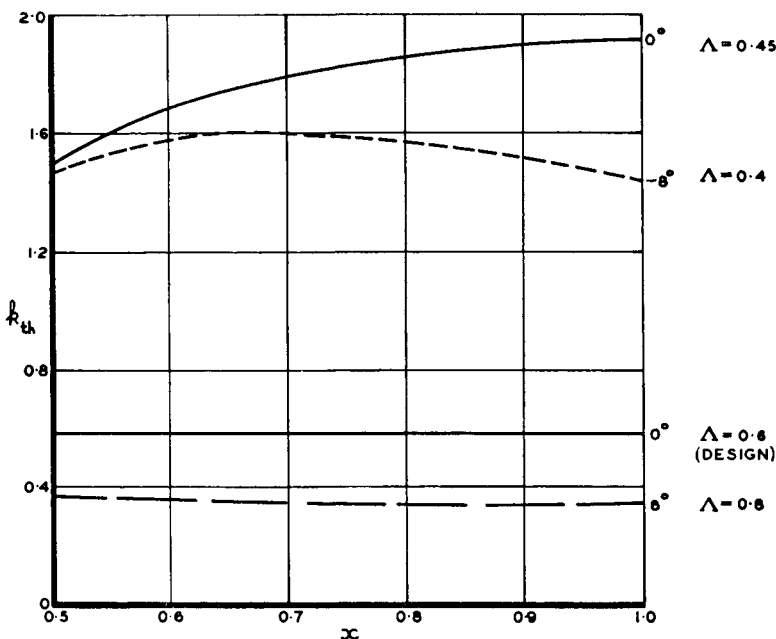


Fig. 21.3. Distributions of total head rise for range of conditions

The question of fixing an upper limit can be considered in terms of lift coefficient magnitude. The maximum lift coefficient is available from isolated aerofoil test data but when the blade solidity is large, these maximum values of lift will not be obtained (Section 7.6). Consideration should also be given to wall boundary layer influences at both ends of the blade. In these regions the actual local lift coefficients will be greater than the values computed on the assumption of uniform axial velocity. When stalling commences at a blade extremity, a decrease in fan efficiency can be expected; this trend will continue as, with increasing load, the rotor approaches a complete stall.

For the rotor in question, the relevant facts are:

- (i) The maximum lift coefficient for the RAF 6E section used is approximately 1.35 at the appropriate Reynolds number (Fig. 4.4).
- (ii) The solidity at the root is 1.24 and hence the allowable  $C_L$  at this station will be less than the maximum quoted above for an isolated aerofoil.

A curve for a computed lift coefficient of unity at the tip has been superimposed on the characteristic curves of Fig. 21.1. Also superimposed is a curve for  $C_{L^*}$  at the root. This curve was obtained by cross plotting the data of Fig. 9.11 on Fig. 21.4 for a solidity of 1.24 and then noting the values of  $\Lambda$  at which the various curves of  $\epsilon_s$  versus  $\Lambda$ , obtained from computations at  $x_b$ , cut this line (Fig. 21.4). Such an approach implies that the optimum lift coefficient,  $C_{L^*}$ , is relatively independent of the actual cambered aerofoil used; this is in fact not strictly true. (The RAF 6E section is a type of cambered aerofoil.) The curves for  $C_L = 1$  and  $C_{L^*}$  intersect at the lower end of the  $\Lambda$  range; it is suggested that high efficiency will be attained for operating conditions lying below this composite curve. When the above criteria are accepted, it will be noted that tip conditions are a governing feature at high  $\Lambda$  while at low  $\Lambda$  conditions at the blade root must be given careful consideration.

The actual local lift coefficients at the tip and root will, owing to wall boundary layers, be greater than the computed values of unity and  $C_{L^*}$  respectively, and may in fact approach the maximum values. Therefore, although the rotor can be

operated for conditions lying above the composite curve, an increasing loss in efficiency must be expected and the approach of stall conditions anticipated.

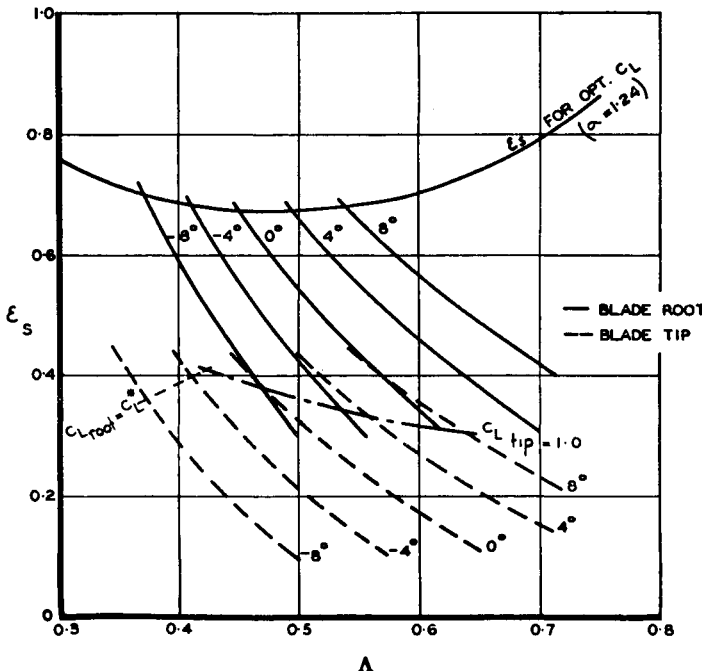


Fig. 21.4. Data used in fixing operational limits

Until the advent of the British cascade aerofoil data it was usually assumed that the design product of lift coefficient and solidity should not exceed unity (Section 7.6). In actual fact the permissible product is a function of  $\epsilon$  and  $\lambda$ . In the present instance the old recommendation agrees with the  $C_{L^*,\text{root}}$  curve (Fig. 21.1) at the lower flow coefficients; here we have blade root values of  $\epsilon_s$  and  $\lambda$  in the vicinity of 0.7 and 0.8 respectively which in turn give a  $C_{L\sigma}$  of approximately unity (see Fig. 8.7).

The procedure for determining a safe upper operating limit may vary in detail from rotor to rotor. The above discussion, however, in combination with experience, should prove of considerable value to the designer approaching this problem.

## 21.4. Variable Pitch Fan Unit

The above rotor will now be designed into a rotor-straightener fan unit. It is desirable that the straightener vanes should have a fixed pitch and yet, within acceptable limits, remove the swirl downstream of the rotor over the entire operating range. Factors affecting the stator design will now be considered.

Since the swirl coefficient,  $\epsilon_s$ , will exceed 0.4, the N.P.L. type of straightener is unsuitable. This means that the cascade method of design must be employed.

When it is assumed that the rotor will always be operated within the upper limit recommended above, the maximum swirl to be removed is represented by  $\epsilon_s \approx 0.7$ . After one or two preliminary calculations, it was decided to design the stators for the rotor condition of zero pitch change and  $A=0.50$ . The tabulated design computations are given in Table 21.3.

Table 21.3. Design of Stators ( $A=0.5, 0^\circ$  rotor pitch change)

$x=r/R$	0.5	0.625	0.75	0.875	1.0
$\epsilon_s$ From rotor analysis	0.544	0.487	0.420	0.372	0.325
$s/c$	1.3	1.35	1.4	1.45	1.5
$\alpha_1 = \tan^{-1} \epsilon_s$ From faired curve	29	25.7	23	20.6	18
$1 - 0.26\sqrt{(s/c)}$	0.704	0.698	0.692	0.687	0.681
$\theta$ eq. (11.7)	41.2	36.8	33.2	30.0	26.5
$\xi$ eq. (11.8)	8.4	7.3	6.4	5.6	4.8
$c (N=11)$ $= 2\pi x R c / s N$ (in.)	1.32	1.59	1.83	2.07	2.28

A linear variation of  $s/c$  along the blade was chosen; the value at the root was based on optimum conditions (see Fig. 11.6) while the recommendation that  $s/c$  should not exceed 1.5 was adopted at the tip.

In attempting to analyse the performance of the stators, a difficulty similar to that discussed in the rotor case again arises at the blade extremities. Downstream of the rotor, the values of  $\omega_s r / u_2$  in these local regions are greatly in excess of the computed ones (see Section 22.4.4). The only practical approach to this problem is to ignore these increases, while bearing in mind the possibility of small local unavoidable regions of separation on the stator blades.

Since the optimum deflection is 80 per cent of the maximum, the maximum deflection for the blade root station

$$\begin{aligned}(\alpha_1 - \alpha_2)_{\max} &= 1.25 \times 29^\circ \\&= 36.3^\circ\end{aligned}$$

For this maximum condition, however,  $\alpha_2$  will not be zero as undeturning will be present. From Fig. 19.3, the ratio  $(i - i^*)/(\alpha_1 - \alpha_2)^*$  at the stall is equal to 0.4 and since  $i^* = 0$

$$\begin{aligned}(\alpha_1 - \alpha_1^*) &= (i - i^*) = 0.4 \times 29^\circ \\&= 11.6^\circ\end{aligned}$$

that is  $\alpha_1$  for the stall condition is equal to

$$\begin{aligned}\alpha_{1,\text{stall}} &= 29^\circ + 11.6^\circ \\&= 40.6^\circ\end{aligned}$$

which corresponds to  $\epsilon_s = 0.86$ . For  $\epsilon_s = 0.7$ , which is the approximate limit fixed by the rotor analysis,  $\alpha_1 = 35^\circ$ . Hence

$$\begin{aligned}(\alpha_1 - \alpha_1^*)/(\alpha_1 - \alpha_2)^* &= 6^\circ/29^\circ \\&= 0.21\end{aligned}$$

Reference to Fig. 10.3 shows that no appreciable increase in drag has occurred for this value and hence the stator design can be considered satisfactory at the root.

The design lift coefficient at the straightener tip is less than the optimum and hence an estimate similar to the above should give a conservative answer in this region.

$$\begin{aligned}\alpha_1 - \alpha_1^* &= 0.4 \times 18^\circ \\&= 7.2^\circ\end{aligned}$$

Therefore

$$\alpha_{1,\text{stall}} = 25.2^\circ$$

which gives a swirl coefficient,  $\epsilon_s$ , of 0.47. From Fig. 21.4 it will be seen that  $\epsilon_s$  is generally below 0.4 when the rotor is operated within the suggested  $C_L$  limit. For  $\epsilon_s = 0.4$

$$\begin{aligned}(\alpha_1 - \alpha_1^*)/(\alpha_1 - \alpha_2)^* &= (21.8^\circ - 18^\circ)/18^\circ \\&= 0.21\end{aligned}$$

This value is identical with that just calculated at the stator root for a similar rotor case and therefore the stator design at the tip can also be considered satisfactory.

The undeturning which occurs at values of  $(\alpha_1 - \alpha_1^*)/(\alpha_1 - \alpha_2)^* = 0.21$  is only 4 per cent of the design deflection; no concern need therefore be felt on this account.

Slight overturning will be present when the fan is operated at low pressure rises. Once again this will be of no consequence, particularly as the drag data for the appropriate gap/chord ratio show no disturbing trends (Fig. 10.3).

In order to estimate the efficiency of the fan unit over the whole operating range, the losses of efficiency in the stators and over the tail fairing must be assessed. Table 21.4 gives a sample tabulation for the stators, when the rotor is at design pitch.

Table 21.4. Analysis of Stators at  $x=0.75$  over Operating Range  
0° Pitch Change

$A=u/\Omega R$	0.45	0.50	0.55	0.60	0.65	0.70
$\lambda = A/x$	0.6	0.667	0.733	0.8	0.867	0.933
$\epsilon_s$ Table 21.2	0.553	0.420	0.314	0.225	0.149	0.083
$\varphi_s$ Section 11.1	74.5	78	81.1	83.6	85.7	87.6
$s/c$ Table 21.3	1.4	1.4	1.4	1.4	1.4	1.4
$C_L$ Fig. 11.3	1.49	1.16	0.87	0.63	0.42	0.23
$C_D$ eq. (10.10)	0.040	0.024	0.014	0.007	0.003	0.001
$C_{D_P}$ Mean value over $A$ range	0.019	0.019	0.019	0.019	0.019	0.019
$\gamma K_S/K_{th}$ eq. (12.2)	0.65	0.70	0.75	0.81	0.87	0.94
$K_S/K_{th}$ eq. (20.7)	0.026	0.026	0.029	0.033	0.046	0.082

For a boss ratio of 0.5 and assuming 80 per cent efficiency in the diffusion over the tail fairing,

$$K_D = 0.088.$$

A final analysis of the rotor-straightener unit at design pitch is given in Table 21.5.

Table 21.5. Final Analysis of Rotor-Straightener Unit  
0° Pitch Change

$A=u/\Omega R$	0.45	0.50	0.55	0.60	0.65	0.70
$K_{th}$ Table 21.2	1.84	1.27	0.86	0.56	0.34	0.18
$K_R/K_{th}$ Table 21.2	0.085	0.078	0.080	0.094	0.132	0.252
$K_S/K_{th}$ Table 21.4	0.026	0.026	0.029	0.033	0.046	0.082
$K_D/K_{th}$ ( $K_D=0.088$ )	0.048	0.069	0.102	0.157	0.259	0.488
$\eta_T$ eq. (14.6)	0.84	0.83	0.79	0.72	0.56	0.18
$K_T = K_{th} \eta_T$	1.55	1.05	0.68	0.40	0.19	0.03

These tabulated results emphasize the great importance of the unavoidable tail fairing losses. It is clear from these results and from Fig. 13.5 that high efficiency operation at low total head rise coefficients can be obtained only when the boss ratio is very small.

The characteristic and efficiency curves for the fan unit operating at various rotor pitch settings are illustrated in Figs. 21.5 and 21.6.

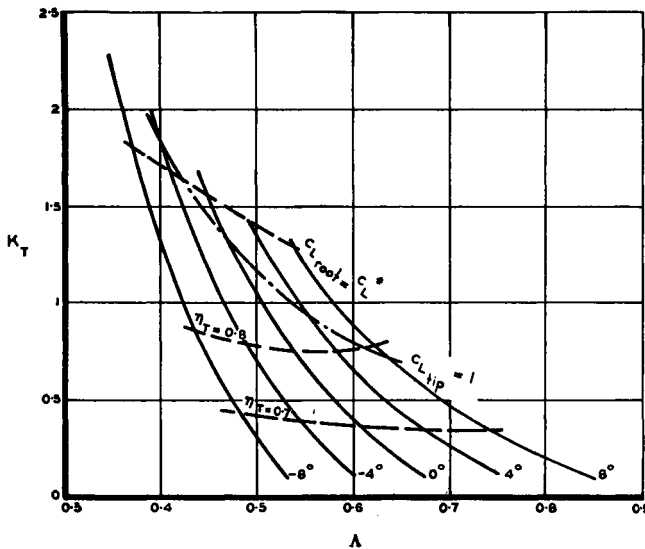


Fig. 21.5. Fan unit characteristics

If the basic aerodynamic data presented in preceding Sections are employed, any type of fan unit incorporating variable pitch rotor or stator blades can be designed on a procedure similar to that followed in the worked example.

The above method should permit the confident design of variable pitch fan units and, since it is simple and speedy, improvements to design can be carried out with the minimum of fatigue. Normally, every effort will be made in the design stage to avoid the possibility of operation near the stall. Accurate information at this extreme end of the range can be obtained only from actual experiments.

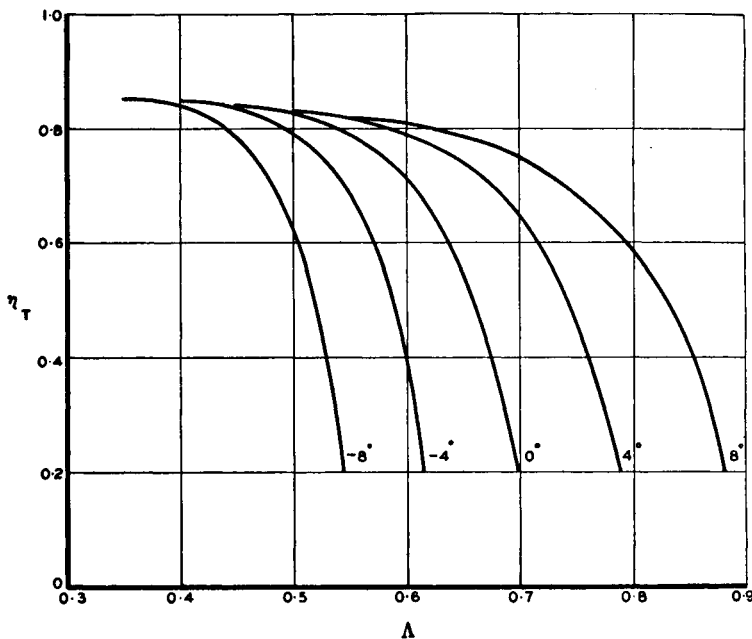


Fig. 21.6. Fan unit efficiency

### 21.5. Analysis of Rotor with Preswirl

A tabulated procedure for dealing with a rotor possessing preswirl is now illustrated by an analysis of the rear rotor of the contra-rotating pair of Reference 68. From the front rotor calculations for design pitch, carried out in Section 21.3, the swirl coefficient,  $\epsilon_s$ , at the midspan station, becomes the swirl coefficient,  $\epsilon_p$ , at the corresponding station on the rear rotor (see Section 7.8).

Table 21.6. Details of Rear Rotor

$x$	0.5	0.625	0.75	0.875	1.0
$\varphi_r + \alpha$	46.0	41.2	37.2	33.8	30.8
$\sigma$	0.841	0.627	0.481	0.374	0.292
$\Phi = \varphi_r + (\alpha - \alpha_{N.L.})$	50.5	45.7	41.7	38.3	35.3

Blade section—RAF 6E ( $m = 5.7$ ,  $\alpha_{N.L.} = -4.5^\circ$ )  
 Fan diameter—1 ft  
 Boss diameter—6 in.

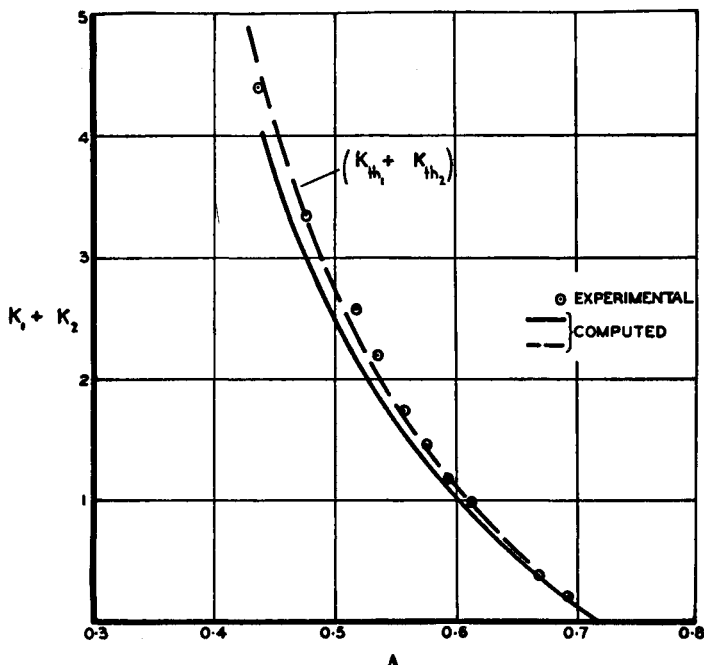


Fig. 21.7. Characteristic of contra-rotating fan unit

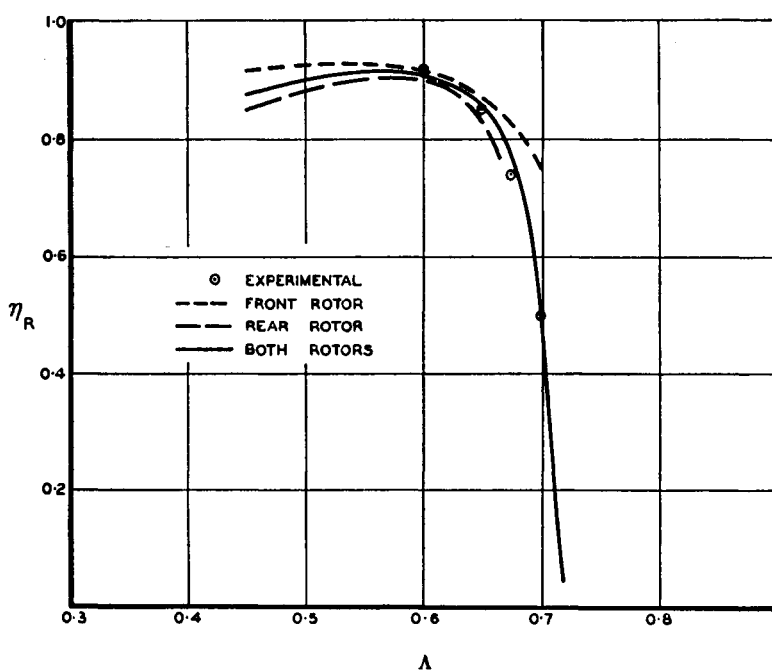


Fig. 21.8. Rotor efficiencies in contra-rotating fan unit

The details of the rotor are given in Table 21.6 which is followed in Table 21.7 by a suggested procedure for analysis.

Table 21.7. Analysis of Rear Rotor at  $x=0.75$   
over Operating Range

$A = u/\Omega R$	0.45	0.50	0.55	0.60	0.65	0.70
$\lambda = A/x$	0.6	0.667	0.733	0.8	0.867	0.933
$\epsilon_p$ Table 21.2	0.553	0.420	0.314	0.225	0.149	0.083
$\lambda_{N.L.}$ eq. (19.2)	1.759	1.431	1.238	1.115	1.028	0.963
$A = 2 \cos \Phi (\lambda_{N.L.}/\lambda - 1)$	2.88	1.711	1.028	0.590	0.281	0.046
$B = 4/m\sigma$	1.458	1.458	1.458	1.458	1.458	1.458
$C = \epsilon_p (2\lambda_{N.L.}/\lambda - 1)$	2.688	1.396	0.746	0.402	0.204	0.088
$\epsilon_s$ eq. (19.7)	0.134	0.079	0.035	-0.005	-0.035	-0.064
$\epsilon_p + \epsilon_s$	0.687	0.502	0.349	0.220	0.114	0.019
$k_{th}$ eq. (8.12)	2.29	1.51	0.95	0.55	0.26	0.04
$\epsilon_p - \epsilon_s$	0.419	0.344	0.279	0.230	0.184	0.147
$\varphi_r$ eq. (8.14)	28.1	30.9	33.6	36.2	38.8	41.2
$C_L$ eq. (8.27)	1.35	1.07	0.80	0.54	0.30	0.05
$C_{DS}$ eq. (10.10)	0.033	0.021	0.012	0.005	0.002	0.001
$C_{DP}$ Fig. 4.4	0.035	0.020	0.015	0.014	0.017	0.030
$\gamma K_R/K_{th}$ eq. (10.4)	2.71	2.53	2.40	2.29	2.21	2.16
$K_R/K_{th}$ eq. (19.16)	0.156	0.117	0.101	0.100	0.160	
$K$ eq. (19.13)	1.93	1.34	0.85	0.50	0.22	

The most convenient method of comparing these computed results with the experimental ones is to take the two rotors as a unit. The computed values for the unit are presented in Table 21.8 and these are compared with experiment in Figs. 21.7 and 21.8.

Table 21.8. Final Analysis of Contra-rotating Rotors

$A = u/\Omega R$	0.45	0.50	0.55	0.60	0.65	0.70
$K_{th_1}$ Table 21.2	1.84	1.27	0.86	0.56	0.34	0.18
$K_{th_2}$ Table 21.7	2.29	1.51	0.95	0.55	0.26	0.04
$\eta_{R_1}$ Table 21.2	0.915	0.92	0.92	0.905	0.87	0.75
$\eta_{R_2}$ Table 21.7	0.845	0.88	0.90	0.90	0.84	
$K_1 + K_2$ Tables 21.2, 21.7	3.61	2.51	1.64	1.01	0.52	
$(K_1 + K_2)/(K_{th_1} + K_{th_2})$	0.88	0.90	0.91	0.91	0.86	

Agreement is well within acceptable limits. Since the experimental values of  $K$  for the unit were measured 0.75 D

downstream of the rear rotor the experimental total head rise will not be subject to an error of the type suggested in Section 21.3 for the front rotor. The overall efficiency of the pair of rotors is reasonable and the computations are in close agreement. No explanation can be advanced for the slight under-estimate of the total head rise coefficient, but this is not likely to be a feature of all designs. Close control must be maintained over the blade sections and settings if consistent results are to be obtained in all cases.

# 22

---

## FAN TESTING

### 22.1. General

Fan testing is a very important aspect of the subject of ducted axial flow fans. From such experiments, progressive improvements in design methods and assumptions can be achieved. In addition, while analytical methods are useful in estimating performance over the main operating range of the fan, rotor characteristics near the stall must be determined experimentally.

When a fan installation proves unsatisfactory, experiments must be undertaken in order to isolate the contributing factors. This may involve a study of

- (a) duct losses
- (b) inlet and outlet conditions to the fan
- (c) rotor and stator performance.

Although there are many aspects of this important experimental field, the main emphasis here will be confined to the broad aerodynamic aspects of fan testing. The reader seeking greater detail on test equipment and methods is referred to the many references quoted.

In general, fan testing can be sub-divided into four main classes :

- (i) Visual studies of the flow through the fan for the main purpose of checking whether there are any local regions of separation on the fixed or rotating surfaces of the unit
- (ii) Static and total pressure measurements at selected reference points

- (iii) Radial traverses upstream and downstream of a blade row for the purpose of measuring velocity, total head and yaw angle distributions
- (iv) Measurements, on the actual rotating blades, of chord-wise static pressure distributions or boundary layer characteristics.

## 22.2. General Test Equipment

An example of a typical fan testing rig is given in Fig. 22.1. Good inlet conditions are essential and hence a streamlined entry to the duct must always be provided. In the test rig shown,

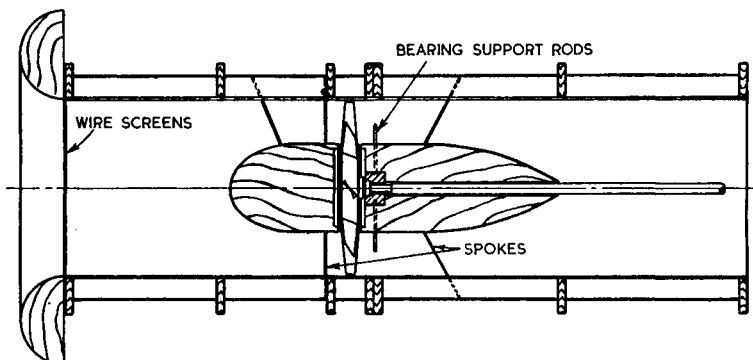


Fig. 22.1. A test rig

wire screens at inlet have been used to vary the pressure rise across the rotor. A more usual arrangement consists of a variable area outlet by which the exit velocity, and hence the discharge loss, can be varied in a continuous manner (see Fig. 22.2). The power unit usually incorporates some form of transmission dynamometer; a simple type is illustrated in Fig. 22.3.

To ensure a good inlet flow distribution, the area in the vicinity of the bellmouth should be kept free of obstructions. The recirculation pattern of the air can also cause experimental difficulties and hence it is advisable either to have the test rig in a large room or to provide a baffle system through which the air has to pass when returning to the inlet end of the room.

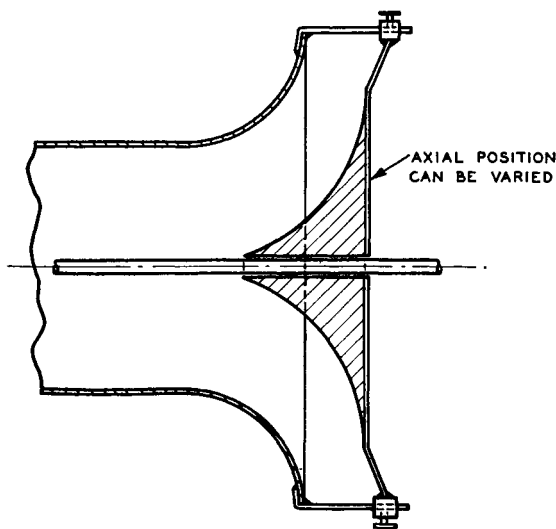


Fig. 22.2. Throttle at exit for varying test conditions

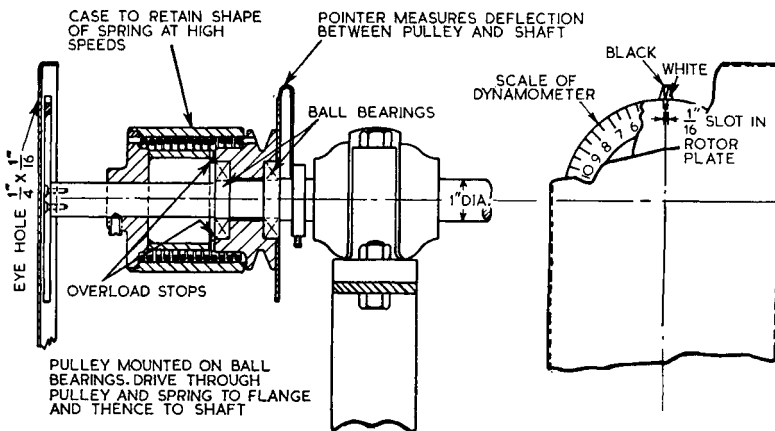


Fig. 22.3. Simple transmission dynamometer (Reference 70)

### 22.3. Test Instruments

The types of instrument most commonly used in fan testing will be considered in broad outline. The manner in which they perform their task of measurement will be indicated in an

attempt to help the comparative newcomer to the field in their correct use.

**22.3.1. Total head.** In measuring the total pressure or head of the stream, the velocity head of the air must be converted to a static pressure without loss. This is usually achieved with a suitable open-ended tube<sup>(83)</sup> pointing into the stream (Fig. 22.4). Air entering the tube is brought to rest when the

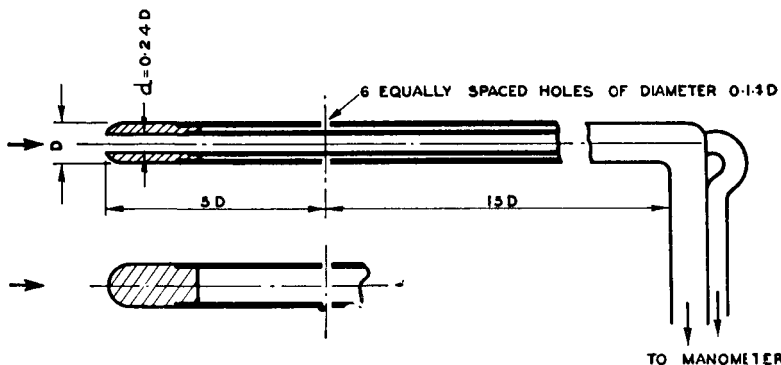


Fig. 22.4. Pressure measuring tubes

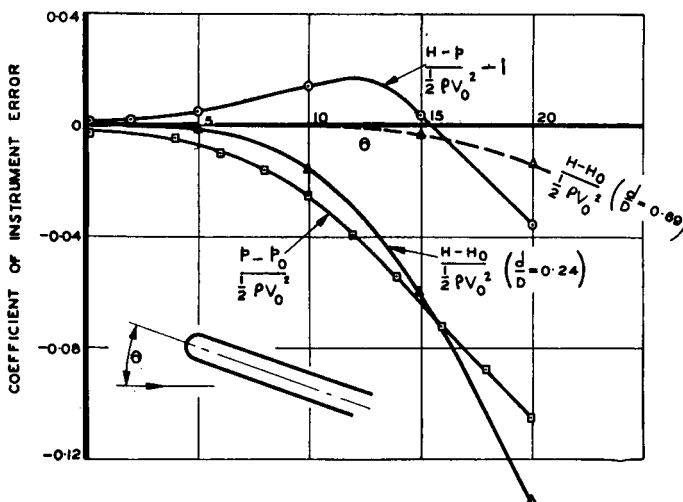


Fig. 22.5. Calibration of instruments in Fig. 22.4

back pressure in the tube equals the dynamic pressure plus the static pressure of the oncoming stream. The back pressure then registers on a manometer as the total head of the stream. From the calibration curves of Fig. 22.5 it will be seen that careful alignment of the tube to the stream direction is important, particularly when the  $d/D$  ratio is small.

An alternative method for measuring total pressure consists in measuring the pressure at the stagnation point of a cylinder, aerofoil or sphere. At such a point the air is divided around the body and the dividing streamline is brought to rest at the surface. Hence the pressure measured, when the small surface

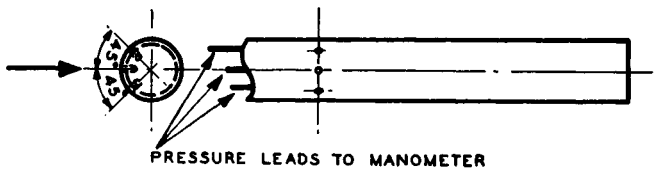


Fig. 22.6. Cylindrical type instrument

hole (see Fig. 22.6) is connected to a manometer, is the total head of the stream. To avoid inaccuracies, the hole should be kept as small as is practicable since the surface region over which the air is virtually at rest is very small. With additional pressure points, a circular tube can be used to measure the stream direction and this feature, plus the compactness of the instrument, makes it a very popular one with test engineers.

**22.3.2. Static pressure.** A small diameter tube, fitted flush with the surface and connected to a manometer, will measure the local static pressure (see Fig. 22.7). This tube cannot

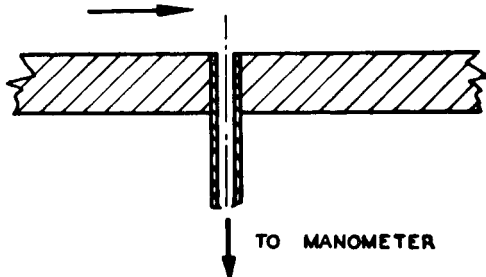


Fig. 22.7. Measurement of static pressure

measure any fraction of the dynamic head as there is no velocity component normal to the surface.

It is important, however, to ensure that the tube is flush with the surface. When the tube protrudes into the stream there is a local speeding up of the flow as it is deflected around the obstacle and hence the static pressure, owing to Bernoulli's relation, will fall below the true value.

When separated flow is present in the vicinity of the tube and when the eddies possess an appreciable dynamic head in a direction normal to the surface, the flush surface tube will give

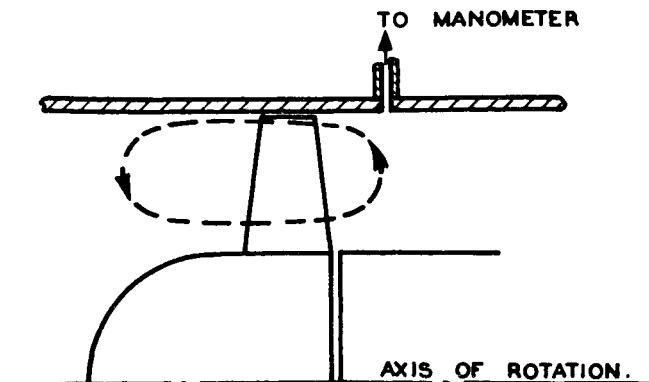


Fig. 22.8. Example of incorrect use of surface tube

an erroneous result. This error may be of large magnitude in the case of recirculation through a stalled rotor (see Fig. 22.8).

The static pressure probe of Fig. 22.4 utilizes the principle of the flush surface hole. The instrument error for a probe yawed to the stream can be deduced from Fig. 22.5; the negligibly small error existing at zero yaw is influenced by a small increase in stream velocity brought about by the tube, which constitutes a flow obstruction, and by the pressure field created by the "stagnation" condition at the tip.

**22.3.3. Velocity.** By means of the combined total head static pressure tube of Fig. 22.4, commonly known as a Pitot-static tube, the dynamic head can be obtained on a manometer as the difference of these two pressures. When the density of the stream is known, the velocity can readily be computed.

This is by far the most common method of velocity measurement. The characteristics of the instrument in the presence of yaw are illustrated in Fig. 22.5.

The cooling effect of an airstream on a heated wire is sometimes employed in the measurement of velocity. With increasing speed, the temperature of the wire is progressively reduced, which in turn changes its electrical resistance. The changes in flow velocity can be measured from the modified current-conducting properties of the wire and a suitable aerodynamic calibration. Except for very special cases, this method is seldom used in fan tests.

Certain types of yawmeter can be used in the measurement of velocity; details of the method will be discussed in the next sub-section.

**22.3.4. Yawmeters.** To measure flow direction accurately, an instrument sensitive to yaw is required. Downstream of a rotor an element of flow is, for all practical purposes, confined to an elementary annulus; hence, when the angle made by the flow with the axis of rotation is known, the flow direction is fully defined. In other words a two-dimensional yawmeter is a suitable instrument for carrying out tests on ducted axial flow fans.

As indicated in Section 22.3.1, the cylindrical tube of Fig. 22.6 is a very attractive instrument when measurements of total head and yaw are required. The present of the tube causes a local speeding up of the flow. A velocity gradient then exists around the surface of the cylinder, with a maximum value in the vicinity of the two holes which have been displaced  $45^\circ$  from the flow axis, and any small change in tube rotation will produce a large change in the surface pressure. When the side tubes are connected to a U-tube manometer, the effect of tube rotation is to reduce the pressure in one tube and increase it in the other. On correct alignment of the tube to the flow, the pressures in both legs of the manometer will be equal. A very accurate measure of flow direction can be obtained with this instrument, particularly when a single inclined manometer tube working on the null point principle is employed. The portion of the instrument projecting outside

the duct is fitted with a suitable scale for measuring the deviation of the flow with respect to some reference line, usually the duct axis. The total head is then given by the central hole facing the oncoming stream (Fig. 22.6).

In using this type of yawmeter, it should be borne in mind that there are points on the downstream side of the cylindrical surface which have pressures similar to those on the upstream side. Hence the side tubes will balance at more than one rotational position. The general direction of the stream is, however, usually known, and hence the above eventuality should never arise.

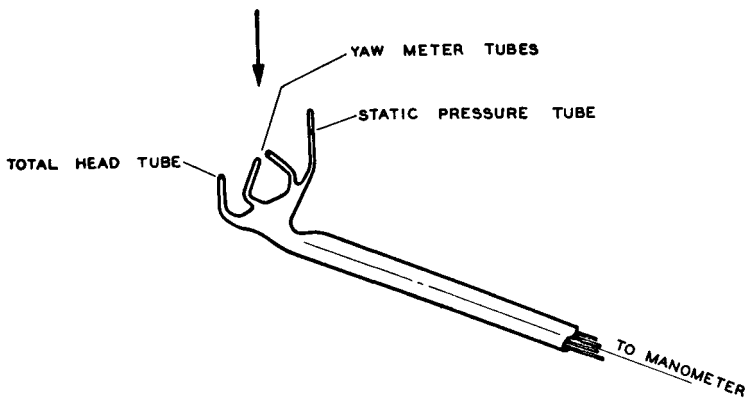


Fig. 22.9. Combination measuring head

The claw type yawmeter, an example of which is illustrated in Fig. 22.9, is based on the known sensitivity of a total head tube at large degrees of yaw (see Fig. 22.5). The two tubes forming the claw are usually aligned at  $45^\circ$  to the flow direction, at which angle small rotational movements produce appreciable pressure changes. As before, the tube is rotated until the pressures measured by the two tubes are equal. Although this type of yawmeter is in common use it suffers certain disadvantages. Compared with the cylindrical type it is less compact and more susceptible to accidental damage, and is more difficult to construct, particularly when the instrument axis of rotation is required to pass through the region of the claw extremities.

Instead of inclining the tubes to the stream direction, a

similar effect can be obtained<sup>(84)</sup> by cutting the tube ends at an angle, as in the Conrad instrument of Fig. 22.10. Owing to the introduction of cross flows, the pressures recorded by the side tubes are less than the total pressure of the stream and are yaw sensitive. Balance of pressure in the two side tubes once again permits the determination of flow direction, while the central tube measures total head.

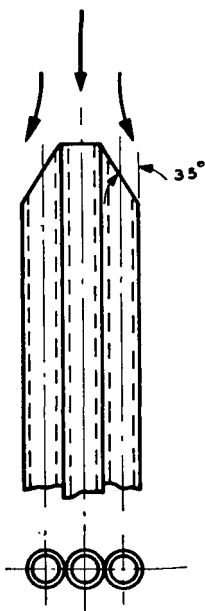


Fig. 22.10. Conrad type instrument  
for measuring yaw

When the direction of flow is unknown in all planes, a spherical instrument<sup>(83)</sup> working on the same principle as the cylindrical tube can be employed. When four holes, in addition to the central total head one, are used, the pressures can be balanced in opposite pairs; a three hole sphere requires a simultaneous balance of all three pressures. Similar modifications can be made to either the Conrad or claw types of yaw-meters by duplicating the tube arrangement in the appropriate plane.

A yawmeter will give a true indication of flow direction only when the total head of the air at each of the pressure orifices is identical. When a large total head gradient exists between orifices, experimental error must be expected.

When the Conrad type instrument is aligned in the stream direction the pressure measured by the side tubes is composed of the static pressure plus some proportion of the dynamic head; the amount is a function of Reynolds number and turbulence. Hence the dynamic pressure of the stream is given by

$$\frac{1}{2}\rho V^2 = C_1(H - p_s) \quad (22.1)$$

where  $C_1$  is a constant

$H$  is total head, measured by central tube

$p_s$  is pressure in side tube.

The constant  $C_1$  must be evaluated in tests for the appropriate Reynolds number and stream turbulence.

A similar expression can be derived for the cylindrical tube yawmeter when the tube is rotated  $45^\circ$  after balancing the side hole pressures. One tube now reads total head while the second one reads a pressure which has properties similar to the pressure recorded by the side tube of the Conrad yawmeter. Once again,

$$\frac{1}{2}\rho V^2 = C_2(H - p_s) \quad (22.2)$$

where  $C_2$  is a new constant and  $(H - p_s)$  is pressure difference between yawmeter holes.

Since it is often difficult to calibrate these instruments in circumstances which are identical with those of the test conditions, their use is not recommended for precision measurement.<sup>(85)</sup> They may on occasions, however, prove an extremely useful tool, provided their limitations are clearly understood.

Hot-wire type instruments, using direction-sensitive elements, can also be designed.

## 22.4. Types of Testing

The measurements involved in determining the characteristic curve of a fan over a range of operating conditions are few and simple. In contrast, when a detailed study of the flow through the fan unit is undertaken, the testing procedures can be very complex and tedious. A survey of various test methods will now be given.

**22.4.1. Visual studies.** A knowledge of the general flow through a unit can be most useful. The simplest and most instructive way of obtaining this information is to render the flow visible by some means. Upstream of the rotor, smoke can be successfully used to indicate the nature of the inlet flow. The dispersion of smoke filaments on passing through the rotor limits the usefulness of smoke for rotor investigations.

Flow visualization is usually associated with the search for possible flow separations within the fan unit or in its neighbourhood. When, as a result of high load conditions, stalling of the rotor blading occurs, a characteristic audible note is given out which can be interpreted by the experienced ear; unsteadiness of the through flow may also be apparent. In the extreme case, blade stalling gives rise to a type of surging which even the novice cannot misinterpret.

In the location of regions of separation, whether on fixed surfaces or on the rotating blades, the common tuft is of immense value. Tufts should be made from low density, flexible strands of material. The length is not critical, but this feature merits consideration in the light of experience. Normally, in an attached flow, silken threads approximately  $1\frac{1}{4}$  in. long are quite suitable. In thin boundary layers the tuft will point steadily in the flow direction, while in thicker layers some movement about the mean flow line will be present. This can be traced to an increase in the scale of the turbulence within the layer. Care should be taken to ensure that increased tuft activity is not caused by a faulty attachment of the tuft to the surface. For example, when cellulose tape is used as a method of attachment and an edge becomes inadvertently turned up, eddies which influence the tuft will be shed by this protuberance.

In separated flow, the tufts will behave in a most irregular manner. They may oscillate in a general upstream direction, turn irregularly through  $360^\circ$  or, when in a region of relatively stagnant air, execute slow, large scale movements.

Flow re-attachment often occurs downstream of severe flow separation and when it does the tufts in the boundary layer usually oscillate with a fairly large angular displacement about the mean flow direction.

The accuracy with which tuft observations can be interpreted

will increase as the operator accumulates experience. Such investigations should, however, be supplemented with other data, visual or otherwise, in order that a fairly accurate picture of the flow field may be obtained.

The type of tuft just described gives an indication of flow conditions near the surface. In order to ascertain the extent of the separation region in which large scale, energy-consuming eddies are present, a single tuft is often secured to the end of a "wand". It is important for the wand to be reduced in diameter as the point of attachment to the tuft is approached ; this is to minimize the possibility that the eddies created by the bluff wand will affect the behaviour of the tuft. A fine stiff wire usually makes an excellent tip to the wand ; attachment of the tuft to the wire should be as neat as possible.

For streamlined flow conditions, a tuft length of approximately 2 in. is quite suitable for a wand. In the presence of separated flow, however, the length has to be matched to the scale of the large eddies. A short tuft will not indicate the extent of the average large eddies, while a long one will suffer interference between adjacent flow patterns.

From the foregoing it will be seen that the tuft is a very useful aerodynamic tool when properly used. It records the mean direction of flow together with the nature of the relatively large scale eddy or vortex motions in attached and separated flow.

Tufts can be applied to rotating as well as to fixed surfaces. The air forces usually have a much stronger influence than the centrifugal forces on the motion of the tufts, and hence tufts are a reliable indicator of the flow condition on rotor blading. The tufts are, of course, viewed with the aid of a stroboscopic light.

Visual tests of the above nature can be carried out quickly and without much effort and are a useful prelude to more detailed studies of the fan performance. In certain cases they may indicate the uselessness of further tests ; alternatively they may suggest the most appropriate type of test to pursue.

**22.4.2. Overall characteristics.** From a commercial point of view it is important to know the overall performance of the

fan unit over a range of operating conditions. The data so obtained are usually listed in the maker's catalogue ; for a chosen capacity in cu. ft/min and a given static head in inches of water, the speed and horse power of the unit can be read off. An outline of one of the test methods employed in obtaining these catalogued data is given below.

The test rig is fitted with two flush surface static pressure tappings one upstream and one downstream of the nose and tail fairings respectively (see Fig. 22.11). On approaching the nose fairing, the flow is deflected more and more ; associated with this deflection is a flow acceleration which will be evidenced by a

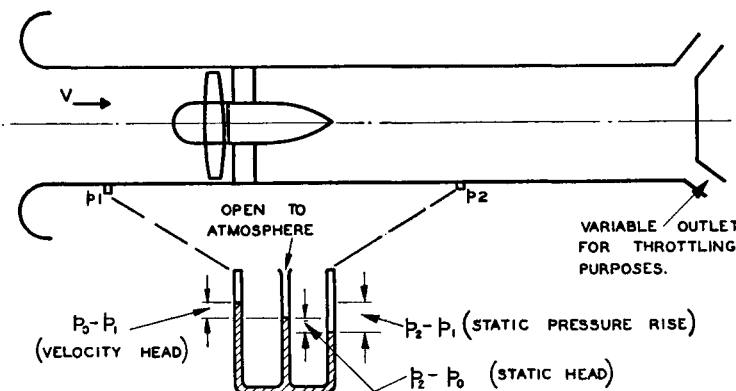


Fig. 22.11. Commercial testing of fans

drop in static pressure along the duct wall. Hence it is important that the pressure tapping should be sufficiently far upstream of the nose fairing to ensure that the flow is approximately axial everywhere across the section. It is advisable to measure the axial distribution of static pressure along the test rig as a prelude to choosing the reference stations. These should be located where the pressure gradients are moderately flat.

It may be assumed that the air eventually sucked into the inlet to the test rig is initially at rest, with a static pressure equal to that of the atmosphere. In the absence of flow resistances such as wire screens at inlet, the total head of the air upstream of the rotor is equal to the atmospheric pressure,  $p_0$ .

As a result of this, the following simple relationships hold:

$$H_0 = p_0 = p_1 + \frac{1}{2} \rho V^2 \quad (22.3)$$

$$\text{cu. ft/min} = 60\pi R^2 \left[ \frac{2(p_0 - p_1)}{\rho} \right]^{1/2} \quad (22.4)$$

When the inlet flow is throttled by means of gauzes, the total head is less than  $p_0$  by an amount equal to the total head loss through the gauze. If a total head measuring tube is inserted on the axis of the duct at the upstream reference station, eq. (22.4) must then be written

$$\text{cu. ft/min} = 60\pi R^2 \left[ \frac{2(H_1 - p_1)}{\rho} \right]^{1/2} \quad (22.5)$$

For the case where the flow leaves the rotor or stator blading in an axial direction, the static pressure difference,  $p_2 - p_1$  is the static pressure rise of the unit and also the total head rise since the mean velocity head is identical at both measuring stations. Writing these relations,

$$\Delta p = \Delta H = p_2 - p_1 \quad (22.6)$$

and from the definition of static head given in Section 1.5,

$$\text{Static head} = p_2 - H_1 \quad (22.7)$$

or when  $H_1 = H_0 = p_0$ ,

$$\text{Static head} = p_2 - p_0 \quad (22.8)$$

When a fan unit designed without stator blading is being tested, the static pressure,  $p_2$ , measured at the wall is not the mean static pressure across the duct since, owing to the rotating flow, there is in existence a pressure gradient,  $dp/dr$ , whose magnitude will depend on the amount of swirl present. The static pressure gradient is positive and hence the pressure,  $p_2$ , will be an over-estimate of the mean static pressure rise in the unit. In addition, the total head rise through the rotor, which includes the swirl momentum, will be greater than  $(p_2 - p_1)$ , but since this momentum is a loss so far as the unit is concerned, the effective total head rise of the unit will be approximated by  $(p_2 - p_1)$ . These factors should be borne in mind when the above type of fan unit is tested by this simple method.

The transmission dynamometer and a rev/min counter provide data from which torque, power and efficiency can be deduced. Rewriting eqs. (15.3) and (15.9) we have

$$\text{Shaft h.p.} = \frac{2\pi Q \times \text{rev/min}}{33,000} \quad (15.3)$$

$$\eta_T = \frac{\Delta H_T \times \text{cu.ft/min}}{33,000 \times \text{h.p.}} \quad (15.9)$$

The static head efficiency is obtained when the total head rise,  $\Delta H_T$ , is replaced by the static head.

In tests of the above type, it is usual to run the rotor at a relatively constant speed and to vary the resistance to flow by means of the outlet throttle. Characteristic curves, based on non-dimensional parameters, can then be drawn.

The data listed in manufacturers' catalogues are obtained from such curves. Although this information is simple to use, it has certain shortcomings from the point of view of an engineer choosing a fan. For example, it is useful to know, first, the proximity of the operating point to the stall, and second, the location of this point with respect to maximum efficiency.

There is a growing tendency to present graphical information in catalogues but the author feels that this should be done more generally. For a given fan, all necessary information can be presented on simple curves in the manner illustrated in Fig. 22.12. With the exception of efficiency, the co-ordinates are not non-dimensional; they are, however, proportional to  $K_{T_v}$  and  $\bar{A}$  for a particular fan unit.

In order to illustrate the use of Fig. 22.12, which was constructed from data extracted from a catalogue for a rotor-straightener unit, a capacity of 30,000 cu. ft/min and a static head requirement of 1 inch of water will be assumed. The head coefficient is therefore

$$\frac{\text{Static head} \times 10^9}{(\text{cu.ft/min})^2} = 1.11$$

Therefore, from Fig. 22.12,

$$\text{c.f.m./rev/min} = 30.2$$

Hence

$$\text{rev/min} = 993$$

To determine the power, the efficiency is obtained from the graph, giving

$$\eta_{\text{static head}} = 0.52$$

and

$$\begin{aligned} \text{h.p.} &= \frac{\text{Static head} \times 5.2 \times \text{cu.ft/min}}{33,000 \times \eta_{\text{static head}}} \\ &= 9.1 \end{aligned}$$

The required installation data have now been established. It will be noted from Fig. 22.12 that the total head efficiency is at a maximum and hence the rotor blades are working under

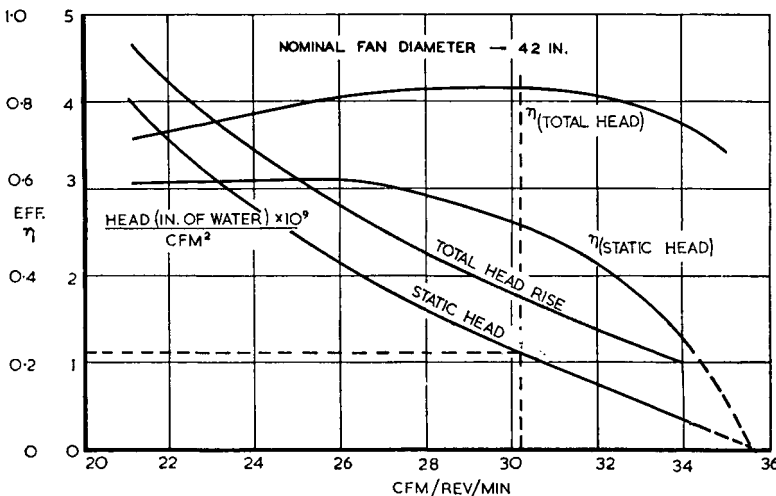


Fig. 22.12. Method of presenting test data

favourable conditions. The difference between the two efficiency curves constitutes a discharge loss. If a larger diameter fan had been chosen the outlet velocity would have been less and as a result the efficiency based on static head would have increased. Alternatively this efficiency can be increased by fitting a diffuser downstream of the fan unit in order to reduce the discharge velocity. When the static head efficiency is the most important factor, it would appear from the above curves that operation at low values of c.f.m./rev/min is desirable. It should, however, be remembered that stall

conditions are being approached at this end of the range and that hence an under-estimate of the required pressure rise could prove troublesome. For the fan in question, the stall characteristics are not available; a study of the efficiency curves, however, suggests that operation for values of c.f.m./rev/min of under 24 should be approached with caution.

It will be seen that the above graphical procedure of presenting test results is a simple one, and as a marked improvement on normal methods it is recommended for fans designed to meet the usual commercial needs. In addition to the data given in Fig. 22.12, the value of c.f.m./rev/min at which blade stalling commences should be indicated.

The foregoing has been confined to the routine testing of fans produced for "off the shelf" buyers. Occasions arise, however, when a fan unit must be tested *in situ* under conditions less ideal than those of Fig. 22.11. The proximity of an upstream corner or diffuser may produce a non-uniform inlet condition while changes in cross-sectional area may cause confusion in specifying the pressure rise. In circumstances such as these it is advisable to avoid rule-of-thumb methods of testing. For example, total head traverses at upstream and downstream stations are recommended; this technique is discussed in Section 22.4.3.

**22.4.3. Traverse experiments.** The type of testing which has just been described is usually adequate for most engineering purposes. If, however, it is desired to increase fan performance by improved design methods a detailed study of certain variables is essential. Such an investigation involves velocity, total head, and flow direction measurements at varying radii in a given cross-sectional plane. When good inlet conditions exist, the flow is axisymmetric and hence measurements are not required over the complete annulus at each station chosen for investigation.

The test rig should be designed so that the streamwise measuring stations are favourably located. For example, it will be noted in Fig. 22.1 that the streamlined nose and tail fairings are combined with cylindrical sections for the purpose of providing an appreciable length of annulus with constant cross-sectional area; measurements can then be obtained under

conditions of constant mean axial velocity. The radial line along which the instruments are traversed upstream of the blading should be so chosen as to avoid wakes or other peculiarities which are not representative of the flow as a whole. Downstream of rotor or stator blading the procedure is not quite so straightforward. Since the rotor is the fan element most commonly investigated in this detailed manner, rotor problems will be considered first. It will be assumed in the subsequent discussion that inlet conditions to the test rig are completely satisfactory.

Since the rotor blades are swept past the measuring instrument, all traversing can be carried out along a single radial line. As each blade possesses a wake, the flow is obviously an unsteady one. Owing, however, to the high frequency with which the wakes pass the pressure recording instruments normally used, the manometer reading remains steady. Experience has shown that the instruments tend to integrate the input and strike a mean in the majority of cases. The survey plane is usually located about one chord length downstream of the blades. Using a total head tube of the type illustrated in Fig. 22.6, the author<sup>(70)</sup> recorded the phenomenon presented in Fig. 22.13. The results obtained immediately downstream of the blade trailing edges are believed to be spurious, as efficiencies calculated from such results are impossibly high. Detailed total head distributions for the cambered plate fan at stations 1 and 3 are given in Fig. 22.14 for a number of operating conditions. The change is more or less constant along the whole blade, thus suggesting that the wall boundary layers are not the primary reason. It is believed that the instrument, when located adjacent to the blades, does not record the true mean value and that mixing in the wakes contributes to the small negative gradients further downstream (see Fig. 22.13).

On occasions it may be impossible to place the instrument as far downstream as one chord length. Under such circumstances, data such as that presented in Fig. 22.13 should be used for the purpose of applying a correction factor.

Downstream of stators, traversing along a single radial line will not provide data from which the mean flow changes in the stator blading can be deduced. A sufficient number of traverses

must be made in the survey plane to ensure a reasonable knowledge of the flow field embracing two adjacent stator blades. Either the instrument or the stator assembly can be moved circumferentially, step by step, in order to obtain the desired number of radial traverses. Location of the survey plane relative to the stator blades may also be important. It is reported in Reference 86 that the mean total head readings at a

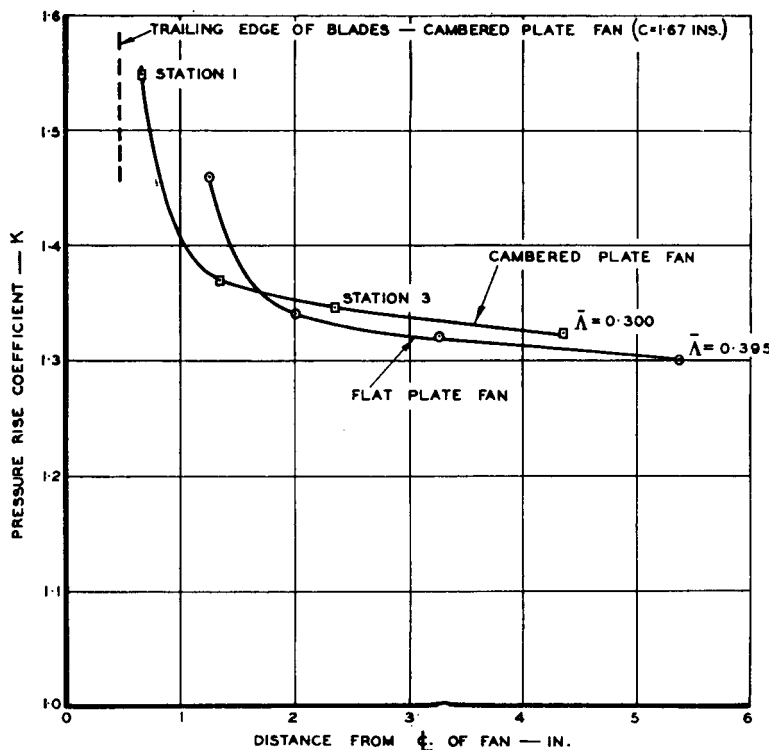


Fig. 22.13. Change in measured total head rise with downstream distance

station a half chord downstream of the stators are approximately 10 per cent higher than those two and a half chords downstream. The difference is attributed to mixing losses associated with the stator wakes. Unfortunately, there are insufficient data to permit the construction of curves similar to those of Fig. 22.13.

It is clear from the foregoing that more than one survey station may be required downstream of rotor or stator blading when any doubt exists concerning the quantities being measured.

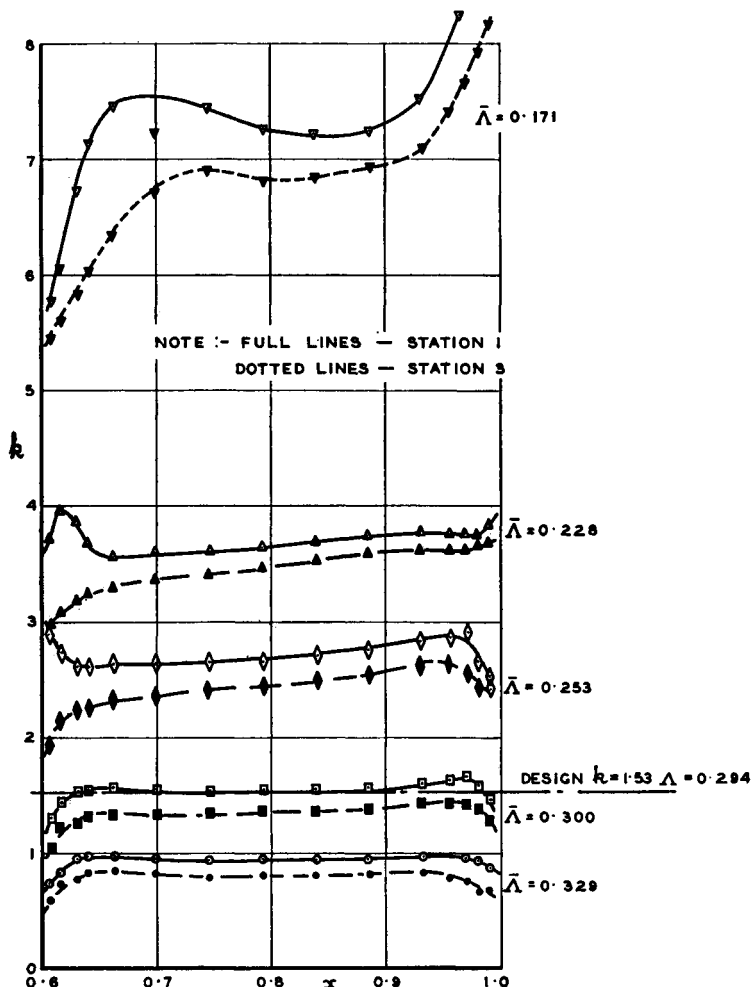


Fig. 22.14. Radial variations in total head rise on cambered plate fan

Provided that a little care is taken in choosing the survey station initially, however, no great concern need be felt concerning the subsequent results.

The use of the instruments described in Section 22.3 will now be considered. The three types illustrated in Figs. 22.6, 22.9 and 22.10 can, with suitable calibration, record total head, dynamic head and flow direction at any given radius either upstream or downstream of the blading under test. When precision is required, however, the Conrad and cylindrical type yawmeters are not recommended for velocity measurement; it is preferable to insert a static pressure measuring tube of the type illustrated in Fig. 22.4, which can be set at the appropriate angles, as determined from a previous yawmeter traverse. The instrument of Fig. 22.9 suffers from a lack of compactness and from susceptibility to damage. Two types of positioning

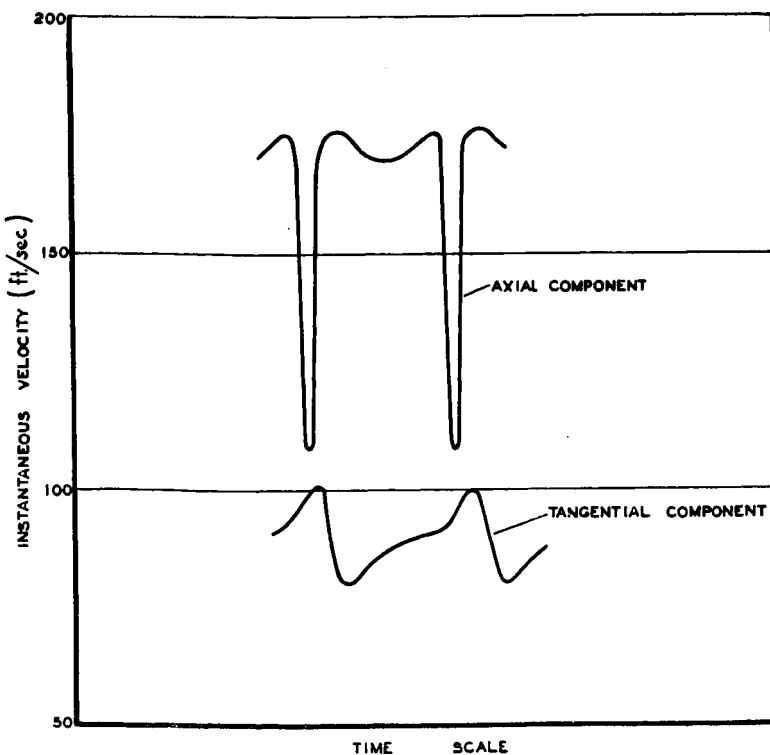


Fig. 22.15. Hot wire measurements of instantaneous velocities downstream of rotor  
(Reproduced by courtesy of Journal of Aeronautical Sciences)

error may also arise from the following sources. First, when the probe is used in the rotating flow downstream of a rotor, the static pressure, total head and yawmeter tubes are not in the same survey plane. Secondly, it is impossible to arrange the instrument so that, for a complete traverse, all measuring elements are at the same radius. The errors arising may be important where flow conditions are changing rapidly, as in the wall boundary layers.

In Section 22.3.3 reference was made to a hot wire instrument suitable for measuring the instantaneous velocities downstream of a rotor. A typical result<sup>(87)</sup> is presented in Fig. 22.15 from which the passage of the blade wakes is readily discernible. It is in a flow field similar to this that the normal pressure measuring instruments are used for the purpose of recording mean values.

It will be noted from the above that an adequate choice of suitable measuring equipment exists. Typical results obtained with these instruments will now be presented.

**22.4.4. Examples of traverse experiments.** Test results have been extracted from a number of publications for the purpose of illustrating the manner in which design assumptions are approximated in practice.

(i) *Axial velocity distributions.* Because of the care usually taken in obtaining good inlet conditions, the excellent upstream velocity distribution illustrated in Fig. 22.16 is representative of most fan tests. The thickness of the boundary layer on the duct wall will vary with the length of inlet ducting; on the other hand, the relatively short nose fairing will always ensure a thin layer on the boss.

Distribution of the axial velocity components downstream of three types of rotor are presented in Figs. 22.16 and 22.17. A thickening of the wall boundary layers is apparent but, in general, the measured values follow the trends assumed in the design theory.

(ii) *Total head distributions.* From the upstream and downstream distributions, the rise in total head is determined at each radius and then converted into a non-dimensional coefficient,  $k$ . This procedure also applies when circumferential differences in total head occur, e.g. downstream of stators.

Non-dimensional distributions for a free vortex rotor fitted with cambered plate blades<sup>(70)</sup> have already been introduced in Fig. 22.14. The design assumption of constant total head rise is closely approached in practice. Except for  $\bar{A}=0.171$ , where blade stalling is well advanced, off-design distributions are also reasonably flat. During the tests on sheet metal bladed fans,<sup>(70)</sup> the tendency for  $k$  to increase rapidly near the tip (Fig. 22.14) appeared to be a function of local stalling. Most of this increase, however, is associated with large swirl

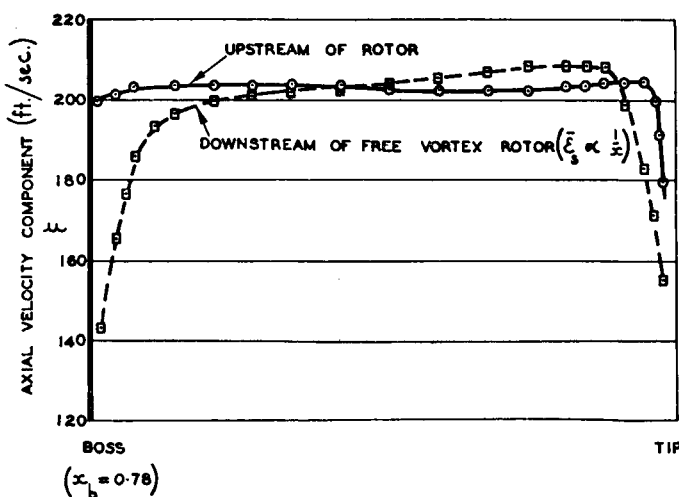


Fig. 22.16. Axial velocity distributions for free vortex rotor

velocity heads, very little of which can be recovered as static pressure. The onset and development of the stall will vary from fan to fan and hence the curve for  $\bar{A}=0.171$  will not be representative of all fans.

Results for the solid rotation rotor introduced in Fig. 22.17 are presented in Fig. 22.18. Once again the agreement with theory is excellent in the design case. The radial position at which  $k$  is equal to  $K$  is close to the midspan point.

One of the available examples of the total head distribution downstream of straighteners<sup>(86)</sup> is illustrated in Fig. 22.19. The contours shown have been constructed from the results of

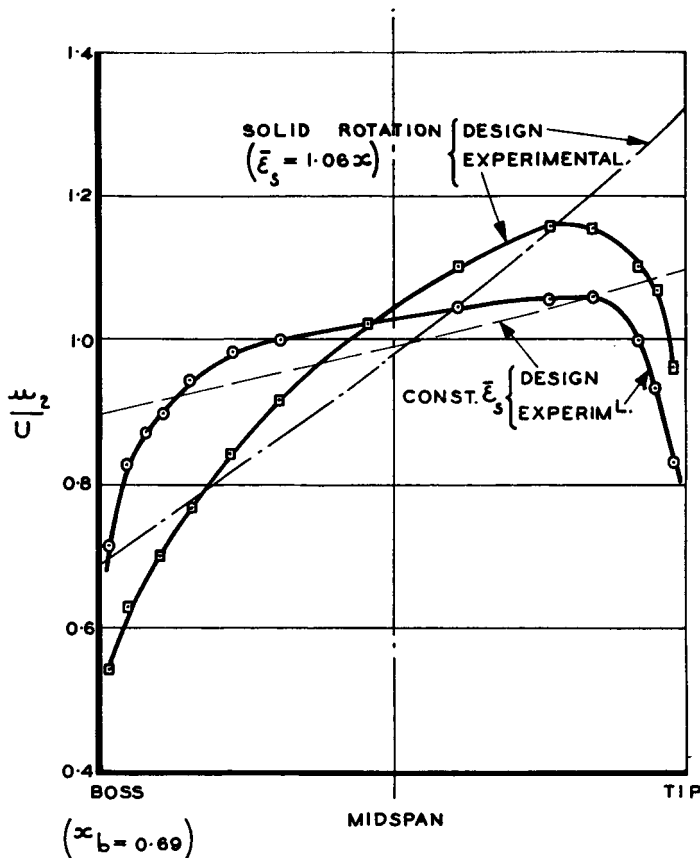


Fig. 22.17. Axial velocity distributions downstream of arbitrary vortex flow rotors

a number of radial traverses. The blade wakes are readily identified with the regions of lowest total head.

(iii) *Swirl velocity distributions.* The induced, or swirl, velocity can be expressed by  $\omega_{sr}/u$  where this ratio is the tangent of the effective yaw angle measured by the yawmeter. The effective yaw is usually taken to be the difference between any slight yaw upstream of the rotor and the angle of yaw downstream. Typical results are illustrated in Fig. 22.20 for two free vortex rotors with different types of blading. Although the above ratio increases rapidly as the boss and duct wall are

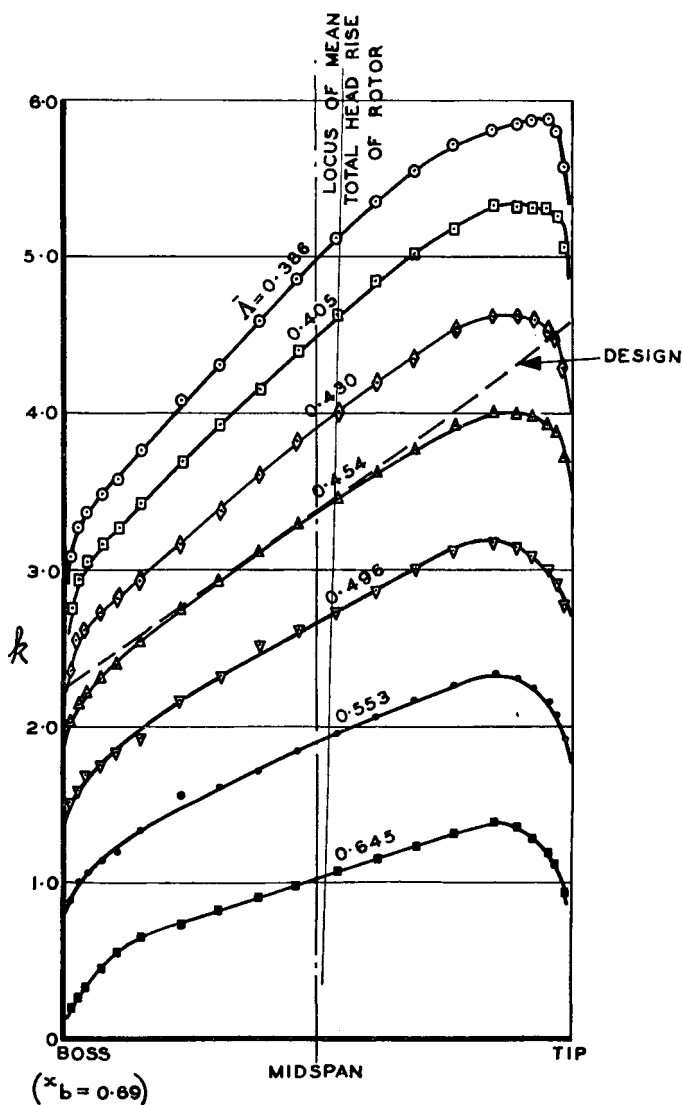


Fig. 22.18. Distributions of total head rise for arbitrary vortex rotor

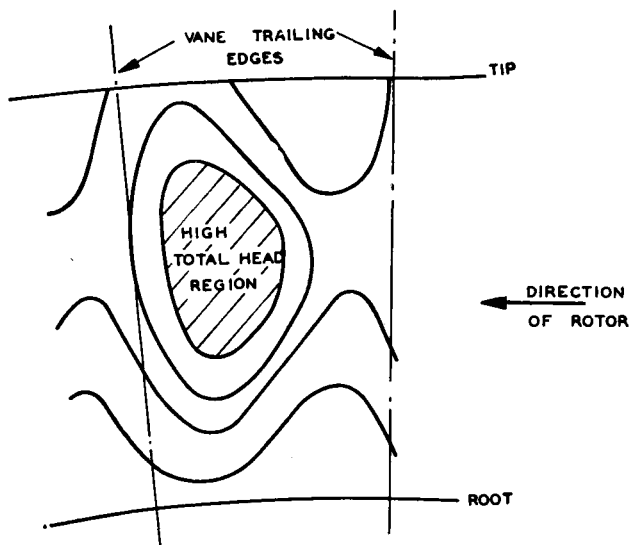


Fig. 22.19. Total head contours downstream of straighteners

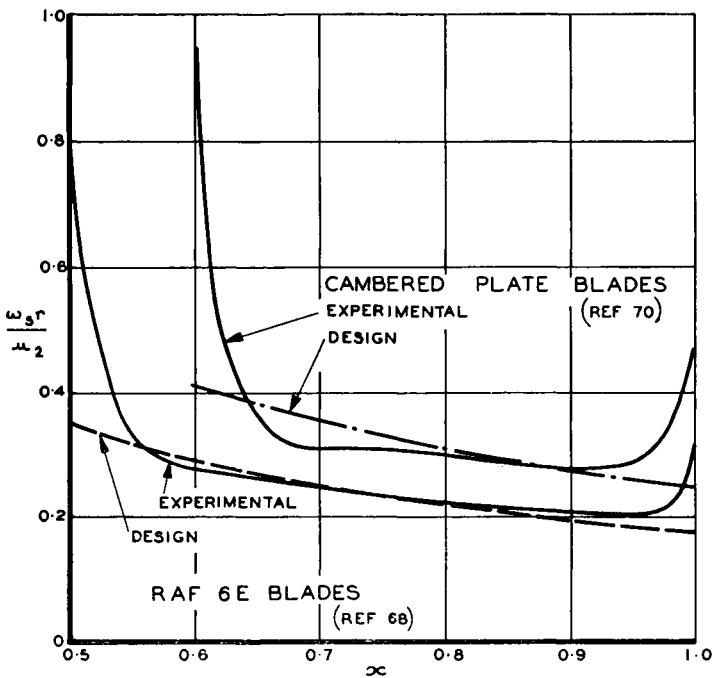


Fig. 22.20. Swirl distributions for two free vortex rotors

approached, the actual swirl velocity,  $\omega_s r$ , need not necessarily increase since  $u$  is being rapidly reduced in the boundary layers. No measurements were made of the downstream axial components in these tests and hence  $\bar{\epsilon}_s$  cannot be computed. Outside the boundary layers, however, the agreement with design theory is reasonably good.

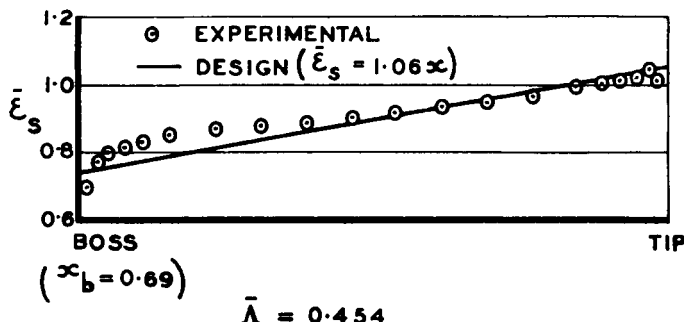


Fig. 22.21. Swirl distribution for arbitrary vortex rotor

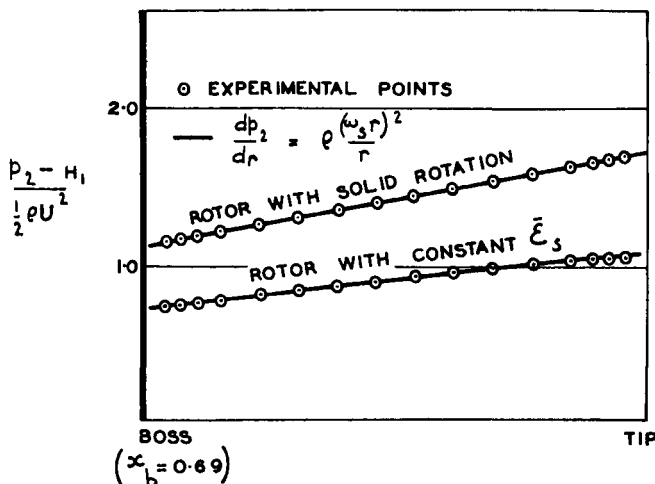


Fig. 22.22. Radial variation of static pressure for two arbitrary vortex rotors

The test data for the rotor with solid rotation permitted the computation of  $\bar{\epsilon}_s$ ; the resulting distribution is demonstrated in Fig. 22.21 and shows satisfactory agreement with theory.

Since this swirl coefficient is based on the mean axial velocity, it follows immediately, from Fig. 22.21, that the swirl velocities near the blade extremities possess no abnormal characteristics.

In determining the theoretical distributions of velocity and total head for the arbitrary vortex rotor designs, it was assumed that equilibrium between the centrifugal and pressure forces acting on a fluid particle is established fairly quickly downstream of a blade stage. In order to check this assumption, Kahane<sup>(72)</sup> has presented the experimental radial pressure gradients for two arbitrary vortex flow cases (Fig. 22.22). Since these, as well as the actual swirl velocity distributions, show excellent agreement with theory, the equilibrium assumption appears to be well founded.

**22.4.5. Determination of mean values.** The relations to be used when computing the mean values of axial velocity and total head will now be indicated. In addition, a method of determining rotor torque from the swirl distribution will be presented.

(i) *Mean velocity.* The mean axial velocity in the annulus follows from eq. (16.8), i.e.

$$U = \frac{2}{1-x_b^2} \int_{x_b}^1 ux \, dx \quad (16.8)$$

This value can then be employed in determining the fan capacity

$$\text{cu. ft/min} = 60U\pi R^2(1-x_b^2) \quad (22.9)$$

(ii) *Mean total head.* When  $\Delta h$  is the total head rise across a rotor at radius,  $r$ , and

$$k = \Delta h/\frac{1}{2}\rho U^2$$

then from a relation similar to eq. (19.14)

$$K = \frac{2}{1-x_b^2} \int_{x_b}^1 kx \, dx \quad (22.10)$$

Double integration must be carried out downstream of stators. The appropriate equation is

$$K = \frac{N}{\pi(1-x_b^2)} \int_{x_b}^1 \int_0^{2\pi/N} kx \, d\theta \, dx \quad (22.11)$$

where  $N$  is number of stator blades. The above relation assumes the flow characteristics between each pair of stator blades to be identical.

When a moderate number of traverses is carried out, with uniform increments in  $\theta$ , eq. (22.10) may be used for each traverse; the results can then be added and divided by the number of traverses made. As an alternative, a plot such as Fig. 22.19 can be divided into a large number of elementary areas to each of which a value of  $k$  can be ascribed. The mean value is then

$$K = \frac{\sum k dA}{\sum dA} \quad (22.12)$$

or, when the elementary areas are of equal size,

$$K = \frac{\sum k}{m}$$

where  $m$  is the number of such areas.

(iii) *Torque*. Although a direct measure of torque is usually obtained from a dynamometer, an estimate can also be obtained from swirl distributions. Reverting to eq. (8.9) and substituting  $(u_1 + u_2)/2$  for  $u$ , it can be shown, for the general case, that

$$Q_c = \int_{x_b}^1 \frac{2(u_1 + u_2)(\omega_s r + \omega_p r)x^2 dx}{U^2} \quad (22.13)$$

The torque,  $Q$ , then follows from eq. (8.25), i.e.

$$Q = Q_c \frac{1}{2} \rho U^2 \pi R^3$$

Some comparisons between the torque coefficients calculated from swirl distributions and those deduced from dynamometer readings are available. By integration of an expression similar to eq. (22.13), Fail<sup>(86)</sup> found that the power coefficients obtained by the two methods agreed to within 1 per cent. Other examples include three free vortex rotors for which eq. (15.1) was used in the reduction of data; it was assumed that the tangents of the yaw angles measured were equal to the swirl coefficients given in this expression and that  $u_1 = u_2 = U$ . Despite these rather bold assumptions, which were made necessary by the lack of velocity distribution data downstream

of the rotors, satisfactory agreement between the two methods of obtaining  $Q_c$  was achieved (see Figs. 22.23 to 22.25).

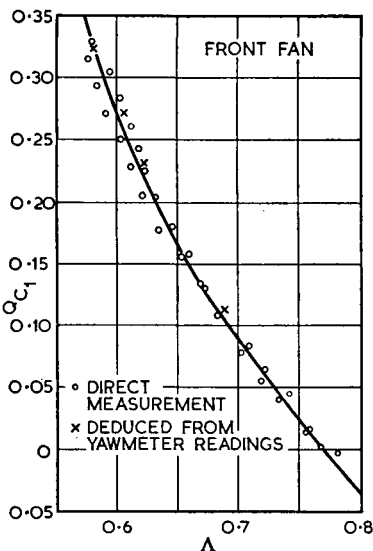


Fig. 22.23. Comparison of torque measuring methods (Reference 68)

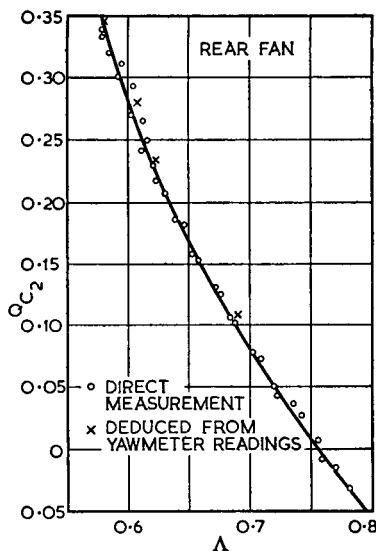


Fig. 22.24. Comparison of torque measuring methods (Reference 68)

(iv) *Efficiency.* The rotor efficiency is given by a rearrangement of eq. (15.9):

$$\eta_R = \frac{K_{\frac{1}{2}} \rho U^2 \times \text{cu. ft/min}}{33,000 \times \text{h.p.}} \quad (22.14)$$

and total efficiency by the relation

$$\eta_T = \frac{K_{T\frac{1}{2}} \rho U^2 \times \text{cu. ft/min}}{33,000 \times \text{h.p.}} \quad (22.15)$$

Alternative expressions which can be used for free vortex flow are

$$\eta_R = \frac{K}{K_{th}} = \frac{KA(1 - x_b^2)}{Q_c} \quad (22.16)$$

and

$$\eta_T = \frac{K_T}{K_{th}} = \frac{K_T A(1 - x_b^2)}{Q_c} \quad (22.17)$$

where substitution for  $K_{th}$  has been made from eq. (15.2).

(v) *Characteristic and efficiency curves.* The mean values obtained by the foregoing methods are normally plotted in the manner illustrated in Fig. 22.25. Similar curves of experimental

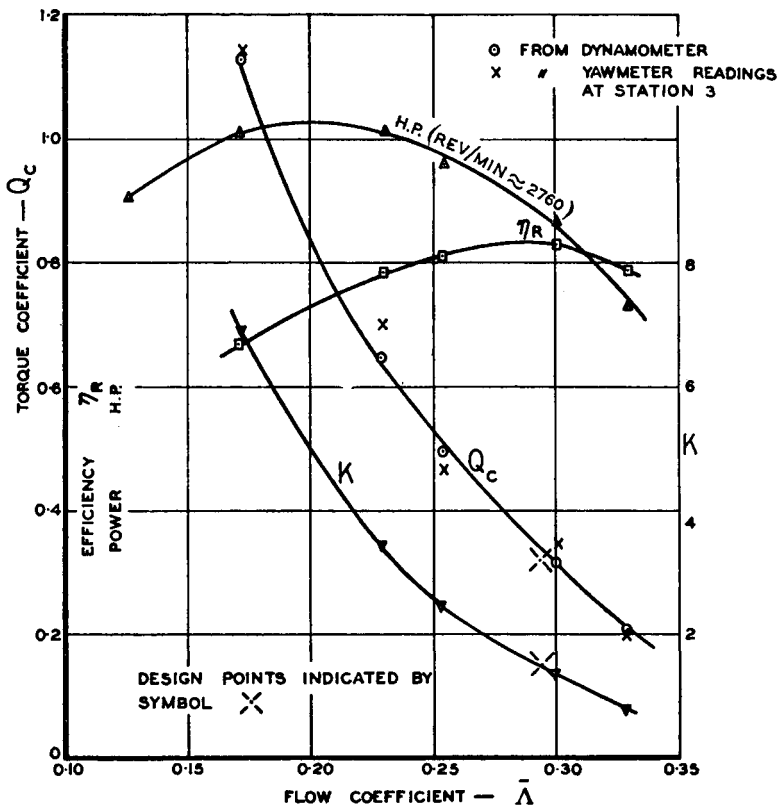


Fig. 22.25. Performance data for cambered plate fan

data for the contra-rotating rotors have already been presented in Figs. 21.7 and 21.8.

The above examples are representative of the close agreement which is, with very few exceptions, achieved between theory and experiment. Increasing tip clearance will, however, result in (a) a decreased efficiency (see Section 10.7), and (b) a reduction in the pressure rise. The data of References 71 and 72 suggest that the pressure drop will be from 2.5 per cent to 5 per cent for

each 1 per cent increase in the tip clearance/blade length ratio.

Earlier in this sub-section, the blade stall of the cambered plate fan was assumed to be well advanced at a flow coefficient of 0.171. This is supported by the horsepower curve presented in Fig. 22.25; in the absence of separation, the power continues to increase with decreasing values of  $\bar{A}$ .

Axial flow units are often known as "limit load" fans for reasons which are clearly illustrated in Fig. 22.25. Since the power varies approximately as the cube of the speed, the "limit load" of a fan unit can usually be expressed by the relation

$$\text{Limit h.p.} \propto (\text{rev/min})^3 \quad (22.18)$$

where the factor of proportionality has to be determined experimentally for the particular fan.

Although the experimental data just presented are confined to rotor properties, it is of course obvious that a similar treatment can be undertaken for the fan unit when the relevant quantities have been determined in the manner indicated previously.

**22.4.6. Measurements on rotating blades.** As stated previously, boundary layer separation and hence blade stalling are the result of relatively large adverse pressure gradients. For this reason, in an attempt to improve the high pressure rise performance of rotors, measurements have been made of the actual pressure gradients present. In this manner the effect of adjacent blades on the chordwise pressure distributions can be obtained for the purpose of improving theoretical calculation methods. With a reliable theory, blade sections for a given rotor can be designed to have pressure distributions which will give a high lift prior to the appearance of critical adverse gradients.

This type of testing really belongs to the subject of axial flow compressors but a brief introduction is relevant. In addition to pressure distributions, boundary layer measurements can be obtained for the purpose of investigating (a) the approach of flow separation, and (b) the centrifugal force effects on the air particles adjacent to the blade surfaces.

Various devices have been employed for the transmission of

the data from the rotating blades. One method<sup>(88)</sup> used is illustrated in Fig. 22.26 where a mercury seal is schematically presented. Another worker<sup>(89)</sup> measured the pressure on a pressure gauge attached to the rotor on the axis of rotation;

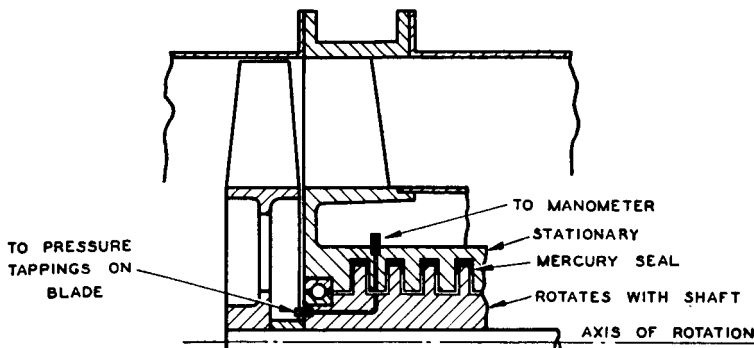


Fig. 22.26. Mercury seal device for multiple pressure leads

the gauge reading was observed by a stroboscopic method. Weske<sup>(90)</sup> employed a relatively complicated mechanical type of rotating seal.

The measured pressures must be corrected for the pressure gradients built up, by centrifugal means, in the rotating pressure leads.

# 23

---

## REVIEW OF DESIGN ASSUMPTIONS

The experimental evidence presented in Sections 21 and 22 has supported many of the assumptions made during the development of the theory. In all the tests referred to, however, inlet velocity distribution was probably more uniform than would normally be the case in an actual duct system. This and other matters of interest will now be discussed briefly.

### 23.1. Effect of Non-uniform Inlet Velocity

The following remarks will be confined to inlet flows which are steady and reasonably axisymmetric. When the stream just upstream of the nose fairing is of the fully developed pipe flow type, the velocity distribution between the axis and the duct wall will be given by the  $H = 1.3$  curve of Fig. 3.5. Due however, to the contraction effect of the nose fairing, the radial gradient of axial velocity immediately upstream of the rotor blades will be less than that illustrated in Fig. 3.5.

In an axial flow compressor, the axial velocity distribution in the annulus deteriorates to a parabolic form after the first two or three stages. Some interesting data relating to this severe condition are available. Comparative tests<sup>(91)</sup> were made on compressors designed for (a) constant axial velocity, (b) the actual axial velocity distribution, and (c) increased total head

rise towards the two blade extremities. The highest efficiency was obtained with the first mentioned design. In the second design, the downstream velocity distribution showed a deterioration, while some improvement in this regard was achieved with the third type of blading. The efficiency loss in this last case was traced to stator stalling brought about by the large swirl angles encountered at the stator extremities. Hence from a practical point of view the constant axial velocity design assumption appears to be as good as any other.

A theoretical analysis will now be made of the effect which a radial variation of inlet velocity is likely to have on a rotor designed for constant axial velocity.

In the absence of preswirl, it follows from Section 19.2 that

$$\frac{d(\omega_s r)}{du} = -2 \tan \psi \quad (23.1)$$

and hence for a given blade element the rate at which the swirl velocity varies with the axial component is constant and negative. Therefore, when the actual velocity is less than the mean value designed for, the swirl component is increased and vice versa. Combining eq. (23.1) with eq. (8.11)

$$\Delta h_{th} = \Delta H_{th} - 2\rho\Omega r \tan \psi du \quad (23.2)$$

so that in regions where  $u$  is less than the mean, the total head rise is greater than the mean and vice versa.

On the assumption of constant static pressure upstream of the rotor, the total head of a elementary annulus will vary from the mean value by an amount

$$\frac{1}{2}\rho(U + du)^2 - \frac{1}{2}\rho U^2$$

When  $du$  is small, this expression reduces to approximately

$$\rho U du$$

It can be shown that this amount is definitely of the same order as the second term in eq. (23.2), being equal to it when  $\bar{\lambda} = 2 \tan \psi$ . Hence it might be expected that the total head, as measured downstream of the rotor, will be relatively constant in the radial direction. In other words, a rotor is a device which automatically tends to compensate for small deviations from the mean velocity assumed in design. Physically, this is due to

an increase in blade incidence and hence lift coefficient when the axial velocity at a given station is less than the mean.

The results of Reference 92 are of interest in this connection. Spoilers were used to produce a considerable thickening of the boundary layer on both the nose fairing and the duct wall. The subsequent losses in pressure rise and efficiency were not very great. In these tests, as in those of Reference 55, the rotor tended to re-energize the boundary layer. Mager,<sup>(55)</sup> however, considers very little of this increased total head rise near the extremities to be useful, as tip and secondary losses tend to absorb it.

From the evidence presented, it appears that the characteristic of a fan is not altered to any noticeable degree by the presence of a fully developed pipe flow upstream of the fan unit. There are, naturally, some accompanying drawbacks. A fan operating in such a flow will be slightly less efficient, and will be more susceptible to tip stalling when the pressure rise through the fan unit is increased. The presence near the root, however, of an axial component greater than the mean will tend to make conditions less critical in this danger region.

In the extreme case of the axial flow compressor, the effect of the velocity distribution is taken into account during design by means of the "work done" factor which can be expressed by

$$\Delta p_{th} = \frac{\Delta p}{\eta_s \times \text{"work done" factor}}$$

where  $\eta_s$  is the stage efficiency and  $\Delta p$  is the pressure rise required.<sup>(66)</sup> This is equivalent to acknowledging that the assumption of constant axial velocity will over-estimate the amount of work which the compressor is capable of doing. The factor normally used is 0.85.

From the foregoing data it follows that the "work done" factor of fans is approximately unity. When inlet conditions do not meet the requirements laid down at the commencement of this sub-section, a "work done" factor will in all probability have to be applied.

## 23.2. Arbitrary Vortex Flow

The assumption likely to cause the most concern in arbitrary

vortex design is that which involves taking the mean of the inlet and outlet velocities for the purpose of estimating flow deflection through the blading. The deviation laws of eqs. (9.17) and (11.13) do not give the correct outlet angles for blades designed by the recommendations of Section 16. This feature can be explained in terms of the changes in chordwise pressure distributions which occur when arbitrary vortex flow is substituted for the more common free vortex flow. For example, an increase in the axial component in passing through a prerotator vane will reduce the static pressure rise on the convex surface of the blade and hence reduce the angle of deviation with respect to the trailing edge. The problem can also be considered from the viewpoint of the interrelation between lift and flow deflection as outlined in Section 4.6. It can be proved satisfactorily that the assumptions adopted in Section 16 give a reasonably accurate estimate of the lift coefficient, and hence the flow deflection must also be within acceptable limits. Since the use of mean values has proved so successful for free vortex designs, serious difficulties are unlikely to arise in the present application of this principle.

### 23.3. Assumptions Involving Neglect of Second Order Terms

The close agreement between theory and experiment, as illustrated in Sections 21 and 22, justifies the practice of discarding second order terms. Probably the most important of the expressions treated in this manner is eq. (8.21). The approximation used in obtaining eq. (8.27) results in an overestimate of the required  $C_L$  by an amount,  $C_D \cot \varphi_r$ ; the appropriate correction to the design figure obtained from eq. (8.27) would therefore be a small reduction in blade incidence. In other words, the design method recommended tends to give the desired pressure rise at a slightly higher value of the flow coefficient. Characteristic curves tend, however, to be relatively steep and hence any errors which may arise owing to the use of eq. (8.27), or to an inaccuracy of two or three per cent in estimated efficiency, will not for a given  $K_{T_v}$  result in any serious deviation from the design flow coefficient.

# **APPENDIX**

## **FREE FANS**

### **A.1. General**

The function of a free fan is to circulate air in a common air space. This may serve the purpose of achieving uniform mixing and hence steady temperature conditions within the air space. The current of air provided by a free fan is often adequate for the purposes of cooling men or equipment working at high room temperatures. In cases of excessive heat, however, the short ducted fan, whose efflux is aimed at the subject, is the most effective means of air cooling.

Generally speaking, therefore, the free fan is restricted to one or two specific duties and in consequence design procedures can be simplified. In addition, the aerodynamic specifications to which the fan is designed are relatively flexible. These circumstances are indeed fortunate as the flow field in the vicinity of the fan blades is a complex one for which no precise analysis is available. Smith<sup>(94)</sup> has, however, managed to develop a design method which is simple and relatively accurate. Useful information on the general characteristics of free fans is also available in this reference.

Although in what follows no attempt will be made to cover the subject of free fans in a comprehensive manner, data sufficient for the purpose of making an informed approach to design problems will be presented. In particular, the design method for near optimum performance, as developed in Reference 94, will be outlined.

### **A.2. General Flow Features**

The fan discharges a jet of air which possesses an unrestrained or free boundary. Owing to turbulent shear the surrounding air in contact with this boundary is accelerated as a result of

momentum transfer from the jet stream. This process of entrainment continues as the air stream moves further away from the fan. Representative data for such a phenomenon are expressed graphically in Figs. A.1 and A.2. The nominal jet boundaries presented are, of course, in regions of large velocity fluctuations; the lines drawn represent a mean condition.

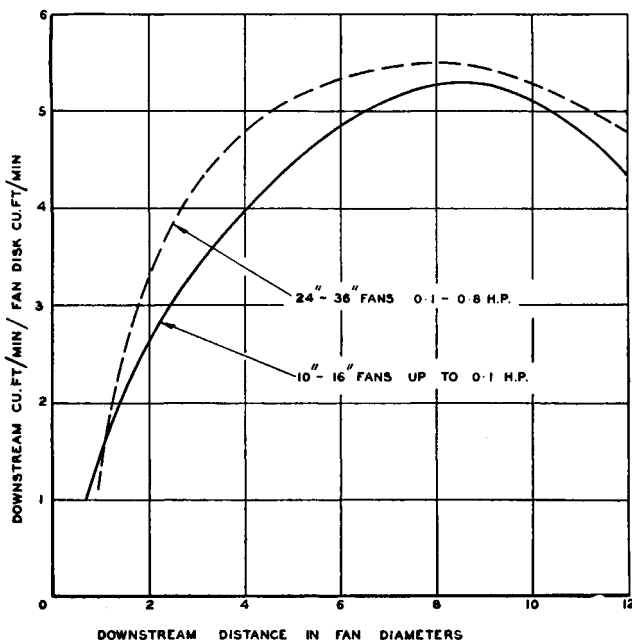


Fig. A.1. Rate of air entrainment into jet downstream of rotor

From Fig. A.1 it will be seen that downstream of 9 diameters, where entrainment ceases, there is a net loss of air through the jet boundaries of Fig. A.2.

When the fan operates in a well defined air space, for example in a room, the air will continue to recirculate through the rotor with a frequency determined to some extent by the size of the room. The recirculation flow pattern can be broadly divided into two parts: (a) the general flow in the room, and (b) the local flow at the blade tips. In the first case, the recirculation pattern is greatly influenced by the size and shape of the room,

the positioning of furniture within the room, and the location and orientation of the fan. In general, the bulk of the air movement in the room occurs on the downstream side of the fan. This implies that the fan is fed principally by air which has returned to the inlet side of the fan by the medium of a converging stream of reverse flow just outside the diverging jet.<sup>(94)</sup> The buffer region between these two flows is one of relatively large-scale random turbulence except in the close

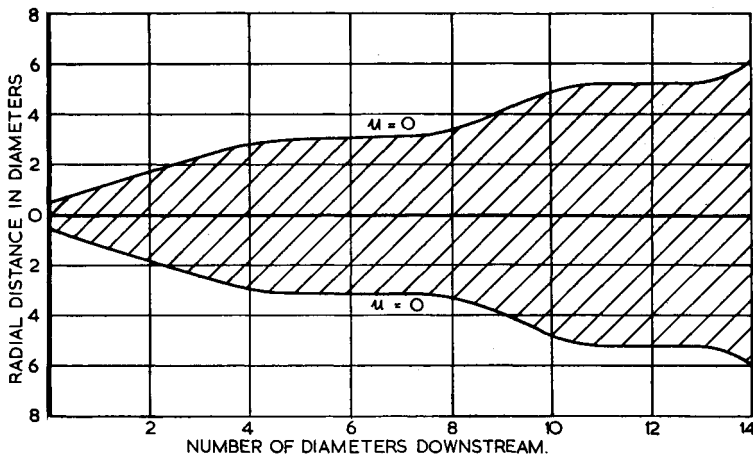


Fig. A.2. Typical jet boundaries

vicinity of the fan where the flow reversal region is very narrow and well defined. The air entrained by the jet, through the action of fluid shear forces, is obtained from this buffer region. When the jet is powerful enough to reach an opposing surface such as a wall, the stream is deflected and this feature results in a relatively wide stream of reverse flow.

The local flow in the vicinity of the blade tips is of considerable interest. According to Smith<sup>(94)</sup> there are two possible flow régimes in this region. The one which he refers to as the "normal state" possesses no appreciable local recirculation of the air through the blade tips. In the second régime, known as the "vortex ring state", a stationary vortex ring of recirculating air is present; this phenomenon is often associated with local blade stalling.

To return to the problem of the general flow field created by the fan, it is possible, by design changes in blade loading, to vary the overall properties of the jet. This fact is illustrated in Fig. A.3 where, for the same power, three different designs have produced markedly different flow patterns. The air jet

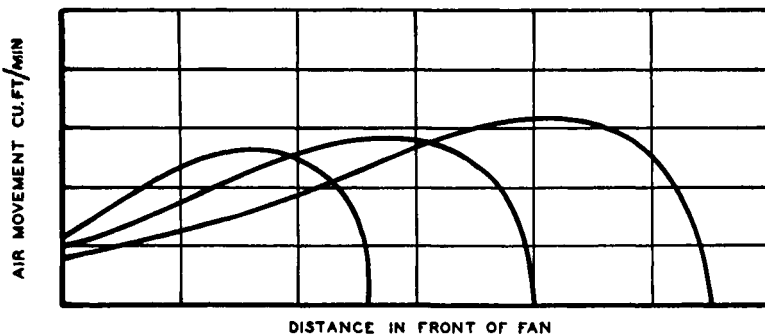


Fig. A.3. Air movements of three different designs (disk diameter and horse power constant)

possessing the greatest penetration properties has a lesser rate of initial entrainment. Variations of this nature are inevitably associated with changes in the reverse flow and vortex conditions just downstream of the rotor blade tips.

### A.3. Test Requirements

In the past, the test codes, B.S. 380:1930 and the American N.E.M.A. Standard, have called for a single velocity traverse at some specified distance downstream of the fan. On integration, the capacity of the fan has been established at this station and this value divided by the power input has been used to specify the service factor of the fan. It is clear from Fig. A.3, however, that this test procedure can produce misleading data. Smith and Chambers<sup>(95)</sup> have therefore suggested the presentation of test data as in Fig. A.4. The combined use of data such as that contained in these latter two figures provides a more satisfactory specification of the fan duty.

In the testing of such fans, the test room must be long enough to ensure that the end wall has no measurable influence

on the jet penetration. Useful comments on test instrumentation and conditions are given in References 94 and 95.

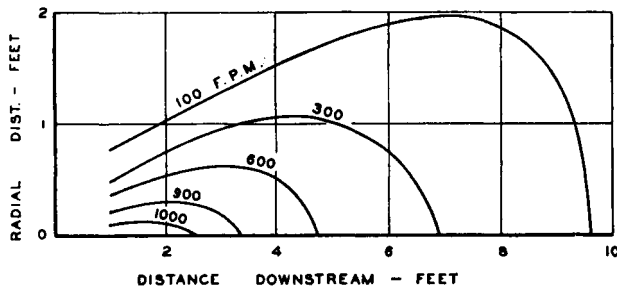


Fig. A.4. Typical velocity contours in a jet

## A.4. Design

As stated previously, the design section will be limited to one specific set of conditions. Before the method is described, the group of assumptions on which design is based will be outlined.

**A.4.1. Design assumptions.** The major design assumption concerns the spanwise distribution of axial velocity for which the fan will be designed. For the general purpose fan, it has been found from design experience and test observations,

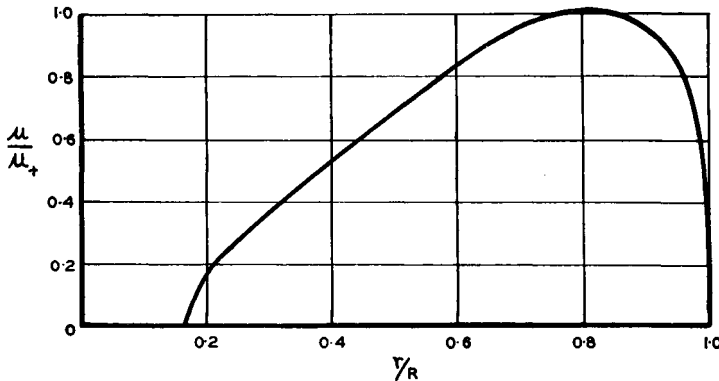


Fig. A.5. Suggested design axial velocity distribution

including visual flow ones, that a velocity distribution such as that presented in Fig. A.5 gives good results. It is believed that the chances of ring vortex formation at the blade periphery

are minimized by designing for a prescribed drop in velocity as the tip extremity is approached, as illustrated in Fig. A.5. The steady decrease in velocity from  $x = 0.8$  inboard is dictated to some extent by aerodynamic design difficulties,<sup>(94)</sup> and by practical difficulties associated with blade shape and attachment. For example, if high velocity were designed for in the inner region, the blade chord and setting angle would both be excessively high. In addition, the curved inflow pattern of the air is such that a smaller axial velocity towards the blade root is, on fundamental grounds, almost inevitable. On the basis of the foregoing evidence, the distribution of Fig. A.5 has here been adopted for design.

In developing the design method, Smith was forced to make many assumptions and approximations. The flow at any given radius is assumed to be truly axial and independent of the adjacent flow. To each elementary annulus of width  $dr$ , the Rankine-Froude "actuator disk" theory has been applied in the process of determining the momentum added to the air; the momentum associated with the velocity head due to swirl is assumed to be negligible in computing the thrust on a blade element. Despite these rather sweeping assumptions very good agreement has been obtained between the design and test values in all cases where the method has been applied.

**A.4.2. Design requirement.** Design specifications may take two forms. Either (a) the design of a fan to make the best use of the power available from a specific electric motor may be called for, or, (b) an air flow condition may be specified for which a fan suitably matched to a motor is required.

From the details to be given, either design can readily be carried out. Since the first specification is the one most commonly encountered, the design method will, in the first instance, be developed for this case.

**A.4.3. Design procedure.** For case (a) above, the torque equation is the key to the design. From Reference 94 this can be written,

$$Q = 4\pi\rho\Omega R^4 u_+ \int_0^1 \frac{u}{u_+} a' x^3 dx \quad (A.1)$$

where  $u_+$  is the peak axial velocity at  $x = 0.8$  and  $a'$  is equal to  $\omega r / 2\Omega r$ .

The notation used in the appendix is consistent with that employed for ducted fans in the main text.

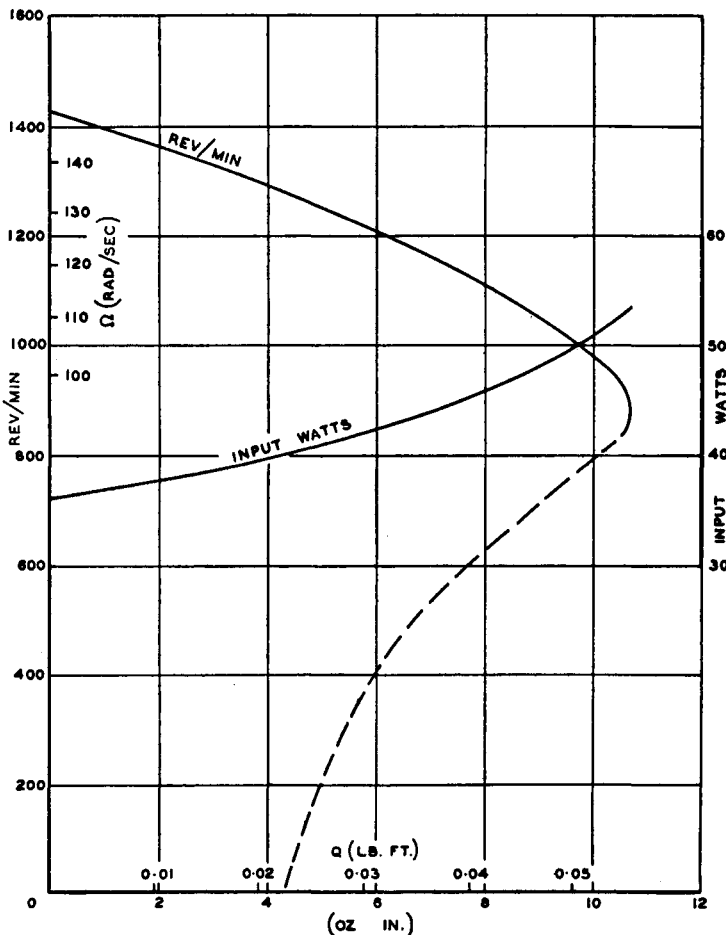


Fig. A.6. Characteristics of a shaded-pole motor

The design values of  $Q$  and  $\Omega$  will be known from motor characteristics similar to those illustrated in Fig. A.6. The three remaining unknowns are  $R$ ,  $u_+$  and the distribution of  $a'$  with respect to  $x$ . Smith's general design method is based on

the relationships graphically presented in Fig. A.7. It will be seen that  $\alpha'$ ,  $C_L\sigma$  and  $\phi$  are all unique functions of  $u/\Omega r$  for a given lift/drag ratio; the design, however, is not very sensitive to changes in this ratio. Since in the present instance  $u/u_+$  is a unique function of  $x$  (see Fig. A.5) it can be shown that the

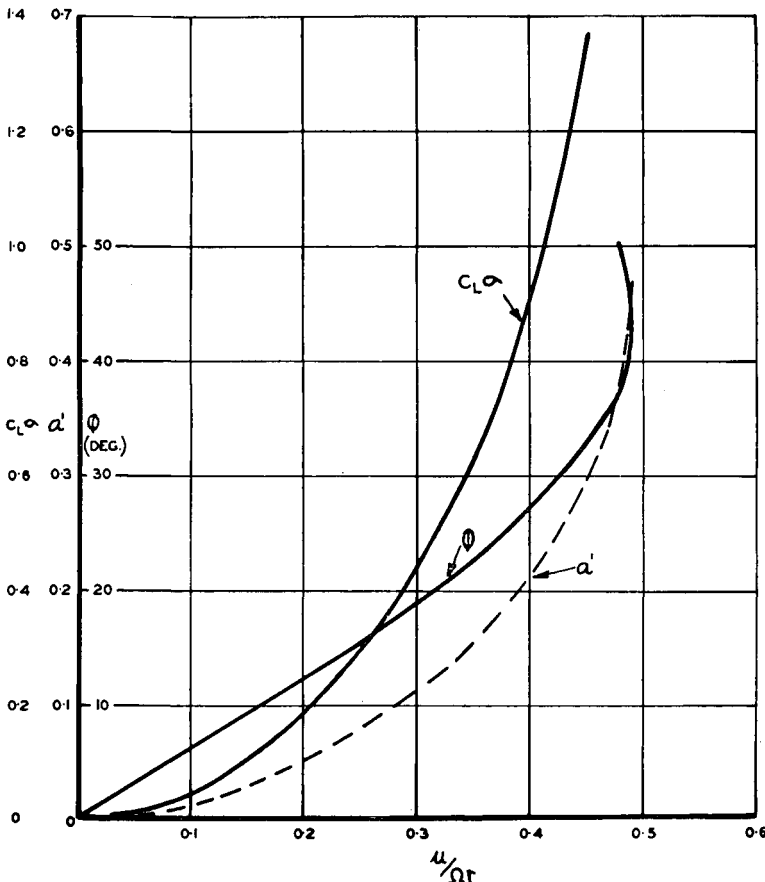


Fig. A.7. Design data for general application,  $C_L/C_{DP} = 50$

above variables are also functions of  $u_+/\Omega R$  and  $x$ . This being so, eq. (A.1) can be rewritten for our particular case as

$$Q = 4\pi\rho\Omega R^4 u_+ f(u_+/\Omega R) \quad (A.2)$$

The function in this equation can be presented as in Fig. A.8.

It will be noted that one variable, namely  $a'$ , has been eliminated and individual integration avoided. It only remains to assume either  $R$  or  $u_+$  and to solve the equation for the given values of  $Q$  and  $\Omega$ .

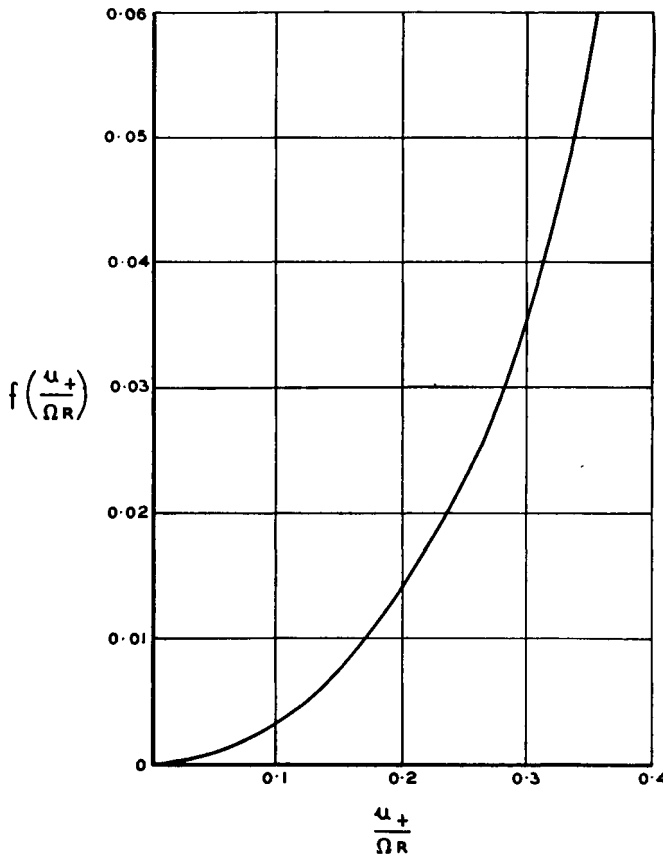


Fig. A.8. Design graph (see eq. A.2)

The volume flow at the fan can now be established from the general equation

$$\text{Vol. flow} = 2\pi R^2 u_+ \int_0^1 \frac{u}{u_+} x \, dx \quad (\text{A.3})$$

which for the above specified velocity distribution reduces to

$$\begin{aligned} \text{Vol. flow} &= C_1 R^2 u_+ \\ &= 2.48 R^2 u_+ \end{aligned} \quad (\text{A.4})$$

The thrust exerted by the fan is given in Reference 94 by

$$T = 4\pi\rho R^2 u_+^2 \int_0^1 \left(\frac{u}{u_+}\right)^2 x \, dx \quad (\text{A.5})$$

or, in our case, by

$$\begin{aligned} T &= C_2 R^2 u_+^2 \\ &= 0.00982 R^2 u_+^2 \end{aligned} \quad (\text{A.6})$$

for standard air conditions (see Section 2.1.3).

The remaining task is the computation of the blade properties at various radii, i.e. values of  $x$ . Using the data previously presented in this sub-section, values of  $\varphi$  and  $C_L\sigma$  are presented as functions of  $(u_+/\Omega R)$  and  $x$  in Figs. A.9 and A.10. Before the design can proceed further a choice of blade section and operating conditions for this aerofoil section must be made.

In very many cases, cambered plate aerofoils are used as blade sections; very good lift/drag ratios can be obtained with this type of blade (see Fig. 4.10). Smith<sup>(94)</sup> has, however, shown that substantial changes in  $C_L/C_{D_p}$  do not have a great influence on the blade design details. The design graphs of Figs. A.8 to A.10 were constructed for  $C_L/C_{D_p} = 50$  and on reference to Fig. 4.10 it will be seen that an 8 per cent cambered plate attains such a value at a  $C_L$  of 1. The angle of incidence corresponding to this lift is  $3^\circ$  (Fig. 4.6). Since  $C_L$  is unity,  $\sigma$  can be read directly off Fig. A.10. The chord,  $c$ , follows from

$$c = \frac{2\pi x R \sigma}{N} \quad (\text{A.7})$$

where  $N$  is the number of blades.

The angle made by the blade chord with respect to the plane of rotation is

$$\varphi + \alpha = \varphi + 3^\circ$$

where  $\varphi$  is obtained from Fig. A.9.

The design is now complete. It will be seen that very little work is involved, particularly when full use is made of a tabulated design sheet and a graphical approach. Data for use in constructing design graphs are presented in the Table Section.

The second type of specification outlined in Section A.4.2 can be met by starting the design at eq. (A.4). If the volume flow

were specified at some given distance from the fan, then Fig. A.1 could be used in conjunction with eq. (A.4) in the choice of values of  $R$  and  $u_+$  to satisfy the requirements.

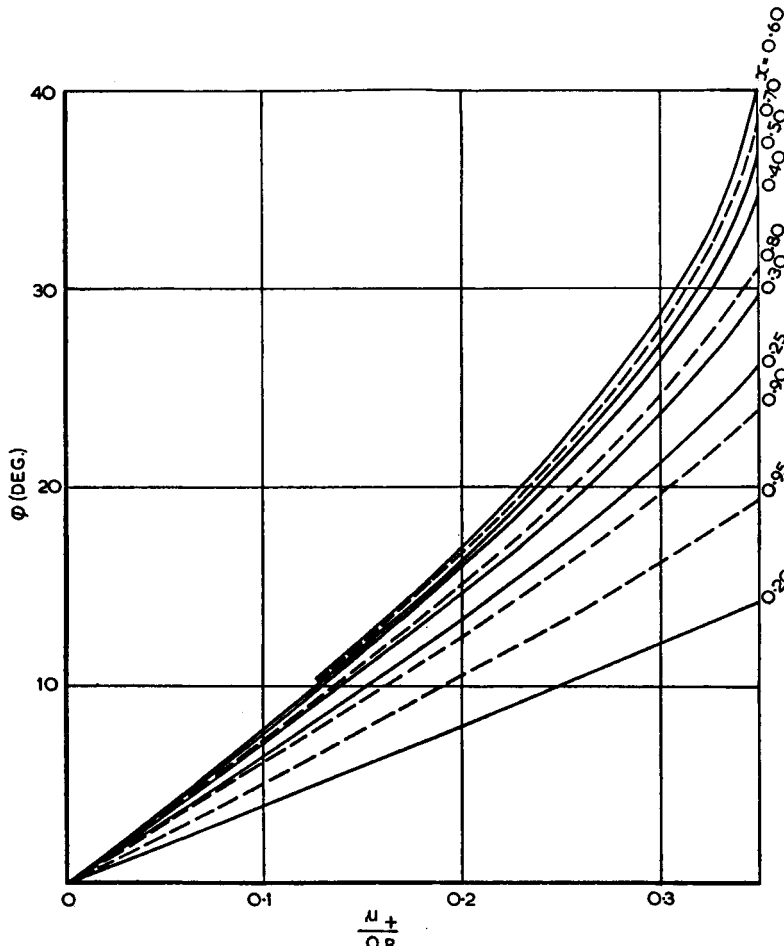


Fig. A.9. Variation of flow angle with  $u_+/\Omega R$  and  $x$  ( $C_L/C_{DP} = 50$ : vel. distribution of Fig. A.5)

The next step requires the matching of the proposed fan to a suitable motor. Eq. (A.2) is now solved by assuming either  $Q$  or  $\Omega$  and computing the other. The resulting relationship

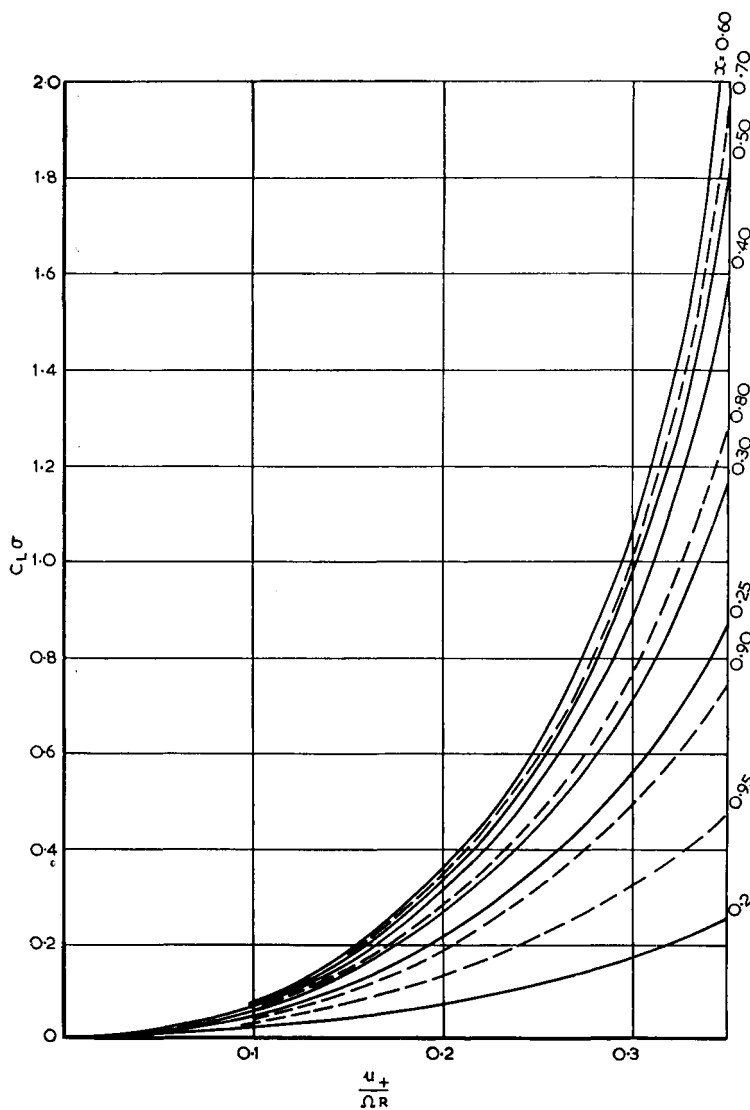


Fig. A.10. Variation of product,  $C_L\sigma$ , with  $u_+/QR$  and  $x$  ( $C_L/C_{DP} = 50$ : vel. distribution of Fig. A.5)

between  $Q$  and  $\Omega$  can be presented as a curve ; when this line is superimposed on the  $Q$  versus  $\Omega$  curves for available shaded pole motors a satisfactory matching of fan to motor may usually be achieved. In some instances it may be desirable to change the values of  $R$  and  $u_+$  in which case a new solution of eq. (A.4) is necessary. Nevertheless, by the above simple trial and error methods, a satisfactory solution of eqs. (A.2) and (A.4) can readily be obtained for chosen values of  $R$ ,  $u_+$ ,  $Q$  and  $\Omega$ .

The design procedure discussed above has been centred around the shaded-pole type of motor which possesses the characteristic of a relatively large variation of speed with torque. For split-phase or three-phase type motors, which are comparatively insensitive to moderate torque changes, the design procedure can be shortened since  $\Omega$  will be known initially.

**A.4.4. Design example.** For a given shaded-pole motor, it is assumed that a suitable operating point is given by

$$Q = 0.065 \text{ lb ft} \quad \text{and} \quad \Omega = 100 \text{ rad/sec}$$

The fan, which is to be 12 in. in diameter, can be computed as follows :

$$M = 4\pi\rho\Omega R^4 = 0.187 \text{ for standard air}$$

$u_+$	12.5	13.0	13.5
$u_+/\Omega R$	0.25	0.26	0.27
$M u_+$	2.338	2.431	2.525
$f(u_+/\Omega R)$ Fig. A.8.	0.0230	0.0252	0.0274
$Q$ eq. (A.2.)	0.0538	0.0613	0.0692

From the above, the design values of  $u_+$  and  $u_+/\Omega R$  are established as 13.25 ft/sec and 0.265 respectively.

$$\begin{aligned} \text{Vol. flow} &= 2.48R^2u_+ \\ &= 8.22 \text{ cusec through rotor} \end{aligned}$$

$$\begin{aligned} \text{Thrust} &= 0.00982R^2u_+^2 \\ &= 0.431 \text{ lb} \end{aligned}$$

The design details for a four bladed rotor utilizing the 8 per cent cambered plate aerofoil are tabulated as follows for various radii.

$x$	0·2	0·25	0·3	0·4	0·5	0·6	0·7	0·8	0·9	0·95
$r = xR$ (in.)	1·2	1·5	1·8	2·4	3·0	3·6	4·2	4·8	5·4	5·7
$\varphi$ Fig. A.9.	10·6	18·2	20·1	22·2	23·0	23·9	23·3	20·8	17·0	14·0
$\sigma(\sigma_{L-1})$ Fig. A.10.	0·134	0·416	0·512	0·623	0·672	0·713	0·694	0·548	0·364	0·247
$c$ (in.) eq. (A.7.)	0·25	0·98	1·45	2·35	3·17	4·03	4·58	4·13	3·09	2·21
$\varphi + \alpha$ ( $\alpha = 3^\circ$ )	13·6	21·2	23·1	25·2	26·0	26·9	26·3	23·8	20·0	17·0

A somewhat similar fan designed and tested by Smith<sup>(94)</sup> demonstrated a close agreement between the theoretical and experimental values of motor speed, torque and thrust. The velocity distribution at the Code test station, namely 2 ft downstream of the rotor, is given in Fig. A.11.

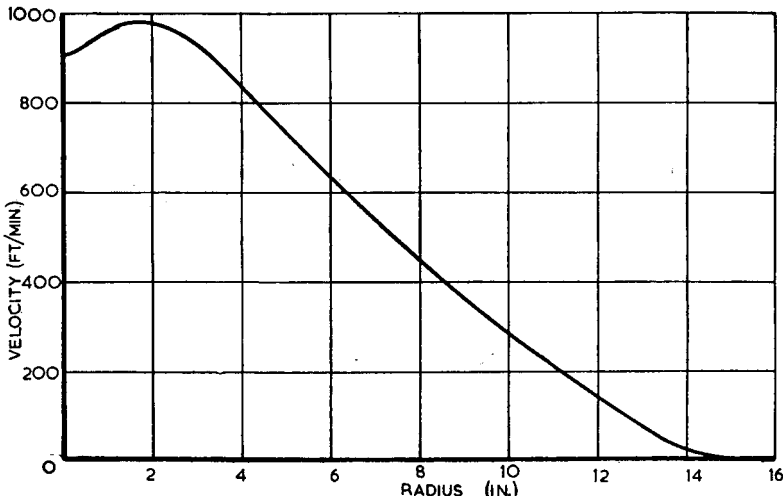


Fig. A.11. Experimental velocity distribution at Code test station for fan design of Reference 94

In setting out the blade planform a measure of "industrial designing" may be employed as suggested in Reference 94. The blade leading edge may be given an arbitrary curvature which then automatically fixes the contour of the trailing edge for the design chord distribution.

### A.5. Fan Analysis

For a given fan of unknown design, a performance estimate by analytical methods is often of great value. Such assessments

may save testing time by showing the fan to be completely inadequate for the task in hand or they may assist in relating experimentally determined downstream circulation patterns with the spanwise blade loading.

Analysis in this instance differs from the ducted fan case in that the free rotor works always under a constant load condition. This eliminates the swirl coefficient as an independent variable. In analysing a free fan the relevant task is the estimation of  $u/\Omega r$  at each spanwise station.

For a given station the values of  $\sigma$  and  $(\varphi + \alpha)$  are ascertained by measurement. When the aerodynamic characteristics of the blade section are unknown, it is essential to choose a roughly equivalent section whose characteristics are known and to replace the original section by this in the computations. From an assumed value of  $C_L$ , a tentative value of  $\alpha$  follows immediately (see Fig. 4.6 for cambered plates). The angle  $\varphi$  then follows by subtraction and this leads to a tentative value of  $u/\Omega r$  from the relationship of Fig. A.7. For this flow coefficient value the corresponding value of  $C_L\sigma$  can be determined (Fig. A.7). A solution of the problem is achieved when this product is equal to that obtained by using the assumed value of  $C_L$  at the commencement of the process.

The distribution of  $u$  with  $x$  is tentatively established when a value of  $\Omega$  is assumed. Eq. (A.1) is now solved for  $Q$  when the remaining variable  $a'$  is extracted from Fig. A.7 for the appropriate flow coefficient. A repetition of the above process permits the construction of a curve of  $Q$  versus  $\Omega$ ; the fan operating point is given by the intersection of this line with the motor curve. With the rotational speed of the rotor thus determined, the velocity distribution follows immediately from the values of  $u/\Omega r$  at each radius. The volume flow through the disk is given by eq. (A.3).

Smith claims that an accuracy of prediction to within 5 per cent can be obtained with the analysis procedure just outlined once experience has been gained.

## A.6. Miscellaneous

In the foregoing no attempt has been made to use or define

an efficiency or figure of merit ; these expressions are of doubtful value in the design of free fans. A better guide to the effectiveness of a particular fan is the dimensions of the downstream area within which the air movement exceeds a specified value (see Fig. A.4) for a given power input.

The influence of the axial flow velocity distribution on jet properties is not well understood and hence a well informed approach to this important design problem is not yet a possibility. Research in this field is obviously desirable.

Lastly, the question of noise is worthy of mention. The principles outlined in Section 17 are equally applicable to the free fan. Vortex noise can be minimized by eliminating regions of disturbed flow and local separation from the blade surfaces. In locating such regions stroboscopic observations of blade surface tufts are invaluable. A simple alternative method of isolating the spanwise blade region from which the noise is emanating involves the use of a stethoscope ; if the detection or sensing piece is placed close to the upstream side of the blades, a radial sweep can be made. Any particular note can now be identified with the region from which it is emanating.

Rotation noise is always troublesome and this can be appreciably reduced by a reduction in speed. Most free fans are, however, directly coupled to a four-pole shaded-pole motor since these motors are very simple and cheap to manufacture. Although a particular fan could readily be redesigned to run on a six-pole motor, the cost of such a motor would make the product hard to sell. In consequence, the greater noise level must be tolerated except in special circumstances where, when a low noise level is essential, the additional cost of a six-pole motor must be accepted as unavoidable.

Careful attention to detailed design and development, however, can usually keep the noise from fans coupled to four-pole motors to an acceptable level.

# NOTATION

## I. Introduction

In Sections 2 to 6 inclusive the generally accepted symbols have been employed. The definitions, which are given in the text, will not be repeated here. Difficulty has, however, arisen in devising a suitable notation to deal with all aspects of fan design, analysis and performance. This is due to the marked lack of uniformity among the various systems in use. For example, while most design methods define flow angles with respect to the plane of rotation, the British compressor theory uses the axial direction as the reference plane. Velocity vectors present the greatest difficulty when a serious attempt is made to develop a comprehensive notation system. The lack of suitable symbols, and the need for elaborate subscript systems to cover all cases are two of the problems encountered. A modified system based on Patterson's well-known fan design work and some British symbols relating to cascade design methods were finally blended into a compromise solution.

The symbols are presented in groups, in order to facilitate understanding of their derivation. Symbols which appear only locally and are in limited use will not be included; these are adequately defined in the text.

## 2. Velocity Vectors

**2.1. Absolute velocities.** The magnitude and direction of the absolute velocity at any given point are not usually required; it is sufficient to know the magnitude of the axial and tangential components.

$u$  Axial velocity component at any radial station in the fan annulus

$U$	Mean axial velocity in annulus swept by rotor blades
$V$	Mean axial velocity upstream of nose fairing
$\omega_p r$	Tangential velocity component just upstream of the rotor as introduced by the prerotor vanes at a station of radius, $r$
$\omega_s r$	Tangential velocity component just downstream of the rotor which has to be removed by the straightener vanes at a station of radius, $r$
suffixes :	
0, 1, 2, 3	These are used in conjunction with $u$ to define the stage reached in the fan unit (see Fig. 8.1 and Section 16)

## 2.2. Relative velocities.

$V_1$	Velocity relative to rotor or stator blade at inlet
$V_2$	Velocity relative to rotor or stator blade at outlet
$\alpha_1$	Angle which $V_1$ makes with axial plane
$\alpha_2$	Angle which $V_2$ makes with axial plane
$w$	Mean velocity relative to rotor or stator blade
$\varphi$	Angle which $w$ makes with plane of rotation
$\Phi$	Value of $\varphi_r$ for no-work condition

suffixes :

$r, p, s$	These are used in conjunction with $w$ and $\varphi$ to denote rotor, prerotor or straightener blade respectively
-----------	---

For rotor blade design, the suffixes for  $V$  and  $\alpha$  agree with the convention just outlined for the axial velocity. It was convenient, however, to retain the same numerals for stator blades and hence 1 and 2 actually define inlet and outlet conditions. In design, no confusion can arise from the above apparent inconsistency.

In British cascade practice,  $V_m$  is used instead of  $w$ , and the angle  $\alpha_m$  instead of its complementary angle,  $\varphi$ .

## 2.3. Rotational speed of fan.

$\Omega$	Angular velocity of rotor
$\Omega_r$	Tangential velocity of a blade element at radius $r$
$\Omega R$	Tangential velocity of blade tip

### 3. Pressures and Pressure Coefficients

#### 3.1. Pressures.

$H$  Total head pressure at a point

$p$  Static pressure at a point

suffixes :

0, 1, 2, 3 These are used in the manner illustrated in Fig. 8.1.

$\Delta$  Signifies a pressure difference

$\Delta h$  Local total head change at any radial station

$\Delta H$  Mean total head change in annulus swept by rotor blades

$\Delta p$  Local static pressure rise at any radial station

suffixes :

The absence of a suffix signifies actual total head or static pressure rise through rotor blading

$th$  Signifies theoretical total head rise through rotor (i.e. 100 per cent efficiency)

$R, P, S, D$  These are used to signify total head losses in the rotor, prerotators, straighteners and tail fairing diffuser respectively

$T$  Relates to the total losses in the duct system, exclusive of those in the fan unit

N.B. Capital letter suffixes always denote total head losses

**3.2. Pressure coefficients.** With two exceptions, which will be mentioned later, all pressure coefficients have been constructed by using the dynamic head,  $\frac{1}{2}\rho U^2$ .

$k$   $\Delta h/\frac{1}{2}\rho U^2$ , total head coefficient at any radial station

$K$  Mean total head coefficient for annulus swept by rotor blades

1st suffixes :

$th$   
 $R, P, S, D$   
 $T$

These have a meaning similar to those used with the pressure differences above

2nd suffixes :

(e.g.  $K_{R\Delta}$ )

$P, S, A$  Signify losses due to profile, secondary and annulus drag respectively

In relating the duct system losses to the total head rise through the fan unit it is convenient to introduce the coefficient:

$K_{T_V}$   $\Delta H_T / \frac{1}{2} \rho V^2$ , where the second suffix denotes that the coefficient is with respect to  $V$ , the mean duct velocity just upstream of the rotor nose fairing

A coefficient derived in Section 16.8 is defined as follows:

$$k_{th}' \quad \Delta h_{th} / \frac{1}{2} \rho \left( \frac{u_1 + u_2}{2} \right)^2$$

#### 4. Lift and Drag Coefficients

No distinction has been made between these coefficients on rotor or stator blades.

$C_L$  Lift coefficient with respect to mean relative velocity,  $w$

$C_L^*$  Optimum lift coefficient as used in cascade design method

$C_D$  Drag coefficient with respect to mean relative velocity,  $w$

$\gamma$   $C_L/C_D$

2nd suffixes:

$P, S, A$  These denote component of drag coefficient due to profile, secondary and annulus losses respectively

#### 5. Flow and Swirl Coefficients

In constructing the flow and swirl coefficients, which are simply velocity ratios, the axial velocity component is the most convenient reference velocity. For *free vortex flows* we have

$\epsilon_s$   $\omega_s r / u$

$\epsilon_p$   $\omega_p r / u$

$\lambda$   $u / \Omega r$

$\Lambda$   $u / \Omega R$

Since  $u$  is equal to  $U$  no difficulty is experienced in establishing the above coefficients.

In designing for *arbitrary vortex flow* the above expressions must be modified. First, in the preliminary design it is more convenient to use  $U$  since the distributions of  $u$  are initially unknown. A bar is then placed over the coefficients to denote that the mean velocity has been used. For example

$$\bar{\epsilon}_s = \frac{\omega_s r}{U}$$

Finally, the design of the individual blade elements requires the use of a velocity which is the mean of the inlet and outlet values at any specific radius, for example,

$$\epsilon_{s_{12}} = \frac{2\omega_s r}{u_1 + u_2}$$

## 6. Efficiencies

The loss in efficiency in each component is expressed as a ratio of the total head loss coefficient to the theoretical total head rise coefficient for the complete unit. The required efficiency is then obtained by subtracting all the relevant ratios from unity. The two efficiencies of greatest interest are,

$\eta_R$	$1 - K_R/K_{th}$
$\eta_T$	Efficiency of complete fan unit (see Section 14)

## 7. Geometric Parameters

### 7.1. General.

$r$	Radius of elementary annulus
$r_b$	Radius of boss
$R$	Radius of duct, i.e. rotor tip approximately
$x$	$r/R$
$x_U$	$(r/R)_{u=U}$
$x_b$	$r_b/R$
$x_m$	$(r/R)_{midspan}$
$c$	Blade chord at any radial station
$s$	Gap between rotor or stator blades at any radial station
$\sigma$	Solidity, $c/s$

To obviate possible errors in the reading of graphs, the rotor data have been presented in terms of  $\sigma$  while  $s/c$  is used in relation to stator design.

### 7.2. Parameters used in cascade design method.

$\beta_1$	Angle camber-line tangent makes with axial plane at leading edge
$\beta_2$	Angle camber-line tangent makes with axial plane at trailing edge
$\theta$	Camber angle of rotor or stator blades
$\xi$	Stagger angle
$\delta$	Angle of deviation
$i$	Local incidence angle

These angles are illustrated in Fig. 9.13.

### 7.3. Parameter used in isolated aerofoil method of design.

$\alpha$	Angle of incidence, or angle which mean relative velocity, $w$ , makes with the reference chord line of the aerofoil.
----------	---

## 8. Greek Letters Used

Letter	Small	Capital
Alpha	$\alpha$	
Beta	$\beta$	
Gamma	$\gamma$	
Delta	$\delta$	$\Delta$
Epsilon	$\epsilon$	
Eta	$\eta$	
Theta	$\theta$	
Lambda	$\lambda$	$\Lambda$
Mu	$\mu$	
Nu	$\nu$	
Xi	$\xi$	
Pi	$\pi$	
Rho	$\rho$	
Sigma	$\sigma$	
Tau	$\tau$	
Phi	$\varphi$	$\Phi$
Psi	$\psi$	
Omega	$\omega$	$\Omega$

# TABLES

In this Section numerical data of slide rule accuracy are presented with the purpose of facilitating the preparation of working design graphs. The use of such graphs cannot be too highly recommended.

Table I. Aerofoil Section Co-ordinates

Distance from L.E.	<i>Distance from chord line</i>				
	CLARK Y (Ref. 23)		RAF 6E (Ref. 22)	C4 (Ref. 54)	NACA 0012 (Ref. 93)
	Upper surface	Lower surface	flat undersurface	symmetrical	symmetrical
0	2.99	2.99	1.15	0	0
1.25	4.66	1.65	3.19	1.65	1.89
2.5	5.56	1.26	4.42	2.27	2.62
5.0	6.75	0.80	6.10	3.08	3.56
7.5	7.56	0.54	7.24	3.62	4.20
10	8.20	0.36	8.09	4.02	4.68
15	9.14	0.13	9.28	4.55	5.35
20	9.72	0.03	9.90	4.83	5.74
30	10.00		10.30	5.00	6.00
40	9.75		10.22	4.89	5.80
50	9.00		9.80	4.57	5.29
60	7.82		8.98	4.05	4.56
70	6.28		7.70	3.37	3.66
80	4.46		5.91	2.54	2.62
90	2.39		3.79	1.60	1.45
95	1.27		2.58	1.06	0.81
100	0.10		0.76	0	0.13
L.E. rad.			1.15	1.2	1.58
T.E. rad.			0.76	0.60	
Chord line	Flat under-surface of aerofoil	Flat under-surface of aerofoil	Axis of symmetry	Axis of symmetry	

All distances are given in percentage of chord distance.

Table II. Streamlined Body of Revolution Co-ordinates

<i>Distance from nose</i>		<i>Per cent</i>																
<i>Total length</i>			0	24.8	34.8	48.4	66.2	86.6	96.8	100	40	50	60	70	80	90	95	100
<i>Diameter at point</i>		<i>Max. diameter</i>																

Table III. Design Data from Momentum Considerations:  $\epsilon_p = 0$   
Used in constructing Figs. 8.4, 8.5, 8.7, and 10.1.

$\lambda$	$\epsilon_s$	$\alpha_1^\circ$	$\alpha_2^\circ$	$\alpha_1^\circ - \alpha_2^\circ$	$\varphi_r^\circ$	$c_L\sigma$	$k_{th}$	$\gamma k_R/k_{th}$
0.2	0.1	78.7	78.5	0.2	11.4	0.0396	1.0	5.12
	0.2		78.2	0.5	11.5	0.0800	2.0	5.00
	0.3		78.0	0.7	11.7	0.121	3.0	4.90
	0.4		77.7	1.0	11.8	0.163	4.0	4.82
	0.5		77.5	1.2	11.9	0.206	5.0	4.73
	0.6		77.2	1.5	12.0	0.250	6.0	4.62
	0.7		77.0	1.7	12.1	0.294	7.0	4.53
	0.8		76.6	2.1	12.3	0.340	8.0	4.43
	0.9		76.3	2.4	12.4	0.387	9.0	4.35
	1.0		76.0	2.7	12.5	0.434	10.0	4.26
0.3	0.1	73.3	72.8	0.5	17.0	0.0583	0.667	3.52
	0.2		72.3	1.0	17.2	0.118	1.333	3.45
	0.3		71.8	1.5	17.4	0.180	2.000	3.34
	0.4		71.2	2.1	17.7	0.243	2.667	3.25
	0.5		70.6	2.7	18.0	0.309	3.333	3.14
	0.6		69.9	3.4	18.3	0.376	4.000	3.06
	0.7		69.2	4.1	18.5	0.444	4.667	2.98
	0.8		68.5	4.8	18.8	0.516	5.333	2.88
	0.9		67.7	5.6	19.1	0.589	6.000	2.79
	1.0		66.8	6.5	19.5	0.667	6.667	2.71
0.4	0.1	68.2	67.4	0.8	22.2	0.0756	0.5	2.82
	0.2		66.5	1.7	22.6	0.154	1.0	2.70
	0.3		65.5	2.7	23.1	0.235	1.5	2.61
	0.4		64.5	3.7	23.5	0.319	2.0	2.51
	0.5		63.4	4.8	24.0	0.406	2.5	2.42
	0.6		62.3	5.9	24.5	0.497	3.0	2.34
	0.7		61.0	7.2	25.0	0.591	3.5	2.25
	0.8		59.5	8.7	25.5	0.688	4.0	2.16
	0.9		58.0	10.2	26.0	0.789	4.5	2.08
	1.0		56.3	11.9	26.6	0.894	5.0	2.00
0.5	0.1	63.5	62.2	1.3	27.2	0.091	0.4	2.40
	0.2		61.0	2.5	27.8	0.187	0.8	2.30
	0.3		59.5	4.0	28.4	0.285	1.2	2.21
	0.4		58.0	5.5	29.1	0.384	1.6	2.12
	0.5		56.3	7.2	29.8	0.497	2.0	2.03
	0.6		54.5	9.0	30.5	0.608	2.4	1.95
	0.7		52.4	11.1	31.2	0.725	2.8	1.86
	0.8		50.2	13.3	32.0	0.847	3.2	1.78
	0.9		48.0	15.5	32.8	0.975	3.6	1.70
	1.0		45.0	18.5	33.7	1.110	4.0	1.62

Table III (cont.)

$\lambda$	$\epsilon_s$	$\alpha_1^\circ$	$\alpha_2^\circ$	$\alpha_1^\circ - \alpha_2^\circ$	$\varphi_r^\circ$	$C_L\sigma$	$k_{th}$	$\gamma k_R/k_{th}$
0.6	0.1	59.0	57.3	1.7	31.8	0.105	0.333	2.16
	0.2		55.7	3.3	32.6	0.215	0.667	2.07
	0.3		53.8	5.2	33.4	0.330	1.00	1.99
	0.4		51.7	7.3	34.3	0.451	1.333	1.89
	0.5		49.4	9.6	35.2	0.577	1.667	1.80
	0.6		46.9	12.1	36.2	0.709	2.000	1.72
	0.7		44.0	15.0	37.2	0.847	2.333	1.64
	0.8		40.9	18.1	38.3	0.991	2.667	1.56
	0.9		37.5	21.5	39.4	1.143	3.000	1.48
	1.0		33.7	25.3	40.6	1.302	3.333	1.42
0.7	0.1	55.0	53.0	2.0	36.0	0.117	0.286	2.03
	0.2		50.9	4.1	37.0	0.241	0.571	1.94
	0.3		48.5	6.5	38.0	0.370	0.857	1.84
	0.4		45.8	9.2	39.1	0.505	1.15	1.76
	0.5		42.9	12.1	40.3	0.647	1.43	1.67
	0.6		39.7	15.3	41.6	0.796	1.713	1.59
	0.7		36.1	18.9	42.8	0.952	2.00	1.52
	0.8		32.2	22.8	44.2	1.115	2.286	1.44
	0.9		27.9	27.1	45.6	1.287	2.57	1.37
	1.0		23.2	31.8	47.1	1.465	2.86	1.30
0.8	0.1	51.3	49.0	2.3	39.8	0.128	0.25	1.95
	0.2		46.4	4.9	41.0	0.262	0.50	1.86
	0.3		43.6	7.7	42.3	0.404	0.75	1.77
	0.4		40.4	10.9	43.6	0.551	1.00	1.68
	0.5		36.9	14.4	45.0	0.707	1.25	1.60
	0.6		33.0	18.3	46.5	0.869	1.50	1.52
	0.7		28.8	22.5	48.0	1.04	1.75	1.45
	0.8		24.2	27.1	49.7	1.22	2.00	1.38
	0.9		19.3	32.0	51.3	1.41	2.25	1.32
	1.0		14.0	37.3	53.1	1.60	2.50	1.25
0.9	0.1	48.0	45.3	2.7	43.3	0.137	0.222	1.92
	0.2		42.3	5.7	44.7	0.281	0.445	1.82
	0.3		39.0	9.0	46.1	0.433	0.667	1.73
	0.4		35.4	12.6	47.7	0.591	0.890	1.65
	0.5		31.4	16.6	49.3	0.758	1.112	1.57
	0.6		27.1	20.9	50.9	0.932	1.333	1.50
	0.7		22.3	25.7	52.7	1.114	1.556	1.42
	0.8		17.3	30.7	54.6	1.304	1.780	1.36
	0.9		11.9	36.1	56.5	1.502	2.000	1.29
	1.0		6.3	41.7	58.6	1.706	2.222	1.24
1.0	0.1	45.0	42.0	3.0	46.5	0.145	0.2	1.90
	0.2		38.7	6.3	48.0	0.297	0.4	1.81
	0.3		35.0	10.0	49.6	0.457	0.6	1.72
	0.4		31.0	14.0	51.3	0.625	0.8	1.64
	0.5		26.6	18.4	53.1	0.800	1.0	1.56
	0.6		21.8	23.2	55.0	0.982	1.2	1.49
	0.7		16.7	28.3	57.0	1.171	1.4	1.43
	0.8		11.3	33.7	59.0	1.372	1.6	1.36
	0.9		5.7	39.3	61.2	1.579	1.8	1.30
	1.0		0.0	45.0	63.4	1.789	2.0	1.25

Table III (concluded)

$\lambda$	$\epsilon_s$	$\alpha_1^\circ$	$\alpha_2^\circ$	$\alpha_1^\circ - \alpha_2^\circ$	$\varphi_r^\circ$	$C_L\sigma$	$k_{th}$	$\gamma k_R/k_{th}$
1.1	0.1	42.3	39.0	3.3	49.3	0.152	0.182	1.92
	0.2		35.3	7.0	51.0	0.311	0.364	1.84
	0.3		31.3	11.0	52.8	0.478	0.545	1.74
	0.4		27.0	15.3	54.7	0.653	0.727	1.66
	0.5		22.2	20.1	56.6	0.835	0.910	1.58
	0.6		17.2	25.1	58.7	1.025	1.091	1.51
	0.7		11.8	30.5	60.8	1.222	1.272	1.45
	0.8		6.2	36.1	63.0	1.426	1.454	1.39
	0.9		0.5	41.8	65.3	1.636	1.637	1.34
	1.0		-5.2	47.5	67.8	1.851	1.818	1.28
1.2	0.1	39.8	36.3	3.5	51.9	0.158	0.167	1.94
	0.2		32.4	7.4	53.8	0.323	0.333	1.85
	0.3		28.1	11.7	55.7	0.495	0.500	1.76
	0.4		23.4	16.4	57.7	0.676	0.667	1.69
	0.5		18.4	21.4	59.8	0.864	0.833	1.61
	0.6		13.1	26.7	61.9	1.059	1.000	1.54
	0.7		7.6	32.2	64.2	1.260	1.167	1.48
	0.8		1.9	37.9	66.6	1.468	1.333	1.43
	0.9		-3.8	43.6	69.0	1.681	1.500	1.38
	1.0		-9.5	49.3	71.6	1.897	1.667	1.33
1.3	0.1	37.6	33.8	3.8	54.3	0.162	0.154	1.97
	0.2		29.6	8.0	56.2	0.333	0.308	1.88
	0.3		25.1	12.5	58.2	0.510	0.462	1.80
	0.4		20.3	17.3	60.4	0.695	0.615	1.73
	0.5		15.1	22.5	62.6	0.888	0.769	1.65
	0.6		9.6	28.0	64.9	1.086	0.923	1.59
	0.7		3.9	33.7	67.3	1.291	1.078	1.53
	0.8		-1.8	39.4	69.7	1.501	1.230	1.48
	0.9		-7.5	45.1	72.3	1.715	1.385	1.43
	1.0		-13.0	50.6	74.9	1.931	1.540	1.39
1.4	0.1	35.6	31.6	4.0	56.4	0.167	0.143	2.02
	0.2		27.3	8.3	58.4	0.341	0.286	1.93
	0.3		22.5	13.1	60.6	0.523	0.429	1.85
	0.4		17.5	18.1	62.8	0.711	0.571	1.78
	0.5		12.1	23.5	65.1	0.907	0.714	1.71
	0.6		6.6	29.0	67.5	1.109	0.857	1.65
	0.7		0.9	34.7	70.0	1.315	1.000	1.59
	0.8		-4.9	40.5	72.6	1.526	1.143	1.54
	0.9		-10.5	46.1	75.2	1.740	1.286	1.50
	1.0		-15.9	51.5	77.9	1.956	1.429	1.47
1.5	0.1	33.7	29.6	4.1	58.3	0.170	0.133	2.07
	0.2		25.0	8.7	60.5	0.348	0.267	1.98
	0.3		20.2	13.5	62.7	0.533	0.400	1.90
	0.4		15.0	18.7	65.0	0.725	0.533	1.83
	0.5		9.5	24.2	67.6	0.923	0.667	1.76
	0.6		3.8	29.9	69.9	1.130	0.800	1.70
	0.7		-1.9	35.6	72.4	1.333	0.933	1.65
	0.8		-7.6	41.3	75.1	1.545	1.067	1.61
	0.9		-13.1	46.8	77.8	1.752	1.200	1.57
	1.0		-18.4	52.1	80.6	1.973	1.333	1.54

Table IV. Design Data from Momentum Considerations:  $\epsilon_s = 0$   
Used in constructing Figs. 8.6, 8.8 and 10.2.

$\lambda$	$\epsilon_p$	$\alpha_1^\circ$	$\alpha_2^\circ$	$\alpha_1^\circ - \alpha_2^\circ$	$\varphi_r^\circ$	$C_L\sigma$	$k_{th}$	$\gamma k_R/k_{th}$
0.2	0.1	78.9	78.7	0.2	11.2	0.0389	1.0	5.31
	0.2	79.1		0.4	11.1	0.0770	2.0	5.40
	0.3	79.3		0.6	11.0	0.114	3.0	5.52
	0.4	79.5		0.8	10.9	0.151	4.0	5.62
	0.5	79.7		1.0	10.8	0.187	5.0	5.71
	0.6	79.9		1.2	10.7	0.223	6.0	5.81
	0.7	80.1		1.4	10.6	0.257	7.0	5.93
	0.8	80.2		1.5	10.5	0.292	8.0	6.04
	0.9	80.4		1.7	10.4	0.325	9.0	6.15
	1.0	80.5		1.8	10.3	0.358	10.0	6.26
	1.1	80.7		2.0	10.2	0.390	11.0	6.36
	1.2	80.8		2.1	10.1	0.422	12.0	6.47
	1.3	81.0		2.3	10.0	0.453	13.0	6.58
	1.4	81.1		2.4	10.0	0.484	14.0	6.69
	1.5	81.3		2.6	9.9	0.514	15.0	6.80
0.3	0.1	73.8	73.3	0.5	16.5	0.0568	0.667	3.72
	0.2	74.2		0.9	16.2	0.112	1.333	3.84
	0.3	74.6		1.3	16.0	0.165	2.000	3.94
	0.4	75.0		1.7	15.8	0.218	2.667	4.05
	0.5	75.4		2.1	15.6	0.269	3.333	4.16
	0.6	75.7		2.4	15.4	0.318	4.000	4.28
	0.7	76.1		2.8	15.2	0.368	4.667	4.35
	0.8	76.4		3.1	15.0	0.414	5.333	4.48
	0.9	76.7		3.4	14.8	0.459	6.000	4.60
	1.0	77.0		3.7	14.6	0.505	6.667	4.71
	1.1	77.3		4.0	14.5	0.549	7.333	4.81
	1.2	77.6		4.3	14.3	0.591	8.000	4.95
	1.3	77.8		4.5	14.1	0.632	8.667	5.07
	1.4	78.1		4.8	13.9	0.675	9.333	5.17
	1.5	78.3		5.0	13.8	0.712	10.000	5.32
0.4	0.1	69.0	68.2	0.8	21.4	0.0730	0.5	3.00
	0.2	69.7		1.5	21.0	0.144	1.0	3.10
	0.3	70.3		2.1	20.7	0.212	1.5	3.25
	0.4	71.0		2.8	20.3	0.278	2.0	3.33
	0.5	71.6		3.4	20.0	0.342	2.5	3.43
	0.6	72.1		3.9	19.7	0.404	3.0	3.54
	0.7	72.7		4.5	19.3	0.463	3.5	3.65
	0.8	73.2		5.0	19.0	0.522	4.0	3.77
	0.9	73.6		5.4	18.7	0.578	4.5	3.88
	1.0	74.1		5.9	18.4	0.632	5.0	4.02
	1.1	74.5		6.3	18.1	0.685	5.5	4.13
	1.2	74.9		6.7	17.9	0.737	6.0	4.26
	1.3	75.3		7.1	17.6	0.787	6.5	4.37
	1.4	75.6		7.4	17.4	0.835	7.0	4.50
	1.5	76.0		7.8	17.1	0.882	7.5	4.63
0.5	0.1	64.5	63.5	1.0	26.0	0.0877	0.4	2.60
	0.2	65.6		2.1	25.5	0.172	0.8	2.71
	0.3	66.5		3.0	24.9	0.253	1.2	2.82
	0.4	67.4		3.9	24.4	0.330	1.6	2.93
	0.5	68.2		4.7	24.0	0.406	2.0	3.04
	0.6	69.0		5.5	23.5	0.479	2.4	3.14
	0.7	69.7		6.2	23.1	0.549	2.8	3.26

## TABLES

Table IV (cont.)

$\lambda$	$\epsilon_p$	$\alpha_1^\circ$	$\alpha_2^\circ$	$\alpha_1^\circ - \alpha_2^\circ$	$\varphi_r^\circ$	$C_L\sigma$	$k_{th}$	$\gamma k_R/k_{th}$
0.5	0.8	70.3	63.5	6.8	22.6	0.615	3.2	3.38
	0.9	71.0		7.5	22.2	0.680	3.6	3.51
	1.0	71.6		8.1	21.8	0.743	4.0	3.63
	1.1	72.1		8.6	21.4	0.803	4.4	3.76
	1.2	72.6		9.1	21.1	0.861	4.8	3.88
	1.3	73.1		9.6	20.7	0.917	5.2	4.02
	1.4	73.6		10.1	20.4	0.973	5.6	4.14
	1.5	74.1		10.6	20.0	1.026	6.0	4.28
	0.1	60.5		1.5	30.2	0.101	0.333	2.37
	0.2	61.8		2.8	29.5	0.197	0.667	2.48
	0.3	63.0		4.0	28.8	0.289	1.000	2.59
	0.4	64.2		5.2	28.2	0.378	1.333	2.70
	0.5	65.2		6.2	27.6	0.463	1.667	2.82
	0.6	66.2		7.2	27.0	0.544	2.000	2.91
0.6	0.7	67.1	59.0	8.1	26.4	0.622	2.333	3.04
	0.8	67.9		8.9	25.8	0.697	2.667	3.16
	0.9	68.7		9.7	25.3	0.769	3.000	3.30
	1.0	69.5		10.5	24.8	0.838	3.333	3.43
	1.1	70.1		11.1	24.3	0.905	3.667	3.55
	1.2	70.8		11.8	23.8	0.968	4.000	3.68
	1.3	71.4		12.4	23.4	1.030	4.333	3.82
	1.4	72.0		13.0	22.9	1.090	4.667	3.97
	1.5	72.5		13.5	22.5	1.148	5.000	4.11
	0.1	56.8		1.8	34.1	0.112	0.286	2.23
	0.2	58.5		3.5	33.2	0.219	0.571	2.33
	0.3	60.0		5.0	32.4	0.321	0.857	2.44
	0.4	61.3		6.3	31.6	0.419	1.15	2.56
	0.5	62.6		7.6	30.8	0.512	1.43	2.67
	0.6	63.8		8.8	30.1	0.601	1.713	2.79
0.7	0.7	64.8		9.8	29.4	0.686	2.00	2.91
	0.8	65.8	55.0	10.8	28.7	0.768	2.286	3.04
	0.9	66.8		11.8	28.0	0.846	2.57	3.17
	1.0	67.6		12.6	27.4	0.920	2.86	3.30
	1.1	68.4		13.4	26.8	0.993	3.15	3.43
	1.2	69.2		14.2	26.3	1.062	3.43	3.57
	1.3	69.9		14.9	25.7	1.128	3.71	3.72
	1.4	70.5		15.5	25.2	1.315	4.00	3.87
	1.5	71.1		16.1	24.7	1.377	4.29	4.02
	0.1	53.5		2.2	37.6	0.122	0.25	2.15
	0.2	55.4		4.1	36.5	0.238	0.50	2.26
	0.3	57.2		5.9	35.5	0.349	0.75	2.37
	0.4	58.8		7.5	34.6	0.454	1.00	2.48
	0.5	60.3		9.0	33.7	0.555	1.25	2.60
0.8	0.6	61.6		10.3	32.8	0.650	1.50	2.72
	0.7	62.9		11.6	32.0	0.741	1.75	2.85
	0.8	64.0	51.3	12.7	31.2	0.829	2.00	2.98
	0.9	65.1		13.8	30.5	0.913	2.25	3.11
	1.0	66.0		14.7	29.8	0.993	2.50	3.24
	1.1	67.0		15.7	29.1	1.070	2.75	3.39
	1.2	67.8		16.6	28.4	1.142	3.00	3.52
	1.3	68.6		17.3	27.8	1.210	3.25	3.69
	1.4	69.3		18.0	27.2	1.276	3.50	3.84
	1.5	70.0		18.7	26.6	1.341	3.75	4.00

Table IV (cont.)

$\lambda$	$\epsilon_p$	$\alpha_1^\circ$	$\alpha_2^\circ$	$\alpha_1^\circ - \alpha_2^\circ$	$\varphi_r^\circ$	$C_L\sigma$	$k_{th}$	$\gamma k_R/k_{th}$
0.9	0.1	50.7	48.0	2.7	40.7	0.131	0.222	2.12
	0.2	52.7		4.7	39.6	0.255	0.445	2.22
	0.3	54.7		6.7	38.4	0.373	0.667	2.33
	0.4	56.5		8.5	37.3	0.485	0.890	2.44
	0.5	58.2		10.2	36.3	0.592	1.112	2.57
	0.6	59.7		11.7	35.3	0.694	1.333	2.69
	0.7	61.1		13.1	34.4	0.791	1.556	2.82
	0.8	62.4		14.4	33.5	0.883	1.780	2.95
	0.9	63.6		15.6	32.7	0.971	2.000	3.09
	1.0	64.7		16.7	31.8	1.055	2.222	3.24
	1.1	65.7		17.7	31.1	1.135	2.445	3.38
	1.2	66.6		18.6	30.3	1.211	2.667	3.54
	1.3	67.5		19.5	29.6	1.284	2.890	3.69
	1.4	68.3		20.3	28.9	1.353	3.112	3.85
	1.5	69.0		21.0	28.3	1.420	3.333	4.02
1.0	0.1	47.7	45.0	2.7	43.6	0.138	0.2	2.10
	0.2	50.2		5.2	42.3	0.269	0.4	2.21
	0.3	52.4		7.4	41.0	0.394	0.6	2.33
	0.4	54.5		9.5	39.8	0.513	0.8	2.44
	0.5	56.3		11.3	38.7	0.625	1.0	2.56
	0.6	58.0		13.0	37.6	0.730	1.2	2.70
	0.7	59.5		14.5	36.5	0.835	1.4	2.83
	0.8	61.0		16.0	35.5	0.931	1.6	2.96
	0.9	62.3		17.3	34.6	1.021	1.8	3.09
	1.0	63.5		18.5	33.7	1.110	2.0	3.25
	1.1	64.5		19.5	32.8	1.191	2.2	3.40
	1.2	65.6		20.6	32.0	1.270	2.4	3.56
	1.3	66.5		21.5	31.2	1.347	2.6	3.73
	1.4	67.4		22.4	30.5	1.420	2.8	3.89
	1.5	68.2		23.2	29.8	1.490	3.0	4.06
1.1	0.1	45.3	42.3	3.0	46.2	0.144	0.182	2.12
	0.2	48.0		5.7	44.8	0.282	0.364	2.22
	0.3	50.4		8.1	43.4	0.412	0.545	2.34
	0.4	52.6		10.3	42.0	0.536	0.727	2.46
	0.5	54.6		12.3	40.8	0.653	0.910	2.58
	0.6	56.5		14.2	39.6	0.765	1.091	2.71
	0.7	58.2		15.9	38.5	0.871	1.272	2.84
	0.8	59.7		17.4	37.4	0.972	1.454	2.98
	0.9	61.1		18.8	36.4	1.067	1.637	3.13
	1.0	62.4		20.1	35.4	1.158	1.818	3.29
	1.1	63.5		21.2	34.4	1.244	2.000	3.44
	1.2	64.6		22.3	33.5	1.326	2.182	3.60
	1.3	65.6		23.3	32.7	1.404	2.364	3.78
	1.4	66.6		24.3	31.9	1.478	2.545	3.94
	1.5	67.5		25.2	31.1	1.549	2.727	4.12
1.2	0.1	43.0	39.8	3.2	48.6	0.150	0.167	2.14
	0.2	46.0		6.2	47.0	0.293	0.333	2.24
	0.3	48.6		8.8	45.6	0.428	0.500	2.36
	0.4	51.0		11.2	44.1	0.556	0.667	2.48
	0.5	53.1		13.3	42.7	0.678	0.833	2.61
	0.6	55.1		15.3	41.4	0.794	1.000	2.74
	0.7	56.9		17.1	40.2	0.904	1.167	2.88

Table IV (concluded)

$\lambda$	$\epsilon_p$	$\alpha_1^\circ$	$\alpha_2^\circ$	$\alpha_1^\circ - \alpha_2^\circ$	$\varphi_r^\circ$	$C_L\sigma$	$k_{th}$	$\gamma k_R/k_{th}$
1.2	0.8	58.5	39.8	18.7	39.0	1.008	1.333	3.04
	0.9	60.0		20.2	37.9	1.107	1.500	3.18
	1.0	61.4		21.6	36.9	1.200	1.667	3.34
	1.1	62.7		22.9	35.9	1.289	1.833	3.49
	1.2	63.8		24.0	34.9	1.373	2.000	3.67
	1.3	64.9		25.1	34.0	1.453	2.167	3.84
	1.4	65.9		26.1	33.1	1.530	2.333	4.01
	1.5	66.8		27.0	32.3	1.602	2.500	4.21
	0.1	41.0		3.4	50.7	0.155	0.154	2.18
	0.2	44.1		6.5	49.0	0.302	0.308	2.29
1.3	0.3	46.9	37.6	9.3	47.4	0.442	0.462	2.40
	0.4	49.5		11.9	45.9	0.575	0.615	2.53
	0.5	51.8		14.2	44.5	0.700	0.769	2.65
	0.6	53.9		16.3	43.0	0.819	0.923	2.80
	0.7	55.8		18.2	41.8	0.933	1.078	2.92
	0.8	57.5		19.9	40.5	1.040	1.230	3.09
	0.9	59.1		21.5	39.4	1.141	1.385	3.24
	1.0	60.5		22.9	38.2	1.238	1.540	3.40
	1.1	61.9		24.3	37.2	1.329	1.692	3.57
	1.2	63.1		25.5	36.1	1.415	1.846	3.75
1.4	1.3	64.2	35.6	26.6	35.2	1.497	2.000	3.92
	1.4	65.2		27.6	34.2	1.575	2.154	4.10
	1.5	66.2		28.6	33.4	1.649	2.308	4.31
	0.1	39.2	35.6	3.6	52.6	0.159	0.143	2.22
	0.2	42.5		6.9	50.9	0.310	0.286	2.33
	0.3	45.4		9.8	49.2	0.454	0.429	2.45
	0.4	48.1		12.5	47.6	0.591	0.571	2.58
	0.5	50.5		14.9	46.1	0.720	0.714	2.70
	0.6	52.8		17.2	44.6	0.843	0.857	2.84
	0.7	44.8		19.2	43.2	0.959	1.000	2.99
	0.8	56.6		21.0	41.9	1.069	1.143	3.14
	0.9	58.2		22.6	40.7	1.173	1.286	3.29
	1.0	59.8		24.2	39.5	1.271	1.429	3.45
1.5	1.1	61.1	33.7	25.5	38.4	1.365	1.571	3.64
	1.2	62.4		26.8	37.3	1.453	1.714	3.82
	1.3	63.6		28.0	36.2	1.537	1.857	4.00
	1.4	64.7		29.1	35.3	1.616	2.000	4.21
	1.5	65.7		30.1	34.3	1.692	2.143	4.40
	0.1	37.5	33.7	3.8	54.4	0.163	0.133	2.27
	0.2	40.9		7.2	52.5	0.317	0.267	2.38
	0.3	44.0		10.3	50.8	0.464	0.400	2.49
	0.4	46.9		13.2	49.0	0.604	0.533	2.63
	0.5	49.4		15.7	47.5	0.737	0.667	2.76
	0.6	51.7		18.0	45.9	0.862	0.800	2.90
	0.7	53.8		20.1	44.5	0.981	0.933	3.05
	0.8	55.7		22.0	43.1	1.092	1.067	3.20
	0.9	57.5		23.8	41.8	1.200	1.200	3.37
	1.0	59.0		25.3	40.6	1.301	1.333	3.53
	1.1	60.5		26.8	39.4	1.395	1.467	3.72
	1.2	61.8		28.1	38.3	1.486	1.600	3.91
	1.3	63.1		29.4	37.2	1.572	1.733	4.09
	1.4	64.2		30.5	36.2	1.655	1.867	4.29
	1.5	65.2		31.5	35.2	1.730	2.000	4.50

Tables V and VI. Optimum Values of  $C_L$ ,  $\sigma$ ,  $\theta$  and  $\xi$  for  $\epsilon_p = 0$ : Cascade Method  
Used in constructing Figs. 9.9, 9.11, 9.14 and 9.16.

$\lambda$	$\epsilon_t = 0.4$			$\epsilon_t = 0.5$			$\epsilon_t = 0.6$			$\epsilon_t = 0.7$			$\epsilon_t = 0.8$			$\epsilon_t = 0.9$			$\epsilon_t = 1.0$							
	$C_L^*$	$C_{L\sigma}$	$\sigma$																							
0.3																										
0.4																										
0.6																										
0.8	1.157	0.551	0.476	1.042	0.577	0.553	0.917	0.707	0.709	0.773	0.869	0.975	0.789	1.04	1.045	0.516	0.494	0.933	0.589	0.631	0.341	0.667	0.793			
1.0	1.179	0.625	0.530	1.050	0.620	0.562	0.947	0.982	1.037	0.868	1.171	1.35	0.811	1.32	0.711	0.22	1.715	0.645	1.143	0.607	0.756	0.789	0.144	0.668	0.894	1.34
1.2	1.222	0.676	0.553	1.125	0.864	0.768	1.042	1.059	1.015	0.993	1.260	1.269	0.971	1.468	1.270	0.545	1.270	1.545	1.217	1.342	1.752	1.305	1.442	1.973	1.37	
1.5	1.368	0.725	0.530	1.292	0.923	0.714	1.250	1.130	0.904	1.254	1.333	1.063	1.270	1.545	1.270	0.545	1.270	1.545	1.217	1.342	1.752	1.305	1.442	1.973	1.37	

$\lambda$	$\epsilon_t = 0.4$			$\epsilon_t = 0.5$			$\epsilon_t = 0.6$			$\epsilon_t = 0.7$			$\epsilon_t = 0.8$			$\epsilon_t = 0.9$			$\epsilon_t = 1.0$		
	$\theta^\circ$	$\xi^\circ$	$\theta^\circ$	$\xi^\circ$	$\theta^\circ$	$\xi^\circ$	$\theta^\circ$	$\xi^\circ$	$\theta^\circ$	$\xi^\circ$	$\theta^\circ$	$\xi^\circ$	$\theta^\circ$	$\xi^\circ$	$\theta^\circ$	$\xi^\circ$	$\theta^\circ$	$\xi^\circ$	$\theta^\circ$	$\xi^\circ$	
0.3																					
0.4																					
0.6																					
0.8	17.5	42.6	14.8	51.6	9.6	63.4	10.8	62.8	12.2	62.1	13.7	61.4	9.2	69.1	8.3	69.1	9.2	68.7	9.2	60.6	15.3
1.0	21.8	34.1	21.0	40.8	24.9	38.9	20.1	49.0	23.2	47.5	26.6	45.8	13.7	61.4	13.7	61.4	15.3	60.6	15.3	30.4	43.8
1.2	25.2	37.2	26.4	31.9	31.1	29.5	36.5	26.8	42.2	23.9	34.4	38.9	21.0	54.3	21.0	54.3	21.0	54.3	21.0	29.2	17.9
1.5	29.1	19.2	35.0	16.2	41.2	13.1	47.6	9.9	54.1	6.7	60.7	3.4	67.1	6.7	67.1	6.7	67.1	6.7	67.1	6.7	0.2

## TABLES

Table VII. Optimum Values for Cascade Design Method

$\sigma$	$\alpha_2 = 70^\circ$			$\alpha_2 = 60^\circ$			$\alpha_2 = 50^\circ$		
	$C_L^*$	$\tan \alpha_1 - \tan \alpha_2$	$C_L\sigma$	$C_L^*$	$\tan \alpha_1 - \tan \alpha_2$	$C_L\sigma$	$C_L^*$	$\tan \alpha_1 - \tan \alpha_2$	$C_L\sigma$
0.6	0.950	0.960	0.570	0.970	0.670	0.582	1.020	0.545	0.612
0.7	0.885	1.062	0.620	0.907	0.738	0.635	0.952	0.595	0.667
0.8	0.830	1.153	0.664	0.855	0.803	0.684	0.900	0.647	0.720
0.9	0.782	1.235	0.704	0.807	0.864	0.726	0.848	0.695	0.763
1.0	0.740	1.318	0.740	0.764	0.922	0.764	0.800	0.740	0.800
1.1	0.705	1.395	0.775	0.727	0.978	0.800	0.760	0.785	0.836
1.2	0.674	1.472	0.809	0.695	1.030	0.834	0.724	0.825	0.869
1.3	0.648	1.541	0.842	0.667	1.077	0.866	0.694	0.862	0.901
1.4	0.623	1.610	0.872	0.642	1.124	0.898	0.668	0.900	0.935
1.5	0.600	1.675	0.900	0.618	1.166	0.927	0.644	0.935	0.966
1.6	0.578	1.735	0.925	0.596	1.210	0.954	0.620	0.969	0.992
1.7	0.558	1.793	0.948	0.577	1.250	0.981	0.600	1.00	1.020
1.8	0.540	1.850	0.972	0.557	1.290	1.002	0.580	1.032	1.042
1.9	0.532	1.905	0.994	0.540	1.325	1.026	0.560	1.061	1.063
2.0	0.506	1.960	1.012	0.522	1.365	1.044	0.541	1.090	1.082

$\sigma$	$\alpha_2 = 10^\circ$			$\alpha_2 = 0^\circ$			$\alpha_2 = -10^\circ$		
	$C_L^*$	$\tan \alpha_1 - \tan \alpha_2$	$C_L\sigma$	$C_L^*$	$\tan \alpha_1 - \tan \alpha_2$	$C_L\sigma$	$C_L^*$	$\tan \alpha_1 - \tan \alpha_2$	$C_L\sigma$
0.6	1.350	0.438	0.810	1.538	0.470	0.922	1.780	0.534	1.068
0.7	1.270	0.483	0.889	1.440	0.520	1.009	1.672	0.593	1.170
0.8	1.203	0.525	0.963	1.362	0.567	1.090	1.590	0.644	1.272
0.9	1.142	0.566	1.029	1.294	0.610	1.165	1.511	0.690	1.360
1.0	1.086	0.603	1.086	1.231	0.650	1.231	1.440	0.733	1.440
1.1	1.036	0.637	1.139	1.177	0.685	1.293	1.372	0.772	1.510
1.2	0.993	0.669	1.192	1.130	0.718	1.357	1.310	0.807	1.571
1.3	0.953	0.700	1.239	1.083	0.750	1.409	1.256	0.842	1.631
1.4	0.915	0.730	1.281	1.040	0.780	1.455	1.204	0.875	1.687
1.5	0.882	0.756	1.323	1.000	0.810	1.500	1.160	0.905	1.740
1.6	0.850	0.781	1.360	0.966	0.836	1.547	1.119	0.933	1.790
1.7	0.822	0.808	1.397	0.933	0.861	1.586	1.080	0.962	1.836
1.8	0.796	0.832	1.433	0.902	0.885	1.624	1.043	0.990	1.880
1.9	0.771	0.855	1.465	0.872	0.910	1.658	1.010	1.015	1.919
2.0	0.750	0.876	1.500	0.844	0.933	1.688	0.980	1.039	1.960

Used in constructing Figs. 9.6, 9.7 and 9.8.

$\alpha_2 = 40^\circ$			$\alpha_2 = 30^\circ$			$\alpha_2 = 20^\circ$			$\sigma$
$C_L^*$	$\tan \alpha_1 - \tan \alpha_2$	$C_L\sigma$	$C_L^*$	$\tan \alpha_1 - \tan \alpha_2$	$C_L\sigma$	$C_L^*$	$\tan \alpha_1 - \tan \alpha_2$	$C_L\sigma$	
1.061	0.464	0.637	1.125	0.434	0.675	1.230	0.428	0.738	0.6
0.995	0.515	0.696	1.059	0.478	0.741	1.148	0.470	0.804	0.7
0.937	0.561	0.750	1.000	0.521	0.800	1.085	0.511	0.868	0.8
0.885	0.604	0.796	0.945	0.562	0.850	1.030	0.550	0.927	0.9
0.840	0.645	0.840	0.897	0.600	0.897	0.980	0.587	0.980	1.0
0.800	0.681	0.880	0.856	0.634	0.942	0.935	0.622	1.029	1.1
0.764	0.717	0.917	0.820	0.667	0.983	0.893	0.656	1.071	1.2
0.732	0.750	0.950	0.786	0.696	1.021	0.857	0.683	1.112	1.3
0.704	0.782	0.985	0.757	0.726	1.060	0.825	0.715	1.154	1.4
0.678	0.813	1.019	0.730	0.754	1.095	0.797	0.741	1.196	1.5
0.655	0.844	1.048	0.703	0.781	1.125	0.770	0.770	1.232	1.6
0.633	0.872	1.076	0.680	0.808	1.155	0.747	0.796	1.270	1.7
0.612	0.900	1.101	0.657	0.832	1.183	0.722	0.820	1.300	1.8
0.595	0.925	1.130	0.636	0.855	1.209	0.700	0.843	1.330	1.9
0.578	0.951	1.156	0.618	0.876	1.236	0.677	0.865	1.354	2.0

$\alpha_2 = -20^\circ$			$\alpha_2 = -30^\circ$			$\alpha_2 = -40^\circ$			$\sigma$
$C_L^*$	$\tan \alpha_1 - \tan \alpha_2$	$C_L\sigma$	$C_L^*$	$\tan \alpha_1 - \tan \alpha_2$	$C_L\sigma$	$C_L^*$	$\tan \alpha_1 - \tan \alpha_2$	$C_L\sigma$	
2.152	0.650	1.290							0.6
2.030	0.711	1.420							0.7
1.922	0.771	1.539	2.420	0.971	1.936				0.8
1.827	0.823	1.643	2.284	1.030	2.061				0.9
1.738	0.871	1.738	2.168	1.085	2.168				1.0
1.655	0.915	1.820	2.055	1.135	2.260				1.1
1.580	0.953	1.897	1.956	1.175	2.345	2.490	1.580	2.990	1.2
1.510	0.988	1.961	1.860	1.212	2.415	2.380	1.548	3.090	1.3
1.445	1.021	2.022	1.775	1.248	2.484	2.267	1.585	3.170	1.4
1.387	1.052	2.080	1.700	1.280	2.550	2.163	1.620	3.250	1.5
1.333	1.083	2.135	1.632	1.312	2.610	2.065	1.653	3.310	1.6
1.284	1.112	2.184	1.572	1.340	2.675	1.979	1.683	3.360	1.7
1.240	1.141	2.232	1.515	1.370	2.726	1.900	1.711	3.420	1.8
1.197	1.170	2.274	1.460	1.398	2.774	1.830	1.740	3.480	1.9
1.160	1.196	2.320	1.405	1.422	2.810	1.770	1.769	3.540	2.0

Table VIII. Optimum Values of  $C_L$  and  $\sigma$ , for  $\epsilon_s = 0$ : Cascade Method Used in constructing Figs. 9.10 and 9.12.

Table IX. Optimum Values of  $\theta$  and  $\xi$  for  $\epsilon_s = 0$ : Cascade Method  
Used in constructing Figs. 9.15 and 9.17.

Tables X, XI, and XII. Design Data for Stators  
Used in constructing Figs. II.3, II.6, II.7 and II.9.

Table X. Values of  $C_L$  as a Function of  $\epsilon_s$  or  $\epsilon_p$ , and  $s/c$  for Stator Design

$\epsilon$	$s/c$						1.5
	0.5	0.6	0.7	0.8	0.9	1.0	
0.2	0.199	0.239	0.279	0.318	0.358	0.398	0.438
0.4	0.392	0.471	0.549	0.628	0.706	0.785	0.863
0.6	0.575	0.690	0.805	0.920	1.035	1.150	1.265
0.8	0.742	0.891	1.040	1.189	1.336	1.485	1.633
1.0	0.893	1.072	1.251	1.430	1.609	1.789	1.968
1.2	1.029	1.234	1.440	1.646	1.851	2.059	2.264
1.4	1.145	1.373	1.603	1.832	2.061	2.290	
1.5	1.200	1.440	1.680	1.920	2.160	2.400	

Table XI. Recommended Values for Straightener Design as Functions of  $\epsilon_s$ 

$\epsilon_s$	0.1	0.2	0.3	0.4	0.5	0.6	0.7	0.8	0.9	1.0
$s/c$	1.5	1.5	1.5	1.5	1.5	1.5	1.5	0.88	0.685	0.540
$C_L$	0.300	0.597	0.890	1.178	1.458	1.310	1.162	1.018	0.886	0.430
$\theta$	8.4°	16.6°	24.6°	32.0°	39.0°	42.9°	46.3°	49.2°	51.9°	54.3°
% camber	1.86	3.67	5.43	7.07	8.62	9.47	10.22	10.86	11.46	12.00
$\xi$	1.5°	3.0°	4.4°	5.8°	7.1°	9.5°	11.8°	14.1°	16.0°	17.8°

Table XII. Recommended Values for Prerotator Design as Functions of  $\epsilon_p$ 

$\epsilon_p$	0.1	0.2	0.3	0.4	0.5	0.6	0.7	0.8	0.9	1.0	1.1	1.2	1.3	1.4	1.5
$s/c$	1.5	1.5	1.5	1.5	1.5	1.5	1.5	1.345	1.215	1.116	1.038	0.975	0.918	0.872	0.840
$C_L$	0.300	0.597	0.890	1.178	1.458	1.725	1.982	2.0	2.0	2.0	2.0	2.0	2.0	2.0	2.0
$\theta$	8.1°	16.2°	23.9°	31.1°	38.0°	44.3°	50.0°	52.9°	55.4°	57.9°	60.2°	62.4°	64.1°	66.1°	67.7°
% camber	1.77	3.58	5.28	6.87	8.40	9.78	11.05	11.69	12.25	12.79	13.30	13.79	14.16	14.60	14.95
$\xi$	4.1°	8.1°	12.0°	15.6°	19.0°	22.2°	25.0°	26.5°	27.7°	29.0°	30.1°	31.2°	32.1°	33.1°	33.9°

Tables XIII and XIV. Loss Coefficient,  $(K_{R_P} + K_{R_S}) / K_{th}$ , for Rotor  
Designed by recommended Cascade Method  
Used in constructing Figs. 10.6 and 10.7.

Table XIII.  $\epsilon_p = 0$ 

$\lambda$	$\epsilon_s$						
	0.4	0.5	0.6	0.7	0.8	0.9	1.0
0.3					0.098	0.095	0.092
0.4			0.080	0.077	0.074	0.072	0.072
0.6		0.061	0.058	0.057	0.055	0.055	0.056
0.8	0.058	0.054	0.052	0.050	0.049	0.048	0.047
1.0	0.057	0.053	0.051	0.049	0.047	0.045	0.043
1.2	0.059	0.055	0.052	0.050	0.049	0.047	0.045
1.5	0.066	0.063	0.060	0.058	0.057	0.057	0.057

Table XIV.  $\epsilon_s = 0$ 

$\lambda$	$\epsilon_p$						
	0.4	0.5	0.6	0.7	0.8	0.9	1.0
0.3				0.125	0.128	0.132	0.160
0.4			0.099	0.103	0.108	0.115	0.137
0.6		0.089	0.092	0.097	0.104	0.111	0.122
0.8		0.087	0.092	0.097	0.104	0.111	0.120
1.0	0.084	0.087	0.092	0.097	0.105	0.114	0.125
1.2	0.086	0.089	0.093	0.099	0.108	0.118	0.131
1.5	0.092	0.095	0.099	0.104	0.112	0.124	0.136

$\lambda$	$\epsilon_p$						
	1.1	1.2	1.3	1.4	1.5		
0.3	0.164	0.169	0.173	0.178	0.185		
0.4	0.142	0.148	0.154	0.162	0.172		
0.6	0.130	0.140	0.150	0.163	0.177		
0.8	0.132	0.144	0.160	0.176			
1.0	0.138	0.154					
1.2	0.145						

The above figures are based on the assumptions :

$$C_{D_P} = 0.016$$

$$C_D = 0.018 C_L^2$$

Tables XV and XVI. Loss Coefficient Data for Stators  
Used in constructing Figs. 12.1 and 12.2.

Table XV. Values of  $\gamma \frac{k_p}{k_{th}}$  or  $\gamma \frac{k_s}{k_{th}}$ . For  $\epsilon_p$  or  $\epsilon_s = 0$

$\epsilon$	$\lambda$						
	0.2	0.3	0.4	0.5	0.6	0.7	0.8
0.2	0.202	0.303	0.404	0.505	0.606	0.707	0.808
0.4	0.208	0.312	0.416	0.520	0.624	0.728	0.832
0.6	0.219	0.328	0.437	0.546	0.656	0.765	0.874
0.8	0.232	0.348	0.464	0.580	0.696	0.812	0.928
1.0	0.250	0.375	0.500	0.625	0.750	0.875	1.000
1.2	0.272	0.407	0.543	0.678	0.814	0.950	1.086
1.4	0.299	0.447	0.597	0.746	0.895	1.044	1.194
1.5	0.314	0.471	0.628	0.785	0.942	1.100	1.255

Table XVI. Values of  $\frac{1}{C_D} \cdot \frac{k_s}{k_{th}}$  for N.P.L. Type of Straightener,  $\epsilon_p = 0$

$\epsilon$	$\lambda$						
	0.2	0.3	0.4	0.5	0.6	0.7	0.8
0.1	1.504	2.005	2.505	3.006	3.508	4.01	4.51
0.2	0.762	1.015	1.269	1.524	1.776	2.030	2.283
0.3	0.517	0.690	0.862	1.035	1.207	1.380	1.552
0.4	0.265	0.398	0.530	0.663	0.796	0.928	1.061
0.5	0.219	0.329	0.438	0.548	0.657	0.767	0.876

Tables XVII and XVIII. Loss Coefficients for Stators Designed by Recommended Cascade Method  
Used in constructing Figs. 12.3 and 12.4.

Table XVII.  $\frac{K_{sp} + K_{ps}}{K_{th}}, \epsilon_p = 0$

$\epsilon_t$	$\lambda$									
	0.2	0.3	0.4	0.5	0.6	0.7	0.8	0.9	1.0	1.1
0.1	0.012	0.018	0.024	0.030	0.035	0.041	0.047	0.053	0.059	0.065
0.2	0.008	0.011	0.015	0.019	0.023	0.027	0.030	0.034	0.038	0.042
0.3	0.007	0.010	0.014	0.017	0.021	0.024	0.028	0.031	0.035	0.038
0.4	0.007	0.011	0.015	0.018	0.022	0.025	0.029	0.033	0.036	0.040
0.5	0.008	0.012	0.016	0.020	0.024	0.028	0.032	0.036	0.039	0.043
0.6	0.008	0.012	0.016	0.019	0.023	0.027	0.031	0.035	0.039	0.043
0.8	0.008	0.012	0.016	0.019	0.023	0.027	0.031	0.035	0.039	0.043
1.0	0.009	0.013	0.018	0.022	0.027	0.031	0.036	0.040	0.044	0.049

Table XVIII.  $\frac{K_{sp} + K_{ps}}{K_{th}}, \epsilon_s = 0$

$\epsilon_p$	$\lambda$									
	0.2	0.3	0.4	0.5	0.6	0.7	0.8	0.9	1.0	1.1
0.1	0.012	0.018	0.024	0.030	0.035	0.041	0.047	0.053	0.059	0.065
0.2	0.008	0.011	0.015	0.019	0.023	0.027	0.030	0.034	0.038	0.042
0.3	0.007	0.010	0.014	0.017	0.021	0.024	0.028	0.031	0.035	0.038
0.4	0.007	0.011	0.015	0.018	0.022	0.025	0.029	0.033	0.036	0.040
0.5	0.008	0.012	0.016	0.020	0.024	0.028	0.032	0.036	0.039	0.043
0.7	0.010	0.015	0.020	0.025	0.030	0.034	0.039	0.044	0.049	0.054
1.0	0.011	0.017	0.022	0.028	0.033	0.039	0.044	0.050	0.055	0.060
1.2	0.012	0.018	0.024	0.030	0.036	0.042	0.048	0.054	0.060	0.066
1.5	0.014	0.021	0.028	0.035	0.041	0.048	0.055	0.062	0.069	0.076

The above figures are based on the assumptions :

$$C_{Dp} = 0.016$$

$$C_{Ds} = 0.018 C_L^2$$

Tables XIX, XX, and XXI. Free Fan Design Data  
Used in constructing Figs. A.7, A.8 and A.5.

Table XIX  $\frac{C_L}{C_{D_p}} = 50$

$u/\Omega r$	$\varphi$	$a'$	$C_L \sigma$
0.05	2.8	0.003	0.014
0.10	5.8	0.013	0.042
0.15	8.9	0.027	0.095
0.20	11.9	0.049	0.170
0.25	15.1	0.075	0.283
0.30	18.5	0.110	0.430
0.35	22.4	0.155	0.635
0.40	26.8	0.214	0.925
0.45	32.7	0.305	1.430
0.48	38.5	0.400	2.010
0.49	43.5	0.485	2.670

Table XX.  $\frac{C_L}{C_{D_p}} = 50$ , velocity distribution of Table XXI

$u_+/\Omega R$	0.05	0.10	0.15	0.20	0.25	0.30	0.35
$f(u_+/\Omega R)$	0.0010	0.0032	0.0075	0.0144	0.0230	0.0350	0.0560

Table XXI.

$x$	0.166	0.20	0.25	0.30	0.40	0.50	0.60	0.70	0.80	0.90	0.95	1.00
$u/u_+$	0	0.136	0.279	0.365	0.525	0.675	0.832	0.957	1.000	0.947	0.843	0

Table XXII. Blade Element Design Data for Free Fans  
Used in constructing Figs. A.9 and A.10.

$x$	0.166	0.2	0.25	0.3	0.4	0.5	0.6	0.7	0.8	0.9	0.95	1.0
$u_+/\Omega R$	0	1.9	3.2	3.5	3.8	3.9	4.0	4.0	3.6	3.0	2.5	0
	0	0.009	0.017	0.019	0.021	0.022	0.023	0.023	0.020	0.016	0.012	0
$\varphi^\circ$		3.9	6.5	7.1	7.6	7.9	8.1	8.0	7.3	6.2	5.1	
		0.022	0.053	0.062	0.073	0.076	0.080	0.078	0.065	0.047	0.034	
$\varphi^\circ$	6.0	9.8	10.8	11.7	12.0	12.4	12.2	11.1	9.3	7.8		
	0.044	0.116	0.140	0.164	0.174	0.184	0.179	0.147	0.103	0.074		
$C_L\sigma$		8.0	13.3	14.6	15.9	16.4	16.9	16.6	15.1	12.5	10.5	
		0.078	0.216	0.266	0.316	0.337	0.360	0.347	0.281	0.190	0.132	
$\varphi^\circ$	10.0	17.0	18.8	20.6	21.4	22.2	21.7	19.4	15.9	13.1		
	0.120	0.364	0.446	0.540	0.576	0.623	0.598	0.475	0.318	0.210		
$C_L\sigma$		12.1	21.1	23.6	26.3	27.3	28.5	27.8	24.5	19.7	16.1	
		0.177	0.564	0.715	0.890	0.970	1.070	1.000	0.765	0.490	0.326	
$\varphi^\circ$	0	14.2	25.9	29.6	34.3	36.6	40.0	38.0	30.9	23.9	19.3	0
	0	0.253	0.865	1.160	1.570	1.790	2.280	1.950	1.280	0.732	0.470	0

$\frac{C_L}{C_{D_P}} = 50$ , velocity distribution of Table XXI

## REFERENCES

1. Pankhurst, R. C., and Conn, J. F. C. "Physical properties of the standard atmosphere". R. and M. 1891. Aero. Res. Council. 1941.
2. Reynolds, Osborne. "An experimental investigation of the circumstances which determine whether the motion of water shall be direct or sinuous and of the law of resistance in parallel channels". *Phil. Trans.* Part 111, 935-982. 1883.
3. Goldstein, S. (Editor). *Modern Developments in Fluid Dynamics*. Oxford University Press. 1938. Vol. I, p. 321.
4. Goldstein, S. *op. cit.* Vol. I, p. 158.
5. Thwaites, B. "Approximate boundary layer calculations". *Aeronaut. Quart.* 1, 3, 245. 1949.
6. Rott, N. and Crabtree, L. F. "Simplified laminar boundary layer calculations for bodies of revolution and for yawed wings". *J. aero. Sci.* 19, 8, 553. 1952.
7. Goldstein, S. *op. cit.* Vol. I, p. 20.
8. Spence, D. A. "The development of turbulent boundary layers". *J. aero. Sci.* 23, 1, 3. 1956.
9. Von Doenhoff, A. E. and Tetrovian, N. "Determination of general relations for the behaviour of turbulent boundary layers". N.A.C.A. Tech. Report 772. 1943.
10. Ross, D. and Robertson, J. M. "An empirical method for calculation of the growth of a turbulent boundary layer". *J. aero. Sci.* 21, 5, 355. 1954.
11. Ludwig, H. and Tillmann, W. "Investigations of the wall shearing stress in turbulent boundary layers". N.A.C.A. Tech. Memo. 1285. 1950.
12. Coles, D. "The law of the wake in the turbulent boundary layer". *J. fluid Mech.* 1, 2, 191. 1956.
13. Dryden, H. "Air flow in the boundary layer near a plate". N.A.C.A. Tech. Report 562. 1936.
14. Liepmann, H. W. "Investigation of boundary layer transition on concave walls". N.A.C.A. Adv. Confidential Report 4J28. 1945.
15. Cowley, E. H. "The effects of surface irregularities on transition in the laminar boundary layer". A.R.L. Report A86. 1954.

16. Goldstein, S. *op. cit.* Vol. II, p. 380.
17. Goldstein, S. *op. cit.* Vol. II, p. 382.
18. Prosser, L. E. and Worster, R. C. "The hydro mechanics of fluid flow" in *Some Aspects of Fluid Flow* (Institute of Physics symposium). Edward Arnold and Co. London. 1951. p. 65.
19. Persh, J. and Bailey, B. M. "Effect of surface roughness over the downstream region of a 23° conical diffuser". N.A.C.A. Tech. Note 3066. 1954.
20. Glauert, H. *The Elements of Aerofoil and Airscrew Theory*. Cambridge University Press. 1926. p. 208.
21. Jacobs, E. N. and Abbott, I. H. "The N.A.C.A. variable density wind tunnel". N.A.C.A. Tech. Report 416. 1932.
22. Patterson, G. N. "Ducted fans: design for high efficiency". Australian Council for Aeronautics. Report ACA 7. 1944.
23. Pinkerton, R. M. and Greenberg, H. "Aerodynamic characteristics of a large number of aerofoils tested in the variable density wind tunnel". N.A.C.A. Tech. Report 628. 1938.
24. Wallis, R. A. "Wind tunnel tests on a series of circular arc plate aerofoils". A.R.L. Aero. Note 74. 1946.
25. Andrews, S. J. "Tests related to the effect of profile shape and camber line on compressor cascade performance". R. and M. 2743. Aero. Res. Council. 1949.
26. Glauert, H. *op. cit.* p. 43.
27. Goldstein, S. *op. cit.* Vol. II, p. 360.
28. Wallis, R. A. and Cumming, R. W. "Industrial aerodynamics". *J. Instn Engrs Aust.* **24**, 12, 221. 1952.
29. Patterson, G. N. "Modern diffuser design". *Aircr. Engng.* **10**, 267. 1938.
30. Squire, H. B. "Experiments on conical diffusers". R. and M. 2751. Aero. Res. Council. 1953.
31. Schubauer, G. B. and Spangenberg, W. G. "Effect of screens in wide angle diffusers". N.A.C.A. Tech. Note 1610. 1948.
32. "Fluid mixing device". U.S.A. Patent 2,558,816. July 1951.
33. Patterson, G. N. "Corner losses in ducts". *Aircr. Engng.* **9**, 205. 1937.
34. Wirt, L. "New data for the design of elbows in duct systems". *Gen. Elect. Rev.* **30**, 6, 286. 1927.
35. Henry, J. R. "Design of power plant installation pressure loss coefficients of duct components". N.A.C.A. Adv. Restricted Report L4F26. 1944.
36. Gray, S. "A survey of existing information of the flow in bent channels and the losses involved". Power Jets Report 1104. 1945.
37. Weske, J. R. "Pressure loss in ducts with compound corners". N.A.C.A. Adv. Restricted Report Feb. 1943.
38. Weske, J. R. "Experimental investigation of velocity distributions downstream of single duct bends". N.A.C.A. Tech. Note 1471. 1948.

39. Harper, I. "Tests on elbows of a special design". *J. aero. Sci.* **13**, 11, 587. 1946.
40. Palme, H. O. "An investigation of the effect of boundary layer suction on the air resistance in channel elbows". K. tekn. Högsk. Aero. TN2, Stockholm, 1948.
41. Salter, C. "Experiments on thin turning vanes". R. and M. 2469. Aero. Res. Council. 1952.
42. Dimmock, N. A. "The development of a simply constructed cascade corner for circular cross section ducts". N.G.T.E. Memo. 78. 1950.
43. Friedman, D. and Westphal, W. R. "Experimental investigation of a 90° cascade diffusing bend with an area ratio of 1·45:1 and with several inlet boundary layers". N.A.C.A. Tech. Note 2668. 1952.
44. MacPhail, D. C. "Experiments on turning vanes at an expansion". R. and M. 1876. Aero Res. Council. 1939.
45. Hoerner, S. F. *Aerodynamic Drag*. Otterbein Press. Dayton, U.S.A. 1951.
46. Goldstein, S. *op. cit.* Vol. II, p. 439.
47. Fage, A. and Johansen, F. C. "On the flow of air behind an inclined flat plate of infinite span". R. and M. 1104. Aero. Res. Council. 1927.
48. Wieghardt, K. E. G. "On the resistance of screens". *Aeronaut. Quart.* **4**, 186. 1953.
49. Mair, W. A. "The design of fans and guide vanes for high speed wind tunnels". R. and M. 2435. Aero. Res. Council. 1951.
50. Collar, A. R. "Cascade theory and the design of fan straighteners". R. and M. 1885. Aero. Res. Council. 1940.
51. Lighthill, M. J. "A mathematical method of cascade design". R. and M. 2104. Aero. Res. Council. 1945.
52. Hansen, A. G. and Yohner, P. L. "A numerical procedure for designing cascade blades with prescribed velocity distribution in incompressible potential flows". N.A.C.A. Tech. Note 2101. 1950.
53. Koffman, J. L. "Fans for traction applications". *Diesel Rly Tract.* **5**, 65-70 and 87-94. 1951.
54. Howell, A. R. "Fluid dynamics of axial compressors". *Proc. Instn mech. Engrs, Lond.* **153**, 441. 1945.
55. Mager, A., Mahoney, J. J. and Budinger, R. E. "Discussion of boundary layer characteristics near the wall of an axial flow compressor". N.A.C.A. Tech. Report 1085. 1952.
56. Carter, A. D. S. "Three-dimensional flow theories for axial compressors and turbines". *Proc. Instn mech. Engrs, Lond.* **159**, 255. 1948.
57. Turner, R. C. and Hughes, H. P. "Tests on rough surfaced compressor blading". Current Paper 306. Aero. Res. Council. 1956.

58. Bogdonoff, S. M. and Herrig, L. J. "Performance of axial flow fan and compressor blades designed for high loadings". N.A.C.A. Tech. Note 1201. 1947.
59. Squire, H. B. and Winter, K. G. "The secondary flow in a cascade of aerofoils in a non-uniform stream". *J. aero. Sci.* **18**, 4, 271. 1951.
60. Hawthorne, W. R. "Secondary circulation in fluid flow". *Proc. roy. Soc.* **206**, A1086. 1951.
61. Hansen, A. G., Herzig, H. Z. and Costello, G. R. "A visualization study of secondary flows in cascades". N.A.C.A. Tech. Note 2947. 1953.
62. Howell, A. R. "The present basis of axial flow compressor design. Part II, Compressor theory and performance". R.A.E. Report E 3961. 1942.
63. Gray, S. "Fluid dynamic notation in current use at N.G.T.E.". N.G.T.E. Memo M93. 1950.
64. Blight, F. G. "An introduction to the aerodynamic theory of compressors and turbines". A.R.L. Engines Report E56. 1947.
65. Howell, A. R., Mettam, M. and Nock, J. "Some general notes on axial flow compressor design". Power Jets Report R1088. 1945.
66. Cox, Sir H. Roxbee (Editor). *Gas Turbine Principles and Practice*. George Newnes. London. 1955. Chapter 5.
67. Howell, A. R. "The present basis of axial flow compressor design. Part 1, Cascade theory and performance". R. and M. 2095. Aero. Res. Council. 1942.
68. Scholes, J. F. M. and Patterson, G. N. "Wind tunnel tests on ducted contra-rotating fans". Australian Council for Aeronautics Report ACA 14. 1945.
69. Carter, A. D. S. and Cohen, E. M. "Preliminary investigation into the three-dimensional flow through a cascade of aerofoils". R. and M. 2339. Aero. Res. Council. 1946.
70. Wallis, R. A. "Performance of sheet metal bladed axial flow fans". A.R.L. Report A90. 1954.
71. Ruden, P. "Investigation of single stage fans". N.A.C.A. Tech. Memo. 1062. 1944.
72. Kahane, A. "Investigation of axial flow fan and compressor rotors designed for three-dimensional flow". N.A.C.A. Tech. Note 1652. 1948.
73. Patterson, G. N. "Ducted fans: effect of the straightener on overall efficiency". Australian Council for Aeronautics. Report ACA 9. 1944.
74. Carter, A. D. S. "The low speed performance of related aerofoils in cascade". Current Paper 29. Aero. Res. Council. 1950.
75. Reeman, J. "Performance of cascades of aerofoils at positive stagger". Power Jets Memo. M1203. 1947.

76. Ainsley, D. G. "Performance of axial flow turbines". *Proc. Instn mech. Engrs, Lond.* **159**, 230. 1948.
77. Warner, E. P. *Airplane Design-Performance*. McGraw-Hill. New York. 2nd edition. 1936. p. 349.
78. Johnston, I. H. "The effect of inlet conditions on the flow in annular diffusers". Current Paper 178. Aero. Res. Council. 1954.
79. Rebiffet, P. *Aerodynamique Expérimentale*. Librairie Polytechnique Ch. Béranger, Paris. 2nd edition. 1950. p. 281.
80. Batchelor, G. K. "Sound in wind tunnels". Australian Council for Aeronautics. Report ACA 18. 1945.
81. Olson, H. F. *Elements of Acoustical Engineering*. Van Nostrand. New York. 1940.
82. Wallis, R. A. "Sheet metal blades for axial flow fans". *Engineering, Lond.* **171**, 681. 1951.
83. Bauerle, H. "Measuring instruments for pressure, velocity, and direction measurements". A.V.A. monographs, Reports and Translations 951 (British). 1947.
84. Bryer, D. W., Walshe, D. E. and Garner, H. C. "Pressure probes selected for mean flow measurements—Exploration of turbulent boundary layers". Aero. Res. Council 17997. 1955.
85. Wallis, R. A. "Note on a boundary layer probe". A.R.L. Aero. Note 79. 1949.
86. Fail, R. "Tests on a high solidity engine cooling fan in the R.A.E. full scale fan testing tunnel". RAE. Report Aero. 2068. 1945.
87. Pearson, C. E. "Measurement of instantaneous vector air velocity by hot wire methods". *J. aero. Sci.* **19**, 2, 73. 1952.
88. Runchel, J. F. and Davey, R. S. "Pressure distribution measurements on the rotating blades of a single stage axial flow compressor". N.A.C.A. Tech. Note 1189. 1947.
89. Khalil, K. H. "Rotational effects on a cascade of aerofoil blades". *Engineer, Lond.* **193**, 831. 1952.
90. Weske, J. R. "An investigation of the aerodynamic characteristics of a rotating axial flow blade grid". N.A.C.A. Tech. Note 1128. 1947.
91. Andrews, S. J., Jeffs, R. A. and Hartley, E. L. "Tests concerning novel designs of blades for axial compressors.  
Part I. Blades designed for increased work at root or tip.  
Part II. Blades designed to operate in a parabolic axial velocity distribution".  
R. and M. 2929. Aero. Res. Council. 1956.
92. Boxer, E. "Influence of wall boundary layer upon the performance of an axial flow fan rotor". N.A.C.A. Tech. Note 2291. 1951.
93. Abbott, I. H. and von Doenhoff, A. E. *Theory of Wing Sections*. McGraw-Hill. New York. 1949. p. 321.

94. Smith, V. J. "Air circulator fans: a design method and experimental studies". A.R.L. Report A119. 1960.
95. Smith, V. J. and Chambers, E. W. "The technique of testing air circulating fans". A.R.L. Aero. Tech. Memo 88. 1952.

### Additional Useful References

- Keller, C. *The Theory and Performance of Axial Flow Fans*. McGraw-Hill. New York. 1937.
- Horlock, J. H. *Axial Flow Compressors*. Butterworth Scientific Publications. London. 1958.
- Pope, A. *Wind Tunnel Testing*. John Wiley and Sons. New York. 1947.
- Pankhurst, R. C. and Holder, D. W. *Wind Tunnel Technique*. Sir Isaac Pitman and Sons. London. 1952.
- Ower, E. *The Measurement of Air Flow*. Chapman and Hall. London. 3rd edition. 1949.
- American Society of Heating, Ventilating and Air-Conditioning Engineers *Guide*. 1958.
- Berry, C. H. *Flow and Fan-Principles of Moving Air through Ducts*. Industrial Press. New York. 1954.
- Beranek, L. L. *Acoustics*. McGraw-Hill. New York. 1954.
- Richardson, E. G. *Technical Aspects of Sound*. Elsevier, Amsterdam, 1953. Vol. I.
- Van Niekerk, G. G. "Measurement of the noise of ducted fans". *J. acoust. Soc. Amer.* 28, 681. 1956.

### Fan Testing Codes

Where the ability of a fan to carry out a specific task with good efficiency must be demonstrated to the satisfaction of the customer it is essential to have test codes in which standard requirements are laid down. Revisions of existing codes are planned but at the end of 1959 the controlling bodies and the codes sponsored by them were:

British Standards Institution  
2 Park Street  
London W 1

B.S. 380:1958 Performance of desk type electric fans  
B.S. 707:1936 The testing of mine fans  
B.S. 848:1939 Testing of fans for general purposes

Fan Manufacturers' Association Ltd.  
Copthall Avenue  
London E C 2

F.M.A. 3:1952 Fan performance tests

Air Moving and Conditioning Association Inc.  
2159 Guardian Bldgs  
Detroit 26  
Mich.  
U.S.A.

Bulletin No 110:1952 Standards, definitions, terms and test codes  
for centrifugal, axial and propeller fans

With the exception of B.S. 380, all codes are under revision.  
Codes B.S. 707 and 848 are to be combined and republished under  
the code number 848. Reference to the above bodies should be made  
if at any time further information concerning revisions is required.

# INDEX

- Aerodynamic smoothness, 48  
Aerofoils  
camber of, 55–56, 70, 119, 149–153, 169–170, 237, 239  
cascaded, 59–62, 70–71, 120, 123, 137–145, 169–175, 230–234, 249–251  
co-ordinates for, 335  
definitions of, 54–55  
effect of Reynolds number, 71–72, 121, 159–160, 239  
effect of roughness, 52  
isolated, 63–70, 123, 137, 225–230, 234–236, 241–249  
pitching moment, 57  
stall, 21, 58–59, 72, 239, 249, 266  
Aerofoil forces  
drag, 26–27, 57–59, 63, 111, 121, 130, 156–157, 167, 177, 247, 252, 256  
lift, 26–27, 56–57, 63, 119, 131, 139–145, 163–165, 167, 221, 226–227, 243, 246–247, 266–267, 312, 322  
Analysis  
prerotator, 254–256  
rotor, 241–253, 263–267, 272–275  
rotor-straightener unit, 270  
stator, 270  
straightener, 257–258, 268  
Angle of incidence, 27, 54, 119, 137  
Angle of local incidence, 149, 153, 170, 173, 249, 255  
Angular momentum, 9, 59, 75, 128  
Arbitrary vortex flow, 77, 118, 200–211, 298, 303, 311–312  
analysis, 247–249, 253, 255–256, 258  
design, 200–211, 232–236  
design limits, 208–210  
fan efficiency, 211  
Atmospheric properties, 13–14  
Axial velocity distribution  
in ducted fans, 118, 126–127, 203, 205–207, 297  
effect of non-uniformity, 309–311  
in free fans, 317, 327  
Bernoulli's equation, 15–16, 127–128, 202  
Blade aspect ratio, 238  
Blade elements, 118–120, 129, 136–155, 166, 207–208, 318  
design limits of, 119, 123–124, 154, 168, 170, 173, 188, 208–210, 221, 229  
forces, 56, 130–131, 238  
load distribution on, 117–118, 200, 205, 209, 298  
sections, 70  
solidity, 119–120, 131, 141–143, 154, 226, 245, 266  
types of, 5, 56, 70  
Bose ratio, 4, 123, 155, 183, 188, 201, 235, 271, 309  
Boundary layer  
equations of motion, 29–31  
growth, 19–20, 32, 38  
laminar, 18, 29–30, 31–33, 46–48, 239  
separation, 20–21, 33, 38, 42, 53, 58–59, 72, 91, 97, 101, 111–112, 188, 209, 214, 239, 255, 281, 286, 328  
skin friction, 16, 24–26, 33–37, 40–42, 49–53, 57  
thicknesses, 16–18, 23, 31–32, 38  
transition, 19, 23–24, 42–46, 86  
turbulent, 18–19, 30, 37–42, 48–53, 86, 89  
Branched duct systems, 85  
Camber, 55–56, 70, 119, 149–153, 169–170, 237, 239  
Capacity, 8, 288, 303  
Characteristic  
of duct, 8  
of fan, 8, 246–253, 263–264, 271, 306–307  
Chord, 54  
Coefficients  
drag, 26–27, 57–59, 63, 111, 121, 130, 156–157, 167, 177, 247, 252, 256  
flow, 116, 124, 129, 146–148, 241  
force, 24–27  
lift, 26–27, 56–57, 63, 131, 139–145, 163–165, 167, 221, 226–227, 243, 246–247, 266–267, 312, 322  
non-dimensional, 21–28  
pitching moment, 57  
pressure, 27–28, 128

- Coefficients (*contd.*)  
 swirl, 115–116, 124, 128, 146, 150,  
 241–242  
 thrust, 132, 198–211  
 torque, 132, 197, 211, 304–305  
 Compressibility, 11, 14, 119, 123, 215–  
 216  
 Conrad tube, 284–285  
 Contractions, 81, 89–91  
 effect of, 16, 20, 42, 89–91, 107, 109  
 losses caused by, 90  
 Corners  
 aspect ratio, 102  
 compound, 104  
 cross-sectional shape, 102, 109–110  
 diffusing, 110–111  
 flow in, 78–79, 100–101  
 losses, 101–105, 109–110  
 radius ratio, 102  
 secondary flow in, 78, 100  
 special types, 105–107  
 turning angle, 102  
 vanned, 79–80, 107–110
- Deviation angle  
 accelerated flow, 173  
 retarded flow, 150
- Diaphragm mounted fans, 3
- Diffuser angle, 93–94, 184–185, 188
- Diffusers  
 annular, 184–185  
 area ratio of, 94  
 cross-sectional shape of, 94–95  
 devices for improved flow in, 97–99  
 efficiency of, 92, 184–185  
 flow in, 92–93  
 inlet condition effects, 96  
 Reynolds number effects, 95, 189  
 Discharge loss, 6, 82, 195, 225, 291  
 effect of diffuser on, 6, 92, 195, 291
- Disk drag, 162
- Drag  
 annulus, 121, 161, 180  
 disk, 162  
 profile, 57–59, 121, 252, 256  
 secondary, 59, 80, 121, 160–161,  
 179–180  
 total, 121, 158, 162–165, 182, 247,  
 256
- Drag coefficient, 26–27, 57–59, 63,  
 111, 121, 130, 156–157, 167, 177,  
 247, 252, 256
- Ducts, 6–8, 78–79, 81–114, 194  
 assessment of losses, 82–89  
 components of, 81–82  
 equivalent, 21, 82, 87  
 straight, of constant cross-sectional  
 area, 85–89
- Efficiency  
 of fan unit, 121–122, 192–194, 225,  
 259, 261  
 of rotor, 156–165, 193, 305–306  
 preswirl effects on, 164–165, 193,  
 231  
 residual swirl effects on, 190–192  
 static, 194–196, 237, 290  
 surface roughness effects on, 52, 121  
 system, 194–196  
 tip clearance effects on, 162, 238  
 total, 192–193  
 wall boundary layer effects on, 311
- Equation of continuity, 30
- Equation of state, 14
- Equations of motion, 29–30
- Fairings  
 belt, 239  
 nose, 4, 230, 240  
 tail, 4, 183, 194, 201, 209, 230, 271,  
 336
- Fan units  
 definition of, 2, 4  
 ducted fan types, 9  
 duty of, 6  
 general types of, 2  
 layout design of, 4, 121, 127, 229,  
 239–240  
 special types of, 10  
 static pressure head in, 6, 194–195,  
 288  
 static pressure rise in, 9–11, 120,  
 128, 139, 209  
 total head rise of, 4, 6, 81, 119, 128,  
 234, 244, 289, 293, 298, 303
- Fineness ratio, 187–189, 230
- Flow coefficients, 116, 124, 129, 146–  
 148, 241
- Flow deflection, 59–62, 72, 80, 120,  
 127, 249, 312
- Flow direction, measurement of, 282–  
 285
- Flush surface tube, 280
- Force coefficients, 24–27
- Free fans, 2, 313–328  
 analysis of, 326–327  
 design of, 317–325  
 noise in, 328  
 recirculating flow in, 313–315  
 testing of, 316–317, 326
- Free vortex flow, 77, 118, 123, 126,  
 130, 246–247, 298
- design for, 225–232
- Head  
 fan static pressure, 6, 194–195,  
 288–289

- Head (*contd.*)  
     total, 15, 127–128, 279–280  
     velocity, 15, 27
- Hot wire instruments, 282, 285, 296–297
- Hydraulic mean radius, 87
- Impulse fan, 10
- Inlets, 90–91, 277, 288
- Interference factor, 120–121, 228
- Internal bodies in ducting, 111–114
- Kinematic viscosity, 30, 226
- Lift, 26–27, 56–57, 63, 119, 131, 139–145, 163–165, 167, 221, 226–227, 243, 246–247, 266–267, 312, 322
- Limit load, 307
- Loss coefficients, 84, 128, 158, 176, 185–187, 331
- Losses  
     duct, 82–85  
     rotor, 121–122, 128, 156–165  
     stator, 128, 176–182  
     tail fairing, 185–187
- Manufacturing methods, 5–6
- Mean value computation, 84, 303–307
- Mechanical blade design, 238
- Momentum thickness, 18
- Multiplane interference, 55, 120–121, 154, 307
- Noise, 119, 212–217, 239–240, 255, 328
- Notation, 125, 329–334
- Obstructions to flow, 111–114, 238–239
- Operating point, 8
- Optimum conditions, 136, 138–148, 163, 170
- Pipe flow  
     entry length, 23, 45, 86  
     fully developed, 19, 23, 36–37, 41, 49–51, 83, 86, 311  
     laminar, 36  
     losses, 83, 85  
     mean velocity, 36, 41  
     roughness, 49–51  
     transition, 23, 43, 45–46, 86  
     turbulent, 41, 86
- Pitching moment, 57
- Pitot-static tube, 281
- Power, 198–199, 224, 291, 307
- Prerotation, 9–10, 120, 122, 127, 231
- Prerotators, analysis of, 254–256
- Pressure coefficients, 27–28, 128
- Radial equilibrium, 74–76, 118, 126, 202, 303
- Resistance laws, 8, 84, 89, 95, 103, 199, 307
- Reynolds number, 22–24, 71–72, 84, 86, 95–96, 103, 121, 159–160, 189, 226, 239
- Rotor analysis, 241–253, 262–267, 272–275
- Rotor construction, 5–6
- Rotor losses, 156–165
- Rotors  
     contra-rotating, 9, 123, 193, 262, 272–274  
     variable pitch, 260–271
- Roughness  
     in adverse pressure gradients, 52–53  
     in pipes, 49–51  
     on flat plates and aerofoils, 52  
     surface, 46–53, 87–88, 121
- Similarity, 21–22
- Skin friction, 16, 24–26, 33–37, 40–42, 49–53, 57
- Solidity, 119–120, 131, 141–143, 154, 226, 245, 266
- Specific speed, 116–117
- Stagger angle, 150, 152–153, 170, 172–173
- Stagnation point, 280
- Stall  
     aerofoil, 21, 58–59, 72, 239, 249, 266  
     fan, 10, 81, 137, 146, 195, 214, 249, 266, 286, 292, 298, 307, 315  
     stator, 257
- Static efficiency, 194–196, 237, 290
- Static pressure head in fan units, 6, 194–195, 288
- Static pressure, measurement of, 280–281
- Static pressure rise in fan units, 9–11, 120, 128, 139, 209
- Stator analysis, 254–258, 270
- Stator design, 166–175
- Stator losses, 176–182
- Stators, variable pitch, 245, 254
- Straighteners  
     analysis of, 257–258, 268  
     cascade type, 169–172, 178  
     N.P.L. type, 168, 178
- Stressing of blades, 238

- Swirl  
  coefficient, 115–116, 124, 128, 146, 150, 241–242  
  distribution, 77, 118, 201, 203  
  effect of on efficiency, 9, 190–192, 194  
  sign convention for, 127, 242
- Testing, 276–308  
  codes of, 316, 360  
  commercial, 287–292  
  classes of, 276–277  
  determination of mean values, 303–307  
  equipment, 277–278, 288, 308  
  instantaneous measurements, 297  
  instruments, 278–285  
  measurements on rotating blades, 307–308  
  traverse experiments, 292–303  
  visual studies, 272, 286–287, 328
- Thrust, 132, 197–198, 322  
  coefficient, 132, 198, 211  
  gradient, 132, 211
- Tip clearance effects, 162, 238
- Torque, 132, 197, 304–305, 318, 320  
  coefficient, 132, 197, 211, 304–305  
  gradient, 132, 211  
  measurement of, 304–305
- Total head, 15, 127–128, 279–280
- Transition, 19, 23–24, 42–46, 86
- Tufts, 286–287
- Turbulence, 18–20
- Unducted fans, 2, 313–328
- Vanes, turning, 79–80, 107–110
- Variable pitch rotors, 260–271
- Variable pitch stators, 245, 254
- Velocity, mean, 23, 36, 41, 84, 128, 203, 303
- Velocity, measurement of, 281–282, 285
- Vibration, 213, 215, 238
- Viscosity, 14, 16–18, 30, 226
- Volume flow, 203
- Vortex flow, 74–77  
  arbitrary, 77, 118, 200–211, 232–236, 247–249, 253, 255–256, 258, 298, 303, 311–312  
  free, 77, 118, 123, 126, 130, 225–232, 246–247, 298
- Vortex generators, 99
- Vortex ring state, 315
- Wakes, 72–73, 214
- Wire screens, 94, 97, 111–112, 114
- “Work done” factor, 311
- Yawmeters, 282–285, 299